Methods for increasing the sensing performance of metal oxide semiconductor gas sensors at ppb concentration levels

Dissertation
zur Erlangung des Grades
des Doktors der Ingenieurwissenschaften
der Naturwissenschaftlich-Technischen Fakultät
der Universität des Saarlandes

von

Dipl.-Ing. Martin Leidinger

Saarbrücken

2018

Tag des Kolloquiums:	03.07.2018
Dekan:	Prof. Dr. Guido Kickelbick
Berichterstatter:	Prof. Dr. Andreas Schütze
	Prof. Dr. Helmut Seidel
Vorsitz:	Prof. Dr. Michael Vielhaber
Akad. Mitarbeiter:	Dr. Jonas Sander

Abstract

Metal oxide semiconductor gas sensors are in general well suited for high volume gas sensing applications, e.g. air quality monitoring, due to their low cost and high sensitivity. However, in many applications, the gases to be detected can occur in very low concentrations, which complicates selective measurement of specific components.

In this thesis, several methods are presented which improve the performance of such sensors for the detection of gases at trace concentrations.

First, the design and characterization of a gas mixing system is described, which allows generation of test gases in the ppb (parts per billion) concentration range. Several well established techniques are then tested for their applicability at these low concentration levels. Key elements are cyclic modulation of the sensor temperature and signal processing based on methods for pattern recognition, for both single sensors and combined sensor signals. A novel development is an integrated micro system in which gas pre-concentration is realized in combination with the sensor. In addition to the technical developments, the reproducibility of the results has been investigated in an inter-laboratory comparison, where a measurement system for benzene has been characterized in two different setups for test gas generation.

The presented methods provide a basis for using low-cost metal oxide semiconductor gas sensors for potential applications in the field of trace gas analysis.

Kurzfassung

Metalloxid-Halbleiter-Gassensoren (MOS) sind aufgrund ihrer hohen Sensitivität und geringen Preises grundsätzlich gut geeignet für Gasdetektion in Anwendungen mit hohen Stückzahlen, zum Beispiel für die Überwachung von Luftqualität. In diesen können die zu detektierenden Gase jedoch in sehr niedrigen Konzentrationen auftreten, was eine gezielte Messung einzelner Komponenten erschwert.

In dieser Arbeit werden Verfahren vorgestellt, mit denen die Leistung solcher Sensoren für die Detektion von Gasen in Spuren-Konzentrationen verbessert wird.

Zunächst werden das Design und die Charakterisierung einer Gasmischanlage beschrieben, die eine zuverlässige Generierung von Testgasen im ppb-Bereich (parts per billion) ermöglicht. Mehrere etablierte Verfahren werden dann auf ihre Eignung für diesen niedrigen Konzentrationsbereich getestet. Zentrale Elemente sind hierbei eine zyklische Änderung der Sensortemperatur und Signalverarbeitung basierend auf Methoden zu Mustererkennung, sowohl für einzelne Sensoren als auch für kombinierte Signale. Eine neue Entwicklung ist ein integriertes Mikrosystem, in dem zusätzlich zum Sensor eine Gas-Aufkonzentration realisiert ist. Neben den technischen Entwicklungen wurde die Reproduzierbarkeit der Ergebnisse in einer Vergleichsmessung in zwei Labors untersucht; hier wurde ein Messsystem für Benzol in zwei unterschiedlichen Setups zur Gasaufgabe getestet.

Die vorgestellten Methoden bieten eine Grundlage zum Einsatz der günstigen MOS-Gassensoren für Anwendungen im Bereich von Spurengasen.

Table of contents

1 Introduction and motivation

In recent years, in the fields of gas analysis and gas measurement technology a lot of research and development effort has been put into systems for the detection, identification and quantification of trace gases. Some of the most active fields of applications for gas detection technologies are presented in the following segments, and in all these domains the measurement of gas concentrations at levels of sub-ppm (parts per million) or even ppb (parts per billion) is of high relevance.

Traditionally, analytical equipment is used for detection of low concentration of gases, such as gas chromatography (GC) [1]-[3], mass spectrometry (MS) [4]-[6] or special types of infrared spectroscopy (IR) [7]-[9], all of which are available in various variations and optimizations for different application scenarios. These methods can also be used in combination; especially the coupling of gas chromatography with mass spectrometry (GC-MS) is utilized very widely [10]-[13]. The advantages of such systems are their high performance in terms of selectivity, accuracy, and flexibility regarding the range of the detectable compounds. As they are usually sophisticated laboratory equipment, some disadvantages are high system and running costs, often complex and time-consuming sample preparation, and very limited mobility.

Due to these restrictions, many attempts have been started to try to achieve similar performance as the analytical systems with systems that use smaller, cheaper and more robust gas sensing technologies. A wide variety of low cost gas sensor and gas sensor system technologies is available, although not all of them can be used for ppb level gas sensing; some of the most important, both for trace gases and higher concentrations, are:

- Electrochemical cells [14][15]
- Lambda oxygen sensors [16][17]
- Catalytic sensors (pellistors) [18][19]
- Infrared sensor systems [20][21]
- Metal oxide semiconductor (MOS) gas sensors [22][23]
- Field effect devices [24][25]

All of these technologies have been used for developing gas measurement systems for specific applications in research and commercial usage, many of which require the measurement of ppb level gas concentrations.

1.1 Applications for ppb level gas detection

Selected of fields of applications for trace level gas detection are presented in this chapter.

1.1.1 Air quality monitoring

The monitoring of the air we breathe has gained high relevance, for both indoor and outdoor scenarios [26]-[30]. As people spend more and more time in buildings, more than 85% [35], the air quality especially in homes and workplaces can have a significant influence on our health. In indoor air, a large number of gaseous compounds can have negative effects on humans. In addition to some inorganic permanent gases like carbon monoxide (CO), carbon dioxide (CO_2) and nitrous oxides (NO_x), a large number of different volatile organic compounds (VOCs) can be present indoors. They can cause a variety of symptoms ranging from skin irritations and short-term respiratory problems [28][31] to chronic conditions [32][33] and, for some VOCs, cancer [34]. For many of these substances, a single short time exposure is not dangerous, but permanent exposure over long periods of time can cause the mentioned health risks. Diseases caused by contaminated indoor air have been labeled “sick building syndrome” [36][37].

As most important VOCs for indoor air quality (IAQ) monitoring, three compounds have been identified by the World Health Organization (WHO): benzene, formaldehyde, and naphthalene [38]. The recommended concentration thresholds for human exposure for these compounds, as well as other relevant gases and particulate matter are presented in Table 1.

Table 1: Overview of the most relevant indoor air pollutants; based on [39], © 2014 IEEE.

Pollutant	Exposure limit		Country	Year	Remarks	Ref.
Benzene	2 µg/m³	0.6 ppb	France	2016	long term exposure;	[40]
					no safe level for exposure (WHO)	[38]
Formaldehyde	100 µg/m³	80 ppb	Germany	2006	30 min average	[41]
	30 µg/m³	24 ppb	France	2015	short-term (for exposure of 2 h)	[40]
Naphthalene	10 µg/m³	1.9 ppb	Germany	2010	annual average	[38]
Carbon monoxide	10 mg/m³	8.7 ppm	WHO	2010	8 h average	[38]
Nitrogen dioxide	200 µg/m³	105 ppb	WHO	2013	short-term (for exposure of 1 h)	[42]
Radon	167 Bq/m³		WHO	2010	annual average; excess lifetime risk 1 per 1000 for non-smokers	[38] [43]
Styrene	70 µg/m³	16 ppb	WHO	2000	30-min average	[44]
Tetrachlor-ethylene	0.25 µg/m³	36 ppb	WHO	2010	annual average	[38]
Toluene	3 mg/m³	783 ppb	Germany	2016	guide value II (RWII)	[45]
Trichlor-ethylene	230 µg/m³	42 ppb	WHO	2010	excess lifetime cancer risk 1:10,000	[44]
PM10	50 µg/m³		WHO	2005	24-hour mean	[42]

Table 1 shows that for many gases the recommended limit values are at a sub-ppm levels, for some even in the single-digit or sub-ppb range (benzene, naphthalene). Especially when long-term exposure is considered, 8 h per day or more, the relevant gas concentrations are very low.

The monitoring of specific gases in indoor air poses a number of particular challenges, especially if gas sensors with limited selectivity are used. Indoors, complex gas matrices can occur, and benign interferent gases can be present in comparatively high concentrations, such as ethanol, solvents (e.g. from cleaning agents), or odorants (e.g. from perfumes). Furthermore, some indoor scenarios have a very high baseline of chemical compounds in the air, e.g. kitchens, which can make the detection of specific substances very difficult.

In outdoor scenarios, some of the target gases are identical to IAQ, especially benzene has a high relevance [46][47], and nitrogen oxides (NO_x) occur in higher concentrations [48]-[50]. Additional relevant compounds are Ozone (O_3) [51][52] and Sulfur dioxide (SO_2) [53][54], all of which are associated with respiratory diseases and asthma.

For indoor as well as outdoor applications, measurement systems are required to be small, robust and low-cost compared to analytical laboratory equipment, as there is usually a number of systems deployed to achieve a certain spatial resolution. For example in a private home, the air quality can differ significantly in different rooms (e.g. kitchen, bathroom, living room) and thus a high number of sensor nodes is required to accurately measure the pollutants in different areas of the home. A number of research activities have focused on small networked gas sensor systems for air quality control [55]-[57].

For outdoor applications, mobility is another key aspect, as many approaches include mobile systems that are installed on buses [58], trams [59], cars [60], bikes [61], or pedestrians [62], to generate air quality maps of cities.

1.1.2 Breath analysis

Another emerging field of application for ppb level gas detection is the analysis of exhaled breath [63]-[65]. A number of medical conditions cause the composition of the exhaled breath gases to change in a specific way, e.g. diabetes [66], asthma [67],

tuberculosis [68] or different types of cancer (e.g. lung cancer [69], gastric cancer [70] or breast cancer [71]). In many cases, the relevant gas concentrations are in the ppm range or lower, e.g. for asthma diagnosis, the measured concentrations for NO (nitric oxide) are between 100 and 400 ppb [67], and one study on gastric cancer found the relevant concentrations of VOCs below 100 ppb [72].

So far, breath analysis measurements are mostly performed by analytical methods like different kinds of mass spectrometry [73][74], but as with air monitoring, development of cheaper and smaller gas sensor systems is pursued. These sensor systems often use some of the same sensor technologies as are used for air quality monitoring, such as MOS gas sensors [75]-[77], but other methods or combinations of technologies are used as well, such as infrared / electrochemical [78], colorimetric [79] or potentiometric sensors [80].

1.1.3 Odor monitoring

Odor is also a parameter of gaseous substances which is interesting for some applications [81]-[83]. In some cases, the occurring concentrations of specific gases are not harmful, but generate unpleasant odors. Monitoring of such odors can be desired in order to efficiently use countermeasures or just for monitoring of processes. Many studies have been performed measuring the odors generated by chemical plants [84][85], waste treatment facilities [86][87] or agricultural farms [88][89]. The goal of such studies usually is the generation of objective data about the odor nuisance to the surrounding population. The reported gas concentrations are mostly in the ppb range. One study measuring a wide variety of analytes at a landfill detected all relevant VOCs in the single or low double digit ppb range [90].

1.1.4 Food spoilage detection

Another interesting application of odor monitoring is the detection of spoilage of food products via the emitted gases. Some investigations have attempted this, and found

clear relations between the freshness of certain food items and the emitted matrix of gases. These gases differ significantly for different groups of food, e.g. fish [91][92], meat [93][94], fruit [95][96] or even water [97][98]. But, as in the other presented applications, the emitted gas compositions can be monitored only if the sensor system can detect ppb levels of the relevant compounds.

1.1.5 Safety applications

Safety and security applications are additional fields of use where gas concentrations are often very low, e.g. detection of chemical warfare agents [99][100], explosives [101][102] or drugs [103][104]. In these scenarios, the substances often have very low vapor pressures [105] and thus the emitted gas concentrations are low as well. As in the other presented examples, both analytical methods and gas sensors are used, with low-cost sensor systems gaining more and more relevance to allow comprehensive coverage of relevant areas.

1.2 Electronic noses

As the presented fields of applications and the literature show, for most of these fields of use analytical measurement systems are the first step in analyzing the measurement task. However, after identification of the target analytes and target concentrations, in all of the examples low-cost gas sensor systems have been and are being investigated and developed. A term that is often used to describe such sensor systems is “electronic nose” [106]-[108]. This term usually refers to the whole system, including sensors, electronics, signal processing and communication. Such devices have been explored for the presented fields of air quality monitoring [109]-[112], breath analysis [113]-[116], odor monitoring (outdoor [117]-[120] and food items [121]-[124]) and safety applications [125]-[128]. Often, they do not use single sensors but an array of different types of sensors for increasing the range of detected gases and for suppression of the effects of interfering gases. To enhance the performance of the systems, a great

number of methods are used for combining the signals of the different sensors and to compute the desired output values. A significant drawback of such systems is the limited stability of the sensors and thus the whole system, depending on the chosen sensors and operating modes.

The large number of publications on the topic of electronic noses shows the relevance of low-cost gas sensor systems trimmed for performing specific measurement tasks, many of which focus on low gas concentrations.

1.3 Test gas generation

For development, testing, characterization and calibration of gas sensor systems, test gas mixtures have to be provided. Besides the respective target gases for the application, there are usually variations in interferent gases and other environmental parameters (e.g. gas humidity) which might affect the performance of the sensor system. Therefore, a highly dynamic and versatile generation of gas mixtures is necessary.

Generating low concentrations of VOCs is a special challenge, for several reasons: Many VOCs have a low vapor pressure and are not available in standard gas cylinders, so different methods for generating these species have to be employed, which makes the overall test gas generation system more complex [129]. Another problem is the required low concentration range. While gas cylinders with low concentrations of the desired compounds can be produced quite accurately, there is always a residual contamination in the produced gas. Usually, test gases are produced at purity 5.0, which means a purity of 99.999 %. In such a gas mixture, the contaminations can still be up to 10 ppm, so the concentration of the contamination could be higher than that of the test gas if it is mixed with a share in the low ppm range. Several methods can be used to overcome these problems, e.g. generating test gases from high purity liquids (e.g. using evaporation or injection) [130], using permeation devices [131][132] or diluting the high concentration cylinder gas in a very high ratio with a pure carrier gas (usually air or nitrogen) [129][133]. In the last mentioned method, the background

carrier gas should have a high temporal consistency and low contamination levels. This keeps the total level of contaminations steady at the sensor or system to be tested. If the test gas is present in the background, the gas concentration from the cylinder is added to this existing concentration, so the total level can be higher than intended. However, in any application there is also a ubiquitous background of a large number of gases, and in most cases multiples of these background concentrations are to be detected. From this perspective, a (very) low level of impurities in the carrier gas is acceptable - if it is stable at the sensor - as it is closer to applications than a completely clean background would be.

Other properties of the gas mixing system that can have significant effects for ppb level gas concentrations are adsorption and desorption effects of the installed components (e.g. tubing or seals) and effects of unwanted dead volumes which can cause tailing effects when gases or gas concentrations are switched.

1.4 Scope of this thesis

This thesis focuses on one of the presented types of gas sensors – MOS sensors – and one of the presented fields of application – air quality monitoring. The goal is to increase the sensing performance of MOS gas sensors with regard to the most relevant gases for air quality, especially indoor air, in order to increase the usability and reliability of such sensors for use in versatile gas sensor systems or electronic noses.

In a first step, the issue of test gas generation is addressed and the design, testing and evaluation of a new gas mixing system are presented. This is the basis for being able to reliably test several methods intended to maximize the abilities of MOS based low-cost gas sensor systems.

One of the biggest challenges when using MOS gas sensors is their very limited selectivity, as they are essentially broadband sensing devices. Several previous research activities have reported successes regarding increased selectivity and sensitivity when the sensor is not operated at a constant temperature but if the temperature is changed dynamically. This temperature cycled operation (TCO) is used

for all gas sensor measurements in this thesis. As a MOS gas sensor shows different responses to different gases at different temperatures, this has been called a virtual multisensor. Analyzing the generated signals from a sensor operated in such a way requires more complex data processing techniques, basically pattern recognition algorithms. Several such computational methods are used in this work.

The virtual multisensor approach has also been combined with a real multisensor approach, with a set of several different MOS gas sensors all being run in TCO and combining the dynamic signals of all sensors in the data processing.

An important aspect for assessing the performance of measurement systems or devices is testing them in varying conditions. A sensor system for ppb level benzene detection was subjected to an inter-laboratory measurement campaign and tested for the target gas at two different labs using two very different test setups.

Another option for improving sensing performance which has been explored is the use of gas pre-concentration. In general, pre-concentration describes the accumulation of the target gas in a suitable material, usually a solid, followed by a sudden release of the gas, often thermally induced, which generates a short gas pulse with a higher concentration compared to the initial value.

In a nutshell, this thesis explores the method of dynamic gas dilution for ppb level test gas generation and presents several methods for increasing the performance of MOS gas sensors, such as temperature-cycled operation, combined data processing of multi-sensor systems, gas pre-concentration and advanced pattern recognition data analysis. For verification of the obtained results, a gas sensor system was also tested in a second laboratory.

2 Fundamentals

2.1 Metal oxide semiconductor gas sensors

In this thesis, gases are detected using metal oxide semiconductor (MOS) gas sensors. These devices are used widely in many applications and research projects, as they are inexpensive, can be operated very easily and offer great sensitivity to a large number of gases. However, using these sensors is still challenging, as selectivity and stability of the signals are not as good as for other sensing principles. Both the strengths and the weaknesses of these devices result from their operating principle, which is presented in this chapter, along with the basics of an operation mode which can reduce these issues while also boosting sensing performance.

2.1.1 Basic Operating principle

The transducing element of MOS gas sensors is, as the name suggests, a layer of a semiconducting metal oxide material. A number of different materials is used in such sensors, including tin dioxide (SnO_2), tungsten trioxide (WO_3), zinc oxide (ZnO), magnesium oxide (MgO), indium(III) oxide (In_2O_3), titanium dioxide (TiO_2), and many more [134][135].

The transducing effect is a change of the electrical conductivity of this layer caused by changes of the surrounding gas atmosphere. It can be explained well for the example of SnO_2, which is an n-type semiconductor and one of the most used materials for gas sensors. The electrical conductivity of the material is depending on the interaction of the material with oxygen (O_2) and other gases, which adsorb and desorb at the surface of the sensing layer. As the oxygen adsorbs at the material, it binds electrons from the semiconductor material and thus leads to the formation of a depletion layer [136]. If molecules of oxidizing or reducing gases are also present in the surrounding atmosphere, they can react with the adsorbed oxygen ions, and the formerly bound electrons are available again as charge carriers in the sensor material, which results in

an increase in conductivity. The electrical current which is used to measure the conductivity of the layer has to pass through this area, which represents an energy barrier in the electronic band structure of the semiconductor, as shown in Figure 1.

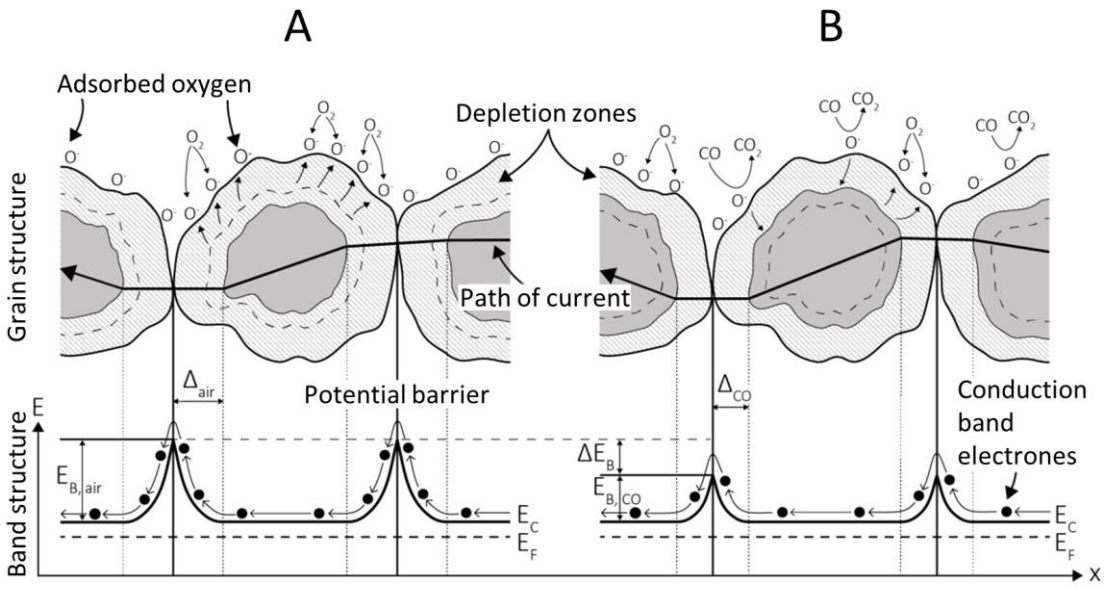

Figure 1: Simplified operating principle of a MOS gas sensor. The polycrystalline structure and the band structure of the semiconductor are visualized for two states: the MOS structure in air without reactive gas (A) and with CO in the surrounding atmosphere (B); adapted from [137] (modeled after [136],[138],[139]).

In the shown example, on the left side (A) no reactive gas is present in addition to oxygen. The oxygen binds electrons from the MOS material and the depletion zones at the edges of the grains increase in width. The junctions between the grains pose significant potential barriers for the conducting electrons to overcome, which means the electrical conductivity is reduced. If a gas is added, carbon monoxide in this example (Figure 1 B), a chemical reaction takes place. The CO reacts with the adsorbed oxygen, the formerly bound electrons are released into the MOS material, the width of the depletion zones is reduced and the height of the energy barrier at the junction of the grains is decreased. As a result, the electrical conductivity of the structure is increased.

The effect is boosted by a large number of grain boundaries that have to be passed. Therefore, usually highly granular materials are produced and used as gas sensitive layers. Investigations on variations of the grain size show higher responses to gases (i.e. changes in conductivity) for smaller grain sizes [140][141].

The dynamics of the adsorption and desorption processes as well as the gas reactions and the conductivity of the semiconductor material are all significantly dependent on temperature [142]. Therefore, gas sensing materials are usually deposited on a substrate which can be temperature controlled via an integrated heater structure [140][143]. Often, temperatures of 400 °C or more can be achieved by the heater [144][145].

There are two basic technologies for MOS sensor substrates: ceramic based substrates [146][147] and micromachined membranes [148][149]. Ceramic substrates are usually produced in sizes of several millimeters. They offer high robustness and can be used for high temperature applications. Various designs have been published; these substrates can be tube shaped, with the heater being placed inside the tube, and the sensing material at the outer wall of the tube (Figure 2 A), which offers a very large sensing area; or they can be planar substrates (Figure 2 B). Planar substrates allow for a wide range of sensing layer deposition techniques. In his case, the heater structure is placed either on the backside of the substrate or between the substrate and the sensing layer. A disadvantage of ceramic substrates is their comparably large thermal capacity, which results in large time constants of at least several seconds when the sensor temperature is changed.

Micromachined sensor substrates, on the other hand, consist of a thin membrane, with a thickness in the range of several µm, which allows for very fast changes of the sensor temperature (time constants of several tens of milliseconds). These structures are generally much smaller than the ceramic substrates, sometimes the dimensions of the heated areas are in the sub-mm range. Two examples are shown in Figure 2 C and D. Gas sensor platforms produced in microtechnology require advanced equipment for manufacturing, but are easily fabricated in large numbers. They require much less electrical power for heating the sensing layer, as the thermal mass and thermal

conductivity of the membrane, which is usually surrounded by a cavity for improved insulation, are very low. The disadvantages, compared to ceramic substrates, are a higher vulnerability to high temperatures and lower durability in harsh conditions.

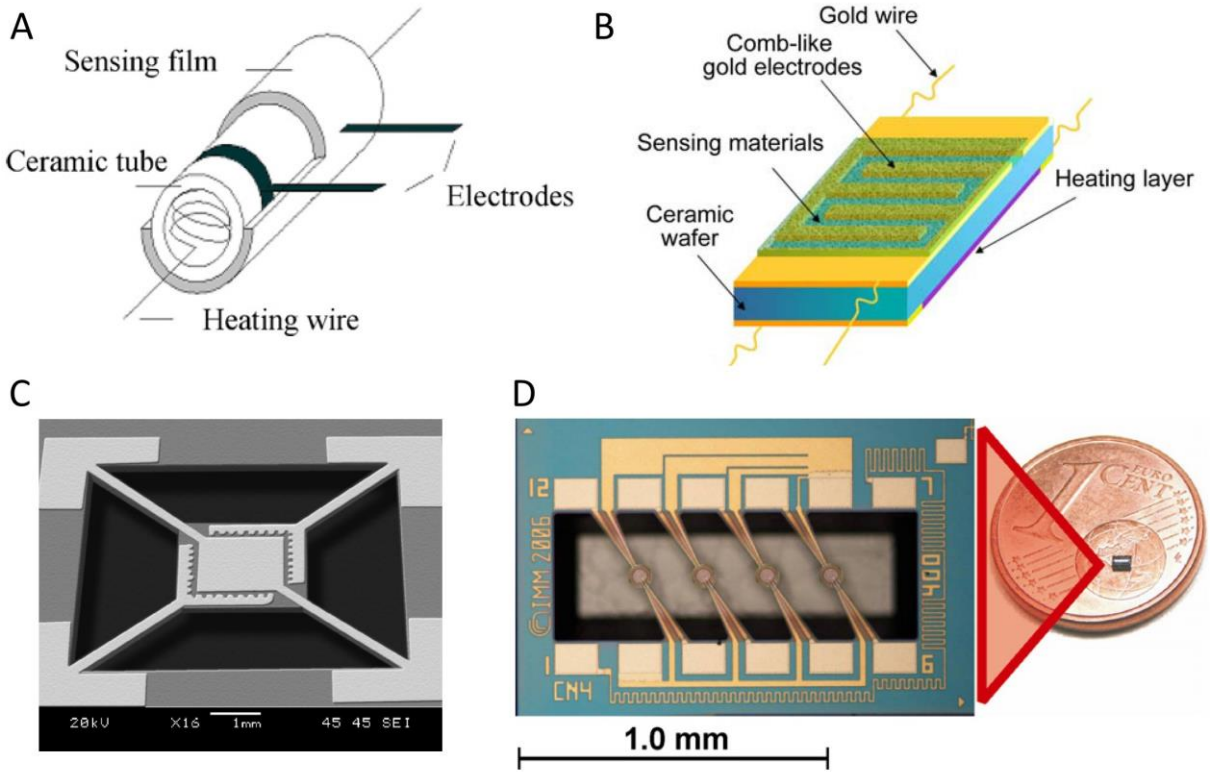

Figure 2: Examples of designs of MOS gas sensors; ceramic substrates can have tube shapes as shown in A [146], but are today usually planar as in B [147]; micro machined devices can be prepared as single sensors, shown in C [148], or as multi sensor platforms as in example D [149].
Figures A, C, D reprinted with permission from Elsevier; B licensed under CC BY-NC-SA 3.0.

The heater structure which is integrated into the sensor substrate is essential for the operation of MOS gas sensors. The sensitivity of the sensor to certain gases as well as the selectivity of the device can be influenced drastically by changing the temperature of the heater and thus the sensing layer; this is discussed further in the next chapter.

2.1.2 Temperature cycled operation

As already mentioned, for most MOS gas sensors the temperature of the gas sensing layer material can be increased using an integrated heater structure. MOS gas sensors are usually heated to temperatures above 100 °C, as their conductivities can be too low to be measured properly at lower temperatures and because the gas reactions at the surface are dependent on an elevated temperature. The temperature of the sensor has a direct effect on the amount of ionosorbed oxygen, which contributes significantly to the operation of the gas sensing material by reacting with the surrounding gases. At high temperatures, more oxygen is ionosorbed at the surface compared to lower temperatures. The transitions from a low to a high temperature and vice versa are non-equilibrium states for the sensors and are particularly interesting, as additional effects gain importance compared to the steady-state operation at a constant temperature. The transitions and the corresponding effects on the conductance of a sensing material, especially for temperature changes with time constants in the millisecond range, have been described in detail in [150] and are illustrated in Figure 3.

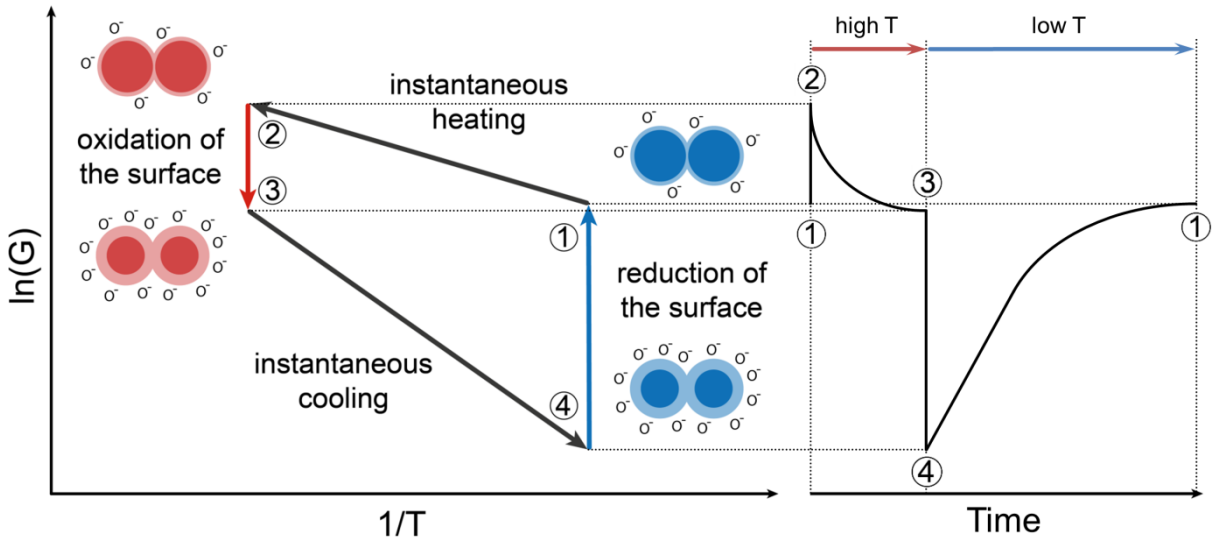

Figure 3: Schematic visualization of the states of a MOS gas sensor during high temperature / low temperature TCO cycle, shown as an Arrhenius plot; the red and blue illustrations represent the states of the grain boundaries and depletion zones at the different temperatures; the right part shows the corresponding signal over time; adapted from [150],[151].

Starting point in this example is a stationary low temperature (state 1), which results in low oxygen coverage. A fast temperature step is assumed to achieve state 2, which represents a high temperature and low oxygen coverage immediately after the temperature step, as the oxygen reaction process is much slower than the temperature change. Given sufficient time, more oxygen ionosorbs on the surface and the conductance of the material decreases until it reaches a new steady state (state 3). A rapid decrease of the temperature, shown as the transition from state 3 to state 4, shows the opposite effect as the previous transition. Due to the low temperature and the high oxygen adsorption on the surface, the sensing material reaches a very low conductance. As after the temperature increase, relaxation effects eventually lead to the steady state which is state 1.

Using active temperature modulation, every point inside the shown trapezoid of states (Figure 3) can be set or passed during a relaxation process, while a sensor at constant temperature operation is limited to one of these states. Therefore, varying the temperature of a MOS gas sensor is an established method for increasing the performance of such a device, which means increase of the selectivity, sensitivity, stability, and speed of the sensor [152]-[156].

Experiments have shown that a MOS gas sensor in TCO can cover more than 5 orders of magnitude in conductivity [157]. Therefore, the read-out of the sensor requires more sophisticated electronics compared to sensors operated in a steady state. One approach to this challenge is the use of logarithmic operational amplifiers, which has been successfully tested in previous works [158].

2.1.3 Pulsed laser deposition for manufacturing MOS gas sensing layers

The desired porous structure of the sensing material results in another problem with MOS gas sensors: reproducibility of the layers and their gas sensing characteristics. Sensors of the same type can show poor uniformity in electrical conductance, which can pose significant problems for the calibration of sensor elements or sensor systems. Manufacturing technologies which address this issue are being developed. One of

them is the deposition of the sensing layer material from a target of this material using laser ablation; the method is called pulsed laser deposition (PLD) [159]-[161]. Pulses of a high energy laser are shot at the target, which is placed inside a vacuum chamber. The high energy of the laser, which is adsorbed by the surface, causes evaporation of the target material and leads to formation of a plasma, which expands into the vacuum chamber. The evaporated material condenses on the surface of the substrate, which is placed face-to-face to the target, and forms a thin coating layer. By controlling the energy, the pulse length and the pulse frequency of the laser as well as the temperature of the substrate and the background gas in the chamber, the structure of the deposited layer can be influenced to generate a large number of variations for a single target material. These parameters can significantly influence the properties of the sensing layer, e.g. the porosity of the structure is influenced by the oxygen partial pressure in the vacuum chamber during the PLD process [162][163]. Examples of SEM (scanning electron microscope) images of the surfaces of three different materials are shown in Figure 4.

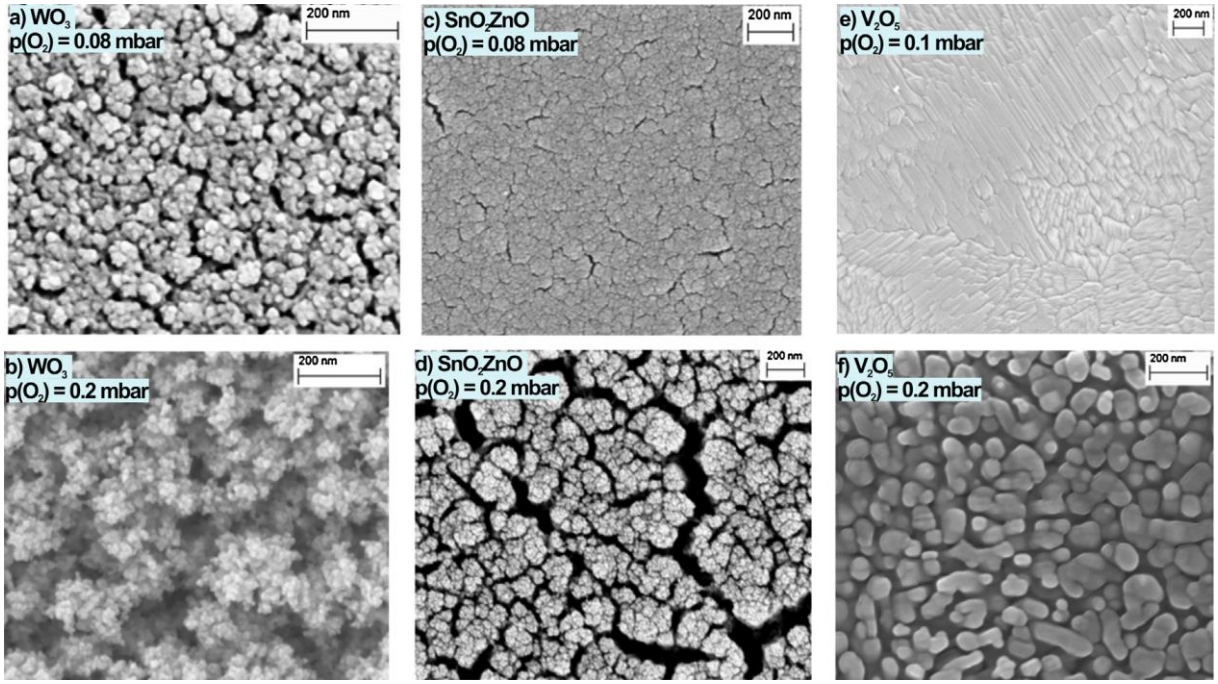

Figure 4: SEM micrographs of the surfaces of three MOS layers generated by PLD (WO_3, SnO_2(ZnO) and V_2O_5), each deposited with two variations of oxygen partial pressure ($p(O_2)$) with a difference of approx. a factor of 2 [163].

For all three investigated materials, an increase of oxygen partial pressure ($p(O_2)$) during deposition results in a more porous structure, while the lower $p(O_2)$ value results in dense layers for two of the samples, Figure 4 c) and e).

Using PLD, very thin layers of the gas sensing material can be produced, down to less than 10 nm [164][165], which is relevant for gas sensors if TCO operation with fast temperature changes is intended. The method has been used widely for preparation of gas sensing MOS layers [162]-[164][166].

2.2 Pre-concentration of gases

A method used to enhance the performance of many analytical measurements, especially for detecting low concentrations of gases (or liquids), is pre-concentration of the target compounds. The goal of gas pre-concentration is to artificially increase the concentration of gases, or of a specific target gas, to a level much higher than that present in the target atmosphere. To achieve this, the gas is collected (adsorbed) in an adsorber material over a certain time and then desorbed quickly, resulting in a short pulse of a high concentration of the gas, which can then be detected and measured. For analytical applications, a wide variety of methods is available [167]. A widely used technique is sampling of gases in sorbent tubes, followed by thermal desorption in the analytical measurement system [168]-[170]. Another method is solid-phase microextraction (SPME), in which a thin polymer coated fiber is inserted in the gas or liquid and the molecules adsorb on the fiber [171]-[173]. The adsorbed gas is then also desorbed thermally for analysis. A disadvantage of these methods is that the usual procedure for such measurements is sampling the gas at the site of its occurrence, transporting the samples to the laboratory, and performing the analytical measurements there. This approach is very time-consuming and the sample might change during transportation. Also, on-line monitoring of a gas atmosphere is not possible.

Therefore, the combination of pre-concentrator devices and small or mobile gas sensor systems has gained interest. The examples shown later in this chapter focus on new

developments on pre-concentrator devices for continuous measurements and the combination of pre-concentrators with gas sensors.

The combination of gas pre-concentrators with MOS gas sensors in low-cost integrated systems has been explored in this thesis; the principles of gas pre-concentration are described in this section. The process of adsorption and desorption is depicted in Figure 5.

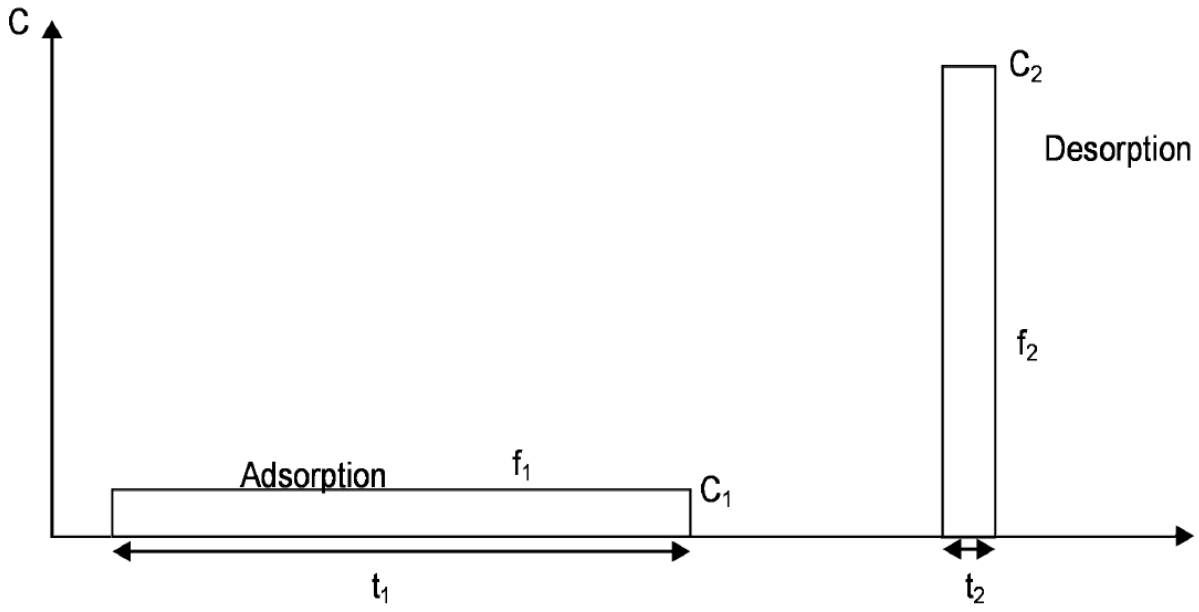

Figure 5: Basic sequence for a pre-concentrator adsorption / desorption cycle, showing the long adsorption period and the short desorption peak; adapted from [174].
Figure reprinted (adapted) with permission from ACS Publications, Copyright 2015 American Chemical Society.

The relevant influences for the pre-concentration factor, i.e. the ratio of the desorbed gas concentration C_2 and the initial gas concentration C_1, have been identified in [174] as the initial gas concentration (C_1), the gas flow rates at adsorption (f_1) and desorption (f_2), and the times of adsorption (t_1) and desorption (t_2). In an ideal system, the relation of these parameters at gas adsorption and desorption can be described by:

$$C_1 \cdot f_1 \cdot t_1 = C_2 \cdot f_2 \cdot t_2$$

The pre-concentration factor k can be defined as:

$$k = \frac{C_2}{C_1} = \frac{f_1 \cdot t_1}{f_2 \cdot t_2}$$

While these formulas point out the basic idea behind gas pre-concentrators, in real devices these relations are not as simple, as experiments and simulations have shown [175].

2.2.1 Physical principles

If gas molecules come into contact with a solid surface, they can adsorb at this surface, i.e. form physical or chemical bonds with the molecules or atoms of the solid and stay attached to them [176]-[178]. The forces for physical adsorption (physisorption) can be van-der-Waals forces and additional electrostatic contributions: polarization, field–dipole and field gradient–quadrupole interactions. These forces are weak compared to chemical bonds (chemisorption), which can also be very selective [178]. For the application of gas pre-concentration, physisorption is the relevant effect [179], as the involved temperatures could not break up chemisorption bindings for desorption.

The number of molecules that can adsorb on a surface is dependent on the number of adsorption sites on the surface of the solid material. To increase the number of available sites, microporous materials are used. This means that the material contains pores with widths not exceeding 2 nm; additionally, mesopores are defined by sizes between 2 nm and 50 nm; pore widths greater than 50 nm are called macropores [176].

A common way to depict and compare the adsorption behavior of materials is by using adsorption isotherms, which show the amount of adsorbed gas versus the equilibrium relative pressure p/p_0 of the gas at a constant temperature, p_0 being the saturation pressure of the gas at the given temperature [176][180].

Recommendations from IUPAC (International Union of Pure and Applied Chemistry) suggest classification of adsorption isotherms in eight groups [176], which are shown in Figure 6.

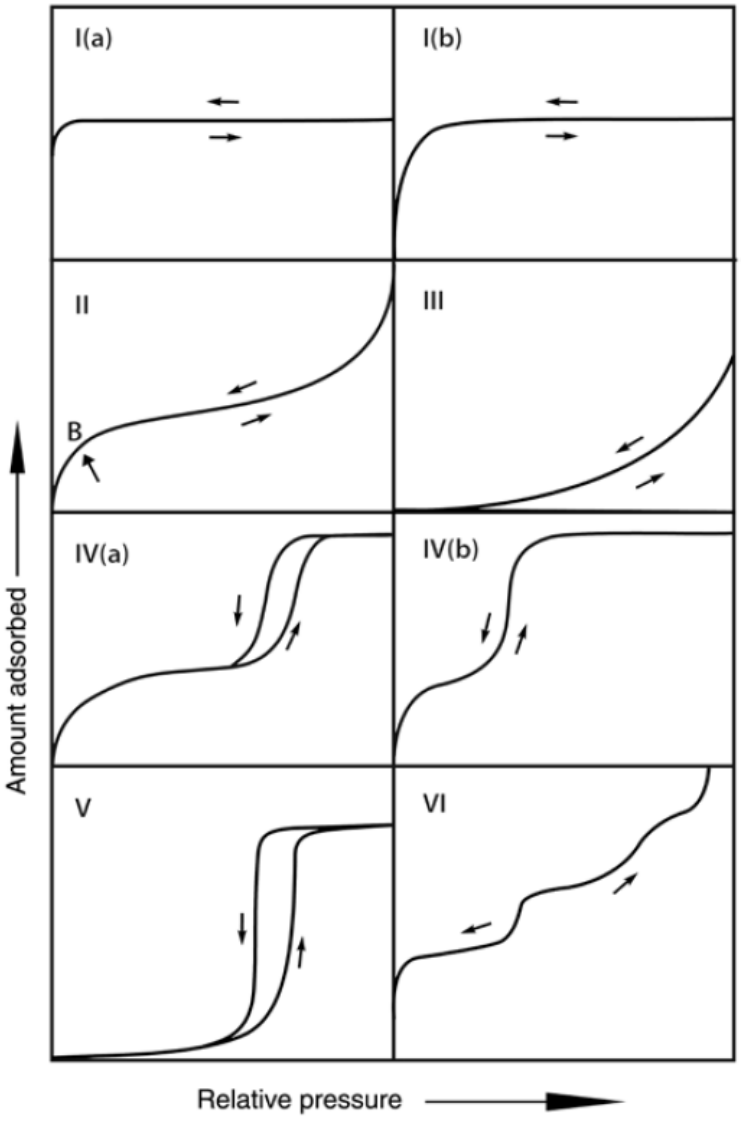

Figure 6: Classification of different isotherms that can occur in physisorption processes, depending on the involved materials and surface characteristics [176].

- Type I isotherms are free of hysteresis and typical for microporous solids which have a relatively small external surface area. After a steep rise in amount of adsorbed gas at very low p/p_0 values, it quickly reaches a limiting value, which is

caused by filling of the available micropore volume. Depending on the exact pore sizes and pore size distributions, Type I(a) isotherms (mainly narrow micropores) or type I(b) isotherms (higher variety in pore size distribution) can occur.

- Type II isotherms do not show hysteresis effects either, and are generated by physisorption of gases on non-porous or macroporous materials, which leads to unrestricted monolayer-multilayer adsorption up to a high value of p/p_0. The point of the curve marked with "B" usually corresponds to the completion of monolayer formation and the beginning of multilayer adsorption.
- Unlike type II, type III isotherms do not show a point "B" to mark the transition from monolayer to multilayer adsorption, as there is no significant formation of monolayers. The forces between gas and solid material are comparably weak and adsorbed molecules cluster around favorable sites. Such behavior also indicates a non-porous or macroporous solid.
- Isotherms of type IV are characteristic for mesoporous materials. For low pressures its shape is similar to type II isotherms, however, after reaching saturation vapor pressure, pore condensation of the adsorbate occurs. Depending on the pore size, hysteresis effects can occur (type IVa) for wide mesopores; for smaller mesopores no hysteresis can be observed (type IVb).
- The behavior of type V isotherms is similar to that of type III for low relative pressures, with relatively weak interactions between the adsorbate and adsorbent. For higher pressures and microporous and mesoporous materials, clustering of adsorbate materials occurs and ultimately pore filling, which leads to hysteresis effects, comparable to type IVa.
- Type VI isotherms are characteristic for reversible layer-by-layer adsorption on uniform non-porous material surfaces. Each step represents a new layer of adsorbate, with the step heights representing the capacities of the layers.

Different models for mathematical description of isotherm have been developed; the most commonly used ones are:

- The Henry model [180]-[182], which is a simplified model based on the assumption that the adsorbed molecules are independent of each other. This results is a linear model for the relative adsorbed gas volume Θ, which is calculated from the partial pressure p of the gas with the Henry constant h [178]:

$$\theta = h \cdot p$$

This approximation is accurate especially for very low adsorbate concentrations.

- The Langmuir model [177][178][183] is suitable for describing monolayer adsorption. Basic assumptions are that only one adsorbate molecule can adsorb at each adsorption site, that all adsorption sites are energetically equal, that there are no interactions between adsorbed molecules and that there is no pore condensation. It can be used at high adsorbate concentrations, where the Henry model becomes inaccurate. It describes isotherms by the following equation [178]:

$$\theta = \frac{V}{V_{mon}} = \frac{K \cdot p}{(1 + K \cdot p)}$$

Θ describes the fraction of the monolayer that is occupied, V represents the volume of the adsorbate, V_{mon} represents the monolayer volume, p is the gas partial pressure and K is a constant. For low pressures, the adsorption is nearly linear, while for higher pressures, the formula describes a saturation effect.

- Another model is the Freundlich model [177][178], which can take into account multi-layer adsorption and inhomogeneous surfaces, i.e. differences in adsorption site energies. It describes isotherms by a power law [178]:

$$\theta = k \cdot p^{\frac{1}{n}}$$

Θ is the relative adsorbed amount and p is the gas partial pressure; k and n are empirical constants for the adsorbent / adsorbate combination.

- A generalization of the Langmuir model for multilayer adsorption is given by the Braunauer-Emmett-Teller model (BET model) [180][184]. Its main assumption is adsorption of a monolayer followed by adsorption of a second layer on top of the first layer and so on. As in the Henry and Langmuir model, for the BET model no interactions between molecules on the same layer are taken into account. The surface coverage θ is calculated with this equation [180]:

$$\theta = \frac{p}{\left(1 - \frac{p}{p^*}\right) \cdot \left(\frac{p^* - p}{C} + p\right)}$$

p is the partial pressure of the gas, p* describes the saturation vapor pressure of the gas, C is a temperature-dependent constant specific for the adsorbate / adsorbent combination

Examples for the basic shape of isotherms for each model are plotted in Figure 7.

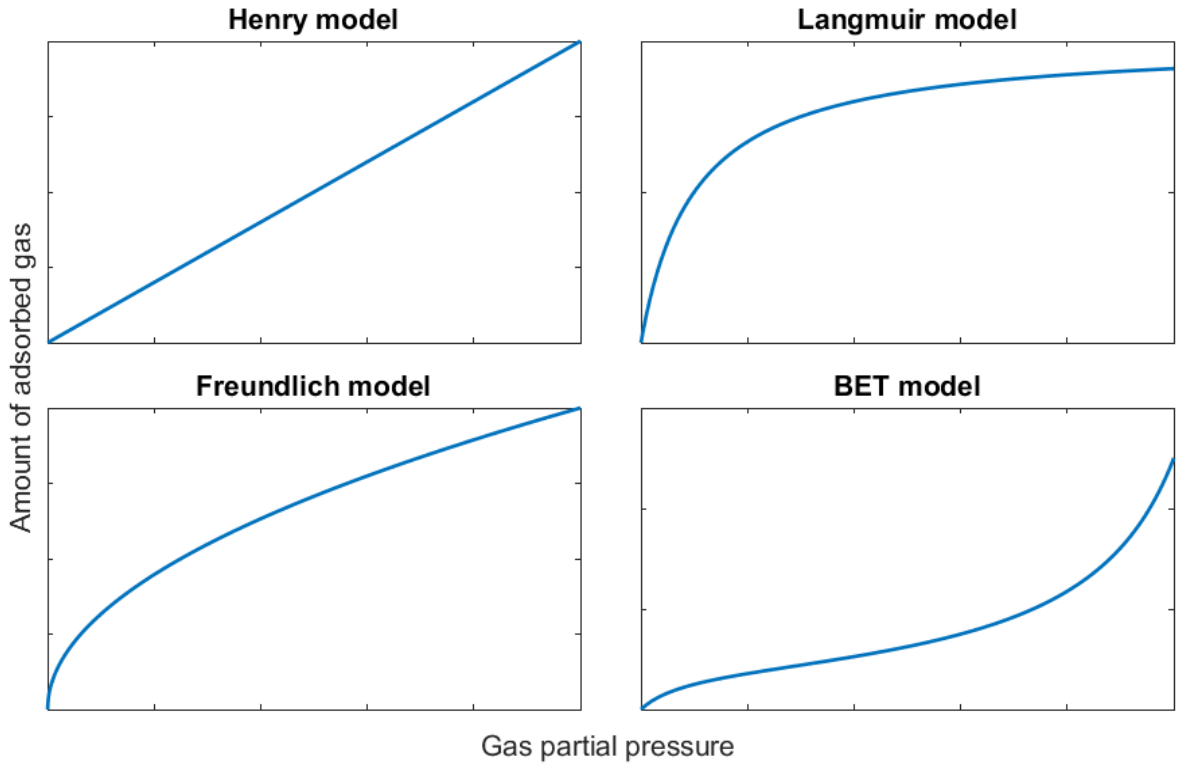

Figure 7: Examplary adsorption isotherms based on the four presented isotherm models.

The models fit – at least for certain segments of the curves – very well with the basic classes of isotherms shown in Figure 6. However, these models can not account for all effects that occur in real isotherms, e.g. hysteresis effects, but can still be used for characterization or comparison of adsorption materials.

As materials for gas pre-concentration, a wide variety of options are available. For example, use of carbon in different configurations [185][186], Tenax® TA [187][188], Carbopack™ [189][190] and zeolites [191] have been reported.

2.2.2 Metal-organic frameworks as pre-concentrator materials

In this thesis, the compounds used for pre-concentrators are metal-organic framework materials (MOFs). These are hybrid materials containing inorganic as well as organic components [179][192][193]. Their structure is determined by a three-dimensional net, which consists of inorganic "nodes", e.g. single metal atoms or metal atom clusters, which are connected by organic molecules, called "linkers". This structure generates pores with sub-nm sizes [194], which results in a large surface area and a large number of adsorption sites, while at the same time the microstructure is very open, allowing easy access of gases into the pores. The surface areas of these materials can be very large, often exceeding 1000 m^2/g [179]; values up to 5900 m^2/g have been reported [195]. Therefore MOFs are in principle very well suited for the application of gas pre-concentration, as a great uptake of target gas in the material should be possible. Figure 8 shows examples for MOF structures.

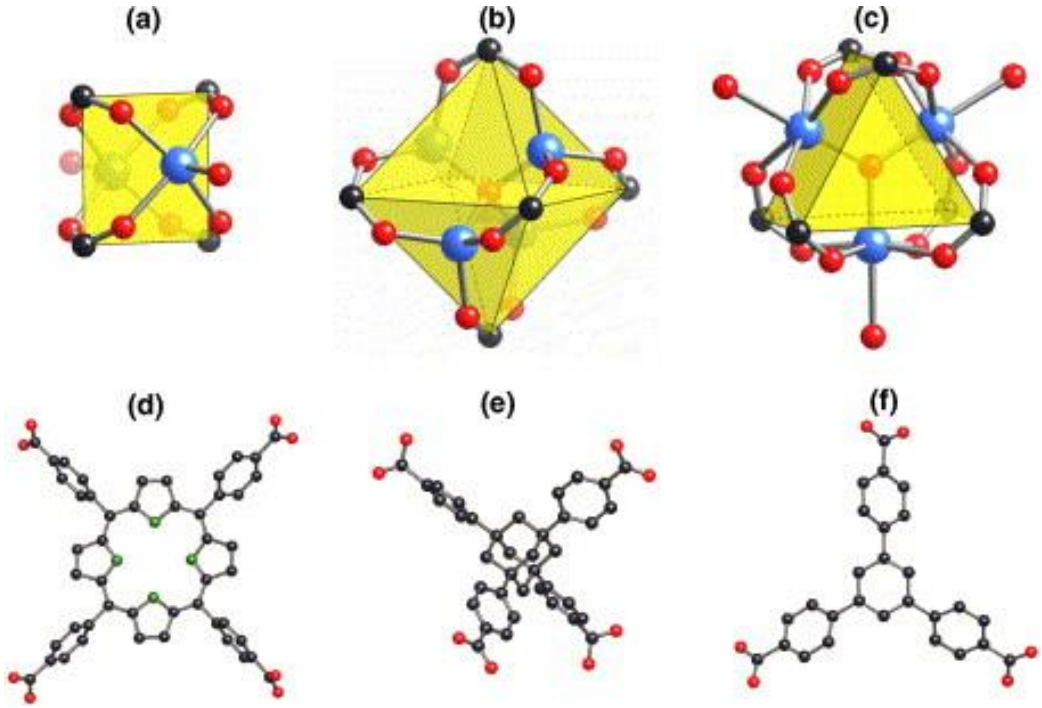

Figure 8: Different common structures occurring in metal-organic frameworks; (a)-(c) so-called "secondary building units", which represent the metal clusters; (d)-(f): examples of organic linker structures which connect the metal nodes; metals are represented by blue spheres, carbon is shown as black spheres, oxygen as red spheres and nitrogen as green spheres [193].
Figure reprinted with permission from Elsevier.

The presented examples show the variety of different pore sizes and shapes that can be achieved by variation of the MOF components, i.e. nodes, linkers, and synthesis method. By controlling these parameters, MOFs can be designed to achieve a certain selectivity regarding gases they can adsorb, e.g. if the pore sizes are designed to be very small, large gas molecules can not enter the MOF and reach adsorption sites; such a MOF would adsorb and pre-concentrate only small gas molecules.

The two types of MOF investigated more closely in this work are HKUST-1 [196], a copper based material (Cu_3BTC_2, BTC: benzene-1,3,5-tricarboxylic acid, also known as trimesinic acid), and MIL-53 [197], a MOF based on Aluminum (AlBDC, BDC: benzene-1,4-dicarboxylic acid, also known as terephthalic acid). Rendered 3D depictions of the structures of the two materials are shown in Figure 9.

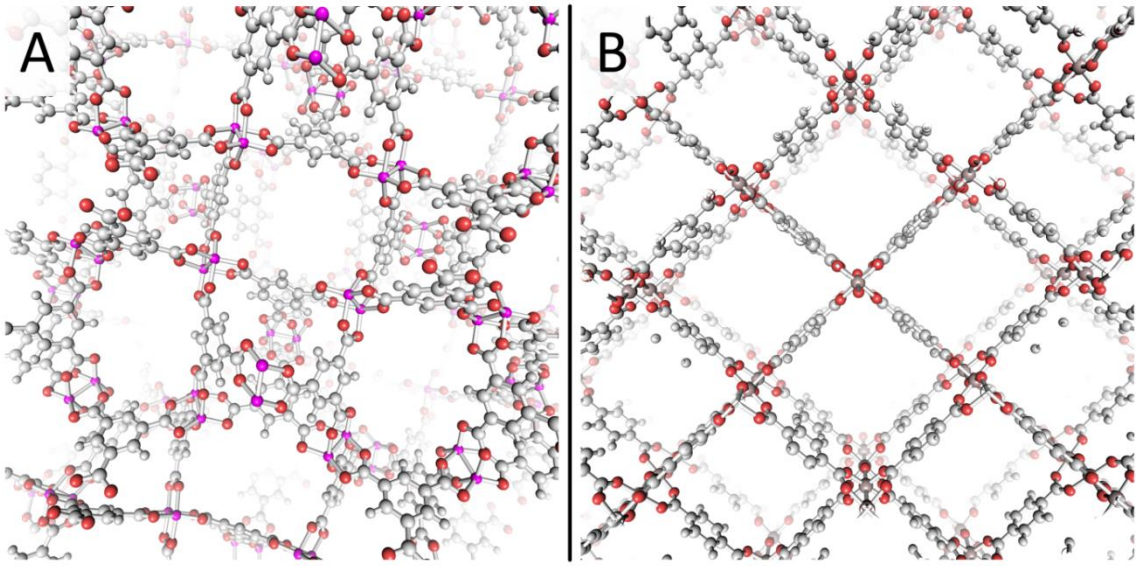

Figure 9: Rendered structures of the two MOFs HKUST-1 (A) and MIL-53 (B); copper atoms are colored pink, aluminum is brown, oxygen is red and carbon is shown in white [198].

A clear difference in the structures of the two MOFs is visible. HKUST-1 (Figure 9 A) forms cavities of different sizes, which enclose single adsorption sites. In MIL-53 (Figure 9 B), the structure is very open in one direction, and straight channels along this axis are formed. For both materials, the pores have diameters of about 1 nm [194].

2.2.3 Examples and applications for gas pre-concentrators

Many research groups have experimented with gas pre-concentration, and a variety of different designs for different applications have been explored.

The usual approach is to design the pre-concentrator as a discrete device with a size of several mm, which is then placed in a larger measurement system. Some examples are given in Figure 10, which shows setups from four publications, all containing pre-concentrator elements as parts of complicated setups.

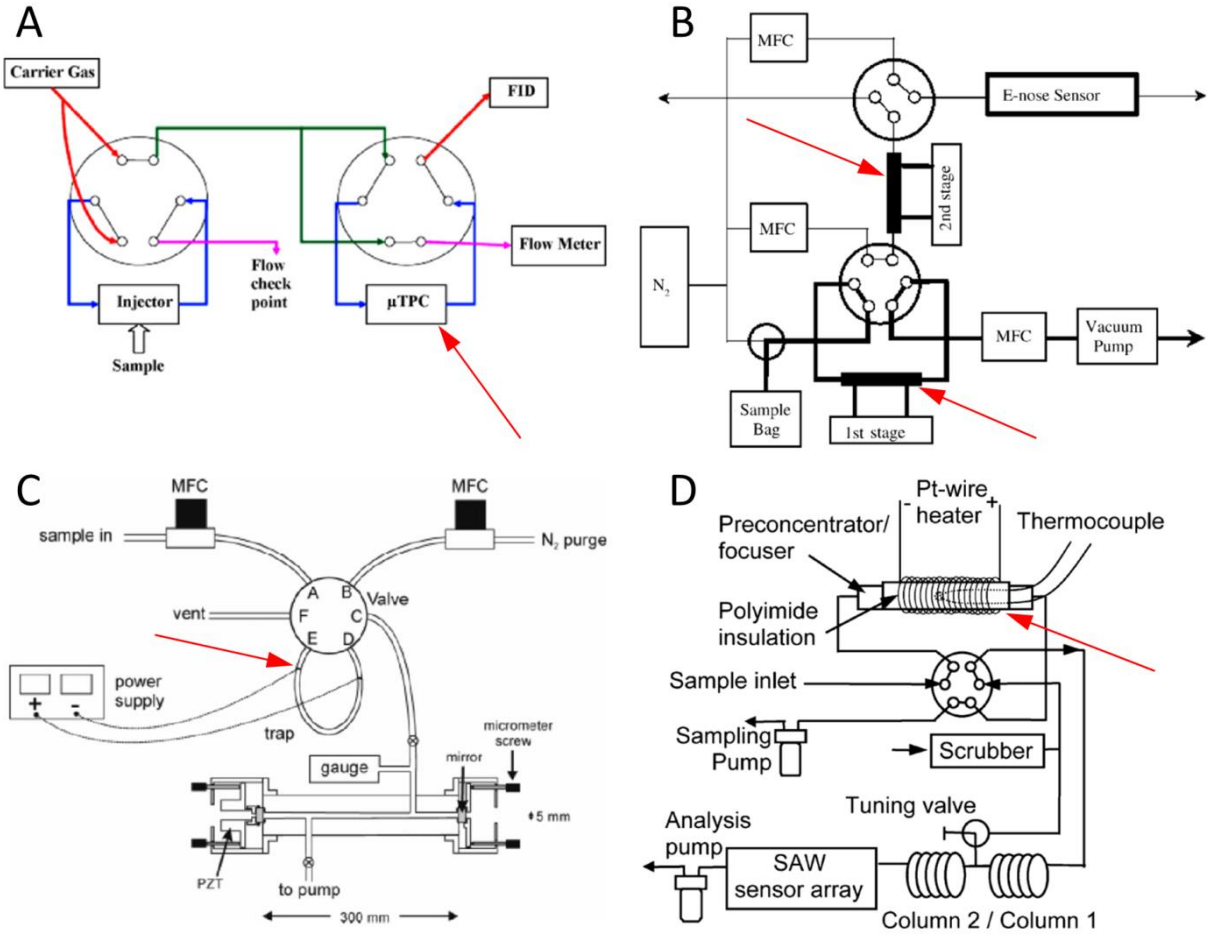

Figure 10: Examples of testing systems for pre-concentrator performance; the pre-concentrator devices are marked by the red arrows; A [188], B [186], figures reprinted with permission from Elsevier; C [191], figure reprinted with permission from ACS Publications, Copyright 2004 American Chemical Society; D [190], figure reprinted with permission from the Royal Society of Chemistry.

In all these examples, the pre-concentrator devices are connected to six-port valves and the valve positions are switched between adsorption and desorption phases. All these fluidic and mechanical components may be necessary for characterization of the pre-concentrators, but would be too large or expensive for many potential applications.

A simpler setup, which consists only of the pre-concentrator device and a modified commercial gas sensor, was presented in [174]. The principle of the setup is shown in Figure 11.

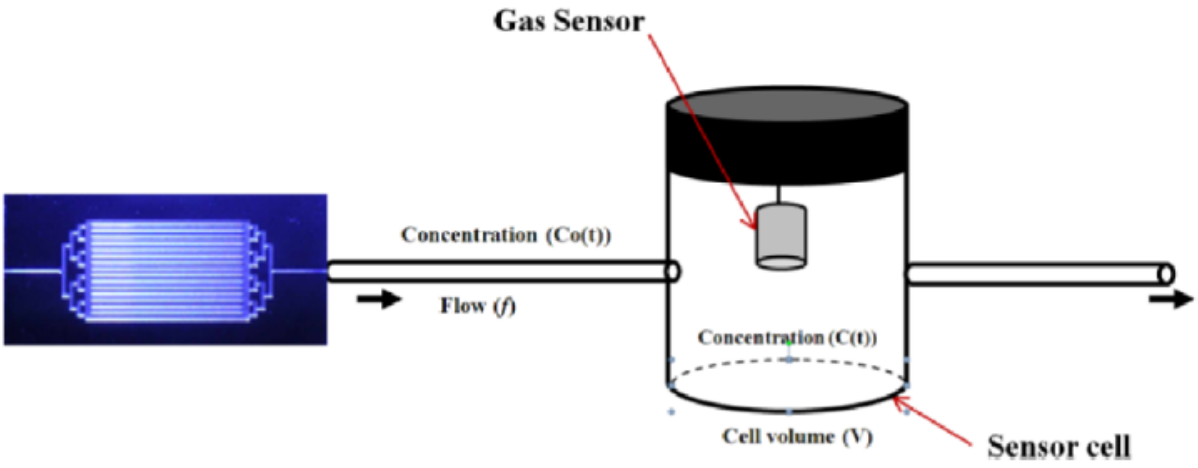

Figure 11: Schematic diagram showing the fluidic interconnection of a pre-concentrator device and a gas sensor; this represents a simple setup compared to other test benches (cf. Figure 10) [174].

Using this setup, the effect of independent adjustments of the gas flow during the adsorption and desorption phase has been investigated. This increased the overall performance of the system; however, the active transfer of the target gas to the pre-concentrator, via pumps or mass flow controllers, which has been a central element in the design of all the presented systems in this section, is expensive and also limits the number of possible fields of use.

As for the mechanical design of the pre-concentrator devices, there are often three-dimensional structures incorporated into the gas flow, which are coated with the

adsorbent material in order to increase the surface area and thus the amount of adsorbent material that is in contact with the gas. Two examples for such 3D structures, produced using MEMS technology and processes, are shown in Figure 12.

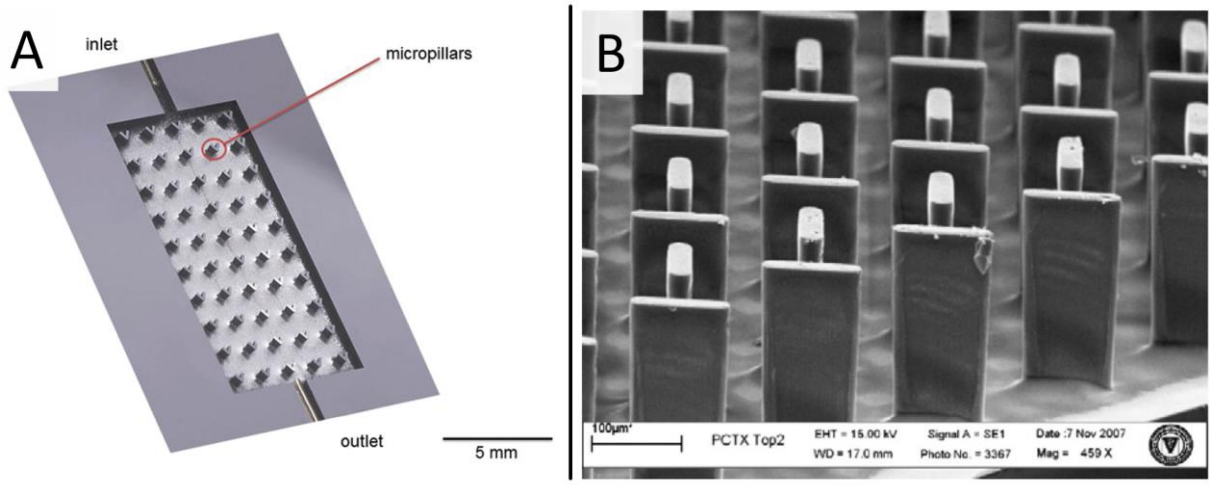

Figure 12: Examples of internal 3D structures of pre-concentrator devices; A: arrow-shaped micro-pillars with a height of 400 µm etched in a silicon substrate and coated with activated carbon [185]; B: rectangular pillars in different angles with a height of 240 µm coated with Tenax® TA [188], figure reprinted with permission from Elsevier.

The two devices show similar basic structures; the gas is directed through a chamber in which pillars are designed into the path of the gas flow. The pillars have sizes of several hundred nm, and increase the amount and surface area of the adsorbent material by a large factor compared to a plain chamber floor.

Pre-concentrators have been investigated for many different applications and in many different setups. Often they have been used in combination with analytical measurements, e.g. GC-FID [186]-[188] or GC-MS [189]. Such setups are suited especially for characterization of the pre-concentrator, as the analytical measurements allow a high degree of sensitivity and selectivity. A number of groups are using pre-concentrators in combination with SAW sensors (surface acoustic wave) [190][199], which are usually set up as arrays of devices with different sensing materials. Pre-concentrators have also been coupled with MOS gas sensors, both commercial sensors

[174] and proprietary ones [185]. Other sensor principles used for testing pre-concentrators are optical cavity ring-down spectroscopy [191] and electrochemical sensors [205].

Many of the published articles focus on air quality monitoring as a possible application for gas pre-concentration. The setups are tested with benzene [174][189] or gas mixtures containing several gases relevant for IAQ [190][191][199], cf. section 1.1.1. Other backgrounds used for development and characterization of pre-concentrator devices include breath analysis [186], safety applications such as detection of explosives [205], detection of specific single gases like ammonia [185] or general characterization of the device performance with a variety of gases without validation for a specific application [187][188].

In the presented examples, the pre-concentrator performance was tested with target gas concentrations from the sub-ppm range, e.g. 400 ppb of BTEX components (benzene, toluene, ethylbenzene, xylenes) [199] or 250 ppb of benzene [174], down to the ppb range, e.g. 17 ppb of heptane [186] or 6 ppb of ethane [191]. In all examples, significant pre-concentration effects were achieved; the highest reported pre-concentration factor was 1000 [188], using the device shown in Figure 12 B in the setup shown in Figure 10 A; the applied test gas was nonane and the adsorbent material Tenax® TA.

These results show the potential of gas pre-concentrators for trace gas analysis, but the design and setup of such devices must be significantly scaled down and simplified to facilitate mass production, which is a key aspect for many of the intended applications.

2.3 Signal processing

The temperature dynamic operation of MOS gas sensors requires and allows for more complex signal processing than sensors operated at constant temperatures. The techniques used in this thesis are presented briefly in this chapter.

2.3.1 Signal pre-processing

Raw gas sensor signals can be affected by noise and drift effects, which reduce the performance of signal processing algorithms. Therefore, pre-processing can be applied to the data in order to minimize some of these influences.

The most common methods for first stage signal treatment in gas sensors are smoothing and normalization of the signals [200][201]. Smoothing can reduce the noise of the sensor signals; however, it must be applied carefully, as the shape of the signal holds the information in TCO sensor signals, and smoothing can also influence this shape and thus the information contained in the signal. A smoothing algorithm must be found for a specific application which removes the noise while maintaining the underlying information. For example, critical segments in TCO data are fast temperature changes of micro hotplate gas sensors, which cause quick changes in the signal that contain useful information, e.g. a peak height, but might be flattened significantly by a smoothing algorithm. Commonly used smoothing methods are moving average [202] and the Savitzky-Golay convolution filter [203]. Depending on the quality of the raw signals and the extent of the sensor response to the gases, using no filter might be the best option, as all information of the signal is preserved, but this choice is dependent on the individual signal situation.

Normalization of the signals is a method that can counteract other influences on the sensor, such as long-term drift effects in the baseline or the sensitivity [204]. For TCO signals, normalization is usually performed per temperature cycle. Proven methods for normalization are division of each signal value by the mean value of the cycle signal or mapping the signal of each cycle to a specific interval, e.g. [0..1] or [-1..1].

Normalization by division by the cycle mean value is performed with the following formula for a signal vector sig_{TCO}, which contains n signal values of a TCO cycle:

$$sig_{norm} = \frac{sig_{TCO}}{mean(sig_{TCO})} = \frac{sig_{TCO}}{\frac{1}{n} \cdot \sum_{i=1}^{n} sig_{TCO}^{i}}$$

i represents the index of the vector.

Normalization with this method is used especially for compensation of baseline drift effects.

Mapping of the signal to the interval [0..1] is performed by the following formula, for other intervals it can be adapted:

$$sig_{norm}^{i} = \frac{sig_{TCO}^{i} - \min(sig_{TCO})}{\max(sig_{TCO}) - \min(sig_{TCO})}$$

Such a normalization can be useful if the information of the signal is contained mostly in the shape instead of the absolute values. On the other hand, if the absolute levels of the signal hold significant information, such a normalization step can result in loss of quality of the following signal processing. As with signal smoothing, the usefulness of a specific method must be tested and evaluated for each application.

2.3.2 Quasi-static sensor signals

The most basic approach to analyzing cyclic sensor signals next to comparing single cycles is the generation of quasi-static sensor signals. To generate such a signal, the sensor signal value of a chosen point in time during the temperature cycle is extracted for each cycle. This generates a simplified sensor signal which represents the signal for the chosen state of the sensor inside the cycle. An example is given in Figure 13.

Figure 13 A shows a raw sensor signal during a ramp up / ramp down temperature cycle. The chosen point for a quasi-static signal was chosen at 20 s, indicated by the dashed line. The signal value at this point of the cycle was extracted for all cycles of a measurement with several concentrations of three gases and a section of approx. 1100 cycles is shown in Figure 13 B. For the chosen point, the sensor shows a clear response to the naphthalene test gas and very low responses to the other two gases.

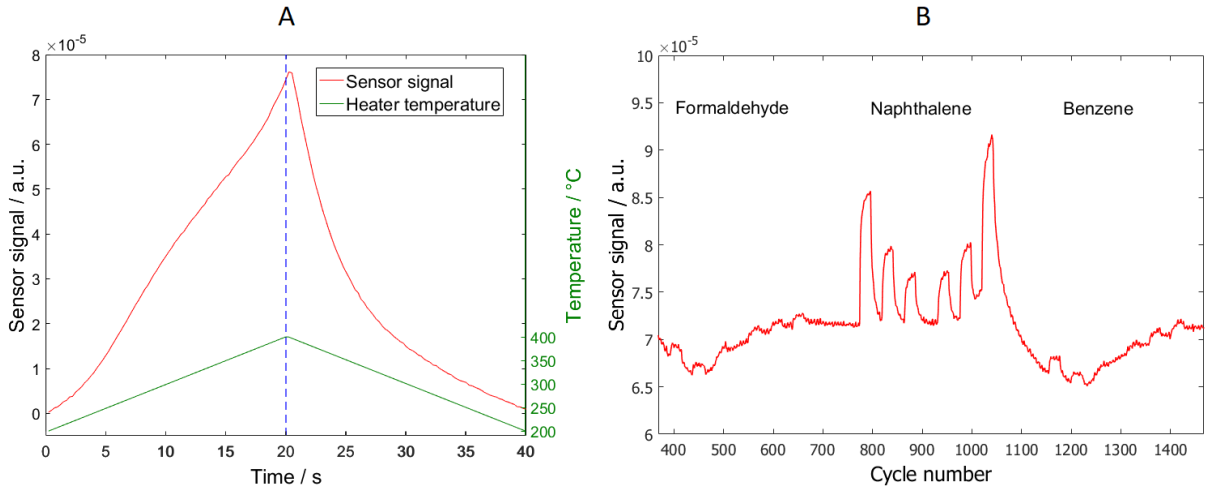

Figure 13: A: Visualization of a gas sensor temperature cycle (linear ramps from 200°C to 400 °C and back down to 200 °C, green) and corresponding gas sensor signal (red); the dotted line shows the point of the cycle selected for a quasi-static signal, which is shown in B for a measurement of three gases in three concentrations each [206].

This representation of the sensor signal allows for a quick and transparent evaluation of the sensor response to the test gases, without employing more advanced and more complicated signal processing. However, the effort for manually evaluating quasi-static sensor signals of larger numbers of points of the temperature cycle take a lot of effort and this approach might not be useable for very small signal changes, which is why advanced signal processing is required for many applications.

2.3.3 Feature extraction

When MOS gas sensors are operated in TCO, the signals cannot be described by a single value. Generating quasi-static signals, as described in the previous section, extracts only a very limited amount of the information that is contained in a temperature cycle signal. To increase the extracted information, a set of values is computed from the cyclic signals, called features. There are many options for doing this; commonly, this is used as a dimension reduction of the complex raw TCO sensor signals. The process and techniques of the feature extractions used in this thesis have

been explained and discussed in detail in previous theses [207]-[210] and publications [211][212], therefore a brief introduction is given in this chapter.

In the presented signal evaluations, features have been extracted from sensor signals which represent these signals while reducing the number of data points that are used in the subsequent signal processing methods. For example, raw signals consisting of 1800 data points have been reduced to 32 features, which describe the shape of the sensor signal curve.

To generate such features, the TCO cycle is first divided into several segments in which the features are calculated. An example is shown in Figure 14.

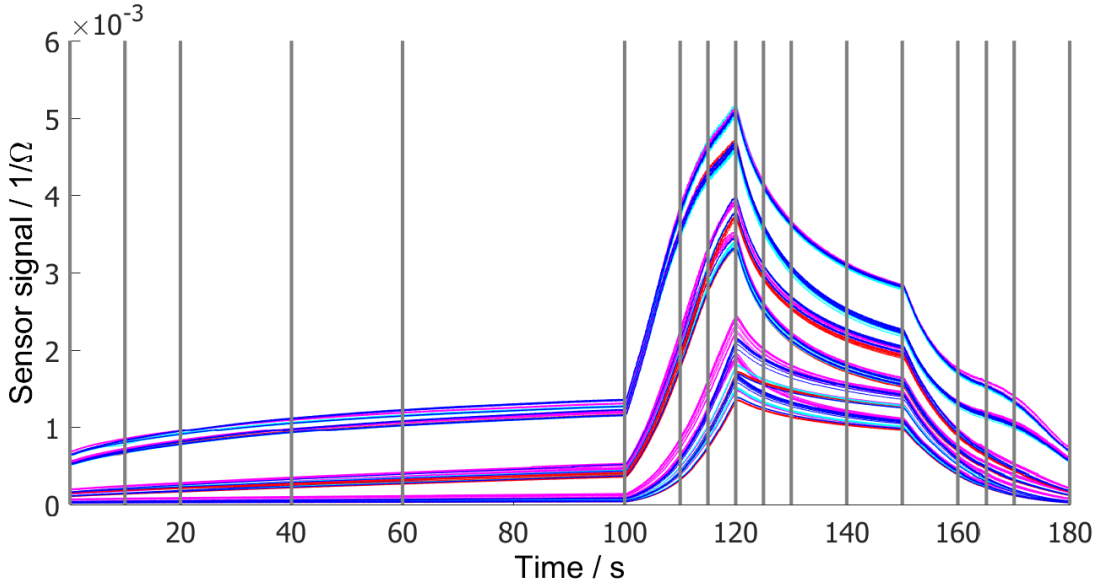

Figure 14: Example of segmentation of a TCO signal cycle for feature extraction in 16 segments; several TCO signals are plotted to see where changes occur in the signal and to enable a suitable choice of segment intervals.

The segments are chosen to represent the different states, i.e. temperatures or temperature ramps, of the sensor, and each state is further divided into several segments. To generate features, the same calculations are performed with the sensor signal in each segment. Many calculations are possible, the most commonly used ones are calculating the mean values and the slopes of the signal segments, but further

options such as calculation of curvatures, fit function parameters (e.g. for polynomial or exponential fits), minimum or maximum values, or Fourier transformations are possible [156][213][214].

In the example (Figure 14), it is obvious that many of the depicted signal curves differ significantly in mean values and slopes for the chosen segments and can be clearly separated using these features. The positions of the segments are chosen by the dynamic of the sensor signal during different states, e.g. the signal changes quickly after a fast temperature change (cf. chapter 2.1.2), therefore the segments are chosen to be shorter in such phases compared to long phases of static temperatures.

This approach creates a set of values, called “feature vector” in this thesis, for each sensor cycle. This vector is then used for further signal processing, i.e. multivariate analysis techniques such as linear discriminant analysis (LDA) or partial least squares regression (PLSR), which were utilized for some of the presented gas measurements.

2.3.4 Linear discriminant analysis and classification

Linear discriminant analysis (LDA) is a method for calculating a transformation rule which separates data sets according to their assigned target classes [215]. The target class for each data set must be known; therefore it is called a supervised learning algorithm. It is a generalization of Fisher’s linear discriminant, which was published in 1936 [216], and can handle data sets representing two or more classes [217]. LDA, which is often used for pattern recognition applications (e.g. face recognition [218]-[220]), calculates a function which represents a linear combination of the input data set *f* (in this case the extracted gas sensor feature vector) and a coefficient set *c*:

$$\begin{pmatrix} DF_1 \\ \vdots \\ DF_{n-1} \end{pmatrix} = \begin{pmatrix} c_{1,0} \\ \vdots \\ c_{n-1,0} \end{pmatrix} + \begin{pmatrix} c_{1,1} & \cdots & c_{1,m} \\ \vdots & \ddots & \vdots \\ c_{n-1,1} & \cdots & c_{n-1,m} \end{pmatrix} \cdot \begin{pmatrix} f_1 \\ \vdots \\ f_m \end{pmatrix}$$

$$= \begin{pmatrix} c_{1,0} + c_{1,1} \cdot f_1 + c_{1,2} \cdot f_2 + \cdots + c_{1,m} \cdot f_m \\ \vdots \\ c_{n-1,0} + c_{1n-1,1} \cdot f_1 + c_{n-1,2} \cdot f_2 + \cdots + c_{n-1,m} \cdot f_m \end{pmatrix}$$

The resulting vector *DF* contains the so-called discriminant functions of the LDA.

The optimization the LDA algorithm performs is finding a set of coefficients c which maximizes the distance between the groups/classes and minimizes scatter within the groups:

$$\Gamma = \frac{scatter\ between\ groups}{scatter\ within\ groups} \stackrel{!}{=} max$$

When the LDA projection is applied to a data (feature) vector, it is transformed into a data point in the new coordinate system, but not yet classified into one of the groups that were used for determination of the LDA parameters. Therefore, a classifier is necessary, which assigns the new data point to one of the existing groups, e.g. a type of gas. In the examples in this thesis, the k-nearest neighbor (knn) classifier is used. It is one of the simplest algorithms for this task, as it calculates the distances of the new data point to the k nearest known data points and then assigns it to the class to which most of these points belong to. Several types of distances can be calculated, here the Euclidian distance was the chosen method:

$$d_{Euclidian} = \sqrt{\sum_{i=1}^{n} (q_i - p_i)^2}$$

The number of observed neighbors, *k*, is usually an odd number in the range from 3 to 11; in the presented data evaluations it was set to 5.

Figure 15 shows an example of an LDA projection of gas sensor signals with a 2-dimensional output, i.e. mapping of the input feature data sets of two discriminant functions.

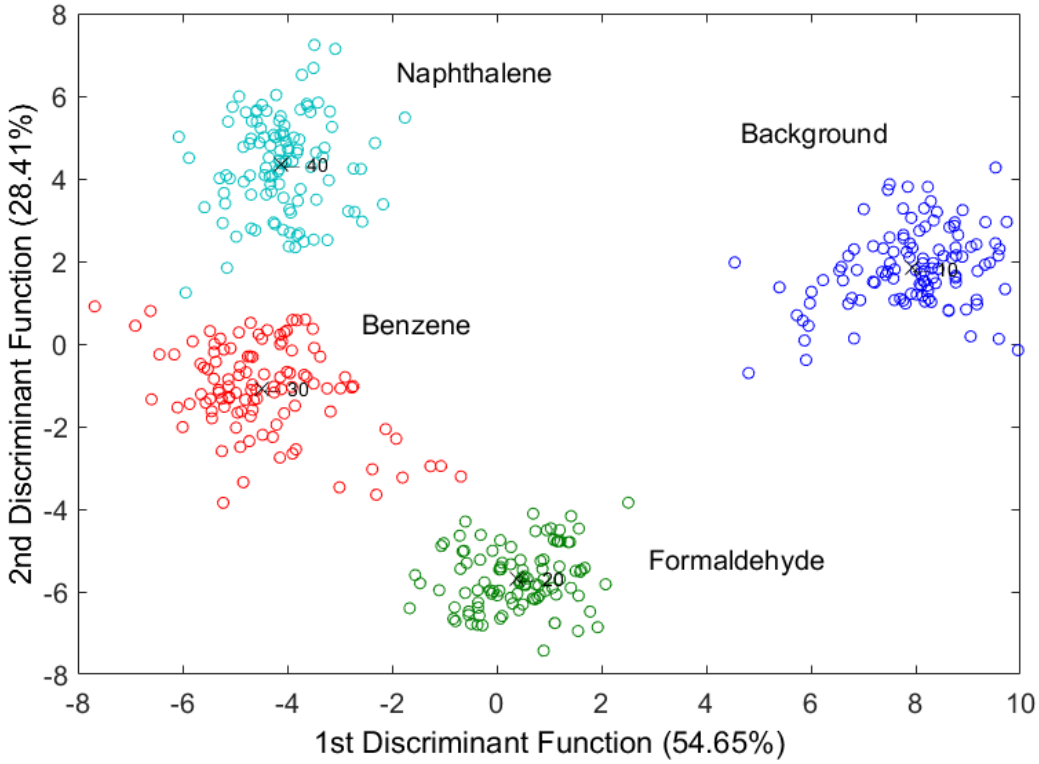

Figure 15: Plot of a 2D LDA data processing for identification of four different classes [221].

The LDA algorithm calculates the output functions in a way that separates the 4 input classes, each representing a different gas condition, in the 2 dimensions. The separation of the groups in this example is not optimal; there is some slight overlap between the groups of naphthalene/benzene and benzene/formaldehyde, respectively. The scatter within the groups is not ideal as well, as the groups are not very compact and there are some outliers.

2.3.5 Partial least squares regression

A disadvantage of using LDA (+ classification) is that it treats every target class independently and does not take into account relations of the target classes, e.g. numerical relations if they represent different gas concentrations. For example, if the gas concentrations 1 ppm, 2 ppm, and 10 ppm are the target classes, the LDA algorithm tries to maximize the distances of all classes, even though the distance

between 1 ppm and 2 ppm should be much smaller than the distance between 2 ppm and 10 ppm.

Regression algorithms, in this case more specifically partial least squares regression (PLSR) [222][223], are used in data processing if the input data is mapped to a continuous numerical target value range, e.g. a gas concentration. Therefore, quantitative information can be extracted from the input, in contrast to LDA with knn, which performs a qualitative classification. The PLSR algorithm calculates a linear model which maps the input variables (e.g. gas sensor signal features) to a response variable (e.g. gas concentration). PLSR has been shown to yield good results even if the input variables are collinear, which is a problem for other methods.

An example for a result of a PLSR signal processing of features extracted from gas sensor signals is given in Figure 16.

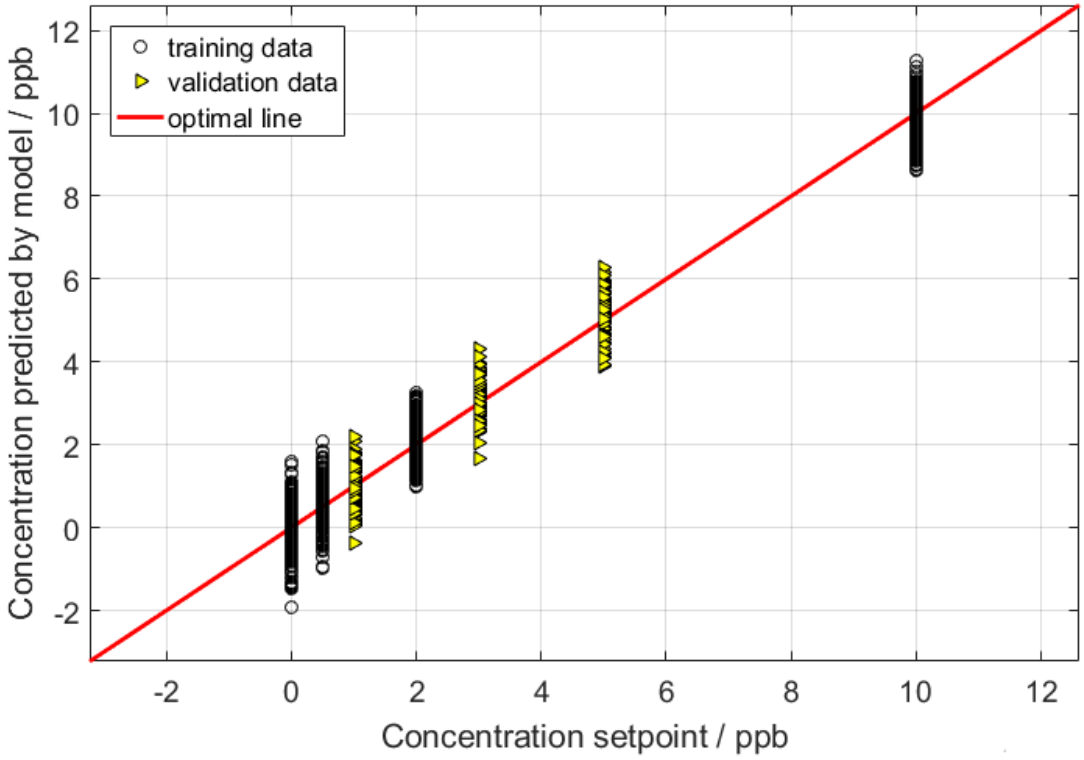

Figure 16: PLSR gas quantification results; the PLSR model was trained with the data marked by hollow circles; the data sets of the data points marked by yellow triangles were projected into the model; further processing of data presented in [224].

In the plot, the set gas concentration is plotted on the x-axis, and the corresponding PLSR output value, i.e. the predicted concentration for each input data set, is plotted on the y-axis. In this example, the PLSR model was calculated with the sensor data (features) from the gas concentrations 0, 0.5, 2 and 10 ppb, and evaluated for the same input data sets ("training data", circles). Then, the feature sets from the sensor signals recorded at 1, 3, and 5 ppb were also mapped to the output concentration range by the model ("validation data", yellow triangles). With ideal data, all data points would be placed on the optimal line (red). In the example, there is an error in the prediction of the gas concentration of less than ± 2 ppb, which is the case for both the training data as well as for the interpolated gas concentrations.

2.3.6 Validation of signal processing methods

The obtained output of such a signal processing run does not yet give an assertion about the quality of the result. Therefore, a validation step is necessary, which evaluates the output, e.g. by checking how many input data sets are classified correctly and between which groups misclassifications occur. This is also crucial for comparing different processing parameters, e.g. different classifiers.

Another important aspect is checking the model for applicability to new data that was not used for training. This cross-validation can be done in several ways, the most effective and most challenging for the model is to evaluate a completely new data set, e.g. repetition of a measurement several weeks after the training measurement was performed. Another method is excluding certain groups of data sets from the training (e.g. gas concentrations, cf. Figure 16) and checking if interpolation or extrapolation are possible with the model. A number of other methods are used for dividing the data set into training data and validation data; many are described in [225]. These methods, such as bootstrap, k-fold cross-validation or leave-one-out cross-validation, represent techniques for fixed or random generation of data splits from a given data set for calculating the signal processing model and data to validate the model. The most simple of these cross-validation methods, which was also used for all LDA validations

in this thesis, is leave-one-out cross-validation (LOOCV). It is performed as many times as there are input data vectors, in this case TCO feature vectors. In each run, one data vector is left out of the training, then projected into the calculated model and classified by the classifier algorithm. After a full run, the result shows how many data vectors are classified correctly or incorrectly, and which class they are assigned to. This allows for a detailed analysis of the performance of the model, and an objective evaluation of different methods and classifiers.

3 Characterization and calibration of gas sensor systems at ppb level – a versatile test gas generation system

Martin Leidinger, Caroline Schultealbert, Julian Neu, Andreas Schütze and Tilman Sauerwald

Saarland University, Lab for Measurement Technology, Saarbrücken, Germany

Originally published in *Measurement Science and Technology, 29 (1), 015901, 2018*

doi: 10.1088/1361-6501/aa91da

Synopsis

As already mentioned in the introduction (section 1.3), adequate generation of test gases is an essential prerequisite for the development of gas sensor systems for the detection of low target gas concentrations. Therefore, a gas mixing system has been developed for this task, based on a previous design [129]. The chosen method for gas generation was dynamic gas dilution; no other methods were incorporated in the system, as the predecessor system offers sufficient channels for additional use of permeation devices. The combination of these two methods can cover a very wide range of target gases and concentrations. The application in mind for the design was characterization of gas sensors and gas sensor systems for indoor air quality monitoring; therefore the facility was equipped to handle permanent gases and VOCs,

with the exclusion of semi volatile organic components, which are not available in gas cylinders in suitable concentrations.

In the design of such a system, several aspects are important and have to be addressed. Most obvious is the performance of the system in terms of accuracy of the generated gas concentrations. The applied technology in this case, mass flow controllers (MFCs), offers active gas flow control and high accuracy of these flows over a wide range. The MFCs used in the presented system (MKS MF1) have an accuracy of ± (0.5 % of reading + 0.2 % of FS (full scale)) and a control range of 2 % to 100 % of FS [226]. The relative accuracy of the set flow therefore decreases significantly when the setpoint is close to the lower limit of the controller, as some examples in Table 2 show.

Table 2: Relative accuracy values for different setpoints of the chosen mass flow controllers.

Setpoint	**Error**
100 % FS	0.7 % of setpoint
50 % FS	0.9 % of setpoint
10 % FS	2.5 % of setpoint
5 % FS	4.5 % of setpoint
2 % FS	10.5 % of setpoint

Therefore, the MFC setpoint calculations of the gas mixing system software have been limited to 5 % FS as the lowest applicable value, although the MFC itself could set even lower flow rates. This limitation assures a maximum error in gas flow of approx. 5 % of the setpoint. Other relevant aspects are response times of the active components (MFCs, pressure regulators, valves) or compatibility of the used materials (tubing, seals, etc.) with the gases regarding chemical stability and adsorption effects, respectively. These aspects are discussed and tested in the publication.

What is also important for such a system is the control software. The program used for the presented facility is an updated version of the one presented in [129], and controls all fluidic components. Additionally, the sensor operation (TCO parameters) and sensor read-out (TCO gas sensors, temperature/humidity sensors and any analog signal sensors) are realized in the same program. The advantage of such a combined software is the inherent synchronization of sensor signals and gas mixing system status, which facilitates interpretation of sensor signals and debugging of the system. The software also allows for active synchronization of gas sensor operation and gas mixing, via coupling of gas state transitions to starting times of TCO cycles.

The publication addresses the design of the fluidic setup of the system regarding possibilities of gas generation and mixing as well as issues of material compatibility for ppb level VOCs and unwanted tailing effects due to dead volumes.

IOP Publishing Measurement Science and Technology
Meas. Sci. Technol. **29** (2018) 015901 (10pp) https://doi.org/10.1088/1361-6501/aa91da

Characterization and calibration of gas sensor systems at ppb level—a versatile test gas generation system

Martin Leidinger, Caroline Schultealbert, Julian Neu, Andreas Schütze and Tilman Sauerwald

Department of Systems Engineering, Lab for Measurement Technology, Saarland University, Saarbrücken, Germany

E-mail: t.sauerwald@lmt.uni-saarland.de

Received 2 July 2017
Accepted for publication 9 October 2017
Published 7 December 2017

Abstract

This article presents a test gas generation system designed to generate ppb level gas concentrations from gas cylinders. The focus is on permanent gases and volatile organic compounds (VOCs) for applications like indoor and outdoor air quality monitoring or breath analysis. In the design and the setup of the system, several issues regarding handling of trace gas concentrations have been considered, addressed and tested. This concerns not only the active fluidic components (flow controllers, valves), which have been chosen specifically for the task, but also the design of the fluidic tubing regarding dead volumes and delay times, which have been simulated for the chosen setup. Different tubing materials have been tested for their adsorption/desorption characteristics regarding naphthalene, a highly relevant gas for indoor air quality monitoring, which has generated high gas exchange times in a previous gas mixing system due to long time adsorption/desorption effects. Residual gas contaminations of the system and the selected carrier air supply have been detected and quantified using both an analytical method (GC-MS analysis according to ISO 16000-6) and a metal oxide semiconductor gas sensor, which detected a maximum contamination equivalent to 28 ppb of carbon monoxide. A measurement strategy for suppressing even this contamination has been devised, which allows the system to be used for gas sensor and gas sensor system characterization and calibration in the low ppb concentration range.

Keywords: gas mixing, trace gases, test gas generation, metal oxide semiconductor gas sensor, volatile organic compounds, FEM simulation

(Some figures may appear in colour only in the online journal)

Introduction and motivation

The detection of trace gases gained high importance within the last decade [1–3]. One major driving force is the rising concern for cleaner air indoors [4–6] in private homes, in public buildings and workplaces as well as outdoors in urban areas and in locations with specific pollution sources like industrial agriculture [7] and waste treatment [8, 9]. In most of these applications, gases at low concentrations in the ppb range need to be measured with high accuracy [10–12]. Most important for the health aspect is a good estimation of the exposure of humans to pollution [13], which drives the development of distributed sensor systems or sensor networks, aiming at supplementing the existing grid of environmental monitoring stations with low-cost sensor nodes offering high spatial and temporal resolution [14–17]. First studies for outdoor air show that the burden of pollution can be very local; highly polluted areas in cities can be located closely to almost clean areas [18]. In indoor environments a strong variation from household to household has already been reported for many years [19, 20].

Meas. Sci. Technol. **29** (2018) 015901 M Leidinger *et al*

Besides the demand for environmental monitoring, new fields of applications are emerging quickly. Numerous medical studies show that the measurement of (gaseous) metabolites, e.g. from exhaled breath [21], but also as from other sources [22], can be used as non-invasive method for diagnostics or therapy monitoring. For these studies and for later applications the detection of a complex mixture of gases covering a wide concentration range in an even more complex gas matrix is required [23].

All presented applications require trace gas generation methods for the development, characterization and calibration of gas sensors and gas sensor systems. Analytical chemistry and its metrology have established various methods for the generation of gas standards; however, new challenges such as high flexibility, high throughput and low costs per item are specific for sensor systems and have to be addressed. Moreover, sensor systems often use detector principles that are different from the methods of chemical analytics. Some of these methods require a higher concern for the gas matrix that may contain hidden interfering gases. For example, metal oxide semiconductor (MOS) gas sensors for detection of VOCs (volatile organic compounds) also respond to hydrogen whereas other methods such as flame ionization or photo ionization detectors do not. Test gas as well as ambient air may contain hydrogen at different concentrations. These aspects need to be considered in novel concepts for test equipment [3]. In the last years only few systems dedicated to the test of gas sensor systems at ppb level have been reported. Gerboles and Spinelle [24] demonstrate an approach using circulating air in a toroidal glass duct. Target gas concentrations can be closed-loop controlled by reference measurement methods. This approach is capable of testing larger devices such as complete sensor systems and it therefore also addresses the influence of environmental parameters like, e.g. air flow. The closed loop approach allows using larger gas flow rates and continuous reference measurements. However, a drawback of this approach is the requirement for real time reference analytics leading to high costs and considerable efforts for adaptation of the test gas profile. A different approach is the use of continuous flow mixing systems [25] with dynamic dilution that use mixtures of various mass flows. These systems can be highly adaptable to various gas profiles; however, the gas flow rate is often limited. For ppb concentration levels this approach has two additional challenges: The generation of very small continuous mass flows for very low concentrations and the minimization of side effects, e.g. sorption on the tubing or dead volumes. In an earlier work [26] some of us presented a successful adaptation of two methods for the generation of continuous flow of ppb level target gases by multi-step dynamic dilution for high volatile compounds and by permeation for low volatile compounds. Using the permeation method Pogany *et al* [27] presented a system for generating ammonia trace gases including a study on the sorption effect on various tubing materials. Haerri *et al* [28] compared the generation of nitrogen oxides and sulfur dioxide traces by dynamic dilution with the permeation method.

In this work we present the improvement of a dynamic dilution gas mixing system for the characterization of sensor systems with a focus mostly on MOS gas sensor based systems. For the semiconductor gas sensors a novel quantification approach [29, 30] can be used that is able to estimate an upper limit value for sensor active gas background in the facility in order to compensate the effect of gas background variations of the system.

Upgrade of previous gas mixing system concept

The design of the new gas mixing system is following the line of our earlier concept [26]. However, the new system focuses on the multistep dynamic dilution and is therefore suitable only for volatile gases with high vapor pressures which are available in gas cylinders at elevated concentrations; using permeation ovens or other methods for low volatile compounds has not been implemented. The motivation for using elevated test gas concentrations in the gas cylinders is the residual contaminations of these cylinders, which are still up to 10 ppm at a test gas purity of 5.0. Therefore, test gas concentrations of at least 100 ppm should be used in order to have a ratio of less than 10% of contaminations compared to the test gas concentration.

In addition to having the ability to generate low concentration test gases, another design goal was to minimize delay times when switching gases or concentrations and to minimize dead volumes in the system, as these can generate tailing effects which hinder the generation of clean gas pulses. This is relevant for the simulation of applications in which gas pulses or quick concentration changes must be monitored, e.g. breath analysis or gas chromatography.

All gas mixing is realized by mass flow controllers (MFCs). The setup can be divided into several sections, see figure 1.

As carrier gas, zero air from two cascaded zero air generators (Nitrox CO2RP280, Parker Hannifin, USA, and Ultra Zero Air generator N-GT15000, Schmidlin Labor + Service SA, Switzerland) is primarily used. The first device reduces the VOC content using an active charcoal filter and also removes water and CO_2 by a molecular sieve with pressure swing. The second stage oxidizes residual hydrocarbons (C1–C3), carbon monoxide and hydrogen using a noble metal catalyst. Nitrogen is installed as a second carrier gas; this allows for generation of reduced oxygen atmospheres down to almost 0% oxygen, i.e. for simulation of exhaust gas mixtures or exhaled breath. Part of the carrier gas stream is humidified to nearly 100% RH by passing the gas flow through a washing bottle which is temperature controlled to a temperature slightly below room temperature to avoid condensation of water in the tubing. To minimize contaminations of the gas by the water, HPLC grade water is used.

All carrier gas fractions are controlled by 500 ml min^{-1} MFCs, allowing the full range of oxygen and RH for total flow rates up to 500 ml min^{-1}, which is normally used, and reduced ranges for higher flow rates, i.e. 50% RH only for 1 l min^{-1} total flow.

One-stage and two-stage dynamic gas dilution of the test gases into the carrier gas stream have been realized. In one-stage dilution, the test gas from the gas cylinder is dosed into

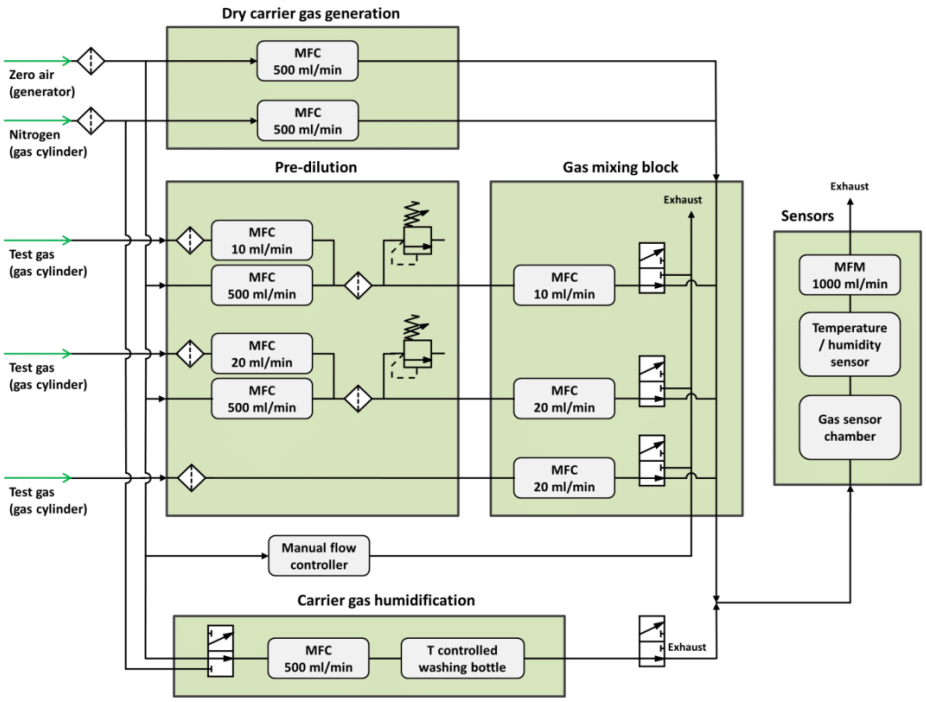

Figure 1. Schematic diagram of the gas mixing system. The different segments are: mixing of the dry carrier gas, test gas dosing with and without an added dilution step, carrier gas humidification, and application of the full gas mixture to a sensor panel.

the carrier gas stream by a single MFC. Two-stage dilution uses an additional dilution step in which a low flow of the test gas from the gas cylinder is mixed with a high flow of the dry background gas before being dosed into the carrier gas stream by a third MFC. This setup is more complex, as not only two additional MFCs per line are needed but also a pressure regulator between the two stages to ensure correct and constant pressure values for the final MFC stage. Currently, four test gas lines are set up as two-stage gas dilution lines and two lines are installed without pre-dilution; these lines can however be upgraded if needed. In the mechanical setup, the MFCs are installed on two levels. The first stage pre-dilution MFCs and the MFC for setting the humid carrier gas are located on the bottom level, while the MFCs for the dry carrier gas and the second dilution stage are located on the top stage. This setup ensures short tubing from the second stage MFCs to the gas mixing block to minimize dead volumes and delay times when changing gas concentrations.

The gas mixing system should be able to provide well-defined gas mixtures. One important aspect is the precision of gas pulses. To provide precise gas pulses the switching time of the mass flow controllers should be as short as possible. We tested three different types of mass flow controllers for their settling time to reach a defined flow for a typical test gas profile. In the previous system [26], MFC types 8715 (bypass sensor with heated resistors) and 8713 (MEMS sensor) from Bürkert (Christian Bürkert GmbH & Co. KG, Germany) were installed for the test gases and for the carrier gases, respectively. These MFCs were found to have long switching times between flow setpoints after receiving the respective command. If the change in flow is large, it can take up to 5 s until

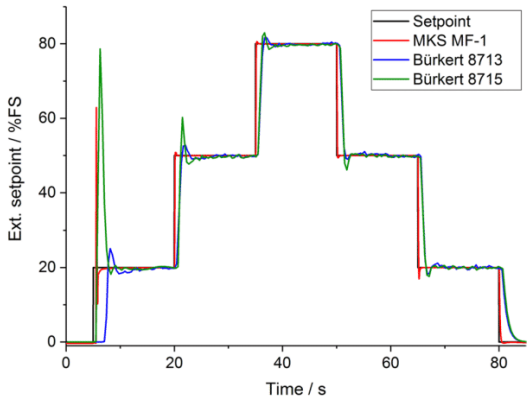

Figure 2. Comparison of settling times for various setpoint changes for three mass flow controller types.

the new gas flow is reached at a steady level for both types. If fast changes in gas concentration or short gas pulses are required, the temporal performance of these controllers is not sufficient. Furthermore, the stability of the gas flow is not ideal.

Therefore, faster MFCs are used in the new system, with a controller settling time of <800 ms according to the datasheet (type MF-1, MKS Instruments Deutschland GmbH, Germany). The settling times for the three controller types were compared by switching the nominal output flow between several values and recording the output signals, see figure 2.

The MF-1 MFC changes its output gas flow much faster than the compared Bürkert controllers. For all setpoint changes, the gas flow overshoots from the control are significantly lower as

well. All controllers show a delay and an overshoot when the setpoint is changed from 0 to 20% FS, for all other changes the MF1 shows a very low over- or undershoot, while the Bürkert MFCs show significant signal oscillations for several seconds until a stable output is reached. The measured flow stability of the MKS MFC is considerably better compared to the Bürkert devices. One can see that the error for the setpoint is very high when switching from a zero flow. In general larger relative changes in flow are producing a large error. Therefore, the test gas lines are equipped with an additional valve at the injection to the total gas flow that allows delaying the injection of the mass flow of the test gas until the MFC gas flow has reached a steady state. By this procedure, only the carrier gas stream needs to be compensated to keep the total flow constant and avoid temperature changes of the tested gas sensors. The minor relative changes of the carrier air stream will only cause small deviations of the total gas flow.

The minimum setpoint for the MFCs was chosen as 5% full scale (FS) of each device, as the relative error of gas flow, i.e. 0.5% of the setpoint plus 0.2% of full scale, increases quickly below this value. At 5% setpoint the relative error for the gas dilution is 4.5%. The calculation of the setpoints of the three MFCs involved in a pre-dilution gas line have to be optimized for low bottle gas consumption and low switching time between gas concentrations, with the latter having a higher priority. Low gas consumption has been achieved by always minimizing the gas flow in the first dilution stage and thus minimizing the cylinder gas flow. Fast changes of concentration for gas mixing are implemented into the MFC control by always having the second stage MFC fully open if possible. This ensures a fast gas exchange in the tubing between the two MFC stages. At a gas volume of approx. 0.8 ml between the two stages, which are installed on two levels of the mechanical setup, the time for gas exchange could take up to 96 s if the second stage MFC with a maximum flow rate of 10 ml min^{-1} is set to 5% FS, based on the MFC configuration and the second stage MFC setpoint. If the second stage MFC is fully opened, the gas exchange time is reduced to 4.8 s in this configuration example.

The total concentration range that can be covered with a two-stage dilution spans four orders of magnitude and is divided into five segments; in most segments the setpoints of two MFCs are fixed while the third one is varied. Figure 3 gives an example for a dilution line with a 20 ml min^{-1} test gas MFC and a 500 ml min^{-1} carrier gas MFC in the first stage, and another 20 ml min^{-1} MFC in the second stage. In the example, the total gas flow at the sensors is set to 400 ml min^{-1} allowing maximum and minimum concentrations of 5% and $5 \cdot 10^{-4}$%, respectively, of the test gas bottle concentration corresponding to 5 ppm and 0.5 ppb, respectively, for a 100 ppm test gas bottle.

1. For the lowest concentration, the dilution carrier gas flow is set to its maximum and the MFC setting the gas flow from the bottle is set to its minimum. The second stage MFC is varied from its minimum to 100% FS.

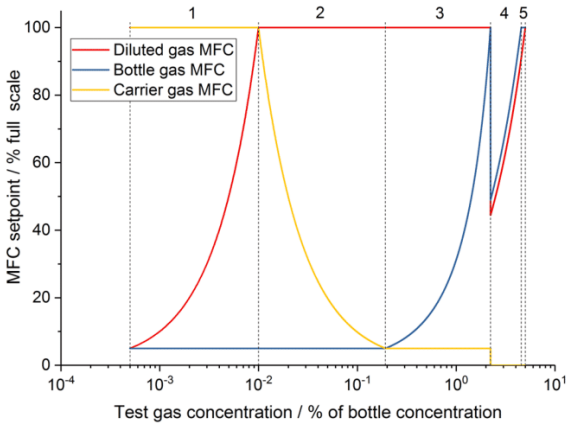

Figure 3. Setpoints for the three MFCs of a two-stage dynamic gas dilution line for a configuration with 20 ml min^{-1} bottle gas MFC, 500 ml min^{-1} carrier gas MFC and 20 ml min^{-1} MFC for the diluted gas into the carrier gas; calculated for a total gas flow at the sensors set to 400 ml min^{-1}.

2. In the second segment, the gas bottle flow is set to its minimum, the second stage MFC is fully opened (for low gas exchange times between the stages) and the dilution gas is varied over its full range.
3. In the third segment, the second stage MFC is kept fully opened, the dilution gas is fixed to its minimum, and the bottle gas MFC is varied over its full range.
4. For the fourth segment, the dilution gas is switched off, the gas concentration between the MFC stages is the same as in the gas bottle. To maintain the pressure drops over both MFC stages, the gas flow of the first stage test gas MFC is set 10% higher than the second stage MFC.
5. In the last segment, the first stage test gas MFC is set to fully open, the dilution gas MFC is closed, and the second stage MFC is varied between 90% FS and 100% FS.

If the full control range of the MFC is used (down to 2% FS, which means the error can be up to 10% of the setpoint), the dynamic range can be increased to 1:62 500 in this example. Two pre-dilution lines of the assembled system are equipped with 10 ml min^{-1} MFCs for both test gas and diluted gas to achieve lower gas concentrations by a factor of 4 compared to the setup with two 20 ml min^{-1} MFCs. For single MFC lines without pre-dilution the dynamic range is 1:20 (limit at 5% FS) and can be extended to 1:50 (flow setpoint down to 2% FS).

Another important aspect in this setup is to assure that the gas flow exiting stage 1 is larger than the gas flow exiting stage 2. This is ensured in segments 1–3 (figure 3) by the carrier gas flow, which is always higher than the MFC flow of the second stage. In segment 4, where the carrier gas for pre-dilution is switched off, the test gas MFC flow in the first stage is set 10% higher than the second stage flow. This ensures a slight overflow and a stable gas pressure between the MFC stages. In the last segment the overflow slowly reduces to zero.

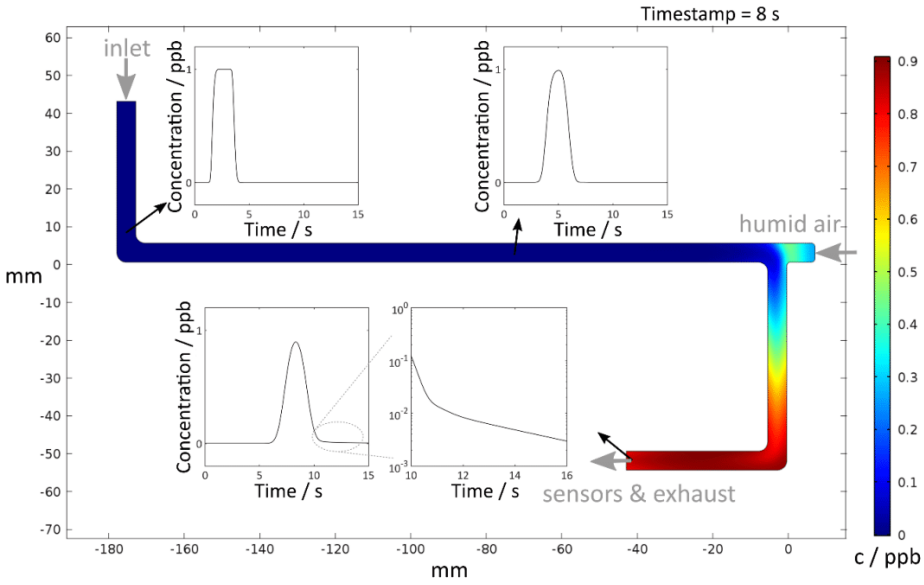

Figure 4. FEM model and gas concentration (color map) for the gas path behind the test gas dosing containing an exemplary dead volume (the humidified carrier gas inlet). A total flow of 100 ml min^{-1} and a 2 s rectangular gas pulse ($c = 1$ ppb) realized by valve switching are assumed at the inlet (top left); through diffusion, a Gaussian peak establishes. Insert at bottom left shows the almost ideal Gaussian peak that reaches the sensors. A dead volume, which for example occurs in our system when no humidity is added to the gas flow, results in significant tailing ($T = 1.0746$, IUPAC notation) where the peak concentration is only reduced by 2 orders of magnitude even after several seconds (time constant $\tau = 6.86$ s).

FEM modelling of critical system components

As already mentioned, another aspect that was optimized was the attention on dead volumes in the system. By designing the mechanical setup in a way that uses short tubing connections between fluidic parts and small diameter tubing, dead volumes which could prolong gas exchange times have been minimized. The effect of a dead volume which is not flushed by a gas stream has been simulated using FEM (finite element method) modelling. For the simulations COMSOL Multiphysics was used. Since laminar flow conditions are dominant throughout the system (Reynold's number Re = 17.5 in the presented example), diffusion is the main gas mixing mechanism. Therefore, attention should be paid to mixing paths (e.g. inside pre-dilution lines) as well as to dead volumes (to avoid carry-over effects). FEM models have been used to evaluate and optimize the most time critical system components; one example is given in figure 4.

Figure 4 shows a 2D model of the tubing path behind the test gas dosing and the adding of the humidified carrier gas via a T-fitting. When no humidity is used, this inlet is a dead end and thereby a large dead volume (minimum 1.5 ml, assuming a T-fitting with a cap nut). Regarding the overall system, this is the longest path and the highest dead volume, so it can be regarded as the most critical component. At the dry air and test gas inlet a total flow rate of 100 ml min^{-1} is assumed and a smoothed 2 s rectangular peak with a concentration of 1 ppb starting at $t = 1$ s is applied. The rectangular shape originates from valve switching. Inside the gas mixing block dead volumes and gas paths are very short, so that at this point a rectangular shape of the gas peak is a valid approximation. Due to the smoothing (0.05 s transition zone) the concentration can be evaluated correctly, because FEM needs steady conditions, and moreover a perfectly rectangular shape does not represent realistic conditions. The tube diameter along the gas path is 5 mm. A diffusion constant of $D = 8 \cdot 10^{-6}$ m² s^{-1} is used for the simulation, which represents toluene as a typical VOC [31]. Due to diffusion, the gas pulse gradually approaches a Gaussian shape with increasing FWHM (full width at half maximum) along the path, starting at FWHM = 2 s at the inlet and reaching FWHM = 2.13 s at the outlet. The time constant τ for the concentration decrease also increases from $\tau = 0.1$ s to $\tau = 0.37$ s at the outlet. At the dead-end, gas molecules are sheared off and, since there is no flow at this point, stay inside this dead volume (see the coloring inside the channel, which stands for concentration). Again, due to diffusion these molecules are carried out of the system very slowly. Behind the T-fitting the pulse shape is no longer perfectly Gaussian. Molecules diffusing out of the dead volume cause tailing effects ($T = 1.0746$, IUPAC notation) and a second time constant of $\tau = 6.86$ s in the decrease of concentration appears, which can be seen in the logarithmic graph in figure 4. The concentration may seem to be very low, but seconds after the peak has passed, still 1% of the maximum concentration reaches the sensors. For sensitive sensors, especially MOS gas sensors with highly non-linear sensitivity, this is significant. In this case, the dead-end could be avoided by using a corner piece instead of a T-fitting when measuring without humidity, but similar effects can also occur inside sensor chambers and sensor housings so sensor chamber design also has to be optimized according to the test conditions.

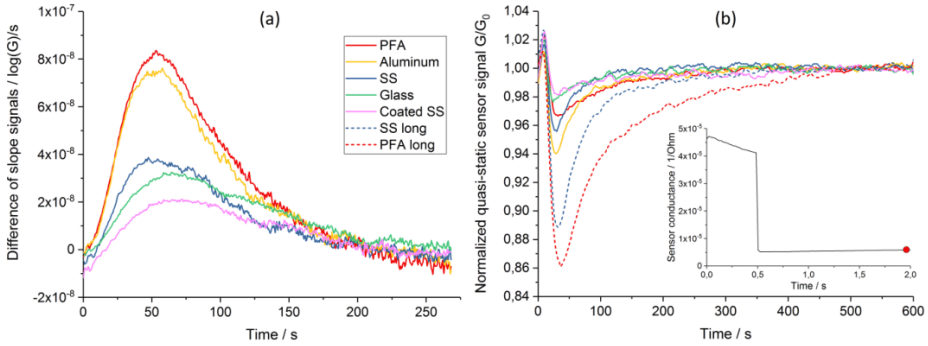

Figure 5. Sensor signals of the adsorption/desorption test measurements. (a) Naphthalene desorption test, the shown signal is the difference of the signal slopes (reference—test) during a low temperature plateau; (b) adsorption test, the shown signal is the quasi-static signal from one point at the end of the low temperature plateau (indicated by the red dot in the insert showing the sensor signal of one temperature cycle).

Comparison of tubing materials

In addition to the geometry of the gas tubing, the material of the tubing can have a significant effect on issues like tailing and purity of gas streams. Various materials are used for gas tubings, e.g. stainless steel, glass, or polymer materials like PFA (perfluoroalkoxy alkanes), depending of the demand of the target gases.

In order to be able to compare the material properties regarding sorption effects of these materials for our intended VOC target gases, five materials were tested for sticking of naphthalene. This low vapor pressure VOC is highly relevant regarding indoor air quality monitoring [32] and has previously been shown to produce significant tailing effects in gas mixing systems [26]. The tested materials are: stainless steel (SS), aluminum, glass, PFA, and SS coated with a silica coating. The tested tubes in a first test measurement had a length of approx. 300 mm and an interior diameter of approx. 4 mm; in a second test two longer, thinner tubes (PFA and SS with a length of 2 m and an interior diameter of approx. 1.65 mm for PFA and 1.4 mm for SS) were added to the test group.

In the first of two measurements the adsorption of naphthalene at the inner walls of the test tubes was investigated by initially loading them with naphthalene and subsequently purging them with zero air, which then was measured by an MOS gas sensor (AS-MLV, ams, Austria). The test tube and a bypass tube were connected to four manually operated 3-way lever valves, which were used to conduct the flow of naphthalene (477 ppb, 100 ml min^{-1}) and zero air (100 ml min^{-1}) through one of the two tubes. The temperature cycled gas sensor was operated with a cycle length of 25 min, with 2 min at 400 °C and 23 min at 275 °C. While the sensor was flushed with zero air through the bypass tube, the test tube was flushed with naphthalene for the length of one sensor cycle. During this loading period the gas molecules are expected to be adsorbed at the inner tube walls. Then the zero air flow was conducted to the loaded test tube by using the lever valves to remove the adsorbed gas molecules. The switching was repeated twice, with the test tube being loaded with naphthalene only once to achieve a differential measurement. The analyzed sensor signal is the difference of conductance slopes of the two cycles (reference and measurement) after the switching. This signal was used to evaluate the effect of adsorbed naphthalene and how fast the molecules are desorbed by the zero air gas flow (figure 5(a)).

In a second measurement, the reverse effect was examined by flushing the sensor with naphthalene and the test tube with zero air for 10 min and then conducting the naphthalene gas flow through the test tube to the MOX gas sensor by switching the valves. For this measurement, very short gas sensor cycles were used (0.5 s at 400 °C, 1.5 s at 275 °C), in order to be able to better track the naphthalene concentration at the sensor during the test runs. For a simple evaluation, the sensor signal at one point of the cycle, at the end of the low temperature plateau, was extracted from each cycle and plotted over time. The change of this quasi-static sensor signal due to the drop of naphthalene concentration caused by adsorption of gas molecules on the test tube surface was used to determine the impact of the adsorption effect. The extracted signals were smoothed using a moving average filter and normalized to the mean value of the last 40 measuring points of each test run. The results of this second measurement are shown in figure 5(b).

In the first measurement, each signal of the tested tubing materials shows a response to the naphthalene loading, which is expressed in different gradients of the signal right after the pre-purging. Considering the difference of slopes of the measurement and reference cycles, this results in peaks of varying height. The slopes differ over a relatively small period of approx. 4 min, which is the time in which the adsorbed molecules are detached by the zero air flow. The signal peaks and therefore the amount of previously adsorbed gas molecules are relatively high for the aluminum and the PFA tube, compared to the glass and both SS tubes. The silica coated SS shows the lowest adsorption effect, followed by glass and uncoated SS. Remarkable is the different peak shape for uncoated SS reaching its maximum approx. 20 s earlier than for glass or coated SS, which implies that the desorption of adsorbed molecules occurs slightly faster for the uncoated SS tube.

The second measurement (figure 5(b)) clearly shows the influence of the tube dimensions in addition to the material. The short increase of the signals at the beginning is assumed to

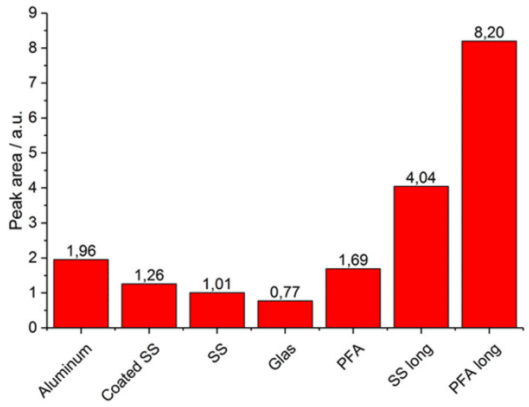

Figure 6. Calculated peak areas of the naphthalene adsorption measurement for various tubing materials (see figure 5(b)).

be due to quick pressure changes caused by manual switching of the valves when redirecting the naphthalene flow. The subsequent signal drop in all signals is caused by a reduced naphthalene concentration reaching the sensor as naphthalene is adsorbed on the clean tube surfaces. The curves of the two longer tubes have significantly lower minima than the shorter tubes of the same material, with PFA still showing worse behavior than SS in terms of minimum value and relaxation time, as observed in the first measurement. The difference due to the length can be explained by a larger possible adsorption area in the longer tubes. However, an analytic relation between the adsorption effect and length cannot be found, since the diameter and therefore the flow velocity differs for the long and short tubes. Regarding the value of the minima of the short tubes, coated SS again shows the lowest peak height, followed by glass, PFA, SS and aluminum, which means that the rate of adsorbed naphthalene is the least for the coated SS. It can also be observed that the curve of uncoated SS has a shorter relaxation time, especially compared to PFA. This means that the inner surface of the tube is saturated with naphthalene molecules more quickly, similar to the faster desorption observed in the first experiment.

In an additional evaluation the peak areas of the signal drops were evaluated as these are related to the total amount of adsorbed gas molecules. The areas enclosed by the different curves and the horizontal line through the normalized value 1 were computed and are shown in figure 6.

The values of the peak areas are given in arbitrary units and are indicative of the amount of adsorbed naphthalene gas molecules. In this measurement the short glass tube and the uncoated SS adsorbed the least amount of naphthalene, followed by coated SS, PFA and aluminum. The order of materials is not the same as for the peak heights (figure 5(b)), as the time constant of the signal relaxation also contributes to the resulting peak area. For the short tubes, glass has the smallest peak area, i.e. the lowest amount of gas adsorbed, followed by the uncoated SS and the coated SS. Aluminum and PFA have larger peak areas, the value of aluminum is about twice that of uncoated SS; the peak area of PFA is approx. 70% larger compared to SS for the short tubes. For the longer, thinner tubes the difference of peak area is higher, slightly above a factor or 2 for PFA over SS. This might be an effect of the different interior diameters of the thin PFA and SS tubes and thus different gas velocities and different adsorption areas inside the tube. Therefore, a direct quantitative comparison of the values is not possible. As a qualitative result the better performance of glass and stainless steel over PFA and aluminum can be extracted from the measurement.

The investigation shows the suitability of standard SS tubes in a gas mixing system regarding its adsorption properties. However, the influence of different flow rates as well as different VOCs on the adsorption/desorption behavior and thus possible carry-over effects has to be studied further.

Contaminations and resulting measurement strategies

The system was checked for intrinsic contaminations using gas sampling on Tenax TA tubes and GC/MS analysis according to ISO 16000-6, as well as by an internal MOS gas sensor. The gas sensor provides an online monitoring that is not possible by sampling tubes. Moreover, MOS gas sensors are able to detect hydrogen, carbon monoxide and also very volatile organic compounds (VVOC) such as formaldehyde [10]. The goal of this investigation was to determine contaminations in the carrier air generated by the zero air generators as well as contaminations introduced by fluidic components such as MFCs, valves, and tubing.

For GC/MS analysis, gas samples were extracted from several locations in the system on sampling tubes. Relevant for determining the general contamination are the zero air going in the system and the mixed gas exiting the mixing block. To take into account all MFCs and valves, zero air was connected to all cylinder gas MFCs, and all six test gas lines (MFCs and valves) were fully opened. The total gas flow was set to 120 ml min^{-1} in all cases, according to the specifications for the sampling method. The humidified carrier air was not taken into account for this analysis. Table 1 gives an overview of the obtained results.

VOC contaminations are generally very low; even with all devices opened the measured TVOC values are below 2 ppb. However, the ISO 16000-6 method is specified for gases with a retention time between hexane and hexadecane. Thus it does not trace some important permanent gases which might still be in the gas mixture, e.g. hydrogen (H_2), carbon monoxide (CO) and methane (CH_4) as well as VVOCs like formaldehyde (CHO).

For determining an upper limit of the permanent gas contamination in the system, a measurement with MOS gas sensors was performed. In previous works, a method for the absolute quantification of low gas concentrations using such gas sensors was developed [29, 30]. This method determines the concentration of a target gas by evaluating the slope of the gas sensor signal, which corresponds to the amount of oxidized surface species, after a rapid change of the sensor temperature from a high to a lower value. The model shows that in this phase re-oxidation of the surface is suppressed by

Table 1. TVOC contaminations inside the gas mixing system measured at various points and under various conditions.

Sampling conditions and location	TVOC content measured by GC-MS
Zero air; at dry carrier air MFC input	0.69 μg m^{-3} (equivalent to 0.18 ppb of toluene)
Dry carrier air; behind gas mixing block	2.60 μg m^{-3} (equivalent to 0.7 ppb of toluene)
All test gas lines fully open; behind mixing block	6.94 μg m^{-3} (equivalent to 1.8 ppb of toluene)

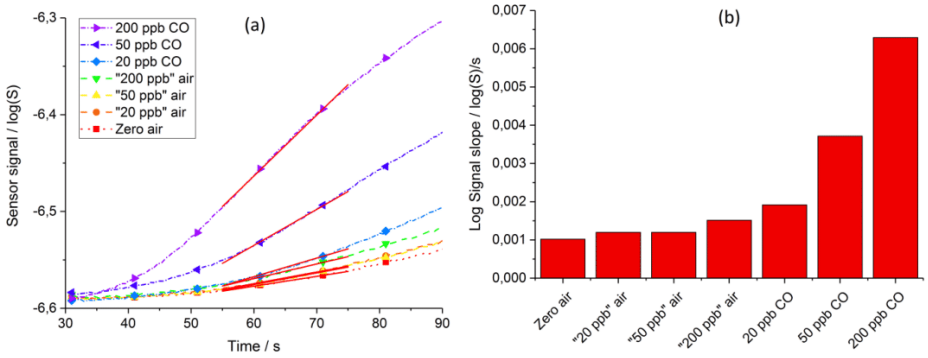

Figure 7. (a) logarithmic sensor signals for all test gases after switching from 400 °C to 175 °C; linear fits marked red; (b) signal slopes calculated from linear signal fits.

several orders of magnitude [29]. Therefore, only reduction processes are observed during this stage. The reduction process was shown to be linear to the reducing gas concentration and proportional to the exposure time. The surface reduction, therefore, gives an upper limit for the reducing gas concentration and, if the concentration is not too low, a good absolute estimate. In the test measurement, a commercial SnO_2 MOS gas sensor (AS-MLV, ams, Austria) was operated at 420 °C for 30 s and then switched rapidly (<10 ms) to lower temperatures. Three low temperature levels were used, 175 °C for 120 s, 250 °C for 90 s, and 325 °C for 60 s, always preceded by a high temperature step to achieve a highly oxidized sensor surface. Carbon monoxide was used as test gas.

One of the pre-dilution test gas lines was equipped with an additional stainless steel manual valve; with this the test gas for the same MFC line could be switched between zero air and carbon monoxide. A measurement run with three variations of the test gas was then performed twice, once with zero air and once with CO (1995 ppm reference gas cylinder). This approach eliminates possible variations of the measurement result caused by using different gas lines (MFCs, valves) and thus guarantees identical conditions for both gases. For CO, three concentrations were chosen: 20 ppb, 50 ppb, and 200 ppb, as this covers the range of expected contaminations. Note that the ubiquitous CO background concentration varies between 100 and 300 ppb with an average of 150 ppb [33]. As the zero air test gas was generated using identical MFC setpoints, the corresponding CO concentrations are used for labeling the three zero air measurement runs.

For signal processing, the lower temperature segments of the temperature cycle were evaluated. In this measurement, the signal slope is evaluated for the zero air test gases, with the CO test gases being used as reference values. One example for the sensor signals is given in figure 7(a); it shows the logarithmic sensor conductivity on the 175 °C temperature plateau for all applied gas mixtures, as the sensor response to CO was found to be highest for this temperature. The range from 55 s to 75 s of the cycle was used for calculating the signal slopes, indicated by the red lines. Figure 7(b) shows a comparison of the signal slopes for all temperature plateaus and test gases.

The logarithmic sensor signals do not show a constant slope over the full temperature plateau; this is probably due to the fact that the measurements were performed in dry air and not with added humidity, which might influence the reactions of the CO on the sensor surface. However, for a qualitative comparison of the applied gas concentrations, the signal slopes still seem to be valid.

In all slopes, the effects of the background contamination and the added test gas are superimposed. At these low concentrations, the effect of this superposition can be assumed as a simple summation of the individual effects on the signal slope.

From the signal slopes at this temperature (figure 7(b)), the following data can be extracted: The effect of CO on the sensor signal slope can be evaluated by calculating the differences in slope values between the slope at a certain CO concentration and the corresponding signal if zero air is connected and the same concentration is set. For 175 °C and 20 ppb of CO, its value is $7.2 \cdot 10^{-4}$ log(S)/s. If a linear correlation between the logarithmic signal slope and the gas concentration is assumed at these low concentrations, a CO-equivalent contamination concentration can be estimated for the zero air carrier gas and the MFC gas line for the tested settings. If 20 ppb of CO generate a slope signal of $7.2 \cdot 10^{-4}$ log(S)/s, the zero air value ($1.03 \cdot 10^{-3}$ log(S)/s) corresponds to 28 ppb CO-equivalent and the '20 ppb' zero air test gas mixed into the carrier gas stream corresponds to 33 ppb CO-equivalent, i.e. the test gas MFCs add 5 ppb of CO-equivalent contamination.

These values represent maximum estimations of the contamination, i.e. there are no more than 28 ppb CO-equivalent

in the carrier gas in the set conditions, and no more than 5 ppb added by the test gas line.

Based on these results, a measurement strategy was devised to compensate the remaining effects of contaminations of the fluidic components in the system. A measurement is performed twice, once with the intended test gases connected to the system and once with zero air connected to the test gas line inputs. With the zero air measurement, a baseline can be recorded for each MFC setpoint configuration of the measurement, and this baseline can be taken into account (e.g. subtracted) for the measurement with the test gases.

Conclusion

In the designed and realized gas mixing system, several issues regarding ppb level VOC gas generation have been addressed and tested. The setup of the fluidic components, especially the two-stage dynamic gas dilution, has been chosen to allow generation of very low test gas concentrations from high concentration gas cylinders, thus minimizing the effect of contaminations in the cylinders. The components and the control algorithms have been optimized to cover a wide range of possible applications, e.g. generation of short gas pulses and fast switching between gas concentrations to allow simulation of complex scenarios like dynamic breath analysis, while minimizing test gas consumption.

Other relevant issues, such as dead volumes, delay times, and influence of gas adsorption/desorption on/from tubing materials, have been identified and taken into account in the system design. FEM simulations show that even small dead volumes can generate significant tailing effects and lead to widening of gas pulses and the need for increased purging periods between test gas injections. Regarding the choice of materials for tubing, two test measurements with naphthalene showed that stainless steel has favorable characteristics over PFA in terms of sticking of the gas to the tube surface. Glass or glass coated steel show even better performance in the tests, but are more expensive and have more restrictions regarding handling and flexibility of use.

The gas contaminations of the system caused by the zero air carrier gas and by the fluidic components have been tested using both standard analytical procedures and a novel approach based on a highly sensitive MOS sensor. Contaminations were found to be below 2 ppb toluene-equivalent for VOCs and in the low ppb range CO-equivalent, respectively, with the two methods. A measurement strategy has been devised to suppress these gas offsets, by running a reference measurement with zero air in addition to the measurement with test gases.

With all these features, reliable gas measurements and exact quantitative calibration in the concentration range down to single ppb level can be performed both for VOCs and permanent gases.

Acknowledgment

Parts of this work were performed within project SENSIndoor, which has received funding from the European Union's Seventh Framework Programme for research, technological development and demonstration under grant agreement No 604311.

References

[1] Penza M and EuNetAir Consortium 2014 COST action TD1105: overview of sensor-systems for air-quality monitoring *Proc. Eng.* **87** 1370–7
[2] Sasahara T, Kato H, Saito A, Nishimura M and Egashira M 2007 Development of a ppb-level sensor based on catalytic combustion for total volatile organic compounds in indoor air *Sensors Actuators* B **126** 371–710
[3] Schütze A, Baur T, Leidinger M, Reimringer W, Jung R, Conrad T and Sauerwald T 2017 Highly sensitive and selective VOC sensor systems based on semiconductor gas sensors: how to? *Environments* **4** 20
[4] Burge P S 2004 Sick building syndrome *Occup. Environ. Med.* **61** 185–90
[5] Wolkoff P 2013 Indoor air pollutants in office environments: assessment of comfort, health, and performance *Int. J. Hygiene Environ. Health* **216** 371–94
[6] Guo H, Lee S C, Chan L Y and Li W M 2004 Risk assessment of exposure to volatile organic compounds in different indoor environments *Environ. Res.* **94** 57–66
[7] Patni N K and Clarke S P 2003 Gaseous emissions in swine barns and during slurry mixing in sub-floor pits *ASAE Annual Meeting*
[8] Dincer F, Odabasi M and Muezzinoglu A 2006 Chemical characterization of odorous gases at a landfill site by gas chromatography-mass spectrometry *J. Chromatogr.* A **1122** 222–9
[9] Voges N, Chaffiol A, Lucas P and Martinez D 2014 Reactive searching and infotaxis in odor source localization *PLoS Comput. Biol.* **10** e1003861
[10] Leidinger M, Sauerwald T, Reimringer W, Ventura G and Schütze A 2014 Selective detection of hazardous VOCs for indoor air quality applications using a virtual gas sensor array *J. Sens. Sens. Syst.* **3** 253–63
[11] Bastuck M, Leidinger M, Sauerwald T and Schütze A 2015 Improved quantification of naphthalene using non-linear partial least squares regression *16th Int. Symp. on Olfaction and Electronic Nose (Dijon, France)* (arXiv:1507.05834)
[12] Leidinger M, Huotari J, Sauerwald T, Lappalainen J and Schütze A 2016 Selective detection of naphthalene with nanostructured WO_3 gas sensors prepared by pulsed laser deposition *J. Sens. Sens. Syst.* **5** 147–56
[13] Plaia A, Di Salvo F, Ruggieri M and Agró G 2013 A multisite-multipollutant air quality index *Atmos. Environ.* **70** 387–91
[14] Spinelle L, Gerboles M, Villani M G, Aleixandre M and Bonavitacola F 2015 Field calibration of a cluster of low-cost available sensors for air quality monitoring. Part A: Ozone and nitrogen dioxide *Sensors Actuators* B **215** 249–57
[15] Spinelle L, Gerboles M, Villani M G, Aleixandre M and Bonavitacola F 2017 Field calibration of a cluster of low-cost commercially available sensors for air quality monitoring. Part B: NO, CO and CO_2 *Sensors Actuators* B **238** 706–15
[16] Heimann I, Bright V B, McLeod M W, Mead M I, Popoola O A M, Stewart G B and Jones R L 2015 Source attribution of air pollution by spatial scale separation using high spatial density networks of low cost air quality sensors *Atmos. Environ.* **113** 1–264
[17] De Nazelle A, Seto E, Donaire-Gonzalez D, Mendez M, Matamala J, Nieuwenhuijsen M J and Jerrett M 2013

Improving estimates of air pollution exposure through ubiquitous sensing technologies *Environ. Pollut.* **176** 92–9
[18] Mead M I *et al* 2013 The use of electrochemical sensors for monitoring urban air quality in low-cost, high-density networks *Atmos. Environ.* **70** 186–203
[19] Geiss O, Giannopoulos G, Tirendi S, Barrero-Moreno J, Larsen B R and Kotzias D 2011 The AIRMEX study—VOC measurements in public buildings and schools/kindergartens in eleven European cities: statistical analysis of the data *Atmos. Environ.* **45** 3676–84
[20] Koistinen K *et al* 2008 The INDEX project: executive summary of a European Union project on indoor air pollutants *Allergy* **63** 810–9
[21] Bajtarevic A *et al* 2009 Noninvasive detection of lung cancer by analysis of exhaled breath *BMC Cancer* **9** 348
[22] Chan D K, Leggett C L and Wang K K 2016 Diagnosing gastrointestinal illnesses using fecal headspace volatile organic compounds *World J. Gastroenterol.* **22** 1639–49
[23] Weber C M, Cauchi M, Patel M, Bessant C, Turner C, Britton L E and Willis C M 2011 Evaluation of a gas sensor array and pattern recognition for the identification of bladder cancer from urine headspace *Analyst* **136** 359–64
[24] Spinelle L, Aleixandre M and Gerboles M 2013 Protocol of evaluation and calibration of low-cost gas sensors for the monitoring of air pollution *EUR* 26112 Publications Office of the European Union
[25] Endres H E, Jander H D and Göttler W 1995 A test system for gas sensors *Sensors Actuators* B **23** 163–72
[26] Helwig N, Schüler M, Bur C, Schütze A and Sauerwald T 2014 Gas mixing apparatus for automated gas sensor characterization *Meas. Sci. Technol.* **25** 055903
[27] Pogány A *et al* 2016 A metrological approach to improve accuracy and reliability of ammonia measurements in ambient air *Meas. Sci. Technol.* **27** 115012
[28] Haerri H-P, Macé T, Waldén J, Pascale C, Niederhauser B, Wirtz K, Stovcik V, Sutour C, Couette J and Waldén T 2017 Dilution and permeation standards for the generation of NO, NO_2 and SO_2 calibration gas mixtures *Meas. Sci. Technol.* **28** 035801
[29] Schultealbert C, Baur T, Schütze A, Böttcher S and Sauerwald T 2017 A novel approach towards calibrated measurement of trace gases using metal oxide semiconductor sensors *Sensors Actuators* B **239** 390–6
[30] Baur T, Schütze A and Sauerwald T 2015 Optimierung des temperaturzyklischen Betriebs von Halbleitergassensoren *Tech. Mess.* **82** 187–95
[31] Erbil H Y and Avci Y 2002 Simultaneous determination of toluene diffusion coefficient in air from thin tube evaporation and sessile drop evaporation on a solid surface *Langmuir* **18** 5113–9
[32] World Health Organization 2010 *WHO Guidelines for Indoor Air Quality: Selected Pollutants* (Copenhagen: WHO Regional Office for Europe)
[33] Deutscher Wetterdienst (DWD) Composition of the atmosphere-trace gases-carbon monoxide (Available online: www.dwd.de/EN/research/observing_atmosphere/composition_atmosphere/trace_gases/cont_nav/co_node.html (Accessed: 28 June 2017))

4 Selective detection of naphthalene with nanostructured WO_3 gas sensors prepared by pulsed laser deposition

Martin Leidinger[1], Joni Huotari[2], Tilman Sauerwald[1], Jyrki Lappalainen[2] and Andreas Schütze[1]

[1] Saarland University, Lab for Measurement Technology, Saarbrücken, Germany
[2] University of Oulu, Faculty of Information Technology and Electrical Engineering, Oulu, Finland

Originally published in *Journal of Sensors and Sensor Systems, 5, pp. 157-156, 2016*

doi: 10.5194/jsss-5-147-2016

Synopsis

This article describes an approach for characterization of two variations of a new gas sensor material. In addition to the characterization of the physical properties of the layers, they were tested for their gas sensing potential for three VOC target gases: formaldehyde, naphthalene and benzene at ppb concentration levels.

The structure of the synthesized materials, which were prepared using pulsed laser deposition (PLD) was analyzed using SEM (scanning electron microscopy), AFM (atomic force microscopy), XRD (X-ray diffraction) and Raman spectroscopy, to

determine parameters like layer thickness, grain sizes and grain structure as well as the influence of deposition parameters and post-deposition annealing on these properties.

Regarding the testing of the gas sensing performance, some of the methods presented in section 2.3 were applied to the TCO sensor signals: quasi-static signals and LDA with extracted features. The results show that LDA generates better data and allows for more detailed analysis of the data compared to the simple quasi-static approach. As the two tested sensing layers show a much higher response to naphthalene than to the other two tested gases, several evaluations of the signals / features are performed to increase the performance of the sensors for this target gas. Identification of the different applied naphthalene concentrations is possible down to 1 ppb with an accuracy of > 99 % for the recorded data set of one of the two deposited sensing layers if no interferent gas is present in the gas mixture. Furthermore, the effect of varying humidity is investigated and the ability of the signal processing to suppress this influence is evaluated.

The results show that the investigated data processing chain of feature extraction, LDA and classification using knn are suitable for gas sensor characterization and it was found that one of the PLD layer variations has a significantly higher potential for naphthalene detection than existing gas sensors.

J. Sens. Sens. Syst., 5, 147–156, 2016
www.j-sens-sens-syst.net/5/147/2016/
doi:10.5194/jsss-5-147-2016

JSSS Journal of Sensors and Sensor Systems Open Access

Selective detection of naphthalene with nanostructured WO_3 gas sensors prepared by pulsed laser deposition

Martin Leidinger[1], Joni Huotari[2], Tilman Sauerwald[1], Jyrki Lappalainen[2], and Andreas Schütze[1]

[1]Saarland University, Lab for Measurement Technology, Saarbrücken, Germany
[2]University of Oulu, Faculty of Information Technology and Electrical Engineering, Oulu, Finland

Correspondence to: Martin Leidinger (m.leidinger@lmt.uni-saarland.de)

Received: 15 October 2015 – Revised: 22 March 2016 – Accepted: 28 March 2016 – Published: 8 April 2016

Abstract. Pulsed laser deposition (PLD) at room temperature with a nanosecond laser was used to prepare WO_3 layers on both MEMS microheater platforms and Si/SiO_2 substrates. Structural characterization showed that the layers are formed of nanoparticles and nanoparticle agglomerates. Two types of layers were prepared, one at an oxygen partial pressure of 0.08 mbar and one at 0.2 mbar. The layer structure and the related gas sensing properties were shown to be highly dependent on this deposition parameter. At an oxygen pressure of 0.2 mbar, formation of ε-phase WO_3 was found, which is possibly contributing to the observed increase in sensitivity of the sensor material.

The gas sensing performance of the two sensor layers prepared via PLD was tested for detection of volatile organic compounds (benzene, formaldehyde and naphthalene) at ppb level concentrations, with various ethanol backgrounds (0.5 and 2 ppm) and gas humidities (30, 50 and 70 % RH). The gas sensors were operated in temperature cycled operation. For signal processing, linear discriminant analysis was performed using features extracted from the conductance signals during temperature variations as input data.

Both WO_3 sensor layers showed high sensitivity and selectivity to naphthalene compared to the other target gases. Of the two layers, the one prepared at higher oxygen partial pressure showed higher sensitivity and stability resulting in better discrimination of the gases and of different naphthalene concentrations. Naphthalene at concentrations down to 1 ppb could be detected with high reliability, even in an ethanol background of up to 2 ppm. The sensors show only low response to ethanol, which can be compensated reliably during the signal processing. Quantification of ppb level naphthalene concentrations was also possible with a high success rate of more than 99 % as shown by leave-one-out cross validation.

1 Introduction

In order to evaluate and assess indoor air quality (IAQ), different types of gaseous chemical compounds have to be considered. In addition to carbon monoxide (CO), carbon dioxide (CO_2) and nitrogen dioxide (NO_2), low concentrations of volatile organic compounds (VOCs) play a significant role in deteriorating the quality of breathing air in buildings (World Health Organization, 2010; Bernstein et al., 2008). Exposure to these substances, even at low concentrations, can lead to severe negative effects on human health. For VOCs, health problems mainly include damage to the respiratory system and skin irritations (Jones, 1999). Additionally, some VOCs are proven to be carcinogenic (e.g., benzene, World Health Organization, 2010) or are suspected to be carcinogenic (e.g., formaldehyde, Guo et al., 2004). Based on toxicity and prevalence, according to the World Health Organization (WHO) and the INDEX project (Koistinen et al., 2008), the highest priority VOCs for IAQ are formaldehyde, benzene and naphthalene. For naphthalene, the WHO guidelines suggest values below 0.01 mg m^{-3} corresponding to 1.9 ppb (World Health Organization, 2010). The main health concerns for naphthalene are lesions in the respiratory tract, including tumors in the upper airways (World Health Organization, 2010).

Published by Copernicus Publications on behalf of the AMA Association for Sensor Technology.

In order to detect such small concentrations of VOCs without the need for expensive and time-consuming analytical measurements (e.g., GC-MS analysis, Wu et al., 2004), metal oxide semiconductor gas sensors can be applied. Detection of VOCs in the ppb range with such sensors has been successfully demonstrated using temperature cycled operation (TCO) and pattern recognition signal processing with ceramic-based thick film sensors (Leidinger et al., 2014); however, significant cross-sensitivity to ethanol was found mainly for SnO_2-based sensors. In order to reduce this cross-sensitivity, WO_3 layers were investigated. To obtain highly sensitive sensors with small thermal time constants, the MOS thin film layers were produced on microheater substrates by pulsed laser deposition (PLD). We found that these sensors show a high response to naphthalene in the relevant concentration range with high selectivity compared to other gases, especially relevant interferent gases for indoor air quality assessment, e.g., ethanol.

Pulsed laser deposition is a method for depositing a variety of materials ranging from epitaxial thin films (Hussain et al., 2005) to highly porous nanostructured layers (Balandeh et al., 2015). Porous nanostructured layers have been studied especially in the context of gas sensing materials (Caricato et al., 2009; Nam et al., 2006). PLD offers many advantages compared to other deposition methods, for example easily controllable film composition by deposition parameters, and a good repetition of stoichiometry of the target material in the films deposited on the substrate. When using nanosecond laser PLD, as in this study, with a high oxygen partial pressure in the deposition chamber, nanoparticle formation starts during the deposition process leading to a highly porous nanostructured layer (Harilal et al., 2003; Infortuna et al., 2008; Huotari et al., 2015). These types of layers are very suitable for gas sensing purposes because of their high specific surface area.

WO_3 as a material has been widely studied as it offers a large range of possibilities in practical applications, e.g., in gas sensing (Kohl et al., 2000; Wang et al., 2008; Balazsi et al., 2008), and photocatalytic water splitting (Pihosh et al., 2015). There are several methods to produce WO_3 layers ranging from thick film and thin films technologies to chemical methods (Zheng et al., 2011). In this study, PLD was utilized for depositing WO_3 layers on MEMS microhotplates to produce low-cost and high-performance gas sensor devices.

The performance of the PLD sensor layers has been evaluated in test gas measurements. The three high-priority VOCs, benzene, formaldehyde and naphthalene, have been applied in concentrations below, at and above the respective guideline values, and ethanol has been added as an interferent gas in much higher concentrations in order to simulate typical IAQ applications with background gases from, e.g., cleaning agents or alcoholic beverages. The sensors were operated in dynamic operation using temperature cycled operation (TCO), which is a well-known method for increasing sensitivity and selectivity of gas sensor systems based on MOS sensors (Heilig et al., 1997; Lee and Ready, 1999; Paczkowski et al., 2013; Baur et al., 2014). The resulting signals, after pre-processing and feature extraction, were analyzed by linear discriminant analysis (LDA), a multivariate pattern recognition method which separates different classes of input data while trying to group data sets of the same assigned group (Klecka, 1980; Gutierrez-Osuna, 2002). The combination of TCO and LDA has shown to improve selectivity and sensitivity of gas sensors, both MOS sensors (Gramm et al., 2003; Meier et al., 2007; Reimann and Schütze, 2012; Leidinger et al., 2014) and other types, e.g., GasFET devices (Bur et al., 2012).

2 PLD sensor layer deposition and characterization

2.1 Sensor layer deposition

A XeCl laser with a wavelength of $\lambda = 308$ nm was used to produce WO_3 layers on both Si/SiO_2 substrates and commercial microheater MEMS platforms from a ceramic WO_3 pellet. The laser pulse length was 25 ns and pulse fluence was $I = 1.25\,J\,cm^{-2}$. In all depositions the substrate temperature was kept at room temperature (RT). Two types of samples have been prepared, one at a low O_2 partial pressures of $p(O_2) = 0.08$ mbar, designation PLD0.08O2, and a second type with a higher partial pressure of $p(O_2) = 0.2$ mbar, designation PLD0.2O2. All samples were annealed in a furnace at 400 °C for 1 h after deposition. The samples deposited on Si/SiO_2 substrates were used as reference samples in structural characterization of the layers, and samples with the MEMS heaters were used in gas sensing measurements.

A Bruker D8 Discover device was used in X-ray diffraction studies, and Raman spectroscopy studies were performed with a HORIBA Jobin Yvon LabRAM HR800 in order to study the crystal structure and symmetry of the layers. The surface morphology and the film composition of the samples were studied with a Veeco Dimension 3100 atomic force microscope (AFM) and with Zeiss Sigma FESEM device.

2.2 Crystal structure characterization of the sensing layers

The grazing incidence diffraction (GID) method of the X-ray diffraction was used to characterize the WO_3 layers annealed at 400 °C for 1 h. The results are shown in Fig. 1. A clear difference in the crystal structure can be seen. The phase composition of layers deposited at $p(O_2) = 0.08$ mbar is mostly of the monoclinic γ phase of WO_3, but in the samples deposited at $p(O_2) = 0.2$ mbar, also the ferroelectric monoclinic ε phase of WO_3 is present. This is emphasized especially by the (110) and (−112) reflections located at $2\theta \approx 24.0$ and 33.3°, respectively (Johansson, 2012). However, one must remember that the crystal structures of the

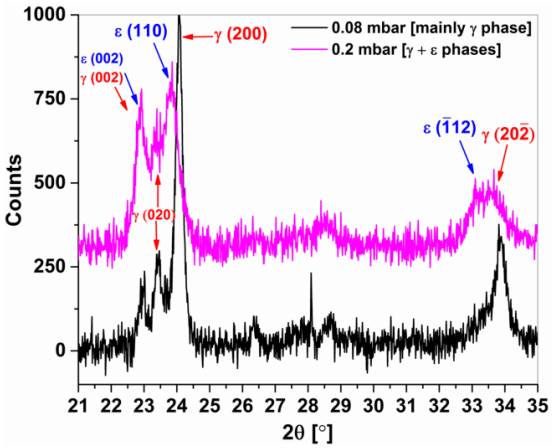

Figure 1. X-ray diffraction spectra of the deposited WO_3 layers after annealing in air (400 °C for 1 h).

γ phase and the ε phase are quite similar, and thus both of them have XRD reflections either in the same 2θ angels or very close to each other. The average grain size of both types of samples after annealing was determined to be around 30 nm using the Warren–Averbach method for XRD data (Marinkovic et al., 2001).

In Fig. 2, the Raman spectroscopy studies performed to the WO_3 layers are presented. The Raman spectra of the as-deposited samples immediately after deposition without any heat treatment are shown in Fig. 2a, and in Fig. 2b the spectra of the layers after annealing at 400 °C for 1 h are presented. An interesting property of the deposition process can be identified in the non-annealed samples. When the O_2 partial pressure is 0.08 mbar, the samples seem to be in an amorphous state after deposition, but when the O_2 pressure is 0.2 mbar, some crystallization is already evident during the deposition process at RT, even before any heat treatment to the layers. However, from Fig. 2b, showing the Raman spectra of the samples after the annealing process, it is clearly seen that after heat treatment in a furnace both films have a more crystallized structure. It is also again evident that the layers PLD0.08O2 are composed mostly of γ phase, but the samples PLD0.2O2 have also the ε phase in their crystal structure, verified from the Raman modes at wavenumbers 67, 97, 144, 183, 203, 272, 303, 370, 425, 644, and 680 cm^{-1} (Wang et al., 2008; Johansson et al., 2012; Souza Filho et al., 2000). Similarly as the reflections in XRD measurements, both γ phase and ε phase have Raman modes either at same wavenumbers or very close to each other.

At this point it should be noted that usually the ferroelectric ε phase only exists in temperatures below −40 °C. However, different studies (Wang et al., 2008; Righettoni et al., 2010; Johansson et al., 2012) show that the ε phase can exist in a solid-state form also at temperatures above RT. The

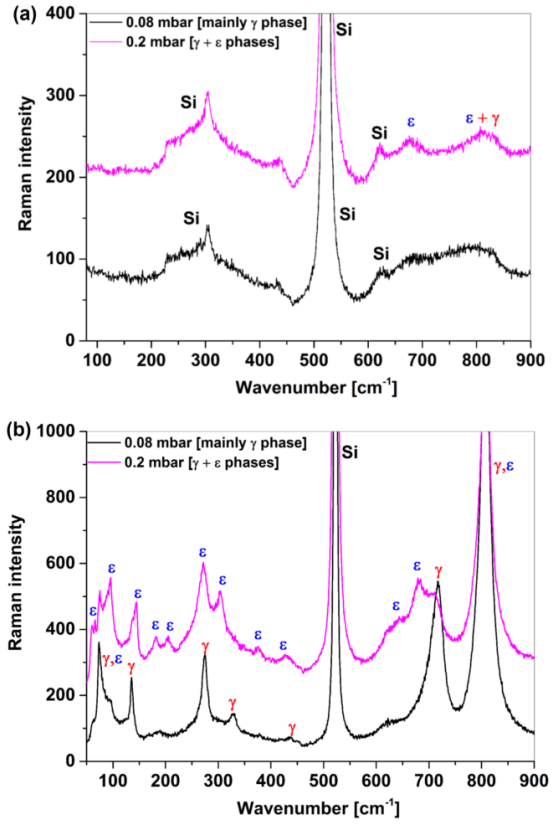

Figure 2. Raman spectra of the deposited WO_3 layers **(a)** as-deposited samples, **(b)** after annealing at 400 °C for 1 h.

reason for this is believed to be the small particle size of the samples, similarly as in the samples presented in this study. Also, the existence of the ε phase in the WO_3 composition has been proven to enhance WO_3 structures sensitivity to acetone (Wang et al., 2008; Righettoni et al., 2010; Sood and Gouma, 2013). The reason was suggested to be the ferroelectricity of the ε phase, namely the spontaneous electric dipole moments it possesses, which are then highly contributing to the chemical reaction between the WO_3 surface and the target gas.

2.3 Film composition characterization of the sensing layers

The surface morphology of the as-deposited and annealed WO_3 samples was studied by atomic force microscopy, and the results are shown in Fig. 3. The surface micrographs of the as-deposited layer and the annealed layer of sample PLD0.08O2 are shown in Fig. 3a and b, respectively. The sample surfaces consist of small agglomerates of nanopar-

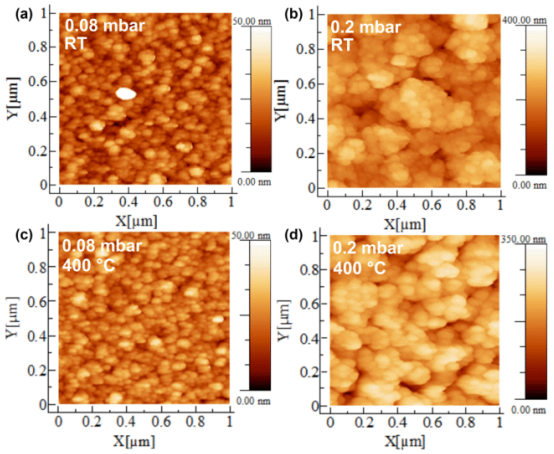

Figure 3. Atomic force microscopy surface micrographs of the deposited WO_3 layers showing the influence of oxygen partial pressure during deposition **(a, b)** as-deposited samples, **(c, d)** after annealing at 400 °C for 1 h.

ticles. In Fig. 3c and d, the surface micrographs of the as-deposited layer and the annealed layer of sample PLD0.2O2 are shown, respectively. The layers consist also of small nanoparticles, but agglomerated to bigger clusters. Also, the layer structure is much rougher and more porous than on the samples deposited at 0.08 mbar O_2. It can also be clearly seen that the annealing process at 400 °C for 1 h does not have a great effect on the surfaces of the samples. In both cases, the average surface roughness value R_q was the same before and after the annealing process, being $R_q = 5.5$ nm for sample PLD0.08O2, and $R_q = 42.2$ nm for sample PLD0.2O2. The crystallization, which is observed for the PLD0.08O2 sample seems to be a local process that does not involve larger-scale material transport.

Scanning electron microscopy was used to further study the film composition of the samples. Both surface micrographs and cross-section micrographs were taken from the samples. In Fig. 4a and b the cross-section micrograph and surface micrograph of the as-deposited sample fabricated at $p(O_2) = 0.08$ mbar are shown, respectively. The cross-section graph shows that the film is composed of small nanoparticle agglomerates formed as pillar-like structures, with some porosity in between the columns. The surface graph shows that the film surface is formed of small nanoparticle agglomerates and thus verifies the measurements made with AFM. The cross-section micrograph and surface micrograph of the as-deposited sample fabricated at $p(O_2) = 0.2$ mbar are shown in Fig. 4b and c, respectively. Now the film composition is much more porous and rough compared to the PLD0.08O2 film, and also the nanoparticle agglomerate size is larger. The agglomerates form clearer pillar-like morphology on top of the substrate. The surface of the film is

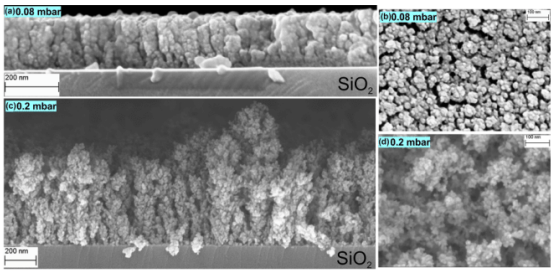

Figure 4. Scanning electron microscopy micrographs (cross sections and top views) of the as-deposited WO_3 layers deposited **(a, b)** at $p(O_2) = 0.08$ mbar, and **(c, d)** at $p(O_2) = 0.2$ mbar.

highly porous, concurrent with the AFM measurements performed.

3 Gas sensor performance

3.1 Gas test measurement setup

The gas sensing performance of the two sensor layers was evaluated in an extensive test measurement. The three target VOC gases were applied in three concentrations each, the middle concentrations representing the respective WHO guideline values of 0.1 mg m^{-3} (81 ppb) for formaldehyde and 0.01 mg m^{-3} (1.9 ppb) for naphthalene (World Health Organization, 2010), as well as the European Union guideline value of 5 µg m^{-3} (1.6 ppb) for benzene (European Parliament, Council of the European Union, 2008). Additionally, ethanol was introduced as a background gas in two concentrations, both much higher than the target gas concentrations. As the third varied parameter, the gas humidity was set in three steps. Table 1 shows all gases and concentrations.

The test gases were generated in a gas mixing system specifically designed for trace gases by Helwig et al. (2014). The gases were mixed into zero air produced by two cascaded zero air generators. Ethanol and formaldehyde test gases were taken from gas cylinders and diluted into the zero air carrier gas stream, either with a one-step dilution (ethanol) or a two-step dilution (formaldehyde). Benzene and naphthalene test gases were generated from permeation tubes in permeation ovens. Each target VOC concentration was set twice during each combination of humidity and ethanol background, first from highest to lowest concentration, then back to the highest concentration. The length of each VOC run was 30 min; between two trace VOC applications the sensors were purged with zero air with the respective ethanol and humidity configuration. In total, 90 different gas mixtures were generated and tested with the sensors; the total length of the measurement was 123 h.

For temperature cycled operation of the sensors, a ramp-up–ramp-down approach was chosen; the temperature of the microheaters was increased from 200 to 400 °C in 20 s and

Table 1. Test gas setup. Each gas concentration was applied at each EtOH background and humidity level for 30 min; between gas exposures sensors were exposed to background for 30 min.

Gas	Concentration (ppb)	EtOH background (ppm)	Humidity (% RH)
Zero air		0; 0.5; 2	30, 50, 70
Formaldehyde	200, 80, 40, 40, 80, 200	0; 0.5; 2	30, 50, 70
Benzene	2.5, 1.5, 0.5, 0.5, 1.5, 2.5	0; 0.5; 2	30, 50, 70
Naphthalene	5, 2, 1, 1, 2, 5	0; 0.5; 2	30, 50, 70

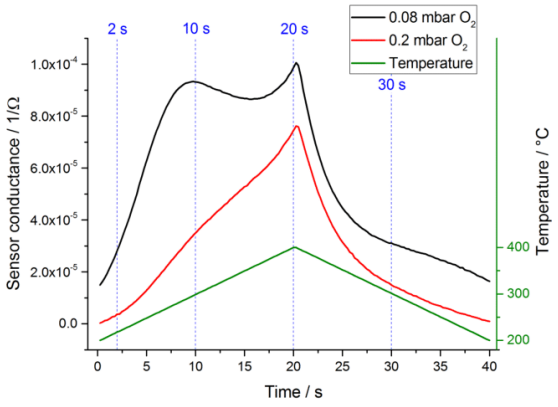

Figure 5. Gas sensor temperature cycle (green) and corresponding sensor signals of the two PLD WO_3 sensors in air at 30 % RH. The dashed lines indicate the selected points for quasi-static sensor signal analysis (cf. Fig. 6).

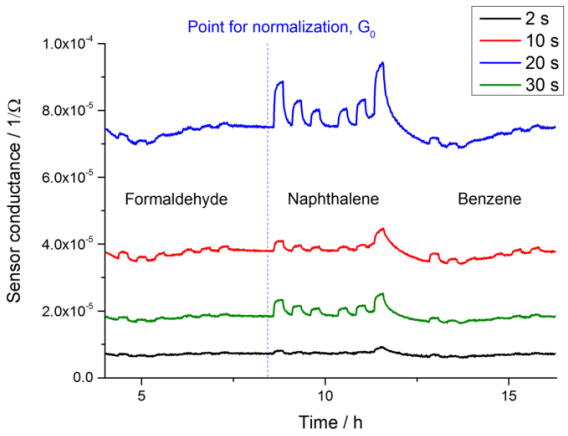

Figure 6. Quasi-static sensor signals for the four points indicated in Fig. 5 during exposure of the PLD0.2O2 sensor to formaldehyde, naphthalene and benzene at relevant ppb levels (Table 1) in air at 30 % RH without EtOH background. For later normalization, the value G_0 was extracted during background before the first exposure to naphthalene as indicated.

then reduced back to 200 °C in the same time, creating a 40 s cycle (see Fig. 5). The two sensor types clearly show differing behavior during the temperature cycle, especially during increase of the heater temperature.

3.2 Gas measurement results

For a first signal evaluation, quasi-static sensor signals were extracted from the raw sensor signal data sets. These signals were generated by plotting the signal value of certain points in the TCO cycle for each cycle, i.e., over the course of the complete measurement. An example of the PLD0.2O2 sensor is given in Fig. 6. Four points of the temperature cycle were selected, indicated in Fig. 5. A section of the measurement was chosen in which all three test VOCs are applied at 30 % RH gas humidity and without ethanol background. The sensor response to all concentrations of naphthalene is clearly visible, as well as the much lower responses to the other VOCs. By normalizing the signals, i.e., calculating the relative change of conductance G/G_0, the sensor response to naphthalene at the different points in the cycle can be determined (cf. Fig. 7). In this plot, it can be seen that the highest sensitivity, of the chosen points in the cycle, is during cooling of the sensor, 30 s after start of the cycle. The

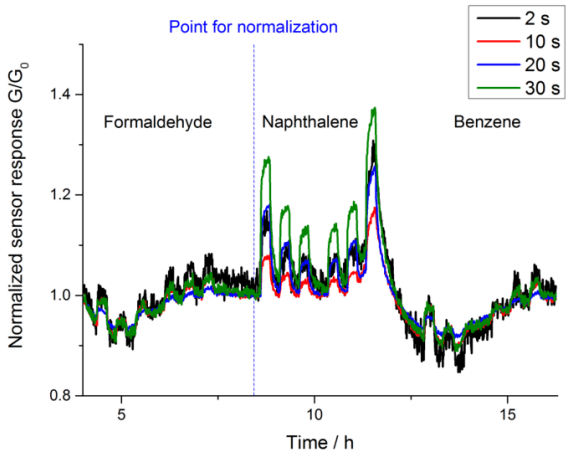

Figure 7. Normalized quasi-static signals for sensor PLD0.2O2 for the four selected points in the temperature cycle (cf. Fig. 5).

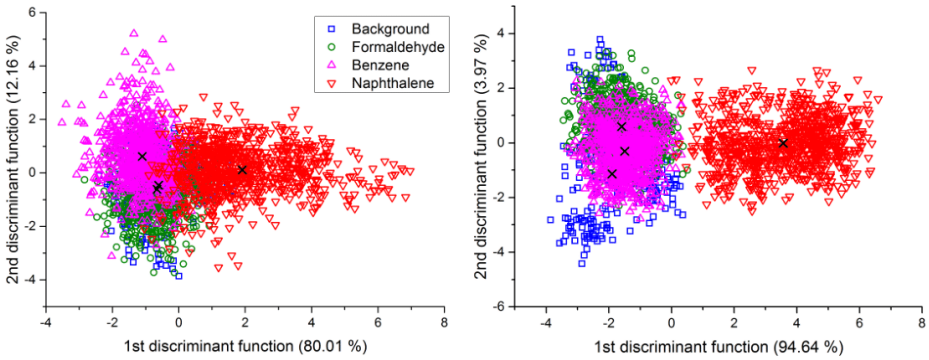

Figure 8. LDA plots for discrimination of different VOCs under varying humidity (30–70 % RH) and changing ethanol background (0–2 ppm), left: PLD0.08O2; right: PLD0.2O2.

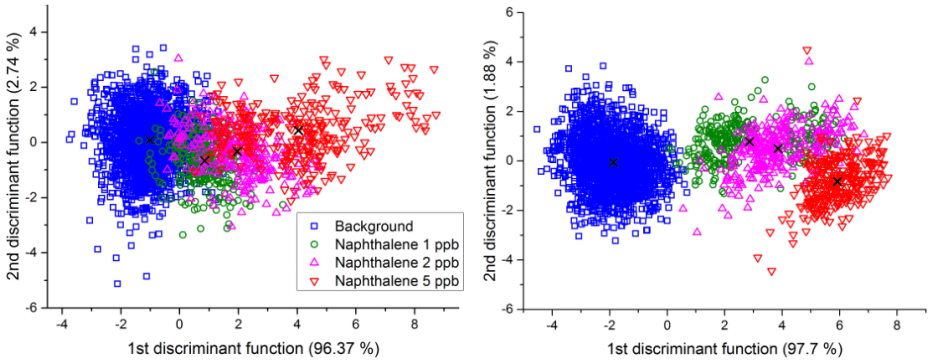

Figure 9. LDA plots for quantification of naphthalene under varying humidity (30–70 % RH) and changing ethanol background (0–2 ppm), left: PLD0.08O2; right: PLD0.2O2.

change of conductance is approx. 15 % for 1 ppb of naphthalene. The reason for the high selectivity to naphthalene is not known in detail and should be studied more closely. However, it was reported earlier that WO_3 has a specific response to aromatic compounds (Sauerwald, 2008) and that in general higher molecular weight leads to an increased sensitivity for this material (Sauerwald, 2008; Kohl et al., 2000).

The dynamic sensor signal patterns were analyzed using LDA. The whole procedure of generating data sets for LDA from dynamic gas sensor signals and the options for LDA application were described by Bur et al. (2014). As input data for each sensor, a limited number of features were extracted from the respective sensor signal of each temperature cycle. In this case, the cycle was divided into 20 segments of equal length (2 s). For each segment, the mean value and the slope of the sensor signal were calculated and used as features. This generates a feature vector with 40 values for each temperature cycle. These data sets were grouped into different groups, depending on the desired data analysis.

For the first analysis, the complete data set, containing 2799 feature vectors, was used as input data for the LDA. All cycles which contain a certain VOC were grouped together, regardless of VOC concentration, humidity and ethanol background. This results in one group for each target VOC and a "background" group, which contains the data sets of the TCO cycles which ran when no trace VOC was applied. This analysis checks the performance of the sensors to discriminate the target gases in varying humidity and background conditions. The LDA result plots for the two sensors with the PLD layers are shown in Fig. 8, left for the PLD0.08O2 sensor and right for the PLD0.2O2 type. For both sensors, the background, formaldehyde and benzene groups are overlapping strongly, while the naphthalene group is more separated. Especially for the PLD0.2O2 sensor the naphthalene group is nearly completely split from the other gases.

As a quantitative measure of the discrimination result, leave-one-out cross validation was performed on the data (LOOCV; Gutierrez-Osuna, 2002), with k nearest neighbors (kNN, $k = 5$) as classifier. This method calculates how many

Table 2. Leave-one-out cross-validation (LOOCV) results for all LDA investigations.

LDA no.	Analysis	PLD0.08O2	PLD0.2O2
1a	Gas discrimination (all gases)	66.5 %	71.9 %
1b	Gas discrimination (naphthalene)	86.3 %	99.2 %
2	Naphthalene quantification (full data set)	83.4 %	94.0 %
3	Naphthalene quantification (reduced data set, only 0 ppm EtOH background)	99.3 %	99.7 %
4	Humidity quantification	100 %	99.7 %
5a	Gas discrimination (all gases, only 50 % RH)	85.4 %	86.7 %
5b	Gas discrimination (naphthalene, only 50 % RH)	91.0 %	100 %

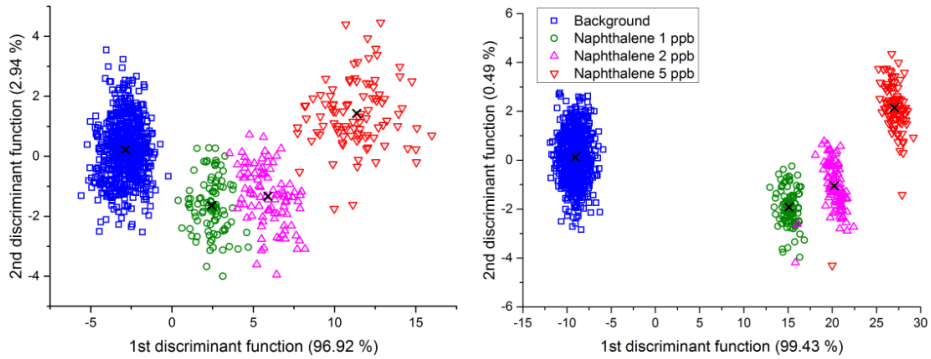

Figure 10. LDA plots for quantification of naphthalene under varying humidity (30–70 % RH) but with 0 ppm ethanol background, left: PLD0.08O2; right: PLD0.2O2.

feature vectors are classified correctly whether the LDA is trained by all other vectors.

Of the two sensors, the one with the PLD0.2O2 layer shows the better discrimination result overall, with 71.9 % correctly classified data points. The PLD0.08O2 achieves 66.5 %. The same order is given for classification of the naphthalene data points. The layer deposited at 0.2 mbar of O_2 shows a much better classification performance (99.2 % correct classifications) compared to the second sensor. The LOOCV results are summarized in Table 2, LDA 1a and 1b.

In the next step, it was checked if a quantification of the naphthalene concentration was possible. The full data set was used again. Each naphthalene concentration was assigned a group (with all humidities and ethanol backgrounds), and the other VOCs were assigned to the background group. The results for both tested sensors are plotted in Fig. 9. In this analysis, the PLD0.2O2 sensor shows the best separation of the groups again. There are some data points from the 1 ppb group located in the 2 ppb group. Otherwise, the three naphthalene concentrations are well lined up along the first discriminant axis. The PLD0.08O2 sensor shows less discrimination of the groups, which is also shown in LOOCV results (see Table 2, LDA 2).

The same analysis was attempted with a reduced data set, which included only the segments of the measurement without the ethanol background (950 sensor cycles in total). This significantly increases the quality of discrimination and thus naphthalene quantification for the sensors (see Fig. 10). Especially the PLD0.2O2 sensor has excellent separation of the naphthalene concentrations along the first discriminant function; the PLD0.08O2 sensor layer has much wider groups. The LOOCV results, listed in Table 2, LDA 3, show nearly 100 % correct classifications for the better sensor (PLD0.2O2); the second sensor layer also has over 99 % success rate.

Another evaluation of the sensor data was performed regarding quantification of gas humidity. The full data set was split into three groups, for the three gas humidities set during the measurement. This LDA run checks the sensors' cross-sensitivity to humidity, which also shows if the sensor would be able to measure the gas humidity. See Fig. 11 for the LDA result plots. These plots and the corresponding LOOCV results (Table 2, LDA 4) show very good discrimination of the humidities, which means that the sensor layers deposited by PLD have considerable sensitivity to water. However, this also means that the sensors could be used to measure the gas humidity or that the sensor performance could be monitored by comparing the predicted gas humidity with the value of a reference humidity sensor.

If the gas humidity is known, either from the gas sensor itself or from an additional humidity sensor, the quality of the signal processing can be improved by calculating different

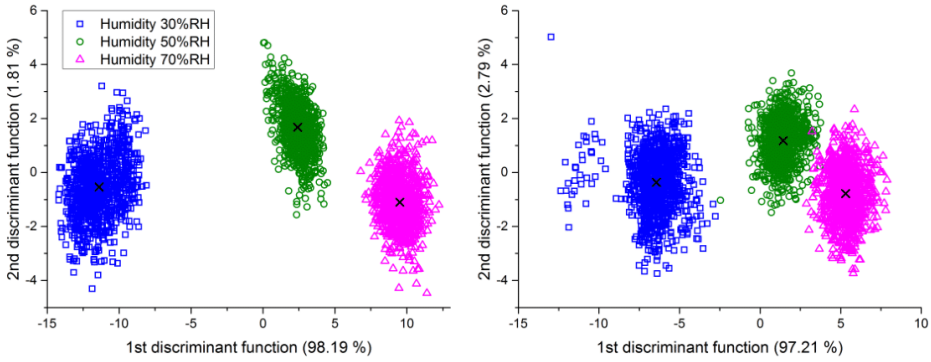

Figure 11. LDA plots for discrimination of ambient humidity levels for all sensor cycles with and without VOCs under varying ethanol background (0–2 ppm), left: PLD0.08O2; right: PLD0.2O2.

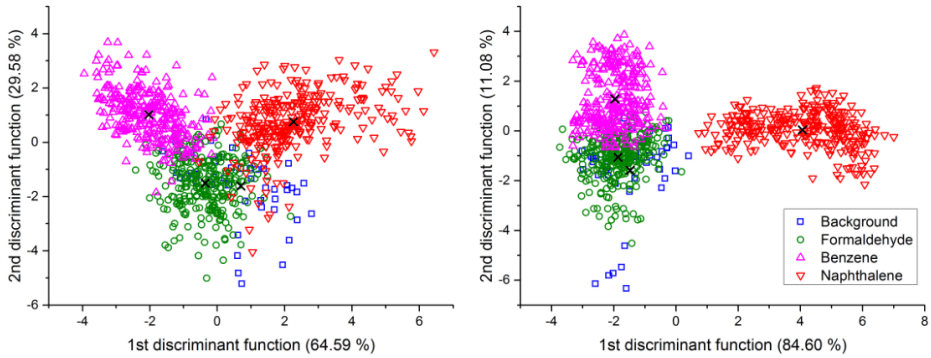

Figure 12. LDA plots for discrimination of different VOCs under constant humidity (50 % RH) and changing ethanol background (0–2 ppm), left: PLD0.08O2; right: PLD0.2O2.

LDA projections for several humidity ranges. A simple version of this approach has been tested by reducing the data set to the sensor signals acquired in one humidity, in this case all cycles measured in 50 % RH. The LDA result for gas identification for this is shown in Fig. 12. Compared to the full data set with three humidity levels (Fig. 8), the separation of the gases is clearly improved, especially for the PLD0.08O2 sensor. LOOCV also shows significant improvement of the classification results (Table 1, LDA 5). For all gases, the ratio of correct classifications was raised from 66.5 to 85.4 % for sensor PLD0.08O2 and from 71.9 to 86.7 % for sensor PLD0.2O2. For the naphthalene group, perfect classification was achieved for the sensor with 0.2 mbar O_2 partial pressure (Table 1, LDA 5b). A hierarchical data processing approach, which in the first step determines the humidity and in the second step classifies the gas, seems promising.

4 Conclusions

Nanoporous WO_3 gas sensing layers have successfully been prepared via nanosecond pulsed laser deposition, characterized, and tested for their gas sensing performance, especially for use in IAQ applications.

The characterization of the PLD sensing layers showed films formed of nanoparticle agglomerates with pillar-like morphology. The films were highly porous in their structure, especially when higher oxygen partial pressure was used during the deposition process. The crystal structure of the films was also dependent on the oxygen partial pressure with higher O_2 pressure resulting in the formation of $WO_3\varepsilon$ phase, which in bulk WO_3 samples is only stable at temperatures below −40 °C. The ε phase in the PLD films was observed to withstand annealing at 400 °C for 1 h probably due to its monocrystalline structure.

The two compared PLD sensor layer samples showed significant differences in their gas sensing performance. The layer deposited at higher oxygen partial pressure displayed improved response and excellent selectivity to naphthalene.

Both discrimination of different target VOCs and quantification of naphthalene were more successful with this sensor.

Naphthalene concentrations down to 1 ppb could be quantified with the sensor layer deposited at 0.2 mbar of O_2 with nearly 100 % success rate as determined by leave-one-out cross validation when no ethanol background was present. Even in varying ethanol background of up to 2 ppm, quantification was still successful for 94 % of all temperature cycles for this sensor. Detection of the presence of naphthalene in concentrations of 1 ppb or more had a success rate of more than 99 %, again determined by LOOCV.

The highly porous structure and possibly the formation of the WO_3 ε phase resulting from the higher oxygen pressure during PLD thus boost the gas sensing performance considerably. With the selected parameters, suitable gas sensing layers for detection and quantification of naphthalene have been obtained. Future investigations will address further improvement of the gas sensitive layers, e.g., by further variations of the deposition parameters as well as introduction of additional nanoparticles for doping and catalytic activation. We are also planning to study PLD deposition based on picosecond laser pulses which allows further optimization of the deposition parameters.

Acknowledgements. This project has received funding from the European Union's Seventh Framework Programme for research, technological development and demonstration under grant agreement no. 604311, Project SENSIndoor.

Edited by: M. Penza
Reviewed by: two anonymous referees

References

Balandeh, M., Mezzetti, A., Tacca, A., Leonardo, S., Marra, G., Divitini, G., Ducati, C., Medad, L., and Di Fonzo, F.: Quasi-1D hyperbranched WO_3 nanostructures for low-voltage photoelectrochemical water splitting, J. Mater. Chem. A, 3, 6110–6117, doi:10.1039/C4TA06786J, 2015.

Balazsi, C., Wang, L., Zayim, E. O., Szilagy, I. M., Sedlackov, K., Pfeifer, J., Toth, A. L., and Gouma, P.-I.: Nanosize hexagonal tungsten oxide for gas sensing applications, J. Eur. Ceram. Soc., 28, 913–917, doi:10.1016/j.jeurceramsoc.2007.09.001, 2008.

Baur, T., Schütze, A., and Sauerwald, T.: Optimierung des temperaturzyklischen Betriebs von Halbleitergassensoren, tm – Technisches Messen, 82, 187–195, doi:10.1515/teme-2014-0007, 2014.

Bernstein, J. A., Alexis, N., Bacchus, H., Leonard Bernstein, I., Fritz, P., Horner, E., Li, N., Mason, S., Nel, A., Oullette, J., Reijula, K., Reponen, T., Seltzer, J., Smith, A., and Tarlo, S. M.: The health effects of nonindustrial indoor air pollution, J. Allergy Clin. Immun., 121, 585–591, doi:10.1016/j.jaci.2007.10.045, 2008.

Bur, C., Reimann, P., Andersson, M., Schütze, A., and Lloyd Spetz, A.: Increasing the Selectivity of Pt-Gate SiC Field Effect Gas Sensors by DynamicTemperature Modulation, IEEE Sens. J., 12, 1906–1913, doi:10.1109/JSEN.2011.2179645, 2012.

Bur, C., Bastuck, M., Lloyd Spetz, A., Andersson, M., and Schütze, A.: Selectivity enhancement of SiC-FET gas sensors by combining temperature and gate bias cycled operation using multivariate statistics, Sensor. Actuat. B-Chem., 193, 931–940, doi:10.1016/j.snb.2013.12.030, 2014.

Caricato, A. P., Luches, A., and Rella, R.: Nanoparticle thin films for gas sensors prepared by matrix assisted pulsed laser evaporation, Sensors, 9, 2682–2696, doi:10.3390/s90402682, 2009.

European Parliament, Council of the European Union: Directive 2008/50/EC of the European Parliament and of the Council of 21 May 2008 on ambient air quality and cleaner air for Europe, Official Journal of the European Union, 51, 2008.

Gramm, A. and Schütze, A.: High performance solvent vapor identification with a two sensor array using temperature cycling and pattern classification, Sensor. Actuat. B-Chem., 95, 58–65, doi:10.1016/S0925-4005(03)00404-0, 2003.

Guo, H., Lee, S. C., Chan, L. Y., and Li, W. M.: Risk assessment of exposure to volatile organic compounds in different indoor environments, Environ. Res., 94, 57–66, doi:10.1016/S0013-9351(03)00035-5, 2004.

Gutierrez-Osuna, R.: Pattern Analysis for machine olfaction: A review, IEEE Sens. J., 2, 189–202, doi:10.1109/JSEN.2002.800688, 2002.

Harilal, S. S., Bindhu, C. V., Tillack, M. S., Najmabadi, F., and Gaeris, A. C.: Internal structure and expansion dynamics of laser ablation plumes into ambient gases, J. Appl. Phys., 93, 2380–2388, doi:10.1063/1.1544070, 2003.

Heilig, A., Bârsan, N., Weimar, U., Schweizer-Berberich, M., Gardner, J. W., and Göpel, W.: Gas identification by modulating temperatures of SnO_2-based thick film sensors, Sensor. Actuat. B-Chem., 43, 45–51, doi:10.1016/S0925-4005(97)00096-8, 1997.

Helwig, N., Schüler, M., Bur, C., Schütze, A., and Sauerwald, T.: Gas mixing apparatus for automated gas sensor characterization, Meas. Sci. Technol., 25, 055903, doi:10.1088/0957-0233/25/5/055903, 2014.

Huotari, J., Lappalainen, J., Puustinen, J., Baur, T., Alépée, C., Haapalainen, T., Komulainen, S., Pylvänäinen, J., and Lloyd Spetz, A.: Pulsed laser deposition of metal oxide nanoparticles, agglomerates, and nanotrees for chemical sensors, Procedia Eng., 120, 1158–1161, doi:10.1016/j.proeng.2015.08.745, 2015.

Hussain, O. M., Swapnasmitha, A. S., John, J., and Pinto, R.: Structure and morphology of laser-ablated WO_3 thin films, Appl. Phys. A, 81, 1291–1297, 2005.

Infortuna, I., Harvey, A. S., and Gauckler, L. J.: Microstructures of CGO and YSZ thin films by pulsed laser deposition, Adv. Funct. Mater., 18, 127–135, doi:10.1007/s00339-004-3041-z, 2008.

Johansson, M. B., Niklasson, G. A., and Österlund, L.: Structural and optical properties of visible active photocatalytic WO_3 thin films prepared by reactive dc magnetron sputtering, J. Mater. Res., 27, 3130–3140, doi:10.1557/jmr.2012.384, 2012.

Jones, A. P.: Indoor air quality and health, Atmos. Environ., 33, 4535–4564, doi:10.1016/S1352-2310(99)00272-1, 1999.

Klecka, W. R.: Discriminant Analysis, in: Quantitative applications in the social sciences, SAGE University Paper, 72 pp., 1980.

Kohl, D., Heinert, L., Bock, J., Hofmann, Th., and Schieberle, P.: Systematic studies on responses of metal-oxide sensor surfaces to straight chain alkanes, alcohols, aldehydes, ketones, acids and

esters using the SOMMSA approach, Sensor. Actuat. B-Chem., 70, 43–50, doi:10.1016/S0925-4005(00)00552-9, 2000.

Koistinen, K., Kotzias, D., Kephalopoulos, S., Schlitt, C., Carrer, P., Jantunen, M., Kirchner, S., McLaughlin, J., Mølhave, L., Fernandes, E. O., and Seifert, B.: The INDEX project: executive summary of a European Union project on indoor air pollutants, Allergy, 63, 810–819, doi:10.1111/j.1398-9995.2008.01740.x, 2008.

Lee, A. P. and Reedy, B. J.: Temperature modulation in semiconductor gas sensing, Sensor. Actuat. B-Chem., 60, 35–42, doi:10.1016/S0925-4005(99)00241-5, 1999.

Leidinger, M., Sauerwald, T., Reimringer, W., Ventura, G., and Schütze, A.: Selective detection of hazardous VOCs for indoor air quality applications using a virtual gas sensor array, J. Sens. Sens. Syst., 3, 253–263, doi:10.5194/jsss-3-253-2014, 2014.

Marinkovic, B., Ribeiro de Avillez, R., Saavedra, A., and Assunção, F. C. R.: A comparison between the Warren-Averbach method and alternate methods for x-ray diffraction microstructure analysis of polycrystalline specimens, Mat. Res., 4, 71–76, doi:10.1590/S1516-14392001000200005, 2001.

Meier, D. C., Evju, J. K., Boger, Z., Raman, B., Benkstein, K. D., Martinez, C. J., Montgomery, C. B., and Semancik, S.: The potential for and challenges of detecting chemical hazards with temperature-programmed microsensors, Sensor. Actuat. B-Chem., 121, 282–294, doi:10.1016/j.snb.2006.09.050, 2007.

Nam, H.-J., Sasaki, T., and Koshizaki, N.: Optical CO gas sensor using a cobalt oxide thin film prepared by pulsed laser deposition under various argon pressures, J. Phys. Chem. B, 110, 23081–23084, doi:10.1021/jp063484f,2006.

Paczkowski, S., Paczkowska, M., Dippel, S., Schulze, N., Schütz, S., Sauerwald, T., Weiß, A., Bauer, M., Gottschald, J., and Kohl, C.-D.: The olfaction of a fire beetle leads to new concepts for early fire warning systems, Sensor. Actuat. B-Chem., 183, 273–282, doi:10.1016/j.snb.2013.03.123, 2013.

Pihosh, Y., Turkevych, I., Mawatari, K., Uemura, J., Kazoe, Y., Kosar, S., Makita, K., Sugaya, T., Matsui, T., Fujita, D., Tosa, M., Kondo, M., and Kitamori, T.: Photocatalytic generation of hydrogen by core-shell WO_3/$BiVO_4$ nanorods with ultimate water splitting efficiency, Sci. Rep., 5, 11141, doi:10.1038/srep11141, 2015.

Reimann, P. and Schütze, A.: Fire detection in coal mines based on semiconductor gas sensors, Sensor Rev., 32, 47–58, doi:10.1108/02602281211197143, 2012.

Righettoni, M., Tricoli, A., and Pratsinis, S: Si : WO_3 Sensors for Highly Selective Detection of Acetone for Easy Diagnosis of Diabetes by Breath Analysis, Anal. Chem., 82, 3581–3587, doi:10.1021/ac902695n, 2010.

Sauerwald, T.: Nachweis von Luftschadstoffen mit Halbleiter-Gassensoren – Möglichkeiten und Einschränkungen, VDI-Berichte 2011, VDI Verlag GmbH, Düsseldorf, 2008.

Sood, S. and Gouma, P.-I.: Polymorphism in nanocrystalline binary metal oxides, Nanomater. Energy, 2, 82–96, 2013.

Souza Filho, A. G., Freire, P. T. C., Pilla, O., Ayala, A. P., Mendes Filho, J., Melo, F. E. A., Freire, V. N., and Lemos, V.: Pressure effects in the Raman spectrum of WO_3 microcrystals, Phys. Rev. B., 62, 3699–3703, doi:10.1103/PhysRevB.62.3699, 2000.

Wang, L., Teleke, A., Pratsinis, S. E., and Gouma, P.-I.: Ferroelectric WO_3 nanoparticles for acetone selective detection, Chem. Mater., 20, 4794–4796, doi:10.1021/cm800761e, 2008.

World Health Organization: WHO Guidelines for Indoor Air Quality: Selected Pollutants, Geneva, 2010.

Wu, C.-H., Feng, C.-T., Lo, Y.-S., Lin, T.-Y., and Lo, J.-G.: Determination of volatile organic compounds in workplace air by multisorbent adsorption/thermal desorption-GC/MS, Chemosphere, 56, 71–80, doi:10.1016/j.chemosphere.2004.02.003, 2004.

Zheng, H., Zhen Ou, J., Strano, M. S., Kaner, R. B., Mitchell, A., and Kalantar-zadeh, K.: Nanostructured tungsten oxide – Properties, synthesis, and applications, Adv. Funct. Mater., 21, 2175–2196, doi:10.1002/adfm.201002477, 2011.

5 Selective detection of hazardous VOCs for indoor air quality applications using a virtual gas sensor array

Martin Leidinger[1], Tilman Sauerwald[1], Wolfhard Reimringer[2], Gabriela Ventura[3] and Andreas Schütze[1]

[1] Saarland University, Lab for Measurement Technology, Saarbrücken, Germany

[2] 3S GmbH, Saarbrücken, Germany

[3] IDMEC – Institute of Mechanical Engineering, Porto, Portugal

Originally published in *Journal of Sensors and Sensor Systems, 3, pp. 253-263, 2014*

doi: 10.5194/jsss-3-253-2014

Synopsis

In the previous chapter, virtual multisensor operation and LDA signal processing were applied to MOS gas sensors in order to improve their performance in the measurement of a specific target gas, naphthalene. The publication in this chapter adds a real multisensor approach to the setup; eventually, the signals of the virtual gas sensor array and the real gas sensor array are fused for further improvement of identification of three target gases in varying humidity and background conditions. Three different gas sensors with different sensing materials were chosen for the task of detection and discrimination of benzene, formaldehyde, and naphthalene in low ppb concentrations. In addition to gas sensors operated by laboratory measurement electronics, integrated

gas sensor systems designed for indoor VOC detection were characterized with the same test gas mixtures. Both the laboratory test setup and the sensor systems use the same types of MOS gas sensors and the same TCO cycle variants, which allows for determination of the influence of parameters which are changed by integrating the sensor devices into compact systems. The most relevant are integration of the sensors on a PCB (printed circuit board) and in a housing, both of which pose additional gas sources in direct vicinity of the gas sensors, as well as switching the method of supplying the test gas to the sensors. The effect of having the sensors integrated in the sensor system has been investigated by sampling and evaluating the gas emissions from the sensor system using TD-GC-MS analysis. This showed a significant increase of VOCs emitted from the systems during operation, which represents a background gas atmosphere for the sensors and results in decreased sensing performance compared to the sensors in the laboratory setup. Regarding the gas transport to the sensors, for the single sensors, a small test chamber volume with a directed flow is used, while the sensor systems are placed inside a larger test volume in which the gas flow rate is much lower. As the sensors are mounted inside the housing behind a number of vents, gas transport is at least partially based on diffusion. This also affects the gas concentration at the sensors, especially after changes in the gas atmosphere, and thus additionally impairs sensing performance.

In the presented measurement campaign, only thick film sensors on ceramic substrates with resulting long time constants are used; therefore, the TCO cycle lengths are quite long at 3 min for two of the sensor types, and 1 min for the third. For the intended application, indoor air quality monitoring, this is sufficient, as the gas composition does not change very quickly. However, the thermal characteristics of the sensors result in a relatively simple temperature profile; for two of the sensor types, both using SnO_2 variations as sensitive layers, only two temperature levels are set, with linear heating and cooling transitions between temperature levels. For the third sensor type, a ramp up / ramp down cycle has been chosen. It has a different sensing material, tungsten trioxide (WO_3), which does not show the relaxation effects of SnO_2 after temperature changes which were described in chapter 2.1.2. Therefore, linear heating

and cooling were chosen, as this mode of operation covers a wide range of temperatures and sensor states.

The measurement results of both the isolated sensor elements and the assembled sensor systems show the potential of the sensors to detect and discriminate the three VOC gases in ppb concentrations, even in the presence of an ethanol background in the ppm range, i.e. three orders of magnitude higher than the target compounds.

The publication addresses three main issues:

- Sensing abilities of different types of thick film MOS gas sensors in TCO for VOCs in the ppb range with additional background in general
- Improvement of gas detection when combining the signals of several sensors during signal processing
- Effects on sensing performance if the sensors are operated in a stand-alone sensor system on a PCB inside a plastic housing

J. Sens. Sens. Syst., 3, 253–263, 2014
www.j-sens-sens-syst.net/3/253/2014/
doi:10.5194/jsss-3-253-2014

JSSS Journal of Sensors and Sensor Systems Open Access

Selective detection of hazardous VOCs for indoor air quality applications using a virtual gas sensor array

M. Leidinger[1], T. Sauerwald[1], W. Reimringer[2], G. Ventura[3], and A. Schütze[1]

[1]Saarland University, Lab for Measurement Technology, Saarbrücken, Germany
[2]3S GmbH, Saarbrücken, Germany
[3]IDMEC – Institute of Mechanical Engineering, Porto, Portugal

Correspondence to: M. Leidinger (m.leidinger@lmt.uni-saarland.de)

Received: 31 July 2014 – Revised: 6 October 2014 – Accepted: 9 October 2014 – Published: 21 October 2014

Abstract. An approach for detecting hazardous volatile organic compounds (VOCs) in ppb and sub-ppb concentrations is presented. Using three types of metal oxide semiconductor (MOS) gas sensors in temperature cycled operation, formaldehyde, benzene and naphthalene in trace concentrations, reflecting threshold limit values as proposed by the WHO and European national health institutions, are successfully identified against a varying ethanol background of up to 2 ppm. For signal processing, linear discriminant analysis is applied to single sensor data and sensor fusion data.

Integrated field test sensor systems for monitoring of indoor air quality (IAQ) using the same types of gas sensors were characterized using the same gas measurement setup and data processing. Performance of the systems is reduced due to gas emissions from the hardware components. These contaminations have been investigated using analytical methods. Despite the reduced sensitivity, concentrations of the target VOCs in the ppb range (100 ppb of formaldehyde; 5 ppb of benzene; 20 ppb of naphthalene) are still clearly detectable with the systems, especially when using the sensor fusion method for combining data of the different MOS sensor types.

1 Introduction

The quality of indoor air (IAQ) is determined by the contamination of the air with various chemical compounds, such as carbon dioxide (CO_2), carbon monoxide (CO), nitrogen dioxide (NO_2) and volatile organic compounds (VOCs). Several investigations have been performed to determine the occurrence of these substances in indoor air, e.g., by Bernstein et al. (2008) or in European projects like the Airmex study (Geiss et al., 2011) and the INDEX project (Koistinen et al., 2008).

Negative health effects of exposure to these substances, even at low concentrations, mainly including the respiratory system and skin irritations, have been observed (Jones, 1999). Additionally, some VOCs (e.g., benzene) are carcinogenic, while others (e.g., formaldehyde) are suspected to be carcinogenic (Gou et al., 2004).

Hazardous VOCs pose a special problem. Despite that threshold limits for single substances are recommended for indoor air, e.g., by the WHO (World Health Organization, 2010), there is currently no online measurement technology commercially available to identify and quantify different volatile organic substances reliably and at reasonable cost. Monitoring total VOC (TVOC) concentrations is state of the art (Umweltbundesamt, 2007), but this parameter is not significant in terms of health effects since it also includes benign substances and cannot be attributed to symptoms like the sick building syndrome (Burge, 2004; Brinke et al., 1998). Selective VOC detection and quantification is today based on gas sampling and analytical techniques, especially gas chromatography coupled with mass spectrometry (GC-MS; Wu et al., 2004). The resulting high cost for individual measurements prevents ubiquitous VOC monitoring in IAQ applications today.

A possible application for selective VOC monitoring is demand-controlled ventilation in smart buildings. VOC levels can be used as an additional parameter for controlling indoor ventilation in addition to other indicators like

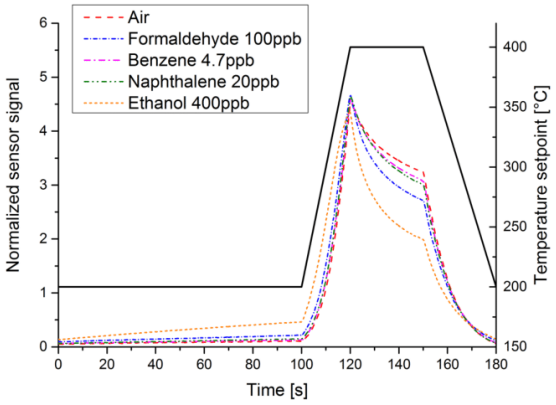

Figure 1. Temperature cycle (solid line) and normalized temperature cycle sensor signals (UST GGS 1330) in the presence of different gases.

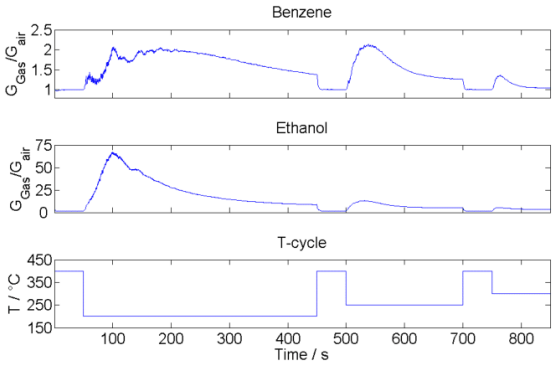

Figure 2. Sensor responses to 25 ppb of benzene and 500 ppb of ethanol during TCO optimization cycle at 12.5 % relative humidity (Fricke et al., 2014).

temperature and CO_2 levels. Then, selective measurement of single VOCs is necessary since ventilation should be increased only if thresholds of hazardous VOCs are exceeded.

From the wide range of VOCs, three compounds were selected for further investigations on selective detection: formaldehyde, benzene and naphthalene, which are three of the first priority harmful VOCs (Koistinen et al., 2008; World Health Organization, 2010). The selected target concentrations of these gases are 10 ppb for formaldehyde, 0.5 ppb for benzene and 2 ppb for naphthalene, based on international and European national regulations (e.g., World Health Organization, 2010; French decree no. 2011-1727, 2011; Sagunski and Heger, 2004). For benzene, the World Health Organization even states that there is no safe level due to its high carcinogenicity (World Health Organization, 2010). Thus, not only a high selectivity is required for identifying these gases but also a very high sensitivity in order to detect ppb levels of these specific VOCs.

One type of sensors which can detect VOCs in this concentration range is a metal oxide semiconductor (MOS) gas sensor (Schüler et al., 2013). MOS sensors in temperature cycled operation (TCO) are used here to measure the selected VOCs against a high background of interfering gas, similar to Reimann and Schütze. (2012). These sensors were also integrated in low-cost sensor systems designed for field testing and as a basis for future commercial online VOC monitoring devices.

2 TCO optimization

Semiconductor gas sensors are very sensitive sensors, but usually they are broadband sensors and show little selectivity to specific gases. One method to improve selectivity, sensitivity and also stability is temperature cycled operation (Lee and Reedy, 1999; Gramm and Schütze, 2003; Schüler et al., 2013). By modulating the operating temperature of the MOS sensing layer, different states of the sensor material itself (i.e., surface coverage with oxygen) and its interaction with gas molecules are activated, and thus different sensing characteristics are obtained. Figure 1 shows normalized sensor signals of the same temperature cycle when different gases are applied to a MOS gas sensor. The differences of the recorded signal shapes (i.e., slopes, average values in different sections) are obvious; these features are characteristic of specific gases.

Three types of ceramic substrate MOS gas sensors were evaluated for detection of the target VOCs: GGS 1330, GGS 2330 (both SnO_2 based) and GGS 5330 (WO_3 based) by UST Umweltsensortechnik GmbH (Geschwenda, Germany).

A method for optimizing the TCO cycle was evaluated. In order to find the most sensitive and most selective temperature transitions, the relaxation behavior from a high temperature to different lower temperatures was investigated. Specifically, temperature changes from 400 to 200 °C, 250 °C and 300 °C were performed with a GGS 1330 SnO_2 sensor with benzene and ethanol as test gases. The results are shown in Fig. 2.

The sensor response was calculated by dividing the sensor signal (conductivity of the sensitive layer) of a cycle in gas by the sensor signal of a cycle in pure air for each point of the cycle. The response has distinct peaks several seconds after the temperature steps from the high temperature to the lower temperatures – e.g., for ethanol 50 s after changing the sensor temperature from 400 to 200 °C. The sensor response after cooldown from 400 to 200 °C reaches approx. 67 for ethanol and then drops to approx. 9 at the steady state. Thus, the sensitivity is significantly increased in TCO mode due to non-equilibrium state of the sensor surface after temperature changes (Sauerwald et al., 2014). For benzene, the sensor

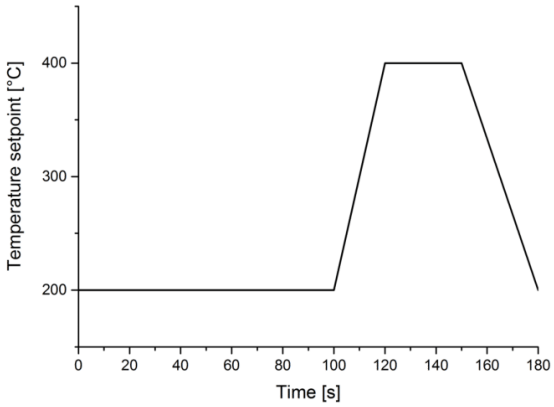

Figure 3. 180 s temperature cycle for the GGS 1330 and GGS 2330 SnO_2-based sensors.

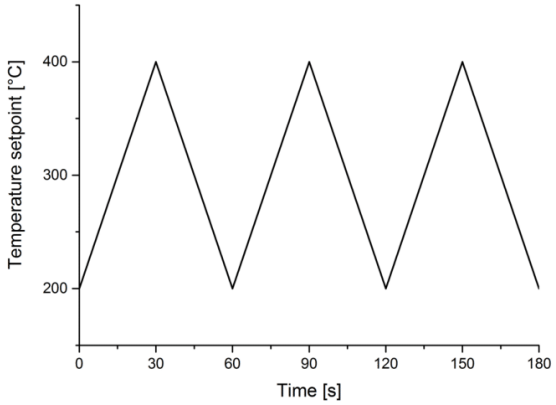

Figure 4. 60 s temperature cycle for the GGS 5330 WO_3-based sensor; three cycles are run in order to synchronize the signals with the 180 s cycle for the SnO_2 sensors.

response rises to 2.1 at the peak 36 s after the temperature transition from 400 to 250 °C compared to 1.3 at the steady state, corresponding to an almost 4-fold increase in sensitivity.

Based on these results, the temperature steps and the lengths of these steps were defined. For the SnO_2 sensors (GGS 1330 and GGS 2330) a two-step temperature cycle with ramp transitions was chosen (see Fig. 3). The ramps were implemented in order to achieve a defined heating up and cooling down of the sensitive layer independent of ambient temperature and humidity. The durations of the ramps are the result of the heating and cooling characteristics of the sensors. Due to the size of the ceramic substrates, heating up the sensors takes up to 20 s and cooling down even longer, up to 30 s. These are the values chosen for the respective ramps.

The length of the low temperature step is 100 s to cover all the response peaks of the previous optimization measurement. The total duration of the temperature cycle is 180 s, which is sufficiently short for the target application in IAQ monitoring.

The WO_3-based sensor (GGS 5330) did not show any delayed response maxima, but only a temperature-dependent response. Thus, a simple ramp up and down between 400 and 200 °C was selected covering the range of maximum sensitivity to the target gases (Fig. 4). The duration of a cycle is 60 s; to synchronize all sensors, three cycles of the WO_3-based sensor are run during one cycle of the two SnO_2-based sensors.

3 Sensor characterization measurements

The three target VOCs were applied in two concentrations each: one at the respective threshold limit value and one at the 10-fold value. Additionally, the measurements were performed with two concentrations of ethanol as a background interference gas and two values for the relative humidity (RH). Table 1 gives an overview for all concentration and humidity values.

The measurements were conducted with a gas mixing system which was designed and set up specifically for trace gas generation with wide concentration ranges by Helwig et al. (2014). The VOCs were diluted into a carrier gas stream of synthetic air (purity 5.0) either from a gas cylinder or from a permeation furnace. Total gas flow was 200 mL min^{-1}; the three sensors were set up in a stainless steel sensor chamber. Each of the 36 VOC gas configurations was applied for 30 min; between the VOC exposures the sensors were flushed with background (humid air plus ethanol) for 30 min to allow their return to the baseline and prevent carryover. The complete data set contained 940 temperature cycles for the SnO_2-based sensors and 2820 cycles for the WO_3-based sensor. Not all of the cycles were used for signal processing; for the "background" groups without the target VOCs, six sections with a length of approx. 15 SnO_2 cycles each were selected, one after each change of the background conditions (humidity, ethanol).

4 Signal evaluation and data processing

4.1 Sensor characterization

As a first analysis of the data, quasistatic sensor signals are examined. These are generated by choosing one point of the temperature cycle and extracting the signal value at this point in the cycle for every cycle of the measurement. These values are then plotted over the respective cycle number, which generates a plot of the sensor signal of a specific point of the cycle over time. An example is given in Fig. 5.

The sensor reactions to all target gases and especially to the ethanol background are clearly visible. This method is

Table 1. Test gas setup

Gas	Conc./ppb (µg m^{-3})	RH/%	EtOH background/ppm (mg m^{-3})
Synthetic air		40; 60	0; 0.4; 2 (0; 0.21; 1.06)
Formaldehyde	10; 100 (12.3; 123)	40; 60	0; 0.4; 2 (0; 0.21; 1.06)
Benzene	0.5; 4.7 (1.6; 15)	40; 60	0; 0.4; 2 (0; 0.21; 1.06)
Naphthalene	2; 20 (10.5; 105)	40; 60	0; 0.4; 2 (0; 0.21; 1.06)

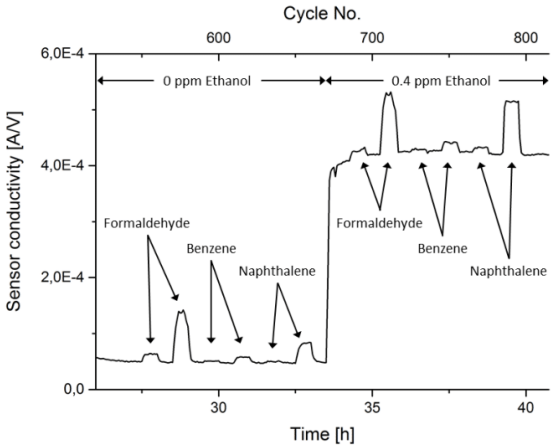

Figure 5. Section of the quasistatic sensor signal, UST GGS 1330, 60 %RH; the selected point of the cycle is the end of the low temperature step at 99 s (see Figs. 3/6).

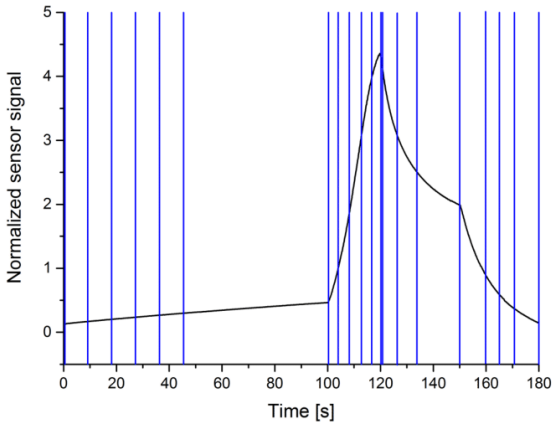

Figure 6. Selected feature ranges of the GGS 1330 and GGS 2330 sensor.

helpful for checking the nominal performance of the gas mixing system and to check the general response of the sensors to the gases. It is independent of the pattern recognition data analysis.

For further signal processing, the method of linear discriminant analysis (LDA) is applied (Gutierrez-Osuna, 2002). This pattern recognition technique can be used to separate different classes of input data while grouping data sets of the same type. In this case, it is used to assign the temperature cycle sensor signals to the different target gases. Thus, in the resulting plots, the algorithm should arrange all cycles of each target gas and background into one compact group while separating the groups of the different target VOCs and the background without VOCs from each other.

The approach used here is basically the same as presented by Bur et al. (2014). Input data sets for the LDA algorithm ("training", i.e., determination of LDA coefficients for the projection, and evaluation) are generated by extracting a set of features from each temperature cycle sensor signal. The temperature cycle is divided into several sections; 20 sections were chosen for the 180 s cycle for the GGS 1330/2330 sensors (see Fig. 6). From each section, features are calculated, in this case the mean value of the sensor signal and the slope of a linear fit. These features were chosen with regard to later implementation of the LDA calculations on the field test system microcontroller since they are easy to calculate. For the GGS 5330 sensor, the 60 s cycle was divided into 14 sections. This generates a data set of 40 (28) values for each sensor for each temperature cycle, which is used as input for the LDA.

As mentioned above, in the presented measurement the aim is identification of the target VOCs. The extracted data sets were therefore assigned to four groups, one group for each target VOC and one for the background gas without any of the three targets. Each of the three VOC groups thus contains the cycles that ran during the application of one VOC with both VOC concentrations, both gas humidities and all ethanol backgrounds, i.e., a total of 12 different conditions. The "background" group contains sections of synthetic air with both humidities and all ethanol background concentrations.

The result of the LDA calculation for the GGS 1330 sensor is shown in Fig. 7. Separation of the four groups is quite successful, but there is still some overlap. As a validation of the results, leave-one-out cross-validation (LOOCV) is performed (Gutierrez-Osuna, 2002). This method checks how many feature vectors are classified correctly if the LDA is trained by all other vectors. For the GGS 1330 sensor, 98.9 % of the 435 used data sets are classified correctly if the method of k nearest-neighbors classification (kNN, $k = 5$) is applied. So despite the overlap of the groups, nearly all TCO feature sets are assigned to the correct gas.

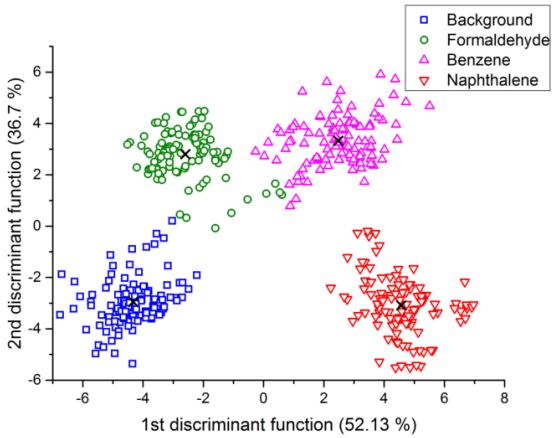

Figure 7. LDA plot of the UST GGS 1330 sensor.

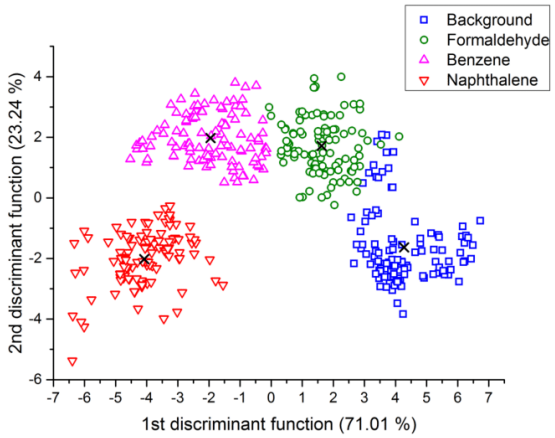

Figure 9. LDA plot of the UST GGS 5330 sensor.

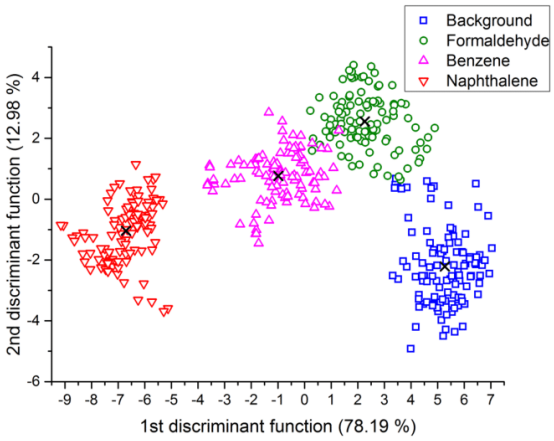

Figure 8. LDA plot of the UST GGS 2330 sensor.

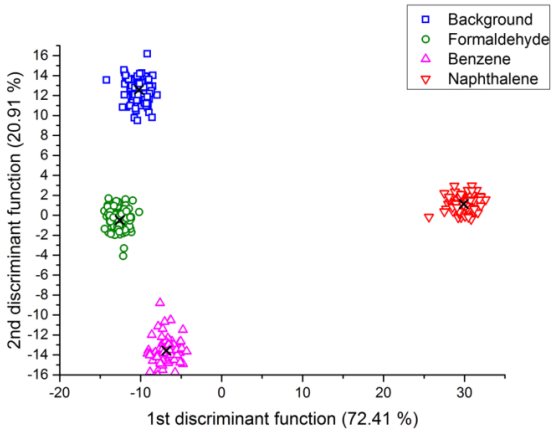

Figure 10. LDA plot based on data fusion of all three sensors.

Figure 8 shows the result of the LDA for the GGS 2330 sensor. Separation of the groups does not appear quite as distinct as for the GGS 1330 sensor, especially with formaldehyde and benzene having slightly more overlap. Leave-one-out cross-validation with kNN results in a correct classification of 96.6 % of all temperature cycles.

The result for the GGS 5330 sensor (Fig. 9) also shows a partial overlap of the groups, especially for formaldehyde and air; compared to the GGS 2230, however, the validation shows a slightly higher number of correct classifications at 98.4 %.

In addition to evaluating the single sensors, a combined processing of the data from the sensors is applied. In this sensor fusion, the feature vectors of two or three sensors are merged into a single data set for each temperature cycle, e.g., a 108-value vector for fusion of all three sensors. LDA calculation with the combined data results in a much better separation of the groups, shown in Fig. 10 for the combination of all three sensor types. Now there is no overlap of the gas groups. Validation shows a classification accuracy of 100 %; all temperature cycles are classified correctly.

4.2 Field test sensor system characterization

For use in field tests, the sensors were integrated into field test electronics (Conrad et al., 2014). The systems are designed to operate two MOS gas sensors independently in temperature cycled operation, with different temperature cycles. Each sensor is mounted on a plug-in PCB (printed circuit board), which also contains an EEPROM (electronically erasable programmable read-only memory) for calibration data and LDA parameters of the individual sensor. With this setup, fast replacement of a sensor is possible without having

Figure 11. Exterior view of modular field test sensor system containing electronics (PCB) with two MOS gas sensors (Conrad et al., 2014).

to perform a new calibration of the overall system. The sensor signals are acquired at a rate of up to 10 ksps and are stored on an SD memory card, which also contains general configuration data and the temperature cycle data sets. An on-board sensor measures air temperature and humidity; in addition, the system can be equipped with a dual-beam NDIR (nondispersive infrared) CO_2 sensor. Online preview of the measured data is possible via a selection of communication interfaces. The electronics are installed in a polymer housing (Fig. 11).

The performance of the systems was determined using the same test gas profile as for the sensor characterization in the stainless steel sensor chamber (Table 1). Three systems were characterized simultaneously, each equipped with two different UST gas sensor types with the temperature profiles identified during the lab optimization. A total of six MOS sensors were operated, two of every type; one sensor of every type was used for offline LDA signal processing. The systems were placed in a stainless steel measurement chamber with a volume of 3.5 L. The total gas flow was set to 800 mL min^{-1}, resulting in an air exchange rate of 13.7 ach (air changes per hour). Signal acquisition, pre-processing and feature extraction was performed identically to the characterization measurement of the sensors in the stainless steel sensor chamber.

The LDA result obtained with data from one of the GGS 1330 sensors is shown in Fig. 12.

Separation of the different gases is significantly less successful compared to the sensor characterization measurement (Fig. 7). Each VOC group is split into two sub-groups, reflecting the two tested VOC concentrations. While the higher concentrations are still discriminated from the background, the lower concentrations can no longer be separated from the background group. Using LOOCV, only 71.7 % of temperature cycles are now classified correctly, a significant reduction compared to the result of the sensor in the stainless steel sensor chamber which achieved 98.9 %.

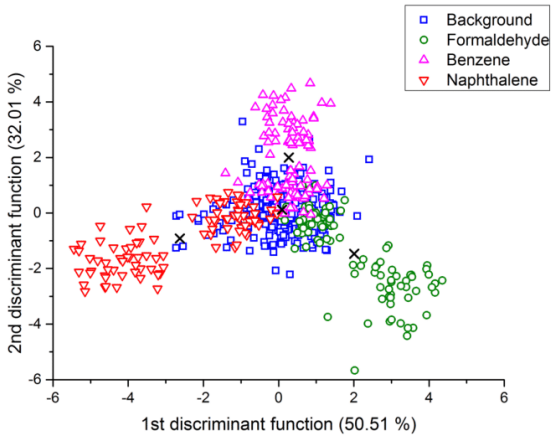

Figure 12. LDA plot of the lab characterization of a UST GGS 1330 sensor integrated in a field test system.

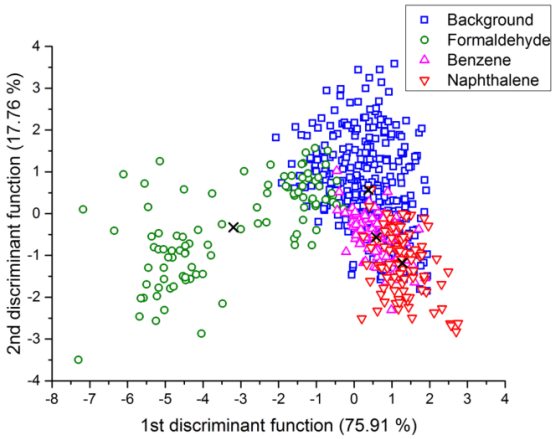

Figure 13. LDA plot of the lab characterization of a UST GGS 2330 sensor integrated in a field test system.

Similar results were obtained for the other two sensor types. In the plot of the GGS 2330 LDA output (Fig. 13), the data groups of naphthalene and especially benzene are hardly separated from the background group and only the high formaldehyde concentration can be clearly discriminated. Only 66.1 % of the temperature cycles are assigned to the correct gas.

The GGS 5330 type sensor is much more sensitive to benzene and naphthalene compared to formaldehyde. This clearly shows in the LDA result (Fig. 14), where both formaldehyde concentrations are plotted overlapping with the background group. However, only the high concentrations of benzene and naphthalene are separated from the background, while the lower concentrations are not. The ratio of correct classifications is 62.0 %.

Table 2. List of leave-one-out cross-validation results with kNN-5 for the LDAs of the single sensors and sensor fusions

Sensor(s)	Correct classifications for the sensors in the stainless steel sensor chamber	Correct classifications for the sensors integrated in the field test systems
GGS 1330	98.9 %	71.7 %
GGS 2330	96.6 %	66.1 %
GGS 5330	98.4 %	62.0 %
GGS 1330 + GGS 2330	100 %	81.6 %
GGS 1330 + GGS 5330	100 %	76.5 %
GGS 2330 + GGS 5330	99.8 %	71.7 %
GGS 1330 + GGS 2330 + GGS 5330	100 %	83.4 %

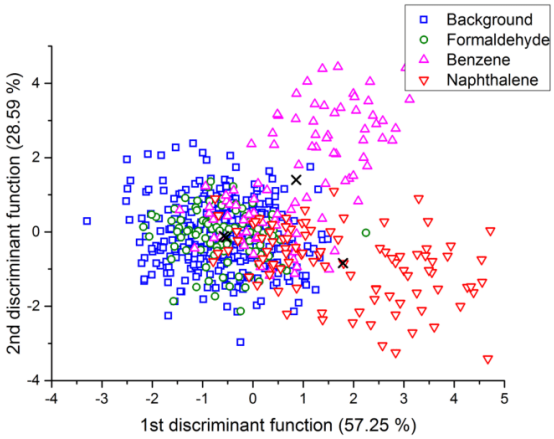

Figure 14. LDA result plot of the lab characterization of a UST GGS 5330 sensor integrated in a field test system.

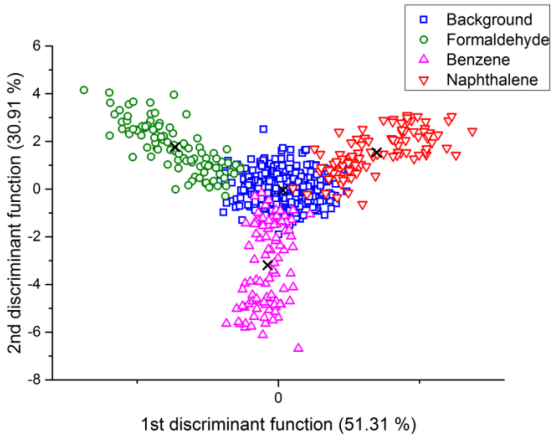

Figure 15. LDA plot based on data fusion of three sensors (one of every type) integrated in field test systems.

Data fusion was applied to the field test system sensor data as well; the resulting LDA plot for fusion one sensor of each of the three sensor types is shown in Fig. 15. As for sensor characterization setup, discrimination of the gases is significantly improved. Not only can the high concentrations of all three target gases be clearly discriminated, but now also the low concentrations are separated more clearly from the background compared to the results obtained with the individual sensors in the systems. LOOCV yields 83.4 % of all temperature cycles classified correctly, an improvement of 11.7 % over the best single sensor (71.7 % for the GGS 1330).

The results of the LDA validations for all the sensors and all possibilities of sensor fusion are listed in Table 2. For the sensors in the stainless steel sensor chamber, fusion of two sensors – GGS 1330 combined with any of the other two sensors – is already sufficient for reliable identification of the VOC. For the sensors integrated in the field test sensor systems, fusion of all three sensors is necessary for best selectivity.

Detailed LOOCVs of the LDA results of the sensors integrated in the systems are listed in Table 3. The different gas sensitivities of the three sensor types are clearly shown by the validation results for the different VOCs. While the GGS 1330 sensor has a similar sensitivity to all the gases, the GGS 2330 has an enhanced sensitivity to formaldehyde and a reduced sensitivity to the other two target VOCs. The GGS 5000 sensor is not very sensitive to formaldehyde but has higher numbers of correct classifications for naphthalene and especially benzene compared to the GGS 2330. These values show that the data from the different sensor types can reasonably be used in sensor fusion as the sensors complement each other in their responses to the target gases.

The reason for the reduced sensitivity of the sensors integrated in the field test systems was investigated further (Leidinger et al., 2014). As the main problem, gas emissions from the sensor system hardware components were determined. These emissions were identified and quantified using analytical methods, namely GC/MS VOC measurements according to the ISO 16000 standard.

Table 3. Detailed LOOCV results of the LDAs of the field test system MOS sensors; ratio of correct classifications for the single groups and overall.

Sensor(s)	Background	Formaldehyde	Benzene	Naphthalene	Overall
GGS 1330	82.8 %	60.8 %	52.6 %	61.5 %	71.75 %
GGS 2330	77.7 %	74.2 %	35.8 %	45.8 %	66.1 %
GGS 5330	84.0 %	11.3 %	48.4 %	46.9 %	62.0 %
GGS 1330 + GGS 2330	84.5 %	87.6 %	67.4 %	79.25 %	81.6 %
GGS 1330 + GGS 5330	84.5 %	66.0 %	61.1 %	72.9 %	76.5 %
GGS 2330 + GGS 5330	80.8 %	79.4 %	35.8 %	66.7 %	71.7 %
GGS 1330 + GGS 2330 + GGS 5330	87.7 %	85.6 %	68.4 %	80.2 %	83.4 %

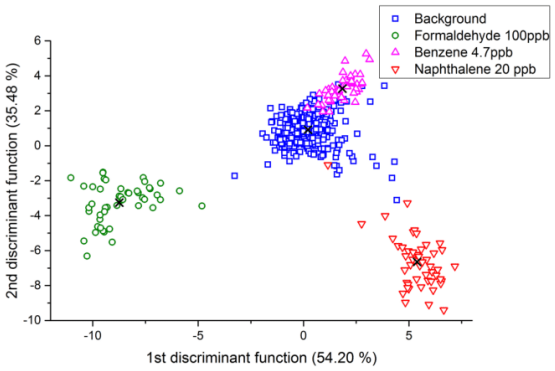

Figure 16. LDA result plot of the lab characterization of a UST GGS 1330 sensor integrated in a field test system, evaluated only for the high VOC concentrations.

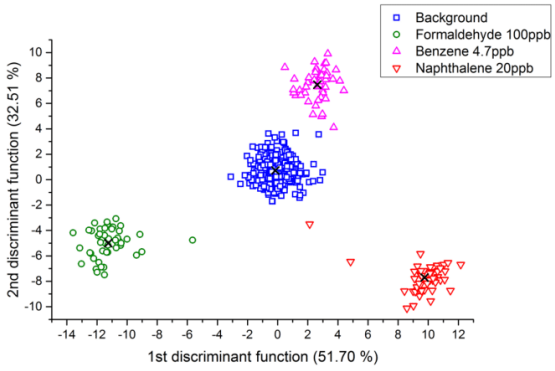

Figure 17. LDA plot based on data fusion of a GGS 1330 and a GGS 5330 integrated in field test systems, evaluated only for the high VOC concentrations.

For gas sampling, Tenax tubes were inserted into the outlet gas flow of the stainless steel measurement chamber containing three field test systems. Due to the requirements of this sampling method, air flow had to be reduced to 120 mL min^{-1} or 2.06 ach. The most significant results of the GC/MS analysis of the gas samples are listed in Table 4. The results obtained with the low flow rate were converted to the high flow rate of 13.7 ach used for the system characterization measurements, assuming that the gas emission rate from the systems is constant and independent of the gas flow at these air exchange rates. The conversion factor is 0.15, which is the ratio of the two gas flows (120 mL min^{-1} vs. 800 mL min^{-1}).

The TVOC value (last row Table 4) proves that there are significant VOC emissions from the systems, especially when heated up during operation. Measured TVOC emissions of three operating systems increase by a factor of approx. 20 compared to the unloaded test chamber and a factor of 12 compared to the systems being switched off and at room temperature. Thus, VOCs are produced by the systems, i.e., outgassing from either the PCB or the polymer housing (cf. Fig. 11). This is also confirmed by the reduced contamination observed after a heat treatment of the field test sensor systems (cf. last row in Table 4).

Looking at the specific gases, the amount of benzene measured is especially conspicuous. A concentration of 11.4 µg m^{-3} was determined, corresponding to 3.6 ppb. This strong benzene background, generated by the systems themselves, readily explains the reduced sensitivity to the applied benzene concentrations, especially the lower concentration of 0.5 ppb, compared to the single sensor measurements.

Naphthalene is not emitted from the systems in relevant amounts; the concentration measured with the systems operating is 0.2 µg m^{-3} or 0.04 ppb. Similarly, the concentration of formaldehyde was 1.2 ppb, or only 10 % of the lower test gas concentration of the calibration measurement. The most significant compound identified in the GC/MS analysis is 1,2-dimethoxyethane, with 168.8 µg m^{-3} or 45.8 ppb. The origin of this substance could not be determined.

Despite the high contamination levels, discrimination is still possible for the high concentrations of the target gases, as shown for the GGS 1330 sensor in Fig. 16. The high concentrations of formaldehyde and naphthalene can be mostly separated from the background. For benzene, discrimination does not seem as clear, but LOOCV shows that 94.5 % of temperature cycles are classified correctly. Sensor fusion further improves discrimination. Figure 17 shows the LDA

Table 4. Measured contaminations caused by outgassing of the field test system, converted from 2.06 ach to 13.7 ach; in $\mu g\,m^{-3}$ according to the ISO 16000 standard (n.d.: not detectable; n/a: data not available).

Compound	Synthetic air 5.0	Measurement chamber, no systems	Systems OFF	Systems ON	Systems ON after heat treatment
Acetone	0.7	9.5	11.5	10.6	n/a
1,3-Dioxolane	0.3	0.4	1.9	24.8	12.8
1,2-Dimethoxyethane	0.1	1.9	12.3	168.8	84.2
Benzene	0.0	0.3	n.d.	11.4	5.7
Toluene	0.1	4.6	4.0	7.3	1.0
m/*p*-xylene	0.1	0.3	0.1	10.2	3.2
Naphthalene	n.d.	0.1	0.0	0.2	2.4
Formaldehyde	n/a	0.3	n/a	1.5	n/a
Acetaldehyde	n/a	n.d.	n/a	1.9	n/a
TVOC	1.74	14.1	22.2	270	164.6

Table 5. List of LOOCV results for the 2-D and 3-D LDAs of the single sensors and sensor fusions of the field test system sensors for the high VOC concentrations.

Sensor(s)	Correct LOOCV classifications with kNN-5, 2-D LDA	Correct LOOCV classifications with kNN-5, 3-D LDA
GGS 1330	94.5 %	97.8 %
GGS 2330	80.7 %	82.2 %
GGS 5330	87.4 %	87.0 %
GGS 1330 + GGS 2330	94.5 %	99.4 %
GGS 1330 + GGS 5330	98.6 %	99.2 %
GGS 2330 + GGS 5330	96.0 %	98.4 %
GGS 1330 + GGS 2330 + GGS 5330	95.3 %	99.6 %

plot for fusion data of a GGS 1330 sensor and a GGS 5330 sensor. With this sensor combination, 98.6 % of temperature cycles are classified in the correct group. The classification results for all sensor types in the field test systems and the combinations are listed in Table 5.

The results can be improved further by calculating 3-dimensional LDAs. Then the ratio of correct classifications reaches more than 99 % with sensor data fusion (Table 5, last column). One example of the 3-D LDA plot is given in Fig. 18.

A method to prevent or at least reduce gas emissions from the systems (PCB and housing) is heat treatment of the devices. This was performed in a climate chamber where the systems were kept for 13 h at 70 °C inside the stainless steel chamber while pure air was continuously flowing through the chamber in order to flush out all emissions from the systems. Afterwards, another gas sample was taken; see Table 4, last column. Obviously, VOC emissions have been reduced significantly by approx. 40 %, but are still more than 7 times higher compared to the unloaded test chamber. Thus, further heat treatment at higher temperature and/or different materials for the housing are required to achieve acceptable contamination levels of the integrated sensor systems.

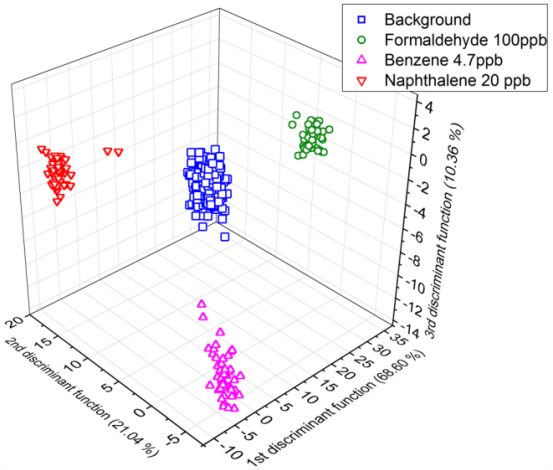

Figure 18. 3-D LDA plot based on data fusion of three sensors (one of every type) integrated in field test systems, evaluated only for the high VOC concentrations.

5 Conclusions and outlook

We have demonstrated that standard metal oxide semiconductor gas sensors operated in dynamic mode using TCO can detect and identify hazardous VOCs at ppb and sub-ppb levels, even in the presence of a much higher background concentration of ethanol (up to a factor of 4000 higher compared to the lower benzene concentration in the measurements).

In the sensor characterization measurements, when the sensors were installed in a stainless steel sensor chamber, the data sets from the sensor signals, containing several ethanol concentrations as well as gas humidities, could be assigned to the correct target gas with high reliability using a one-step LDA algorithm. The results of the data evaluation were improved significantly by sensor fusion, i.e., based on features obtained from two or three different sensors. For this measurement, 100 % of the temperature cycles were assigned to the correct gas by this method as verified by LOOCV. Further optimization of the sensor performance, e.g., using hierarchical data analysis (Schütze et al., 2004) or taking into account the information of further sensors, will be studied in the future.

For the integrated field test systems, however, the classification rate was reduced significantly compared to the sensor tests. Even with sensor fusion, only 83.4 % of the temperature cycles were classified correctly. This was attributed to VOC gas emissions from the system hardware, which have a profound effect on the performance of the individual sensors and the combined sensor array; the sensing capabilities are clearly impaired by the VOC emissions. Using only the high test gas concentrations for LDA processing, the ratio of correct classification rises to more than 95 % in a 2-D LDA and over 99 % in a 3-D LDA. These VOC concentrations, still in the ppb range, can be identified by the systems with a high success rate.

A first test of baking out the system showed promising results, as VOC emissions were significantly reduced. Separate heat treatment of the PCB and the housing would allow for application of a higher temperature to the PCB and should reduce gas emissions even further. The expected positive influence of reduced emissions on the sensing performance of the integrated sensor systems will be verified in future experiments. With these optimized integrated sensor systems field tests will be carried out in various typical indoor environments, e.g., offices and meeting rooms, to validate the performance of these systems for continuous monitoring of indoor air quality.

Acknowledgements. This work was in performed within the MNT-ERA.net project VOC-IDS. Funding by the German Ministry for Education and Research (BMBF, funding code 16SV5480K and 16SV5482) and the Portuguese Foundation for Science and Technology (FCT, ERA-MNT/0002/2010) is gratefully acknowledged.

Edited by: M. Penza
Reviewed by: two anonymous referees

References

Bernstein, J. A., Alexis, N., Bacchus, H., Leonard Bernstein., I, Fritz, P., Horner, E., Li, N., Mason, S., Nel, A., Oullette, J., Reijula, K., Reponen, T., Seltzer, J., Smith, A., and Tarlo, S. M.: The health effects of nonindustrial indoor air pollution, J. Allergy Clin. Immu., 121, 585–591, 2008.

Brinke, J. T., Selvin, S., Hodgson, A. T., Fisk, W. J., Mendell, M. J., Koshland, C. P., and Daisey, J. M.: Development of New Volatile Organic Compound (VOC) Exposure Metrics and their Relationship to "Sick Building Syndrome" Symptoms, Indoor Air, 8, 140–152, doi:10.1111/j.1600-0668.1998.t01-1-00002.x, 1998.

Bur, C., Bastuck, M., Lloyd Spetz, A., Andersson, M., and Schütze, A.: Selectivity enhancement of SiC-FET gas sensors by combining temperature and gate bias cycled operation using multivariate statistics, Sensor. Actuat. B-Chem., 193, 931–940, doi:10.1016/j.snb.2013.12.030, 2014.

Burge, P. S.: Sick building syndrome, Occup. Environ. Med., 61, 185–190, doi:10.1136/oem.2003.008813, 2004.

Conrad, T., Reimringer, W., and Rachel, T.: Modulare Systemplattform zur Bewertung der Luftqualität in Innenräumen basierend auf temperaturmodulierten Metalloxid-Gassensoren, ITG/GMA Fachtagung Sensoren und Messsysteme 2014, ITG Fachbericht 250, VDE Verlag, 2014.

French decree no. 2011-1727: Guideline values for indoor air for formaldehyde and benzene (Translation), original title: relatif aux valeurs-guides pour l'air intérieur pour le formaldéhyde et le benzene, 2011.

Fricke, T., Conrad, T., Sauerwald, T., and Schütze, A: Progress towards an Automatic T-Cycle Optimization Utilizing an Integrated Gas Sensor Testing and Evaluation Toolbox, IMCS2014 – the 15th International Meeting on Chemical Sensors (poster presentation); Buenos Aires, Argentina, 16–19 March, 2014.

Geiss, O., Giannopoulos, G., Tirendi, S., Barrero-Moreno, J., Larsen, B. R., and Kotzias, D.: The AIRMEX study – VOC measurements in public buildings and schools/kindergartens in eleven European cities: Statistical analysis of the data, Atmos. Environ., 45, 3676–3684, doi:10.1016/j.atmosenv.2011.04.037, 2011.

Gramm, A. and Schütze, A.: High performance solvent vapor identification with a two sensor array using temperature cycling and pattern classification, Sensor. Actuat. B-Chem., 95, 58–65, 2003.

Guo, H., Lee, S. C., Chan, L. Y., and Li, W. M.: Risk assessment of exposure to volatile organic compounds in different indoor environments, Environ. Res., 94, 57–66, doi:10.1016/S0013-9351(03)00035-5, 2004.

Gutierrez-Osuna, R.: Pattern Analysis for machine olfaction: A review, IEEE Sens. J., 2, 189–202, doi:10.1109/JSEN.2002.800688, 2002.

Helwig, N., Schüler, M., Bur, C., Schütze, A., and Sauerwald, T.: Gas mixing apparatus for automated gas sensor characterization, Meas. Sci. Technol., 25, 055903, doi:10.1088/0957-0233/25/5/055903, 2014.

Jones, A. P.: Indoor air quality and health, Atmos. Environ., 33, 4535–4564, 1999.

Koistinen, K., Kotzias, D., Kephalopoulos, S., Schlitt, C., Carrer, P., Jantunen, M., Kirchner, S., McLaughlin, J., Mølhave, L., Fernandes, E. O., and Seifert, B.: The INDEX project: executive summary of a European Union project on indoor air pollutants, Allergy, 63, 810–819, doi:10.1111/j.1398-9995.2008.01740.x, 2008.

Lee, A. P. and Reedy, B. J.: Temperature modulation in semiconductor gas sensing, Sensor. Actuat. B-Chem., 60, 35–42, 1999.

Leidinger, M., Sauerwald, T., Conrad, T., Reimringer, W., Ventura, G., and Schütze, A.: Selective Detection of Hazardous Indoor VOCs Using Metal Oxide Gas Sensors, Eurosensors XXVIII, 8–10 September 2014, Brescia, Italy, 2014.

Reimann, P. and Schütze, A.: Fire detection in coal mines based on semiconductor gas sensors, Sensor Rev., 32, 47–58, 2012.

Sagunski, H. and Heger, W.: Richtwerte für die Innenraumluft: Naphthalin, Bundesgesundheitsblatt – Gesundheitsforschung – Gesundheitsschutz, 47, 705–712, 2004.

Sauerwald, T., Baur, T., and Schütze, A.: Strategien zur Optimierung des temperaturzyklischen Betriebs von Halbleitergassensoren, Tagungsband zum XXVIII. Messtechnisches Symposium des Arbeitskreises der Hochschullehrer für Messtechnik, Shaker-Verlag, 2014.

Schüler, M., Helwig, N., Schütze, A., Sauerwald, T., and Ventura, G.: Detecting trace-level concentrations of volatile organic compounds with metal oxide gas sensors, IEEE SENSORS Conference (2013), 3–6 November 2013, doi:10.1109/ICSENS.2013.6688276, 2013.

Schütze, A., Gramm, A., and Rühl, T.: Identification of Organic Solvents by a Virtual Multisensor System with Hierarchical Classification, IEEE Sens. J., 4, 857–863, doi:10.1109/JSEN.2004.833514, 2004.

Umweltbundesamt: Beurteilung von Innenraumluftkontaminationen mittels Referenz- und Richtwerten, Bundesgesundheitsblatt – Gesundheitsforschung – Gesundheitsschutz, 50, 990–1005, 2007.

World Health Organization: WHO Guidelines for Indoor Air Quality: Selected Pollutants, Geneva, 2010.

Wu, C.-H., Feng, C.-T., Lo, Y.-S., Lin, T.-Y., and Lo, J.-G.: Determination of volatile organic compounds in workplace air by multisorbent adsorption/thermal desorption-GC/MS, Chemosphere, 56, 71–80, doi:10.1016/j.chemosphere.2004.02.003, 2004.

6 Highly sensitive benzene detection with metal oxide semiconductor gas sensors - an inter-laboratory comparison

Tilman Sauerwald[1], Tobias Baur[1], Martin Leidinger[1], Wolfhard Reimringer[2], Laurent Spinelle[3], Michel Gerboles[3], Gertjan Kok[4] and Andreas Schütze[1]

[1] Laboratory for Measurement Technology, Saarland University, Saarbrücken, 66123, Germany

[2] 3S GmbH, Saarbrücken, 66121, Germany

[3] European Commission - Joint Research Centre, Directorate for Energy, Transport and Climate, 21027 Ispra, Italy

[4] VSL, Thijsseweg 11, 2629 JA Delft, Netherlands

Originally published in *Journal of Sensors and Sensor Systems, 7, pp. 235-243, 2018*

doi: 10.5194/jsss-7-235-2018

Synopsis

A highly relevant, but often underestimated aspect in testing the performance of a sensor system is to test a variation of the test equipment. If a single test facility is used for characterization and calibration of such a system, any systematic errors of the facility in generation of the target (e.g. gas concentration) remain undetected and are passed on to the sensor system via the calibration. Therefore, inter-laboratory

comparisons are a useful tool for verification of the functionality of both testing facilities and the systems to be tested. Inter-laboratory test measurements are a standard procedure in chemical analysis and are performed between at least two testing facilities [227][228]; however, large numbers of partners can be involved, e.g. the performance of an electronic tongue has been tested in five laboratories [229], different types of glass electrodes for determining the pH value of ethanol have been tested using the same samples by nine participants [230], and for evaluating the reliability of seawater CO_2 content measurements, the results from as many as 50 institutions were compared [231].

In the presented publication, a gas measurement system has been characterized in two test setups for its performance regarding ppb level benzene detection. The intended scenario was outdoor air quality monitoring, where benzene concentrations in the low ppb range are relevant, cf. section 1.1.1. The system was equipped with a commercial MOS gas sensor in TCO; signal acquisition is performed using a logarithmic amplifier. The first tests were conducted at the Lab for Measurement Technology (LMT) at Saarland University (Saarbrücken, Germany), in a low flow rate, low gas volume setup in which only the sensor elements are connected to the generated target gas, cf. chapter 3. A second set of measurements was performed at the Joint Research Centre (JRC, Ispra, Italy), using a high gas volume test chamber in which complete sensor systems can be placed. In both facilities, benzene concentrations in the range from 0.5 to 10 ppb were mixed into the carrier gas. In the first set of measurements (Saarland University), additional interferent gases have been added to the gas mixture, and variations in gas humidity have been performed.

The data recorded at Saarland University has been analyzed in detail, using feature extraction and PLSR processing (partial least squares regression, cf. section 2.3.5). Depending on the gas background variations included in the input data, the benzene concentration could be predicted with an accuracy between ± 0.2 ppb and ± 2 ppb.

For a joint analysis of the two data sets, a PLSR model has been computed using the data obtained in the JRC lab and the signals measured at Saarland University have been evaluated with this model. The results show a slight offset of the data points,

however, the general trend is predicted correctly. The offset probably results from different gas humidities during the two measurement runs or additional gaseous components in the system due to contaminations or degassing from the sensor systems placed in the test gas volume, cf. chapter 5. A second analysis, in which part of the Saarland University data set was used for training and data from both test setups were used for evaluation produces a similar result.

The results show that despite the variation in measurement conditions (humidity) the general transferability of the two measurement setups is valid, and the sensor system yields comparable results in both testing facilities. This confirms a robust operation of the gas sensor system.

J. Sens. Sens. Syst., 7, 235–243, 2018
https://doi.org/10.5194/jsss-7-235-2018

JSSS Journal of Sensors and Sensor Systems Open Access

Highly sensitive benzene detection with metal oxide semiconductor gas sensors – an inter-laboratory comparison

Tilman Sauerwald[1], Tobias Baur[1], Martin Leidinger[1], Wolfhard Reimringer[2], Laurent Spinelle[3], Michel Gerboles[3], Gertjan Kok[4], and Andreas Schütze[1]

[1]Laboratory for Measurement Technology, Saarland University, Saarbrücken, 66123, Germany
[2]3S GmbH, Saarbrücken, 66121, Germany
[3]European Commission—Joint Research Centre, Directorate for Energy, Transport and Climate, 21027 Ispra, Italy
[4]VSL, Thijsseweg 11, 2629 JA Delft, the Netherlands

Correspondence: Tilman Sauerwald (t.sauerwald@lmt-uni-saarland.de)

Received: 29 September 2017 – Revised: 5 February 2018 – Accepted: 11 February 2018 – Published: 5 April 2018

Abstract. For detection of benzene, a gas sensor system with metal oxide semiconductor (MOS) gas sensors using temperature-cycled operation (TCO) is presented. The system has been tested in two different laboratories at the concentration range from 0.5 up to 10 ppb. The system is equipped with three gas sensors and advanced temperature control and read-out electronics for the extraction of features from the TCO signals. A sensor model is used to describe the sensor response in dependence on the gas concentration. It is based on a linear differential surface reduction (DSR) at a low temperature phase, which is linked to an exponential growth of the sensor conductance. To compensate for cross interference to other gases, the DSR is measured at three different temperatures (200, 250, 300 °C) and the calculated features are put into a multilinear regression (partial least square regression – PLSR) for the quantification of benzene at both laboratories. In the tests with the first set-up, benzene was supplied in defined gas profiles in a continuous gas flow with variation of humidity and various interferents, e.g. toluene and carbon monoxide (CO). Depending on the gas background and interferents, the quantification accuracy is between ±0.2 and ±2 ppb. The second gas mixing system is based on a circulation of the carrier gas stream in a closed-loop control for the benzene concentration and other test gases based on continuously available reference measurements for benzene and other organic and inorganic compounds. In this system, a similar accuracy was achieved for low background contaminations and constant humidity; the benzene level could be quantified with an error of less than 0.5 ppb. The transfer of regression models for one laboratory to the other has been tested successfully.

1 Introduction

Air quality is an important pre-requisite for public health. The pollution of the air with gaseous compounds contributes relevantly to the burden of disease in industrial and developing countries (Bernstein et al., 2008). One of the most important pollutants is benzene (WHO Regional Office for Europe, 2010). Due to its toxicity and its carcinogenicity, very low concentrations of benzene should be detected and monitored; threshold limits are in the ppb range, e.g. the European Air Quality Directive set the limit value at 5 µg m^{-3} or 1.6 ppb as the long-term environmental limit (European Parliament and Union, 2008). The benzene detection is also an important topic for indoor air quality and workplace safety, where several national regulations have been put in force, e.g. the Bundesanstalt für Arbeitsschutz und Arbeitsmedizin (2014). For environmental monitoring, analytic techniques, e.g. gas chromatography (GC), are used. In Europe, monitoring of benzene in ambient air is mandatory. The European Air Quality Directive states that the reference method for the mea-

surement of benzene must consist of active or online sampling followed by desorption and gas chromatography (BSI, 2015). Due to the high price and maintenance costs of these methods, the number of points in the measurement network is very limited, but the necessity for a higher spatial resolution of pollution control has been reported (Batterman et al., 1994; Heimann et al., 2015). Within the EMRP project KEY-VOCs, therefore, the use of sensor systems as an indicative method for the measurement of benzene has been tested in order to assess whether the demand for a low-cost measurement device for benzene can be met. A review (Spinelle et al., 2017b) of the existing sensor technology and its commercially available systems has revealed that only very few manufacturers are targeting this concentration range and that it is doubtful whether one of these systems can meet the criteria of detection limit, selectivity and stability (Spinelle et al., 2017a). Therefore, micro analytical systems and prototype sensor systems have been included in the tests. The result of one prototype using metal oxide semiconductor (MOS) gas sensors with temperature cycle operation (TCO) is reported in this paper. This approach has previously been studied for the selective detection of volatile organic compounds (VOCs), e.g. benzene in indoor air (Leidinger et al., 2014; Schütze et al., 2017). MOS gas sensors are very robust and sensitive devices (Morrison, 1981; Sasahara et al., 2004) sensitive to a broad variety of reducing gases. The resistance of the sensor (Eq. 1) is dominated by ionized oxygen at the surface which causes an energy barrier E_B and the height of the barrier depends in a quadratic function on the density of the ionized oxygen N_S.

$$G = G_0 \cdot e^{-\frac{E_B}{k_B T}} \quad \text{with} \quad E_B \propto N_S^2 \tag{1}$$

The reaction of the reducing gas with the reactive surface oxygen reduces the energy barrier and increases the conductance strongly. For constant temperature and gas concentration the change of surface charge can be described by a mass action law of chemisorbed species leading to a power law for the dependence of conductance and gas concentration (Barsan and Weimar, 2001; Madou and Morrison, 1989). While in a few cases the selectivity of the sensors can be increased by special preparation methods for example described in Hennemann et al. (2012), Kemmler et al. (2012), and Leidinger et al. (2016b), typically multi-signal methods like TCO are used. TCO is a well-known method for the improvement of selectivity reported in a multitude of papers, e.g. Eicker (1977), Gramm and Schütze (2003), and Lee and Reedy (1999). It is dynamic operation (Nakata et al., 1998a, b) and in this sense it enables sensor properties that cannot be found in a sensor at any constant temperature. Following this line, some of us could prove in the last few years that an optimized TCO can increase the sensitivity (Baur et al., 2015) and the stability (Schultealbert et al., 2017) of the sensor signal as well. The model-based optimization uses a set of rate equations for the trapping and release in surface states proposed by Ding et al. (2001). For the quantification of VOC concentrations at the ppb level, a technique based on the relaxation of the conductance at a low temperature phase has been demonstrated (Baur et al., 2015). The technique utilizes the fact that the equilibrium surface coverage with ionized oxygen depends on the sensor temperature. At high temperature (e.g. at 450 °C) the surface coverage and thereby the barrier height are higher than at low temperature (e.g. 200 °C) (Schultealbert et al., 2017). For a fast temperature reduction, an excess of surface coverage can be obtained (Baur et al., 2015). At this stage, the reaction at the sensor surface is far from equilibrium as the ionosorption of oxygen is very unlikely. The sensor surface is then predominantly reduced by gases, e.g. benzene, causing a strong increase in sensor response compared to isothermal operation. This increase can be several orders of magnitude in terms of relative conductance. The reduction of the surface is linear to the applied gas dosage or gas concentration given that the concentration is constant over one surface reduction (Baur, 2017). The change in the logarithmic sensor conductance $\ln G_{\text{init}}$ at the beginning of a low temperature plateau (beginning at $t_0 = 0$) is linear to the gas concentration c_{gas}.

$$\frac{\mathrm{d} \ln G_{\text{init}}(t)}{\mathrm{d}t} \sim \text{const} \sim k_{\text{gas}} \cdot c_{\text{gas}} + k_0 \tag{2}$$

Please note that Eq. (2) is only valid if the surface charge is still high above equilibrium; otherwise, the ionosorption of new surface charge is not negligible anymore. A detailed discussion can be found in Schultealbert et al. (2017).

Following this line, we could show that the benzene concentration in the range from 500 ppt to 10 ppb air can be quantified very accurately in a purified air background, whereby compensation of the ubiquitous gas background and interfering gas reduces the accuracy of detection (Leidinger et al., 2017).

2 Experimental

2.1 Sensor system

The sensor system is equipped with three different commercial MEMS gas sensor elements. Two sensor elements are integrated in a dual-sensor package (MiCS 4510 from SGX, Switzerland) and the third sensor is a single-sensor device (AS-MLV from ams Sensor Solutions, Germany). All sensors are operated in TCO with independent control and read-out. A block diagram of the sensor system can be found in the Supplement (Fig. S1). Rapid temperature changes from a high temperature of 450 °C to lower temperatures (200/250/300 °C) are used. The duration of the high temperature plateau is 10 s each, for the 200 and 250 °C plateau the duration is 35 s, and for the 300 °C plateau it is 20 s. The TCO control and the read-out are done using a modified sensor system (SensorToolbox, 3S GmbH, Germany)

that can support up to four sensor modules (ToolboxModule). The sensor signal $S_{\log}$ for each sensor is measured using a logarithmic amplifier comparing the sensor current I_{sens} with a reference current $I_{\text{ref}} = 1\,\text{mA}$. The sensor is operated at a constant voltage of 0.25 V; hence, the sensor current $I_{\text{sens}} = 0.25\,\text{V} \cdot G_{\text{sens}}$ is directly linear to the sensor conductance. The output of the logarithmic amplifier is divided by a subsequent voltage divider to match with the voltage range of the analogue–digital converter of the ToolboxModule (Eq. 1). Corresponding to this, a virtual reference conductance G_{ref} can be calculated. The output of the logarithmic amplifier of $U_{\text{LogAmp}} = 0.5\,\text{V}$ per decade is divided by a subsequent voltage divider to match with the voltage range of the analogue–digital converter of the ToolboxModule, yielding a voltage $U_{\log}$ of 0.25 V per decade.

This output voltage (Eq. 3) is defined as sensor signal $S_{\log}$ which is linear to the logarithm of the conductance G_{sens} of the gas sensing layers.

$$\begin{aligned} S_{\log} &= 0.25\,\text{V} \cdot \log_{10}\left(\frac{I_{\text{ref}}}{I_{\text{sens}}}\right) \\ &= 0.25\,\text{V} \cdot \log_{10}\left(\frac{I_{\text{ref}}}{G_{\text{sens}} \cdot 0.25\,\text{V}}\right) \end{aligned} \tag{3}$$

This measuring method allows us to cover a large signal range, as MOS gas sensor resistances can vary within several orders of magnitude during rapid temperature changes (Baur et al., 2015). Please note that this sensor signal is different from the commonly used sensor response, which is defined as G/G_0. A change in the sensor signal $\Delta S_{\log} = S_{\log} - S_{\log 0}$ can be easily transformed to a sensor response by $S = 10^{\Delta S_{\log}/0.25\,\text{V}}$. However, the definition of $S_{\log}$ allows a facile calculation of the change surface charge as the time-derived sensor signal $S_{\log}$ is proportional to the rate constant k of surface reduction (Eq. 2), which is itself linear depending on the gas (benzene) concentration (Eq. 4).

$$\begin{aligned} &\frac{\mathrm{d}S(t)}{\mathrm{d}t} \sim -\frac{\mathrm{d}\ln G_{\text{init}}(t)}{\mathrm{d}t} \sim -k \sim -c \cdot k_{\text{gas}} - k_0 \\ &\text{for small} \quad (t - t_0) \end{aligned} \tag{4}$$

2.2 Data processing

We used our DAV^{3}E toolbox (Bastuck et al., 2016) for the data processing. The data processing was performed in three steps: feature extraction, feature selection and quantification. The feature extraction reduces the dimensionality of the classification problem.

A set of features of each temperature cycle was extracted from the signals, which describes the shape of the signal (mean values and slopes). The slopes correspond in first approximation to the rate constant (derivative of the sensor signal Eq. (4)). These features were calculated from several segments of the cyclic sensor signal, covering all set temperatures. The ranges of the features have been varied to find the best selection by the feature selection. Feature selection was performed using a recursive feature elimination support vector machine (RFESVM) (Schüler et al., 2017) to choose the best features for classification.

Using these feature sets and the known benzene concentrations, a PLSR model (partial least squares regression) (Bastuck et al., 2015b; Wold et al., 2001) is calculated, which generates a linear combination of the features to allow an estimation of the benzene concentration.

2.3 Gas tests at the Lab for Measurement Technology (LMT)

In the first laboratory (LMT – Lab for Measurement Technology, Saarbrücken, Germany) the sensor system has been tested using a gas mixing apparatus (GMA) operating by the principle of dynamic dilution. The set-up of this system has been reported in detail previously (Helwig et al., 2014). A two-stage dilution system is used to produce the benzene test gas, starting from a gas cylinder containing 50 ppm benzene in synthetic air. The benzene is diluted with zero air, generated from a cascade of two gas purifiers. The first purifier includes a coarse filter to remove particles and oil. Subsequently, humidity and CO_2 are removed by two alternating molar sieves (pressure swing) and hydrocarbons ($>C_3$) are removed by an active charcoal filter. The second purifier has an additional pre-filter and pressure swing followed by a catalytic combustion of hydrogen, carbon monoxide and short chain hydrocarbons ($<C_4$). The catalytic converter is furthermore equipped with a nitrogen oxide scrubber. The pure air is split into eight gas lines, of which five have been used in this investigation. In the first line, pure air saturated with humidity is generated at a dew point of 20 °C using an isothermal blubber with HPLC grade water (low organic carbon). The second line is used for dry air. The third line is a two-step dilution using a dry stream of purified air and diluted benzene test gas from a cylinder in the first dilution step. The second dilution step is the combination with the humid and dry main gas stream from the first two lines. In the fourth line, toluene is added to the test gas; it uses the same set-up as the benzene line. The fifth line uses a two-step dilution to generate a background of 500 ppb hydrogen, 150 ppb carbon monoxide and 1820 ppb methane from a gas cylinder with a dilution of these gases in air. These three gases are the main reducing compounds in pure environmental air (Ehhalt and Rohrer, 2009; Gilge et al., 2010). This gas background has a strong impact on the sensor response as well as on the detection limit of the sensor (Leidinger et al., 2017). A mixture of pure zero air with this background will be defined as standard air. The sensors have been tested directly in gas flow of 200 sccm in a stainless steel sensor housing.

2.4 Gas tests at JRC

For the second laboratory campaign, the evaluation was carried out using the JRC (Joint Research Center) exposure chamber. This chamber allows the control of numerous gaseous mixtures including benzene and a set of selected interfering compounds (toluene, m,p-xylene, ethane, propane, n-butane and n-pentane) plus temperature, relative humidity and wind velocity. The exposure chamber is an "O"-shaped ring-tube system, covered with dark insulation material. The full system has already been described elsewhere (Spinelle et al., 2014). All gaseous compounds are added to pure zero air. The micro-sensors in the stainless steel housing described above were directly placed inside the ring tube. High concentration cylinders were used to generate specific levels of pollutants based on the dynamic dilution principle. A specific LabView software using multiple proportional–integral–derivative (*PID*) feedback loops ensured the stability of the concentration. The reference value for the feedback loop was measured using a PTR-MS (proton-transfer-reaction mass spectrometer) and the reference values were measured by a gas chromatograph with a photo ionization detector (GC-PID 955 from Syntech). The direct input of reference measurements of gaseous compounds, temperature, humidity and and wind speed is used to auto-correct the gas mixture, temperature controlling cryostat and wind velocity by means of an internal fan. In particular, this set-up allows one to set independent criteria for the stability of each parameter and for a defined period of time.

3 Measurement results and data analysis

3.1 Benzene quantification capabilities

The sensor system has been tested in the LMT system in pure zero air towards benzene at six gas concentrations from 0.5 to 10 ppb and three relative humidities (10, 25, 40 %RH) to test the quantification and humidity compensation. Due to the high purity of the zero air, the conductance of the sensors at the beginning of the low temperature phases is very low. The sensor response shows a high noise. The derivative of the sensor response is obviously an even worse signal. Thus, a feature selection tool as described above has been used instead of using the model-based feature directly. The feature selection selected only signals from the less noisy parts of the response curve. To test the quantification of benzene a PLSR has been calculated using the measurement of 0.5, 3 and 10 ppb benzene at 10 and 40 %RH (Fig. 1a). The PLSR is in general a regression of the measured values (e.g. sensor system output) with the "true" values (or a proper estimate, e.g. from a reference measurement). Please note that the value of the concentration set point (x-axis) also adds an additional uncertainty to the regression. As the LMT gas mixing system does not provide continuous reference measurements of the benzene concentration, an estimate of the real value is derived from the mixing ratio of the gas flows and the certified concentration of the gas cylinders. The gas flows are continuously measured and recorded by the gas mixing system. The proper function of the gas mixing system was confirmed as the error of the recorded flow rates is within the error margin. As estimates for the true concentration, the set points of the gas mixing system were used. Figure 1 shows that the PLSR is very accurate. The sensor system output is obviously a linear function for benzene concentration and the compensation of humidity cross-sensitivity is very good. The error of the predicted response is below 0.2 ppb for all trained concentrations. The PLSR model was applied to untrained concentrations of benzene (1, 2 and 5 ppb) at 10 and 40 %RH and to the six concentrations of benzene tested at 25 %RH. This test of the model prediction is shown in Fig. 1b. The full circles denote the trained data points and open circles denote the untrained "test" data point. The test data points do not show any decisive deviation from the trained data points. The interpolation of the benzene concentration and a compensation of an untrained humidity background are demonstrated by this result. However, the quantification of benzene in ambient air at the sub-ppb level cannot be derived from this result since even clean air contains significant inorganic reducing gas components as described in Sect. 2. A similar test therefore has been made under standard air (cf. Sect. 2.2) instead of zero air. The quantification properties have been tested in detail under standard air and other interfering gases in a previous work (Leidinger et al., 2017) showing the strong impact of gas background on the accuracy of the detection. Measurements were made with the dynamic dilution set-up at LMT. In the first case (Fig. 2a), two sweeps of the benzene concentration are included, one in pure zero air without interferents and one with a 2 ppb toluene background, at a constant gas humidity of 25 %RH. The benzene concentrations predicted by the PLSR model still show a very small error of below 200 ppt with respect to the concentration set point. The introduction of standard air has a strong impact on the quantification of benzene. In Fig. 2a the PLSR is shown in standard air, including a variation of the CO concentration between 150 ppb (ubiquitous) and 500 ppb (lightly polluted air). Still, the PLSR shows a linearity between the sensor system output and the set-point concentration, but the error of the prediction is between 1 and 2 ppb depending on the benzene concentration. The addition of interferents like toluene between 2 and 20 ppb (Fig. 2c) seems to reduce the accuracy of the benzene quantification further. However, the strongest impact comes from the standard air conditions. The quantification error can be reduced if the data from 10 %RH are removed from the data set corresponding to a reduction of interfering complexity. Figure 2d contains only two gas humidities; the signals recorded at the lowest value are not taken into account. For this condition the quality of quantification of benzene was improved; compared to the scenarios in Fig. 2b and c, the groups are more compact and error for

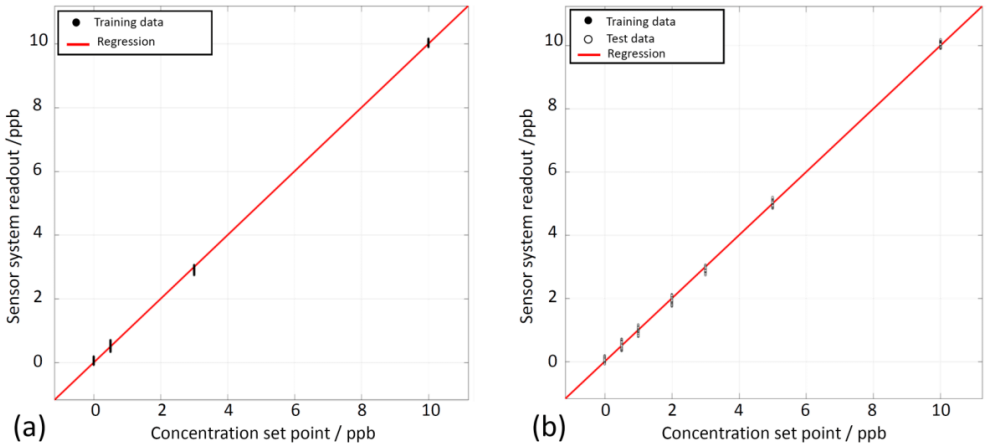

Figure 1. Quantification of benzene in zero air using feature extraction and PLSR. **(a)** Only training data. **(b)** Training and test data.

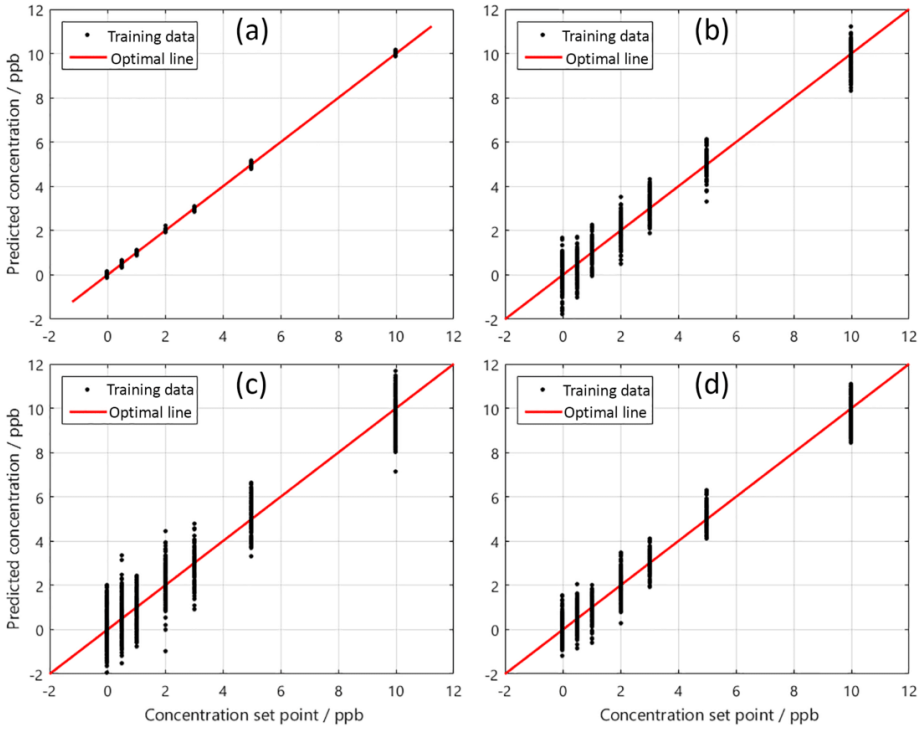

Figure 2. PLSR benzene quantification results for four different background and interferent configurations (Leidinger et al., 2017): **(a)** benzene in pure zero air and with 2 ppb of toluene added, at 25 %RH. **(b)** Benzene in standard air and variation of CO background, 10, 25 and 40 %RH. **(c)** Benzene in standard air and variation of toluene, 10, 25 and 40 %RH. **(d)** Benzene in standard air and variation of toluene and CO, 25 and 40 %RH.

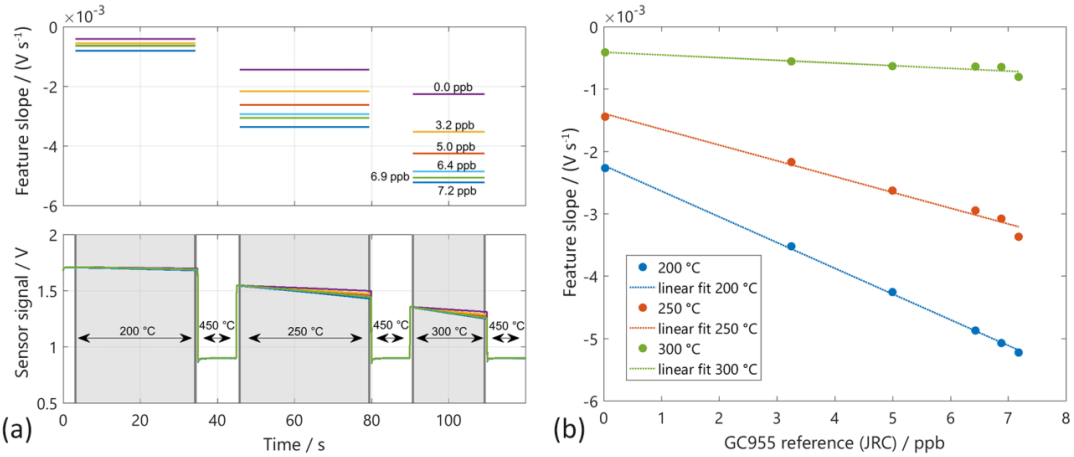

Figure 3. **(a)** Sensor signals in temperature-cycled operation (temperature ranges: blue arrows). The relaxation constants (slope feature) are calculated from the grey marked domains. **(b)** Feature slope over benzene concentration according to the GC955 reference measurement.

the benzene concentration is below 1.8 ppb over the whole concentration range.

3.2 Lab intercomparison

After the initial calibration at LMT, the system was transferred to the JRC. During this transfer, the interface of the read-out electronic of the dual sensor (MiCS4514) was damaged. For the lab intercomparison the remaining sensor (ASMLV) has been used and the signal processing has been retrained. Only tests with zero air background at various humidity and interferent levels have been compared, as in the JRC set-up no addition of the inorganic background was foreseen. The features have been calculated according to Eq. (4) directly, without selection of the feature ranges using RFESVM. However, a short time span at the beginning of the low temperature has been left out manually to reduce the noise (cf. Fig. 3; the sections for feature extraction are marked in grey). The sensor signal $S_{\log}$ in the low temperature plateaus has a good linearity over the full temperature plateau in good agreement with Eq. (4) for all temperature plateaus at all tested benzene concentrations (Fig. 3). Obviously, the strongest response of the sensor to benzene can be found at 300 °C (Fig. 3). Using these features a PLSR model has been trained from the data of the JRC measurement and tested with the data from the LMT measurements. Please note that only three features can be calculated from the single sensor and that the impact of the feature at 200 °C is very small, leading to an incomplete compensation compared to the three-sensor system described in Sect. 3.1. Therefore, only measurement results with pure benzene have been evaluated. For the training of the PLSR, the data of the reference measurement from the GC-PID 955 were used as estimates of the true values. We compared the transfer of a PLSR model obtained by training data of one test system to test data obtained by the other test system (Fig. 4). The transfer of the model trained with JRC test data to LMT test data is shown on the left side in Fig. 4. The black circles denote the trained data points from the JRC lab and the red circles denote the untrained data points from the LMT lab. The benzene concentrations predicted by the PLSR model for the JRC data at 60 %RH still show a very small error of below 200 ppt with respect to the concentration measured by the GC-PID 955. We see two different trend lines of the predicted data points from the LMT lab. Each trend line shows a specific humidity at 10 %RH and 25 %RH. Both trend lines show a good linearity and the same slope, but also an offset to the optimal line. The transfer from the model obtained with LMT data is shown in Fig. 4 on the right. The training was performed with only a single humidity (25 %RH), as obviously the humidity compensation of the single sensor system is not sufficient. The test data from the JRC as well as the test data from the LMT show a good linearity, but also an offset to the training data. The offset is probably due to the humidity as the data with 60 %RH exhibit a negative offset, while the data with 10 %RH exhibit a positive offset.

4 Discussion and conclusion

The presented MOS gas sensor system shows very good performance for benzene quantification, especially in pure air even with low levels of interfering toluene, including the interpolation of unknown benzene concentrations over the full humidity range tested. However, at standard air and a realistic background level of interferents, especially CO, the error of quantification is in the range of 1–2 ppb. For the environmental monitoring, especially in rural areas, even lower

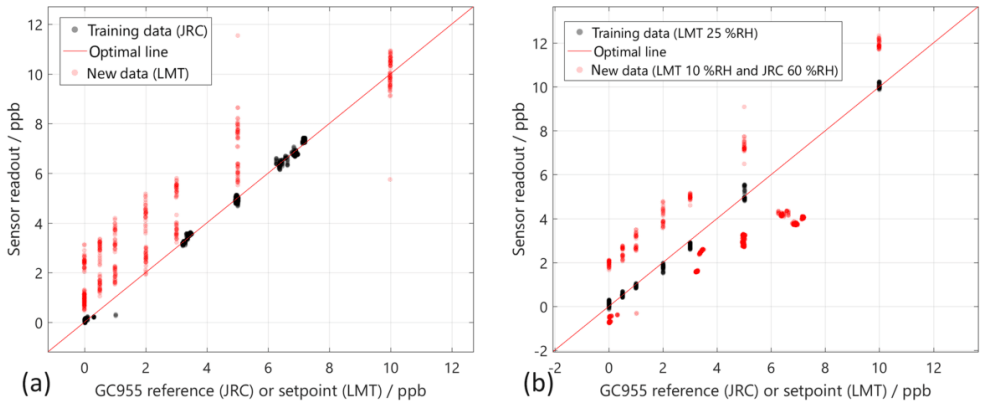

Figure 4. Transfer of the PLSR model from training data of one gas mixing system to test data from another gas mixing system. **(a)** Training using the JRC measurement (60 %RH black solid circles) and test data from the LMT measurement (10 and 25 %RH open red circles). **(b)** Training using LMT measurements (25 %RH black circle) and test using the JRC data (60 %RH) and the LMT data (10 %RH). Both test data are shown in open red circles.

detection limits are needed to monitor the benzene concentration (Schneidemesser et al., 2010). A possible strategy for the further reduction of the detection limit are sensor/preconcentrator micro systems (Leidinger et al., 2016a) and a further optimization of the sensor system electronics to reduce the noise of the signal (Baur and Schütze, 2017). For the quantification of benzene, a combination of the DSR model for feature extraction and a multilinear regression for the compensation of interferents has been tested successfully. Within the measured sensor signals all tested benzene concentrations were in good agreement with the prediction of the DSR model. The multilinear regression yields very good compensation of humidity and even toluene interference. The regression for all conditions shows a good linearity without further pre-processing of the signal; this is an advantage of the system over other TCO modes, which usually does not yield a linear signal with concentration requiring a special pre-processing before PLSR (Bastuck et al., 2015a). The system can be successfully calibrated at different labs and testing conditions, indicating that the very different methods of generating benzene yield similar levels of test gas. The transfer of a regression model from the JRC test data to the LMT test data shows good linearity of the measured benzene concentration but an offset of the response curve on the order of 2 ppb. The observed offset is probably due to the different humidity as the humidity compensation of the single-sensor system is not as good as in the three-sensor system. Moreover, a residual contamination of the GMA with VOC can contribute. Test of the VOC background of the LMT system showed that it is typically in the range of a few $\mu g\,m^{-3}$ (Helwig et al., 2014), which is in the same range as the benzene concentration tested. The result demonstrates the need for the definition of common test standards for trace gas sensor systems and the high potential of those systems for the quantitative detection even of small levels of pollutants like benzene. This is an important step for the development of monitoring grids with high resolution using indicative sensor systems to increase the number of nodes strongly.

Data availability. The underlying measurement data are not publicly available and can be requested from the authors if required.

The Supplement related to this article is available online at https://doi.org/10.5194/jsss-7-235-2018-supplement.

Competing interests. The authors declare that they have no conflict of interest.

Special issue statement. This article is part of the special issue "Sensor/IRS2 2017". It is a result of the AMA Conferences, Nuremberg, Germany, 30 May–1 June 2017.

Acknowledgements. The work has been funded by EMRP Joint Research Project ENV56 KEY-VOCs. The EMRP is jointly funded by the EMRP participating countries within EURAMET and the European Union. Some foundations, especially the set-up of the sensor system, were laid within the SENSIndoor project (funding by the European Union's Seventh Framework Programme for research, technological development and demonstration under grant agreement no. 604311 is acknowledged).

Edited by: Jens Zosel
Reviewed by: two anonymous referees

References

Barsan, N. and Weimar, U.: Conduction Model of Metal Oxide Gas Sensors, J. Electroceram., 7, 143–167, https://doi.org/10.1023/A:1014405811371, 2001.

Bastuck, M., Leidinger, M., Sauerwald, T., and Schütze, A.: Improved quantification of naphthalene using non-linear Partial Least Squares Regression, in: 16th International Symposium on Olfaction and Electronic Nose, Dijon, France, 28 June–1 July 2015, 1–2, available at: http://arxiv.org/abs/1507.05834 (last access: 2 February 2018), 2015a.

Bastuck, M., Bur, C., Sauerwald, T., Spetz, A. L., Andersson, M., and Schütze, A.: Quantification of Volatile Organic Compounds in the ppb-range using Partial Least Squares Regression, Proceedings SENSOR 2015, 19–21 May 2015, Nuremberg, Germany, 584–589, https://doi.org/10.5162/sensor2015/D5.1, 2015b.

Bastuck, M., Baur, T., Schütze, A., and Sauerwald, T.: DAV^{3}E: Data Analysis and Verification/Visualization/Validation Environment für die Multisensor-Datenfusion, 18. GMA/ITG-Fachtagung Sensoren und Messsyst. 2016, 10–11 May 2016, Nuremberg, Germany, 729–734, https://doi.org/10.5162/sensoren2016/P7.3, 2016.

Batterman, S., Chambliss, S., and Isakov, V.: NIH Public Access, Atmos. Environ., 94, 518–528, 1994.

Baur, T. and Schütze, A. T. S.: Detection of short trace gas pulses, Proc. Sens. 2017, 87–91, available at: https://www.ama-science.org/proceedings/details/2497 (last access: 2 February 2018), 2017.

Baur, T., Schütze, A., and Sauerwald, T.: Optimierung des temperaturzyklischen Betriebs von Halbleitergassensoren, Tech. Mess., 82, 187–195, https://doi.org/10.1515/teme-2014-0007, 2015.

Bernstein, J. A., Alexis, N., Bacchus, H., Bernstein, I. L., Fritz, P., Horner, E., Li, N., Mason, S., Nel, A., Oullette, J., Reijula, K., Reponen, T., Seltzer, J., Smith, A., and Tarlo, S. M.: The health effects of nonindustrial indoor air pollution, J. Allergy Clin. Immun., 121, 585–591, https://doi.org/10.1016/j.jaci.2007.10.045, 2008.

BSI: BS EN 14662-3:2015: Ambient air – Standard method for the measurement of benzene concentrations. Automated pumped sampling with in situ gas chromatography, BSI, London, UK, 2015.

Bundesanstalt für Arbeitsschutz und Arbeitsmedizin: TRGS 910: Risikobezogenes Maßnahmenkonzept für Tätigkeiten mit krebserzeugenden Gefahrstoffen, Gmbi (64), 1313, 2014.

Ding, J., McAvoy, T. J., Cavicchi, R. E., and Semancik, S.: Surface state trapping models for SnO2-based microhotplate sensors, Sensor. Actuat. B-Chem., 77, 597–613, https://doi.org/10.1016/S0925-4005(01)00765-1, 2001.

Ehhalt, D. H. and Rohrer, F.: The tropospheric cycle of H2: A critical review, Tellus, 61, 500–535, https://doi.org/10.1111/j.1600-0889.2009.00416.x, 2009.

Eicker, H.: Method and apparatus for determining the concentration of one gaseous component in a mixture of gases, US Patent 4012692A, 1977.

European Parliament and Council of the European Union: Directive 2008/50/EC of the European Parliament and of the Council of 21 May 2008 on ambient airquality and cleaner air for Europe, available at: http://eur-lex.europa.eu/legal-content/EN/TXT/?uri=OJ:L:2008:152:TOC (last access: 2 February 2018), 2008.

Gilge, S., Plass-Duelmer, C., Fricke, W., Kaiser, A., Ries, L., Buchmann, B., and Steinbacher, M.: Ozone, carbon monoxide and nitrogen oxides time series at four alpine GAW mountain stations in central Europe, Atmos. Chem. Phys., 10, 12295–12316, https://doi.org/10.5194/acp-10-12295-2010, 2010.

Gramm, A. and Schütze, A.: High performance solvent vapor identification with a two sensor array using temperature cycling and pattern classification, Sensor. Actuat. B-Chem., 95, 58–65, https://doi.org/10.1016/S0925-4005(03)00404-0, 2003.

Heimann, I., Bright, V. B., McLeod, M. W., Mead, M. I., Popoola, O. A. M., Stewart, G. B., and Jones, R. L.: Source attribution of air pollution by spatial scale separation using high spatial density networks of low cost air quality sensors, Atmos. Environ., 113, 10–19, https://doi.org/10.1016/j.atmosenv.2015.04.057, 2015.

Helwig, N., Schüler, M., Bur, C., Schütze, A., and Sauerwald, T.: Gas mixing apparatus for automated gas sensor characterization, Meas. Sci. Technol., 25, 55903, https://doi.org/10.1088/0957-0233/25/5/055903, 2014.

Hennemann, J., Sauerwald, T., Kohl, C. D., Wagner, T., Bognitzki, M., and Greiner, A.: Electrospun copper oxide nanofibers for H 2S dosimetry, Phys. Status Solidi A, 209, 911–916, https://doi.org/10.1002/pssa.201100588, 2012.

Kemmler, J. A., Pokhrel, S., Birkenstock, J., Schowalter, M., Rosenauer, A., Bârsan, N., Weimar, U., and Mädler, L.: Quenched, nanocrystalline In4Sn3O12 high temperature phase for gas sensing applications, Sensor. Actuat. B-Chem., 161, 740–747, https://doi.org/10.1016/j.snb.2011.11.026, 2012.

Lee, A. P. and Reedy, B. J.: Temperature modulation in semiconductor gas sensing, Sensor. Actuat. B-Chem., 60, 35–42, https://doi.org/10.1016/S0925-4005(99)00241-5, 1999.

Leidinger, M., Sauerwald, T., Reimringer, W., Ventura, G., and Schütze, A.: Selective detection of hazardous VOCs for indoor air quality applications using a virtual gas sensor array, J. Sens. Sens. Syst., 3, 253–263, https://doi.org/10.5194/jsss-3-253-2014, 2014.

Leidinger, M., Rieger, M., Sauerwald, T., Alépée, C., and Schütze, A.: Integrated pre-concentrator gas sensor microsystem for ppb level benzene detection, Sensor. Actuat. B-Chem., 236, 988–996, https://doi.org/10.1016/j.snb.2016.04.064, 2016a.

Leidinger, M., Huotari, J., Sauerwald, T., Lappalainen, J., and Schütze, A.: Selective detection of naphthalene with nanostructured WO_3 gas sensors prepared by pulsed laser deposition, J. Sens. Sens. Syst., 5, 147–156, https://doi.org/10.5194/jsss-5-147-2016, 2016b.

Leidinger, M., Baur, T., Sauerwald, T., Schütze, A., Reimringer, W., Spinelle, L., and Gerboles, M.: Highly sensitive benzene detection with MOS gas sensors, Proc. AMA Conf. 2017, Nuremberg, Germany, 31 May–1 June 2017, 92–97, 2017.

Madou, M. J. and Morrison, S. R.: Chemical Sensing with Solid State Devices, Academic Press, San Diego, USA, 1989.

Morrison, S. R.: Semiconductor gas sensors, Sensor. Actuator., 2, 329–341, https://doi.org/10.1016/0250-6874(81)80054-6, 1981.

Nakata, S., Nakasuji, M., Ojima, N., and Kitora, M.: Characteristic nonlinear responses for gas species on the surface of different semiconductor gas sensors, Appl. Surf. Sci., 135, 285–292, https://doi.org/10.1016/S0169-4332(98)00290-6, 1998a.

Nakata, S., Ozaki, E., and Ojima, N.: Gas sensing based on the dynamic nonlinear responses of a semiconductor gas sensor: Dependence on the range and frequency of a cyclic temperature change, Anal. Chim. Acta, 361, 93–100, https://doi.org/10.1016/S0003-2670(98)00013-0, 1998b.

Sasahara, T., Kido, A., Sunayama, T., Uematsu, S., and Egashira, M.: Identification and quantification of alcohol by a micro gas sensor based on adsorption and combustion, Sensor. Actuat. B-Chem., 99, 532–538, https://doi.org/10.1016/j.snb.2004.01.002, 2004.

Schneidemesser, E. Von, Monks, P. S., and Plass-Duelmer, C.: Global comparison of VOC and CO observations in urban areas, Atmos. Environ., 44, 5053–5064, https://doi.org/10.1016/j.atmosenv.2010.09.010, 2010.

Schüler, M., Schneider, T., Sauerwald, T., and Schütze, A.: Impedance based detection of HMDSO poisoning in metal oxide gas sensors, Tech. Mess., 84, 697–705, https://doi.org/10.1515/teme-2017-0002, 2017.

Schultealbert, C., Baur, T., Schütze, A., Böttcher, S., and Sauerwald, T.: A novel approach towards calibrated measurement of trace gases using metal oxide semiconductor sensors, Sensor. Actuat. B-Chem., 239, 390–396, https://doi.org/10.1016/j.snb.2016.08.002, 2017.

Schütze, A., Baur, T., Leidinger, M., Reimringer, W., Jung, R., Conrad, T., and Sauerwald, T.: Highly Sensitive and Selective VOC Sensor Systems Based on Semiconductor Gas Sensors: How to?, Environments, 4, 20, https://doi.org/10.3390/environments4010020, 2017.

Spinelle, L., Michel, G., and Aleixandre, M.: Report of laboratory and in-situ in itu validation of micro-sensor sensor for monitoring ambient air pollution, ambient air pollution, Publication Office of the European Union, Luxembourg, https://doi.org/10.2788/4277, 2014.

Spinelle, L., Gerboles, M., Kok, G., Persijn, S., and Sauerwald, T.: Performance Evaluation of Low-Cost BTEX Sensors and Devices within the EURAMET Key-VOCs (Lv), MDPI Proceedings 2017, 1, 425, EUROSENSORS 2017, 3–6 September 2017 Paris, France, 30–33, https://doi.org/10.3390/proceedings1040425, 2017a.

Spinelle, L., Gerboles, M., Kok, G., Persijn, S., and Sauerwald, T.: Review of portable and low-cost sensors for the ambient air monitoring of benzene and other volatile organic compounds, Sensors, 17, 1520, https://doi.org/10.3390/s17071520, 2017b.

WHO Regional Office for Europe: WHO guidelines for indoor air quality: selected pollutants, Copenhagen, Denmark, 2010.

Wold, S., Sjöström, M., and Eriksson, L.: PLS-regression: A basic tool of chemometrics, Chemometr. Intell. Lab., 58, 109–130, https://doi.org/10.1016/S0169-7439(01)00155-1, 2001.

7 Integrated pre-concentrator gas sensor microsystem for ppb level benzene detection

Martin Leidinger[1], Max Rieger[2], Tilman Sauerwald[1], Christine Alépée[3] and Andreas Schütze[1]

[1] Lab for Measurement Technology, Saarland University, D-66123 Saarbrücken, Germany

[2] Fraunhofer Institute for Chemical Technology ICT, D-76327 Pfinztal, Germany

[3] SGX Sensortech SA, CH-2035 Corcelles-Cormondrèche, Switzerland

Originally published in *Sensors and Actuators B: Chemical, 236, pp. 988-996, 2016*

doi: 10.1016/j.snb.2016.04.064

Synopsis

The option of using gas pre-concentration for detecting low gas concentrations and some exemplary applications have been introduced in chapter 2.2. The shown pre-concentrator systems all comprise large, complex fluidic setups, which are not usable for low-cost gas sensor systems. For the application of air quality monitoring, such small and inexpensive systems are required, as several sensor nodes are necessary to equip a home, an office building or other indoor as well as outdoor locations.

As an important step towards realization of such systems, the presented work describes the design, simulation and characterization of a fully integrated sensor module, comprising a single (or dual) MOS gas sensor and a MOF pre-concentrator in a single SMD (surface-mount device) package. This is realized by mounting two separate micro hotplates, each optimized for its intended use, next to each other in the package. The dimensions of the integrated device are 5x7x1.5 mm^3.

First, the performance of two MOF materials for gas pre-concentration has been tested with various methods. Using inverse gas chromatography, the partition coefficients of the materials could be estimated for benzene and toluene at several temperatures. These values have been used for simulation of the integrated device operation. A standard adsorbent material, Tenax® TA, was included in these tests as a reference. The two MOF materials have also been deposited on heated ceramic substrates which were placed in a 10 ppm benzene gas stream leading to a mass spectrometer with which the benzene concentration could be monitored continuously. Heating of the substrates after a certain adsorption time generated clear peaks in benzene concentration, which shows the general applicability of the MOFs and which could also be used for further material characterization.

The operating principle of the integrated pre-concentrator has been simulated using FEM simulations and the performance of the system, i.e. the pre-concentration factor, has been estimated from the results. Two different MOF materials have been characterized for their relevant properties, which have been used as input for the simulation model. The MOF that yielded better results in the simulation was then used for real gas tests; measurements with benzene in ppb concentrations have been performed. The addition of the pre-concentrator clearly improves the sensitivity of the gas sensor device compared to a single sensor without pre-concentrator.

The sensor/pre-concentrator devices have later been integrated into gas sensing systems, specifically designed for indoor use, by 3S GmbH (Saarbrücken, Germany), see Figure 17.

Figure 17: Sensor system prototype; Left: PCB with gas sensor / pre-concentrator device mounted in the middle; Center: aluminum flush-mount front panel with gas access; Right: fully assembled system ready for installation [232].

The sensing module is mounted on a PCB which contains electronics for a number of tasks:

- Temperature control of the hotplates (gas sensor and pre-concentrator)
- Acquisition of the sensor signals of the various sensors
    - gas sensor (measurement of the sensing layer conductivity using a log amplifier, cf. chapter 2.1.2)
    - temperature / humidity sensor
    - optical CO_2 sensor
- Data storage
- On-line signal processing
- Control of overall system operation

This list shows that such sensor systems are complex devices, therefore all components, including the sensor/pre-concentrator unit, must be optimized for size and cost, which means integration of as many functions as possible into the separate modules.

The shown systems represent an evolution of the systems presented in chapter 6, the identified issues regarding gas transport and housing materials have been addressed in the new design. The front plate material in the prototypes is made from aluminum, which does not emit VOCs, and the sensor device has been placed directly at the front plate with a seal around it, in order to create a short diffusion path to the atmosphere and to shield it from gas emissions from the PCB.

Graphical abstract

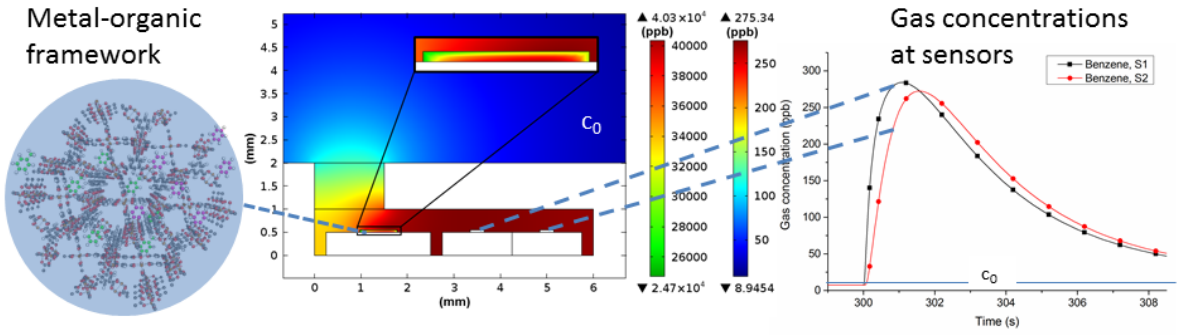

Supplementary material

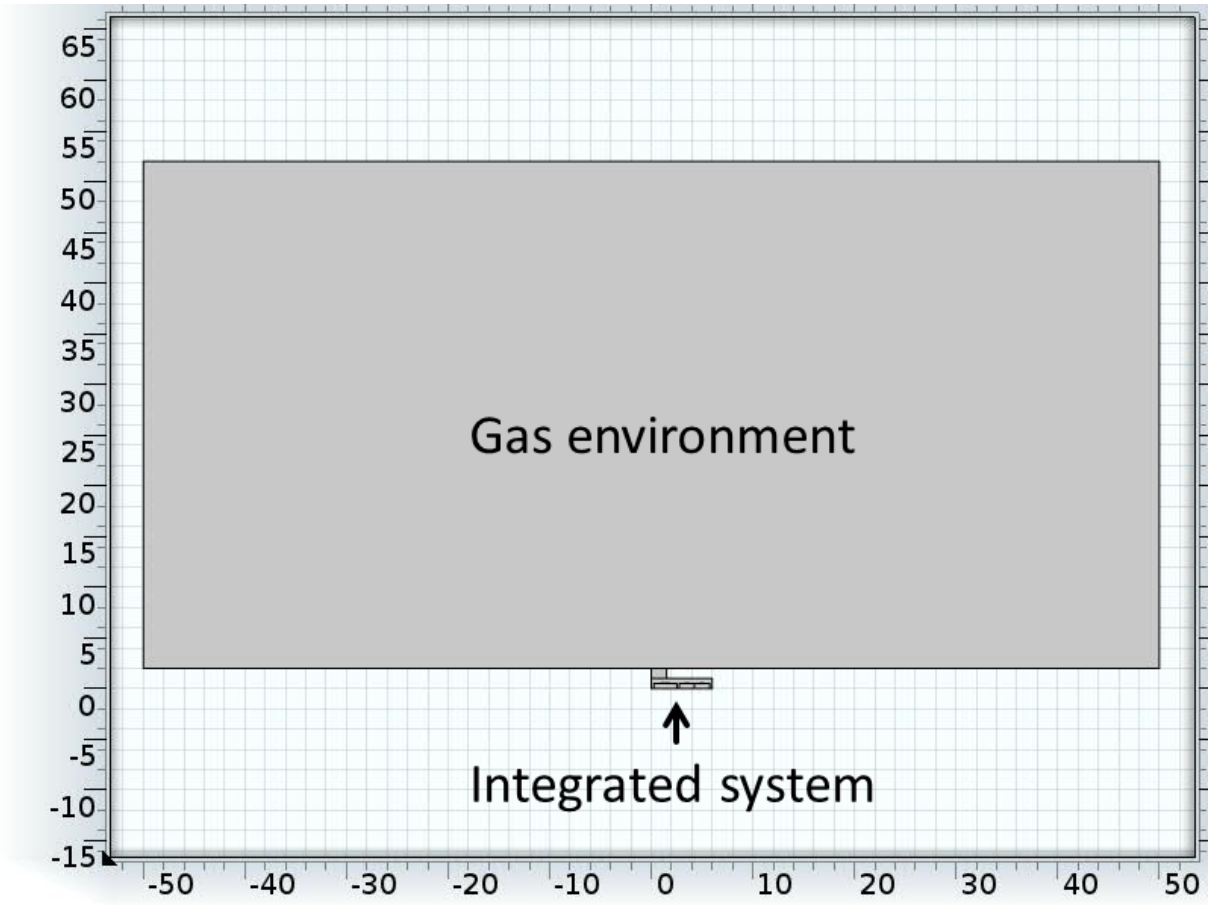

Sensors and Actuators B 236 (2016) 988–996

Contents lists available at ScienceDirect

Sensors and Actuators B: Chemical

journal homepage: www.elsevier.com/locate/snb

Integrated pre-concentrator gas sensor microsystem for ppb level benzene detection

Martin Leidinger[a,*], Max Rieger[b], Tilman Sauerwald[a], Christine Alépée[c], Andreas Schütze[a]

[a] Lab for Measurement Technology, Saarland University, D-66123 Saarbrücken, Germany
[b] Fraunhofer Institute for Chemical Technology ICT, D-76327 Pfinztal, Germany
[c] SGX Sensortech SA, CH-2035 Corcelles-Cormondrèche, Switzerland

ARTICLE INFO

Article history:
Received 31 December 2015
Received in revised form 4 March 2016
Accepted 12 April 2016
Available online 14 April 2016

Keywords:
Gas pre-concentration
Metal-organic frameworks
Integrated gas sensor system
Metal oxide semiconductor gas sensor
Indoor air quality
FEM simulation

ABSTRACT

An integrated microsystem for (indoor) air quality monitoring applications is presented. By combining a gas pre-concentrator based on metal-organic frameworks (MOFs) and a metal oxide semiconductor gas sensor, a device for detecting ppb levels of volatile organic compounds was designed, integrated and tested with benzene as a target gas. Two metal organic frameworks have been characterized for their suitability as gas pre-concentration materials for benzene and toluene using inverse gas chromatography and mass spectrometry measurements in order to obtain breakthrough values for gas adsorption. Both MOFs showed a higher pre-concentration effect compared to Tenax® TA, a state-of-the-art commercial adsorbent material.

By depositing a MOF material on a micro hotplate integrated in a package together with a gas sensor, an integrated gas sensor microsystem was realized. This system has been characterized in FEM simulations concerning its gas pre-concentration capabilities and behavior. Test measurements were performed using benzene at concentrations of 10–1000 ppb. Both the simulations and the measurements show the suitability of the system design for the task. Significantly increased gas concentrations have been observed during thermal desorption from the pre-concentrator after gas adsorption at a low temperature.

1. Introduction

As people spend most time indoors, indoor air quality (IAQ) has become an important health factor. Many different compounds contribute to the problem of potential health issues caused by the air inside buildings. While carbon dioxide (CO_2) is the most commonly monitored species, there are also carbon monoxide (CO), nitrogen dioxide (NO_2) and a variety of volatile organic compounds (VOCs) to be considered [1,2]. The occurrence of these substances has been investigated, e.g. in the INDEX project [3] or the Airmex study [4]. Exposure to VOCs for a long time can have negative effects on human health, including damage to the respiratory system and skin irritations [5]. Moreover, VOCs are the main cause of the sick building syndrome [6,7]. Besides these unspecific adverse health effects, some VOCs are proven to be carcinogenic (e.g. benzene [1]) or are suspected to be carcinogenic (e.g. formaldehyde [8]). Formaldehyde, benzene and naphthalene have been identified as VOCs with the highest priority based on their toxicity and prevalence [1,3]. The respective guideline threshold values for these substances in indoor air are 0.1 mg/m^3 (81 ppb) for formaldehyde [1], 0.01 mg/m^3 (1.9 ppb) for naphthalene [1], and 5 μg/m^3 (1.6 ppb) for benzene [9].

To detect such small concentrations of these gases without expensive and time-consuming analytical measurements like GC–MS analysis [10], solid state gas sensors can be used. It was shown previously that formaldehyde, benzene and naphthalene can be detected in the relevant concentration range using metal oxide semiconductor (MOS) gas sensors in temperature-cycled operation (TCO) and can be discriminated using signal pattern recognition techniques, e.g. linear discriminant analysis (LDA) [11]. These tests were using a changing background of ethanol as a simple model for the interfering background of further VOCs. For more complex VOC backgrounds and for applications under real environmental conditions the performance of the sensor system needs to be enhanced, especially concerning sensitivity and selectivity.

* Corresponding author.
E-mail addresses: m.leidinger@lmt.uni-saarland.de (M. Leidinger), max.rieger@ict.fraunhofer.de (M. Rieger), t.sauerwald@lmt.uni-saarland.de (T. Sauerwald), christine.alepee@sgxsensortech.com (C. Alépée), schuetze@lmt.uni-saarland.de (A. Schütze).

http://dx.doi.org/10.1016/j.snb.2016.04.064
0925-4005/

To this end, a system for gas pre-concentration was realized and tested within this work. With this technique, gases are collected inside a material with a high surface area over a certain time and then a rapid thermal desorption is used to generate a high gas concentration for a short period.

There are several options for pre-concentrator materials, one of them metal-organic frameworks (MOFs). Metal-organic frameworks are a novel class of crystalline porous coordination polymers with a very high surface area (in some cases more than 1000 m^2/g), which means relatively large quantities of gas can be adsorbed and stored in a small volume of the material. They consist of metal or metal clusters (nodes) and spatially interconnecting multidentate organic molecules (linkers) [12]. One-, two- or three-dimensional structures may be formed. Especially the three-dimensionality may render a high interior surface. The resulting network exhibits pores and channels with spatial and chemical uniformity. MOFs can be tailored to a specific need by adapting the synthesis conditions, including choice of linkers, nodes and their molar ratios. Despite their applications in gas storage, separation and catalysis, we focus on using them as a guest molecule trapping-agent for pre-concentration prior to detection.

Recently published computational investigations suggest the usage of MOFs as pre-concentrator materials for small molecules such as xylenes, phosphonates and high explosives (TNT) [13–16]. In this investigation, two MOFs materials, HKUST-1 (Cu_3BTC_2) [17], and MIL-53 (AlBDC) [18], have been characterized regarding their suitability as pre-concentrator materials for benzene, i.e. their adsorption potential at low temperatures and their desorption characteristics at elevated temperature were studied. For comparison, the adsorption potential was also tested for toluene.

A design for an integrated system containing pre-concentrator and gas sensor was developed and implemented. The MOF material was deposited on a MEMS hotplate, allowing for fast temperature cycling of the pre-concentrator. The physical processes inside the system, e.g. gas transport by diffusion and gas enrichment, have been simulated via FEM simulations. Simulations have been performed with benzene as well as toluene, in order to evaluate the possibility to discriminate between these two components with the MOF/MOS combination.

Prototypes of the integrated system were realized and test measurements with benzene were performed. The measurements show the basic functionality of the approach, the pre-concentration effect can clearly be observed in the gas sensor signals.

2. Experimental

For realization of the integrated systems first the two MOF materials were characterized regarding their pre-concentration performance. Checked were their characteristics for adsorption and desorption of benzene and for comparison also their adsorption potential for toluene. For optimizing the basic setup of the pre-concentrator gas sensor system, a model was implemented into FEM simulation software. With this tool, the geometry of the setup of pre-concentrator and sensor in a package could be optimized. A prototype was then integrated and tested for its benzene detection performance.

2.1. MOFs as pre-concentrator materials

The most common method to characterize MOF substances in terms of pore volume and specific surface area is nitrogen sorption isotherms in the BET region. These isotherms, however, only allow determination of the accessible surface area with respect to nitrogen molecules. Measuring equilibrium sorption isotherms for organic vapors is often complicated and requires precisely thermostated equipment. Alternatively, the method of inverse gas chromatography (iGC) [19] can be used to estimate guest molecule sorbent affinities [20]. Heats of adsorption as well as partition coefficients can be calculated from iGC experiments [21].

Table 1
Measured breakthrough volumes for benzene and toluene for MIL-53, HKUST-1 and Tenax® TA, in ml(N_2)/g. Underlined values were extrapolated.

	MIL-53		HKUST-1		TENAX® TA	
T (°C)	Benzene	Toluene	Benzene	Toluene	Benzene	Toluene
50	173117	529840	72174	94534	554	1132
100	8225	46438	3060	14543	375	496
150	1481	5413	1103	5849	197	633
200	556	1386	344	1386	203	478

Two commercially available so-called Basolites®, A100 or MIL-53 and C300 or HKUST-1, were tested in comparison with a standard adsorbent (Tenax® TA in 60–80). Metal-organic frameworks and Tenax® TA were obtained from Sigma Aldrich. The MOF powders showed volume weighted particle diameter means (D [4,3]) of 19.8 μm and 16.2 μm for MIL-53 and HKUST-1, respectively, measured by dynamic light scattering.

A common setup was used to determine breakthrough volumes of organic vapors regarding MOFs. A regular gas chromatograph was equipped with a photoionization detector and a packed column of MOF material was inserted between the injector and detector connecting tube. Using a mass-flow meter and peak maximum retention times it was possible to determine breakthrough or retention volumes of relevant guest molecules on various MOFs. Retention volumes are calculated by subtracting the dead time (methane) and multiplying carrier gas flows (usually 10 ml/min via gas flow meter) with particular retention times. They are normalized by dividing through the respective sorbent mass. A comparison with Tenax® TA was drawn as it is a state-of-the art sorbent for air sampling. The values determined for Tenax® TA differ from values presented in the literature (i.e. SISweb [22]). However, it was also shown that sorbent descriptors of this material differ from that of older lot-numbers [21]. This may be attributed to the manufacturing process and a stronger particle size dependence on equilibration-times during elution of substances. Tenax® TA 60–80 mesh is 177–250 microns while MOF particles are almost one order of magnitude smaller. In some cases the breakthrough volume was so high that the maximum technical chromatogram length of 999 min was exceeded. In these cases the breakthrough volumes were extrapolated using the van't Hoff equation.

The measurement results are composed in Table 1. Results showed that breakthrough volumes varied among benzene and a potential interferent (toluene). As expected, the retention volumes of the MOF materials drop with increasing temperature. This is due to the higher kinetic energy of guest molecules and hampered tendencies to interact with pore walls within and outside the framework. In case of benzene on HKUST-1 breakthrough volumes for benzene drop from 7.22×10^4 ml to 344 ml of nitrogen per gram of absorbent when going up from 50 °C to 200 °C.

MIL-53 shows similar tendencies as HKUST-1 but a higher dynamic retention volume in terms of different temperatures. Benzene and toluene, having retention volumes of 1.73×10^5 ml/g and 5.30×10^5 ml/g at 50 °C, drop to 556 ml/g and 1386 ml/g at 200 °C, respectively.

This is not the case for Tenax® TA. Not even a change of one order of magnitude in retention volume is achieved by a similar temperature jump. Whereas benzene retention volume at 50 °C is about 550 ml/g, it is only reduced to approx. 200 ml/g at 200 °C.

Substance discrimination is another feature to be addressed by the sorbent material. A higher difference in retention volumes on a specific sorbent allows for time-shifted desorption peaks. In case of

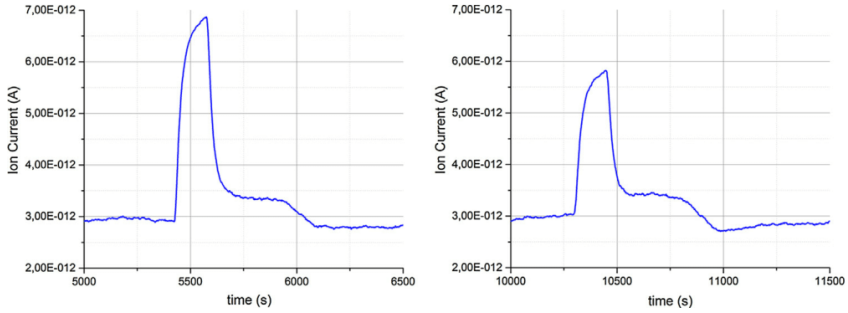

Fig. 1. Desorption peak recorded by mass spectrometry for M = 78 (benzene) after 60 min (left) and 30 min (right) of sampling 10 ppm of benzene on HKUST-1.

a punctiformly loaded lattice of HKUST-1, with both benzene and toluene adsorbed in its structure, a thermal desorption at 200 °C and a carrier gas flow of 10 ml/min will produce a toluene peak maximum after 1.38 min and a benzene peak maximum after 0.34 min, calculated as in [24]. In practical terms, toluene is delayed four-fold compared to benzene. This allows for a dynamic separation. In case of Tenax® TA this discrimination factor is only approx. 2.3 at 200 °C.

2.2. Preparation and test of pre-concentrator devices

By immersing bulk MOF powders in di-*n*-butylether it was possible to create stable suspensions, with respect to sedimentation. These suspensions were drop coated on alumina heater substrates ($3 \times 3\,mm^2$) using capillaries. Approx. 30 mg of the MOF material was deposited on the substrates. For testing thermal gas desorption, selected gas streams were conducted through stainless steel tubing into a measurement chamber containing the pre-concentrators (PCs). In order to determine the pre-concentration efficiency of the film we used a setup presented in [23]. Exiting gas streams were permanently monitored by a mass spectrometer (Pfeiffer GSD 301 quadrupole MS) using multiple ion detection. The system gas flow was regulated using a mass-flow controller and a vacuum pump at the exhaust of the system. Gas samples were supplied in gas sampling bags (Supelco, 30240-U). A T-valve was used to switch between zero air and analyte in zero air. The mass detector's linearity was evaluated by measuring gas sampling bags containing different dilutions of analyte vapor. Linearity was observed for a range from 100 ppb to 100 ppm. A constant flow of analyte loaded carrier gas was conducted through the measurement chamber while the pre-concentrator was kept at room temperature. After a specific sampling time, the pre-concentrator was heated for 500 s to 200 °C for thermal desorption, leading to a particular gain in detector signal (ion current), as shown in Fig. 1. The MS signal shows a clear peak when the heater is switched to desorption temperature.

Examining the desorption peaks, a linear relation of sampling time and desorption peak area could be established below 20 min. Going from 30 min to 60 min of adsorption period, only an area gain of 25% is observed (7.88×10^{-10} As for 60 min and 6.27×10^{-10} As for 30 min). This indicates an approaching saturation or, more correctly, solid-gas-equilibrium.

For the experiment with 10 ppm benzene in the carrier gas we observed an (peak height based) enrichment factor of almost 700% using 60 min of adsorption before thermal desorption and 550 % in case of 30 min. Full widths at half maximum (FWHM) for both desorption peaks are approx. 150 s. The signal drop below the baseline after the heater is switched off (after 500 s of heating) shows the re-adsorption of benzene on the MOF material.

In an experiment with 1 ppm benzene this value drops to 460% for 60 min (Fig. 2). Shorter adsorption intervals (30, 15 and 10 min) lead to preconcentration factors of 310, 210 and 190%, respectively.

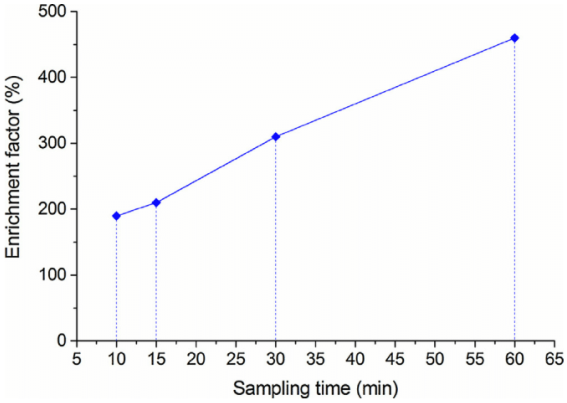

Fig. 2. Enrichment factor vs. sampling time for HKUST-1 and benzene.

This plot of enrichment factors over sampling time shows that at the lower concentration a gas-solid equilibrium is not reached after 60 min of sampling as there is still a linear relationship.

2.3. System integration and FEM simulations

For including MOF pre-concentrators in an FEM simulation, the partition coefficient and the gas diffusion coefficients inside the MOF are required. Partition coefficients for the MOF/gas combinations were estimated using equilibrium sorption constants [24]. These constants are identical to retention volumes of a 50% peak height of an elution peak of an analyte on a sorbent [21]. The values were extracted from the breakthrough volume measurements.

For estimation of the diffusion coefficients of the gases in the MOF, the simulated diffusion coefficients of several MOFs from [25] have been used as a basis. In [25], diffusion coefficients for benzene and toluene have been calculated in the range from $8.3 \times 10^{-6}\,cm^2/s$ to $4.4 \times 10^{-5}\,cm^2/s$ for benzene and from $2.4 \times 10^{-6}\,cm^2/s$ to $2.9 \times 10^{-5}\,cm^2/s$ for toluene, respectively. Simulations showed that for our geometry with a very thin MOF layer (50 μm) this parameter has a negligible influence on the performance of the system. Thus, the average values for the two gases, $2.6 \times 10^{-5}\,cm^2/s$ for benzene and $1.56 \times 10^{-5}\,cm^2/s$ for toluene, were chosen. All material parameters used in the FEM simulations are listed in Table 2.

To set up an integrated pre-concentrator gas sensor system, a pre-concentrator chip and a gas sensor chip were mounted in an SMD ceramic package with external dimensions of $5 \times 7 \times 1\,mm^3$. The design of the integrated system was also implemented into COMSOL Multiphysics. Fig. 3 shows the detailed cross section of the

Table 2
Material parameters used in the FEM simulations.

Parameter	Value	Reference
Partition coefficient at 25 °C		
Benzene	HKUST-1: 3.52×10^{-5} MIL-53: 1.45×10^{-5}	Measurement (extrapolation)
Toluene	HKUST-1: $1.59 \cdot 10^{-5}$ MIL-53: 9.47×10^{-6}	Measurement (extrapolation)
Partition coefficient at 50 °C		
Benzene	HKUST-1: 6.16×10^{-5} MIL-53: 3.89×10^{-5}	Measurement
Toluene	HKUST-1: 4.35×10^{-5} MIL-53: 2.87×10^{-5}	Measurement (extrapolation)
Partition coefficient at 200 °C		
Benzene	HKUST-1: 8.93×10^{-3} MIL-53: 6.01×10^{-3}	Measurement
Toluene	HKUST-1: 2.19×10^{-3} MIL-53: 2.36×10^{-3}	Measurement
Diffusion coefficient in air		
Benzene	8.8×10^{-2} cm²/s	[26]
Toluene	8.7×10^{-2} cm²/s	[26]
Diffusion coefficient in MOF		
Benzene	2.6×10^{-5} cm²/s	Estimation, based on [25]
Toluene	1.56×10^{-5} cm²/s	Estimation, based on [25]

microsystem. A cross section of the full COMSOL model including the gas environment is provided in the supplementary materials.

For the first prototypes, a dual gas sensor chip with two semiconductor sensing layers was used and mounted inside the package next to the pre-concentrator chip. The gas sensor chip is a commercial device by SGX Sensortech SA (Corcelles, Switzerland); the two gas sensitive layers are the same as in the dual sensor device MiCS-4514. Gas access from the environment was limited to a gas port with a width of 1.5 mm and a height of 1 mm at the end of the package at which the pre-concentrator is located. Various options for the gas access, i.e. position and size, have been tested; the highest increase of gas concentrations has been obtained with the presented design.

Using the parameters in Table 2, an adsorption/desorption cycle was simulated, in separate simulations for each of the two gases benzene and toluene, for both MOF materials and different adsorption temperatures. The starting condition for the gas concentration was 10 ppb in the whole geometry, in the environment as well as inside the device package. Adsorption was simulated for 300 s by selecting the partition coefficient for 50 °C. After 300 s the partition coefficient was changed to the value for 200 °C for 180 s to simulate thermal gas desorption, then was changed back again to the low temperature value. Total simulated time for each compound was 600 s. Adsorption was simulated for a temperature of 50 °C, as the partition coefficients for room temperature were not directly available from the measurements but had to be extrapolated. Furthermore, a slightly heated pre-concentrator can have benefits in real applications, e.g., suppressing ambient temperature fluctuations and fluctuations of the background of permanent gases and highly volatile organic compounds.

Gas distributions for benzene inside the device after 6.5 s of adsorption and 1.5 s after start of desorption are shown in Fig. 3, using HKUST-1 as pre-concentrator material. The simulation shows that already 6.5 s after start of adsorption (Fig. 3a), almost the entire gas from inside the package has adsorbed in the pre-concentrator; especially at the location of the two sensors the concentration is reduced by more than one order of magnitude. Moreover, gas from the environment has already started to adsorb in the material, forming an almost hemispherical depletion zone. During gas desorption the highest gas concentration at the location of the two sensor chips was observed after approx. 1.5 s (Fig. 3b).

The gas concentrations just above the centers of the two gas sensor layers were extracted over time, as shown in Figs. 4 and 5.

Table 3
Simulated gas concentration increase factors at the two sensing layers for all MOF/gas combinations.

Gas increase factor (c_{peak}/c_0)	HKUST-1		MIL-53	
	S1	S2	S1	S2
Sampling at 50 °C				
Benzene	28.4	27.2	30.3	29.3
Toluene	16.6	16.4	20.1	19.9
Sampling at 25 °C				
Benzene	36.6	35.1	38.8	37.6
Toluene	22.2	21.9	25.0	24.7

The sensor located closer to the pre-concentrator is labeled S1, the sensor further away in the corner is labeled S2 (see Fig. 3a). At the start of the simulation run the gas concentrations at the sensors decrease rapidly as the gas adsorbs in the pre-concentrator. As the pre-concentrator becomes slowly saturated, gas diffusing from the environment into the housing can pass the pre-concentrator again and reach the sensors. However, even after a sampling time of 300 s the concentration at the sensor is 4.75 ppb (benzene) to 5.75 ppb (toluene) with both MOFs, which is still significantly below equilibrium (10 ppb). After switching the partition coefficient to desorption, there is a significant rise in gas concentration for all gas and MOF material combinations at both sensors. Due to the longer diffusion path, the peak concentration value at sensor S2 is reached approx. 0.5 s after the peak at S1. During the following concentration decrease the values stay slightly higher at S2 compared to S1.

The peak heights differ significantly for the two gases while the MOF material has only a minor influence. Benzene shows higher peaks due to the larger change in partition coefficient from adsorption to desorption temperature. For the same reason MIL-53 generates slightly higher peaks for both gases.

The factors of increase of gas concentrations at the desorption peaks over the initial concentration of 10 ppb are listed in Table 3, for simulations with adsorption at 50 °C and for room temperature (25 °C) based on extrapolated partition coefficient values.

2.4. Test measurements

An integrated prototype system was tested with benzene as test gas and MIL-53 as pre-concentrator material. Benzene was applied in concentrations of 10 ppb, 100 ppb and 1 ppm in dry air. The test

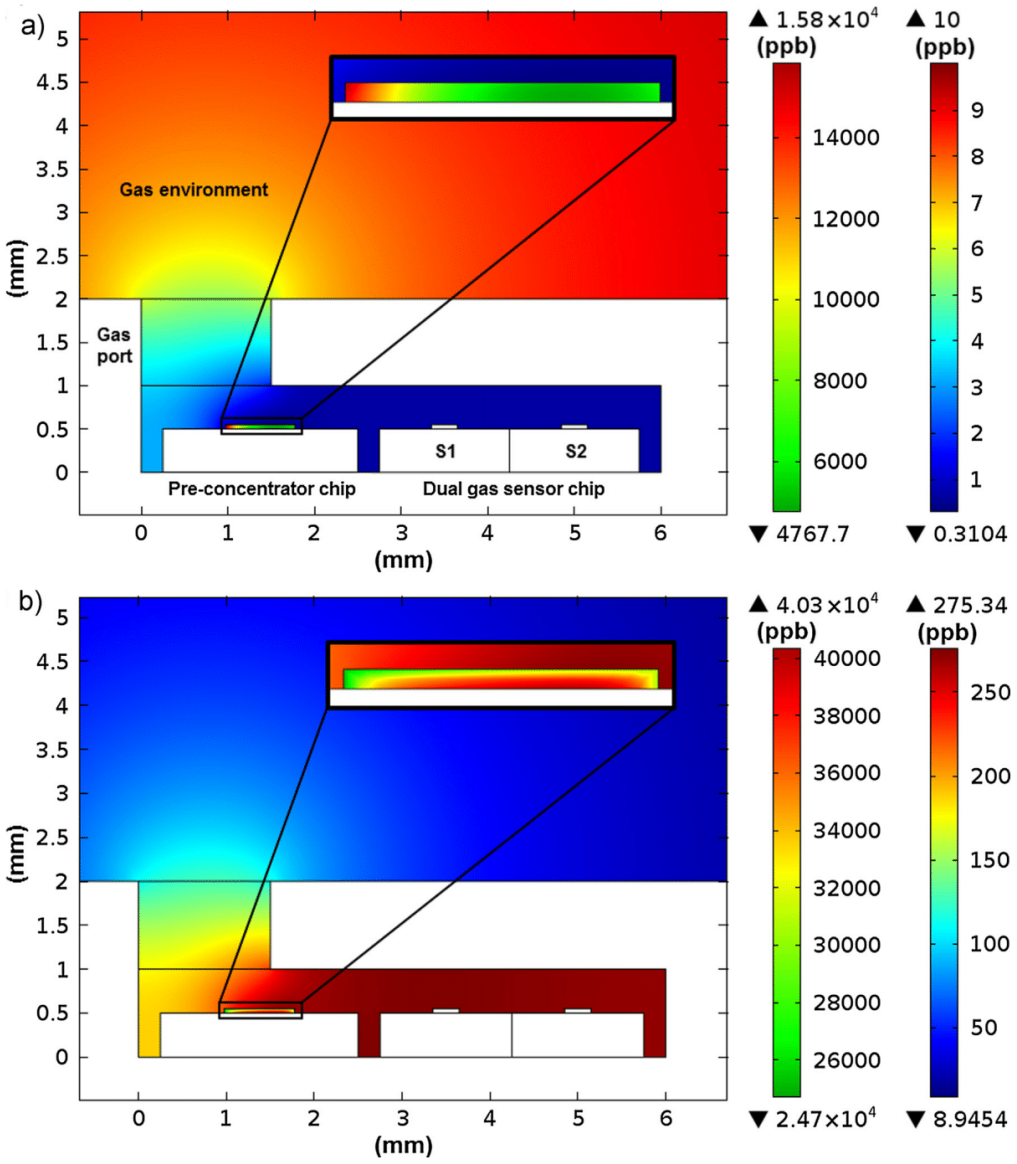

Fig. 3. Simulated gas concentrations inside the pre-concentrator material (left scale) and in the air (right scale), simulated for benzene and HKUST-1 as pre-concentrator material. (a) 6.5 s after start of adsorption at 50 °C. Nearly all gas from inside the package has been adsorbed in the pre-concentrator material. (b) 1.5 s after start of desorption at 200 °C. The highest gas concentration is obtained inside the microsystem, i.e. at the locations of the two gas sensor chips.

gases were generated using a two-step gas dilution of a benzene gas cylinder (50 ppm in air) in a gas mixing system designed specifically for VOC trace gases [27]. The measurements were performed in dry zero air at a total gas flow of 80 ml/min. For the presented first prototypes, not the whole heater area was coated with the MOF materials. Only small suspension drops with a diameter of approx. 300 μm, corresponding to an area of 0.07 mm^2, were deposited on the heaters while the simulations shown above are based on a pre-concentrator area of 0.5 mm^2.

Both the pre-concentrator and the sensors were operated in temperature cycled operation using the TCO electronics *Toolbox* provided by 3S GmbH (Saarbruecken, Germany). Cycle length was 600 s total; the temperature cycles for the pre-concentrator and the gas sensors are shown in Fig. 6. During the first 298 s of the measurement cycle, all devices were switched off. The gas sampling performance of the pre-concentrator is better at lower temperature, hence the gas sensors were switched off to prevent thermal crosstalk to the MOF coated chip. 298 s into the cycle, the gas sensors were heated to a high temperature, 400 °C for 2 s in order to clean the sensor surface before starting the gas desorption from the pre-concentrator. At 300 s, the sensors were switched to 300 °C and the pre-concentrator was switched to desorption at 200 °C for 180 s. The gas sensors remained at 300 °C until the end of the cycle and were then switched off.

Despite of the high functionality and performance of the system the power consumption is low. Beneficial effects are the

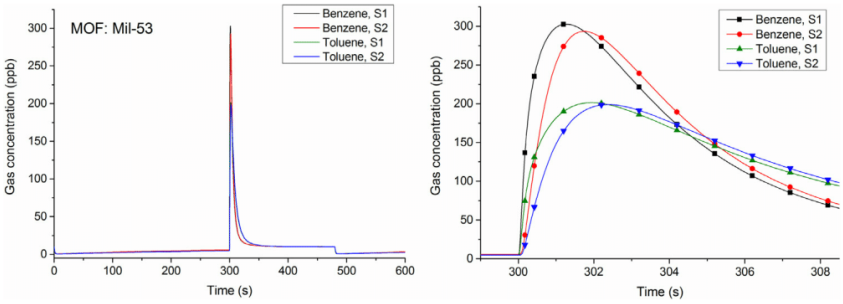

Fig. 4. Simulated gas concentrations at the locations of the two gas sensor layers for the two gases and MIL-53 as pre-concentrator material during an adsorption/desorption run. The pre-concentrator is switched from adsorption to desorption at 300 s and switched back to adsorption at 480 s. Left: full cycles; right: detail of the desorption peaks showing a strong increase of the gas concentration.

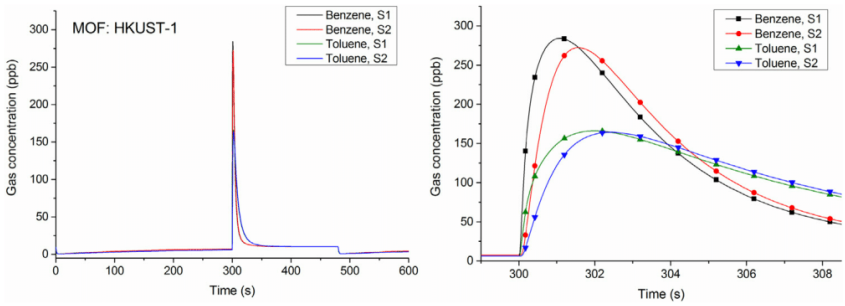

Fig. 5. Simulated gas concentrations at the locations of the two gas sensor layers for the two gases and HKUST-1 as pre-concentrator material during an adsorption/desorption run. The pre-concentrator is switched from adsorption to desorption at 300 s and switched back to desorption at 480 s. Left: full cycles; right: detail of the desorption peaks.

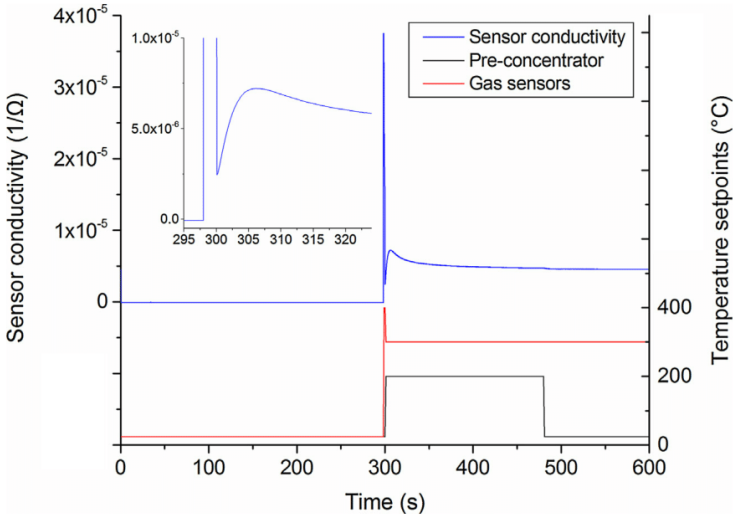

Fig. 6. Temperature setpoints for pre-concentrator and gas sensors as well as measured gas sensor signal during a 600 s TCO cycle [28]. The signal is from the sensor in the corner of the package, "S2" in the simulations. At 298 s the gas sensor is switched to a high temperature of 400 °C for 2 s, and then switched to 300 °C for gas detection. The pre-concentrator is switched from room temperature to 200 °C at 300 s and switched off again at 480 s.

minimization of the heated areas (for the sensors as well as for the pre-concentrator) and the intermittent operation mode. The pre-concentrator heater needs 43 mW at 200 °C for 180 s, the sensor heater 88 mW at 400 °C for 2 s and 60 mW at 300 °C for 300 s. This yields the average power consumption for the dual sensor pre-concentrator system to 73.5 mW for the 600 s cycle. If only one gas sensor is installed, average power consumption is 43.2 mW. We are optimistic that the power consumption could be

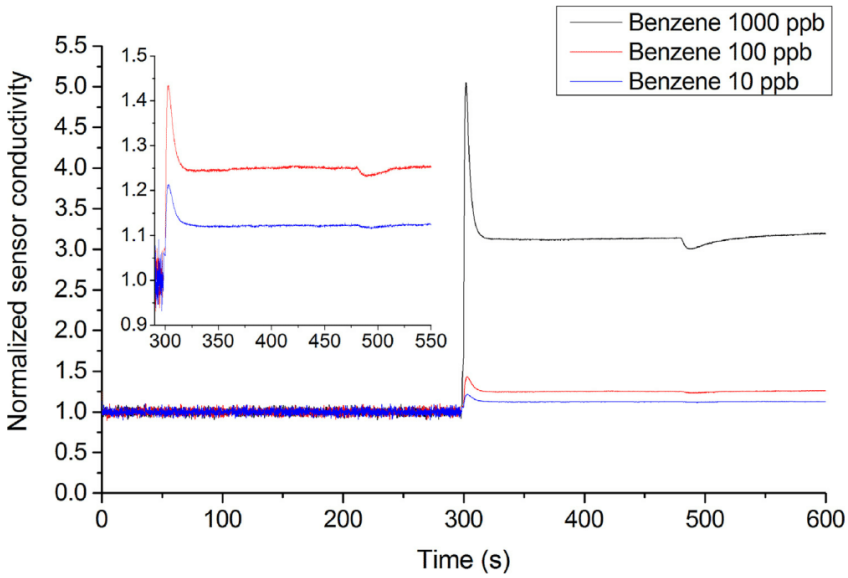

Fig. 7. Normalized sensor signals during a TCO cycle for 1000 ppb, 100 ppb and 10 ppb of benzene. For each concentration, a cycle with benzene was divided pointwise by a cycle in zero air without benzene.

significantly optimized by shortening the power-on times of the devices. For example, if the time the pre-concentrator is switched on is reduced to 20 s and the time the sensors are set to 300 °C is reduced to 40 s, average power consumption for a 600 s cycle drops to 10.0 mW for a dual sensor system and 5.7 mW for a single sensor system.

3. Results

Only the sensor of the dual sensor chip in the far corner of the package (S2 in the simulations) was evaluated for analyzing the basic functionality of the prototype system, the raw sensor signal of a temperature cycle is shown in Fig 6. Before 298 s, the sensor is switched off and the signal close to zero, due to limitations of the read-out electronics at low conductivities. At 298 s, the sensor is switched to a high temperature for 2 s and hits the upper limit of the read-out circuit. At 300 s, when the temperature is switched to 300 °C and the pre-concentrator is switched on, the sensor signal first drops quickly, then rises to a peak after several seconds and then falls towards a steady signal. In this peak, several effects are combined. There is the general sensor layer behavior after a temperature change, the effect of gas desorbed from the pre-concentrator, and a slight influence of thermal crosstalk from the pre-concentrator heater. After switching off of the PC heater at 480 s, the signal drops slightly to a steady value until the end of the cycle indicating gas adsorption in the pre-concentrator.

To separate the effects and extract the signal generated by the gas pre-concentration, a normalized sensor cycle G/G_0 was calculated by dividing a signal cycle measured with benzene pointwise by a signal cycle recorded in pure air. This eliminates all influences but the benzene. This normalization was performed for all three benzene concentrations; see Fig. 7.

During the adsorption phase, there is no significant signal; the calculated quotient is quite noisy as the sensor signals are noisy when the sensors are switched off. The signal peak after heating up the MOF after 300 s is obvious. It represents the gas desorption from the pre-concentrator. After a few seconds, all the gas is desorbed from the MOF so that the sensor signal drops and stabilizes as now only the applied benzene concentration is inside the package. There is a slight signal drop when the pre-concentrator is switched off (at 480 s), the sensor therefore detects the decrease of the gas concentration inside the integrated device which is caused by adsorption in the MOF. Thereafter, the signal increases again at least for several tens of seconds while adsorption and desorption on the MOF is approaching equilibrium (cf. the simulated concentration curves for benzene in Figs. 4 and 5).

The desorption peaks for all concentrations are roughly twice as high as the steady sensor signals. However, the sensor signal is not linear; the peak at 10 ppb of benzene reaches a relative change of conductance of 21%, which is nearly as much as for the steady sensor signal for 100 ppb of benzene indicating a pre-concentration factor of almost 10.

4. Conclusion and outlook

We successfully designed, simulated, integrated and tested an integrated pre-concentrator gas sensor microsystem. Both the simulations and the gas measurements show that the chosen design is suitable for the task of generating short pulses with significantly increased gas concentrations for VOC target gases in the ppb range.

Two MOF materials were tested for their suitability in pre-concentration applications using inverse gas chromatography measurements for adsorption and mass spectrometry measurements for desorption. Using iGC, relative affinities of benzene and toluene towards the two MOFs and a state-of-the-art adsorbent (Tenax® TA) were determined. The MOFs outperformed Tenax® in this setup and are thus suitable for pre-concentrating the two tested compounds benzene and toluene. The affinities of the two gases differ significantly for both MOFs. This may allow for a dynamic separation based on the difference in desorption peaks over time and hereby discrimination of different gases with the integrated sensor system.

An FEM model of the integrated system has been implemented in COMSOL for which gas adsorption and desorption in the pre-concentrator and gas diffusion inside the system as well as gas exchange with the environment could be studied. It was found

that the performance of the system is influenced significantly by the material parameters of the pre-concentrator and the gas, i.e. the partition coefficient. These parameters determine the amount of gas that is adsorbed inside the pre-concentrator and thus the gas concentration at the sensors at desorption. Another parameter that varies significantly with the gas type is the time it takes for the pre-concentrator to be saturated, i.e. the adsorption time that is required for relevant pre-concentration. With the measured values from the iGC material characterizations and the estimations made for the material parameters for the simulations, gas concentrations could be increased by a factor of more than 30. Even though benzene and toluene have fairly similar affinities to the MOF the pre-concentration factor for benzene was more than 50% higher compared to toluene.

The design of the integrated system was successfully tested with benzene gas measurements. The normalized gas sensor signals clearly showed significant peaks at pre-concentrator desorption corresponding to an increase of the gas concentration. For 10 ppb of benzene, the sensor signal during the desorption peak nearly reaches the level of the steady state response for 100 ppb of benzene.

The FEM simulation of the system will be used to further optimize the design of the setup and to study possible operating modes of the system, e.g. to separate gases of different volatilities. The performance of the system will be further enhanced by increasing the MOF coated area and by applying optimized thermal cycling for both the sensors and the pre-concentrator.

Acknowledgment

This project has received funding from the European Union's Seventh Framework Programme for research, technological development and demonstration under grant agreement No 604311, Project SENSIndoor.

Appendix A. Supplementary data

Supplementary data associated with this article can be found, in the online version, at http://dx.doi.org/10.1016/j.snb.2016.04.064.

References

[1] World Health Organization: WHO Guidelines for Indoor Air Quality: Selected Pollutants, Geneva (2010).
[2] J.A. Bernstein, N. Alexis, H. Bacchus, I. Leonard Bernstein, P. Fritz, E. Horner, N. Li, S. Mason, A. Nel, J. Oullette, K. Reijula, T. Reponen, J. Seltzer, A. Smith, S.M. Tarlo, The health effects of nonindustrial indoor air pollution, J. Allergy Clin. Immunol. 121 (3) (2008) 585–591, http://dx.doi.org/10.1016/j.jaci.2007.10.045.
[3] K. Koistinen, D. Kotzias, S. Kephalopoulos, C. Schlitt, P. Carrer, M. Jantunen, S. Kirchner, J. McLaughlin, L. Mølhave, E.O. Fernandes, B. Seifert, The INDEX project: executive summary of a European Union project on indoor air pollutants, Allergy 63 (2008) 810–819, http://dx.doi.org/10.1111/j.1398-9995.2008.01740.x.
[4] O. Geiss, G. Giannopoulos, S. Tirendi, J. Barrero-Moreno, B.R. Larsen, D. Kotzias, The AIRMEX study–VOC measurements in public buildings and schools/kindergartens in eleven European cities: statistical analysis of the data, Atmos. Environ. 45 (2011) 3676–3684, http://dx.doi.org/10.1016/j.atmosenv.2011.04.037.
[5] A.P. Jones, Indoor air quality and health, Atmos. Environ. 33 (28) (1999) 4535–4564, http://dx.doi.org/10.1016/S1352-2310(99)00272-1.
[6] J.T. Brinke, S. Selvin, A.T. Hodgson, W.J. Fisk, M.J. Mendell, C.P. Koshland, J.M. Daisey, Development of new volatile organic compound (VOC) exposure metrics and their relationship to sick building syndrome symptoms, Indoor Air 8 (1998) 140–152, http://dx.doi.org/10.1111/j.1600-0668.1998.t01-1-00002.x.
[7] P.S. Burge, Sick building syndrome, Occup. Environ. Med. 61 (2004) 185–190, http://dx.doi.org/10.1136/oem.2003.008813.
[8] H. Guo, S.C. Lee, L.Y. Chan, W.M. Li, Risk assessment of exposure to volatile organic compounds in different indoor environments, Environ. Res. 94 (2004) 57–66, http://dx.doi.org/10.1016/S0013-9351(03)00035-5.
[9] European Parliament, Council of the European Union: Directive 2008/50/EC of the European Parliament and of the Council of 21 May 2008 on ambient air quality and cleaner air for Europe, Off. J. Eur. Union 51 (2008).
[10] C.-H. Wu, C.-T. Feng, Y.-S. Lo, T.-Y. Lin, J.-G. Lo, Determination of volatile organic compounds in workplace air by multisorbent adsorption/thermal desorption-GC/MS, Chemosphere 56 (1) (2004) 71–80, http://dx.doi.org/10.1016/j.chemosphere.2004.02.003.
[11] M. Leidinger, T. Sauerwald, W. Reimringer, G. Ventura, A. Schütze, Selective detection of hazardous VOCs for indoor air quality applications using a virtual gas sensor array, J. Sens. Sens. Syst. 3 (2014) 253–263, http://dx.doi.org/10.5194/jsss-3-253-2014.
[12] J.L.C. Rowsell, O.M. Yaghi, Metal–organic frameworks: a new class of porous materials, Microporous Mesoporous Mater. 73 (2004) 3–14, http://dx.doi.org/10.1016/j.micromeso.2004.03.034.
[13] J.A. Greathouse, N.W. Ockwig, L.J. Criscenti, T.R. Guilinger, P. Pohl, M.D. Allendorf, Computational screening of metal-organic frameworks for large-molecule chemical sensing, Phys. Chem. Chem. Phys.: PCCP 12 (2010) 12621–12629, http://dx.doi.org/10.1039/C0CP00092B.
[14] K.S. Asha, K. Bhattacharyya, S. Mandal, Discriminative detection of nitro aromatic explosives by a luminescent metal–organic framework, J. Mater. Chem. C 2 (2014) 10073–10081, http://dx.doi.org/10.1039/c4tc01982b.
[15] A. Lan, et al., A luminescent microporous metal-organic framework for the fast and reversible detection of high explosives, Angew. Chem. Int. Ed. Engl. 48 (2009) 2334–2338, http://dx.doi.org/10.1002/anie.200804853.
[16] H. Yamagiwa, et al., Detection of volatile organic compounds by weight-detectable sensors coated with metal-organic frameworks, Sci. Rep. 4 (2014) 6247, http://dx.doi.org/10.1038/srep06247.
[17] S.S.Y. Chui, S.M.F. Lo, J.P.H. Charmant, A.G. Orpen, I.D. Williams, A chemically functionalizable nanoporous material [Cu3(TMA)2(H2O)3]n, Science 283 (1999) 1148–1150, http://dx.doi.org/10.1126/science.283.5405.1148.
[18] T. Loiseau, C. Serre, C. Huguenard, G. Fink, F. Taulelle, M. Henry, T. Bataille, G. Férey, A rationale for the large breathing of the porous aluminum terephthalate (MIL-53) upon hydration, Chemistry 10 (2004) 1373–1382, http://dx.doi.org/10.1002/chem.200305413.
[19] F. Thielmann, Introduction into the characterisation of porous materials by inverse gas chromatography, J. Chromatogr. A 1037 (1–2) (2004) 115–123, http://dx.doi.org/10.1016/j.chroma.2004.03.060.
[20] S. Mohammadi-Jam, K.E. Waters, Inverse gas chromatography applications: a review, Adv. Colloid Interface Sci. 212 (2014) 21–44, http://dx.doi.org/10.1016/j.cis.2014.07.002.
[21] M. Schneider, K.U. Goss, Systematic investigation of the sorption properties of tenax TA, chromosorb 106, porapak n, and carbopak f, Anal. Chem. 81 (8) (2009) 3017–3021, http://dx.doi.org/10.1021/ac802686p.
[22] Scientific Instrument Services, http://www.sisweb.com/index/referenc/tenaxta.htm, 27/12/2015.
[23] M. Leidinger, M. Rieger, D. Weishaupt, T. Sauerwald, M. Nägele, J. Hürttlen, A. Schütze, Trace gas VOC detection using metal-organic frameworks as pre-concentrators and semiconductor gas sensors, Procedia Eng. 120 (2015) 1042–1045, http://dx.doi.org/10.1016/j.proeng.2015.08.719.
[24] J.R. Conder, C.L.Young, Physicochemical Measurement by Gas Chromatography, 1979.
[25] F.D. Lahoz-Martín, A. Martín-Calvo, S. Calero, Selective separation of BTEX mixtures using metal-organic frameworks, J. Phys. Chem. C 118 (2014) 13126–13136, http://dx.doi.org/10.1021/jp411697z.
[26] United States Environmental Protection Agency, Office of Solid Waste and Emergency Response: Soil screening guidance: technical background document, Part 5: Chemical-Specific Parameters, EPA/540/R-96/018, Washington, 1996.
[27] N. Helwig, M. Schüler, C. Bur, A. Schütze, T. Sauerwald, Gas mixing apparatus for automated gas sensor characterization, Meas. Sci. Technol. 25 (2014) 055903, http://dx.doi.org/10.1088/0957-0233/25/5/055903 (9pp).
[28] M. Leidinger, T. Sauerwald, M. Rieger, C. Alépée, A. Schütze, Integrated pre-concentrator gas sensor micro system for trace gas detection, Proceedings Dresdner Sensor-Symposium, Dresden (07.-09. Dec.) 2015 10.5162/12dss2015/5.4.

Biographies

Martin Leidinger received his diploma in mechatronics engineering from Saarland University, Saarbrücken, Germany, in 2013. He is currently a Ph.D. student at the Lab for Measurement Technology at Saarland University. His main research interests are in the fields of dynamic gas sensor operation, gas pre-concentration and design of gas mixing systems for trace gases.

Max Rieger studied chemistry at the University of Würzburg and received his diploma in 2011 in the field of theoretical and pysical chemistry. Since 2011 he is part of the analytics and detection group within the department of energetic materials at the Fraunhofer Institute for Chemical Technology in Pfinztal. He is involved in porous materials characterization and preconcentration methods for explosive and hazardous materials.

Tilman Sauerwald received his PhD in 2007 at the University of Giessen working on the influence of surface reactions to the multi-signal generation of metal oxide sensors. Since 2011 he is working at the Lab of Measurement Technology at the

Saarland University. His current focus is the detection of trace gases by developing of model based techniques for multi-signal generation.

Christine Alépée studied micro-engineering and received her PhD from the Swiss Federal Institute of Technology in Lausanne in 2000. She joined MiCS/SGX in 2001 where she has focused her activities on the development of gas sensing MEMS based on various gas detection principles with the goal of improving commercial gas sensors in terms of sensing properties, power consumption, reliability and fabrication costs.

Andreas Schütze studied Physics and received his doctorate in Applied Physics from Justus-Liebig-Universität in Gießen in 1994 with a thesis on micro gas sensor systems. After some years in industry, he joined the University of Applied Sciences in Krefeld, Germany, as professor for Microsystems Technology from 1998 to 2000. Since 2000 he is a full professor for measurement science and technology in the Department of Mechatronics at Saarland University, Saarbrücken, Germany. His research interests include microsensors and microsystems, especially advanced chemical sensor systems, both for gas and liquid phase, for security and control applications.

8 Discussion of results

In addition to the discussions included in the presented publications, summaries of the results of the single methods and technologies as well as a comprehensive discussion of the achieved results are included in this chapter.

The goal of the investigations presented in this thesis was to improve the sensing performance of MOS gas sensors, especially for very low VOC gas concentrations. A prerequisite for evaluating sensing performance of gas sensors and gas sensor systems is a reliable and accurate generation of test gases; the design and setup of a gas mixing system has been described in chapter 3. The presented system has been tested for its characteristics at generating gas mixtures in the relevant ranges, and performs with sufficient accuracy for ppb level concentrations and even sub-ppb levels. The expected errors in gas concentration due to accuracy of the used fluidic control devices are less than 5 % of the nominal values, and this maximum value applies only to the lower end of the total concentration range. Versatile usability of the system has been ensured by designing it for mixing gases over wide concentration ranges, the dynamic range is 1:10.000 in the presented configuration, and can be increased to 1:62.500 if reduced accuracy is acceptable. This range is sufficient for many applications; for indoor air quality the lowest relevant concentrations are at low ppb levels (e.g. benzene), which can easily be generated from gas cylinders holding sufficiently high gas concentrations of more than 50 ppm. With the presented system configuration, theoretically a dilution factor of 1:12.500.000 of the input concentration can be achieved, if a 10 ml/min MFC line is used, the full MFC setpoint ranges are utilized and the maximum carrier gas flow (1000 ml/min with humidity fixed at 50 %RH) is chosen.

Suitability of the used materials for tubing has been checked in a comparative test of different polymer, metal, and coated tube pieces. The investigation found that stainless steel tubing, which has been installed in the system, shows good performance regarding sticking effects of VOC gases compared to other possible materials, e.g. aluminum. In the design of the mechanical components, the issue of dead times and

tailing effects of gas pulses caused by dead volumes has been addressed and these effects could be reduced, which is relevant for generating short gas pulses.

A drawback of the chosen setup is its limitation to gas cylinders as possible gas sources. Other means of initial gas generation, e.g. permeation, are not included. This means that for some VOCs (e.g. naphthalene), a different test setup must be used. However, for a wide variety of gases, the gas mixing system offers adequate performance regarding accuracy, dilution factor, dynamic range, gas compatibility, number of gases, and switching time between gases or gas concentrations. Combined with the described control software, a useful tool for convenient and versatile generation of complex test gases and test gas sequences has been realized.

Several test measurements with ppb level gas concentrations have been described, using benzene, formaldehyde, and naphthalene as VOC target gases. To generate more realistic scenarios, the gas humidity has been varied in most of the measurements and interferent gases have been added in some of the tests. As explained in the introduction (chapter 1), the possible applications for ppb level sensing usually deal with complex and varying gas conditions, therefore testing of gas sensors and gas sensor systems also needs to include complex gas environments. In such testing conditions, the presented examples of MOS gas sensors operated in TCO showed very promising results. In all tests, trace gas concentrations of different gases could be distinguished or quantified by using pattern recognition signal processing based on features extracted from the dynamic signals. The results show that the gas sensors respond to the investigated gases at different temperatures (chapter 5), therefore operation with temperature variation seems advantageous compared to static heating of the sensors. Additionally, the increase of sensitivity resulting from temperature variations (chapter 2.1.2) can be exploited effectively only in TCO. With the extracted features, advanced signal evaluation could be utilized; the two presented methods were successfully applied to different output data structures: LDA was used for classification of data sets, e.g. identification of gases, and PLSR was used for concentration quantification. However, for the lowest concentrations of the respective gases in complex

backgrounds, LDA classifications still showed significant errors, especially if the measurement runs of different target compounds are combined.

The effect of different sensing materials can also clearly be seen from the presented measurements. The commercial sensors used in chapter 5 show good responses to all applied gases, while the PLD WO_3 layers (chapter 4) offer good selectivity towards one of the three VOCs used in the test run. Effects like this can be helpful in designing systems for specific compounds, which is relevant for some applications.

In addition to characterization of the sensor elements, the effects of installing the sensors in autonomous sensor systems have been identified and described in chapter 5. Improvements for the design of such devices have been derived and incorporated in the next generation of systems. However, the shown second generation uses relatively expensive solutions for certain issues (e.g. metal front plate) and must be revised to allow mass production as a low-cost system.

General performance and stability of MOS gas sensors for specific application scenarios have been proven by the inter-laboratory tests of a sensor system which has been trained and tested for benzene quantification in a simulated outdoor scenario using TCO and PLSR. Using features extracted from three low temperature segments of a SnO_2 gas sensor, benzene could be quantified in a concentration range from 1 to 10 ppb. The results confirm the TCO model presented in chapter 2.1.2; after rapid temperature reductions the conductance value of the sensing layer rises in a logarithmic fashion, and the slope changes with the temperature and the present gas atmosphere. The temperature dependence of the sensitivity is another obvious feature of the presented results. Using PLSR, a model was derived which predicts the benzene concentration of the input signal. The error in quantification was below 2 ppb with the most complex background variation, and was reduced to approx. 0.2 ppb with only low interferent gas variation. While an accuracy of 0.2 ppb is sufficient for indoor air quality monitoring (cf. Table 1), an accuracy of 2 ppb is technically too low for this application, with a desired detection threshold of about 1 ppb for benzene. However, since low-cost sensor systems for such requirements are so far not commercially available, the performance of the system can be rated as sufficient. For outdoor air

monitoring, the performance is adequate, as higher concentrations of benzene occur, especially in cities [47]. For concentrations up to 20 ppb, an accuracy of 2 ppb is satisfactory.

Regarding the transferability of a calibration from one laboratory to measurements from a second laboratory, the system shows deviations of up to 4 ppb; however, this error results, for the most part, from a constant offset. This can most likely be explained by the difference in gas humidity and residual contamination in the two measurement runs. In general, the projected data sets from the second test show good consistency in quantification of the different benzene concentrations, the predicted values increase linearly with linear increase of the actual concentration.

The last presented method is a novel approach on pre-concentration of gases. While a lot of research has been done and is still going on in this topic (cf. chapter 2.2), the approach presented here has a different focus. The goal was to build and characterize a low cost MEMS system with an integrated pre-concentrator / gas sensor design, which uses passive diffusion based gas transport. This goal was achieved; a miniaturized system was set up and tested with benzene as target gas. Thermal desorption of the MOF pre-concentrator layer generated distinct pulses of higher gas concentrations, which could be detected by the gas sensor. Due to the placement of the two elements in direct vicinity, the diffusion based gas transport is fast enough for creation of short gas peaks. While the pre-concentration factor obtained with the presented miniaturized setup is much lower compared to the larger examples presented in chapter 2.2.3, the effect is still significant and increases the quality and decreases the limit of detection for the target gas. For the application of indoor air quality monitoring, the performance has to be optimized further, as 1 ppb of benzene in varying conditions could probably not be detected reliably with the tested setup. Especially the effect of gas humidity, which is always present in real atmospheres but has been eliminated in the shown measurements, will probably decrease the accuracy of benzene detection by influencing both the pre-concentrator and the sensor, as other measurements have shown [232].

Metal-organic frameworks have been identified as suitable materials for gas pre-concentration; their thermal stability, large surface area and large variety make them a promising group of substances for further studies and developments in this area of application. With the created simulation model, the characteristics of the setup can easily be studied further without performing complex measurement series. Characterization and optimization of a larger scale setup has already been carried out based on the MEMS system model [175].

A device like the presented one could be manufactured in high numbers and at low cost. Due to its small size and low energy consumption, it could be used in a wide range of applications, including portable systems for air quality monitoring.

Both temperature cycled operation and micro pre-concentrators have been successfully applied for detection of trace level VOC concentration measurements in laboratory conditions. For transfer of these techniques into field tests and real applications, further optimizations and refinements will be necessary.

9 Conclusion and outlook

In this thesis, several methods for improving the performance of MOS gas sensors at low target gas concentrations have been applied to trace VOC measurements, but are potentially also useful for other gaseous compounds such as permanent gases. An important prerequisite for performing such measurements has been created by the successful design, setup and characterization of a gas mixing system. The system has been optimized for generating very low gas concentrations, which are necessary for calibration and characterization of gas sensors and gas sensor systems.

In several test measurements, the performance of low-cost MOS gas sensors and sensor systems for the intended applications have successfully been tested in laboratory conditions. Temperature-cycled operation in combination with sophisticated signal processing techniques was shown to be an effective approach when using MOS gas sensors for ppb level gas detection. Both gas identification and target gas quantification could be performed successfully using TCO in combination with feature extraction and LDA or PLSR. Adding gas pre-concentration in an integrated gas sensor / pre-concentrator device also yielded very promising results in terms of sensing performance.

In future research, many of the applied methods could be improved further or combined with other techniques. For signal processing with extracted features, a large number of methods are available; some might be more suitable for certain applications than the ones used here. The topic of integrated pre-concentration in particular has many opportunities for further investigations and optimizations. One possibility is the combination of one pre-concentrator with several different sensors or one sensor with several different pre-concentrator chips. These setups could improve especially the selectivity of gas detection. Furthermore, the operation of the pre-concentrator was included in a very simple manner so far. Instead of straightforward on/off operation, more complex adsorption/desorption processes are possible, e.g. using several desorption steps at different temperatures or using ramps for heating of the pre-

concentrator layer. This could further be combined with more complex operation of the gas sensor. In the presented test measurement, a very basic mode of temperature modulation was used for the sensor. Therefore, the introduced methods for advanced signal processing could not be fully applied. Changing the operating mode of the sensor could further improve the performance significantly, and in combination with the mentioned operating modes of the pre-concentrator, the overall performance of such a device could possibly be boosted significantly. Regarding the pre-concentrator design, the samples used in this thesis were not optimized for performance; the achievable pre-concentration factor and the timing of adsorption/desorption cycles could also be improved greatly. Parameters like layer thickness, layer area, distances between chips etc. can all be tweaked for improving the gas measurement capabilities of such an integrated system.

The methods presented in this thesis, and combination of these methods in particular, will allow realization of advanced gas sensor systems for various applications such as air quality, breath, or odor monitoring and analysis; all of which require selective detection and quantification of trace gases, especially of VOCs.

References

[1] Poster, D.L., Schantz, M.M., Sander, L.C., and Wise, S.A.: "Analysis of polycyclic aromatic hydrocarbons (PAHs) in environmental samples: a critical review of gas chromatographic (GC) methods", Analytical and Bioanalytical Chemistry 386 (4), doi:10.1007/s00216-006-0771-0, 2006.

[2] Matisová, E. and Dömötörová, M.: "Fast gas chromatography and its use in trace analysis", Journal of Chromatography A 1000 (1), pp. 199-221, doi:10.1016/S0021-9673(03)00310-8, 2003.

[3] Snow, N.H. and Slack, G.C.: "Head-space analysis in modern gas chromatography", TrAC Trends in Analytical Chemistry 21 (9), pp. 608-617, doi:10.1016/S0165-9936(02)00802-6, 2002.

[4] Beauchamp, J., Kirsch, F. and Buettner, A.: "Real-time breath gas analysis for pharmacokinetics: monitoring exhaled breath by on-line proton-transfer-reaction mass spectrometry after ingestion of eucalyptol-containing capsules", J. Breath Res. 4 (2), doi:10.1088/1752-7155/4/2/026006, 2010.

[5] Španěl, P. and Smith, D.: "Selected Ion Flow Tube Mass Spectrometry for On-Line Trace Gas Analysis in Biology and Medicine", European Journal of Mass Spectrometry 13 (1), pp. 77-82, doi:10.1255/ejms.843, 2007.

[6] Smith, D. and Španěl, P.: "Selected ion flow tube mass spectrometry (SIFT-MS) for on-line trace gas analysis", Mass Spectrom. Rev. 24, pp. 661–700, doi:10.1002/mas.20033, 2005.

[7] Pogodina, O.A., Pustogov, V.V., de Melas, F., Haberhauer-Troyer, C., Rosenberg, E., Puxbaum, H., Inberg, A., Croitoru, N., and Mizaikoff, B.: "Combination of Sorption Tube Sampling and Thermal Desorption with Hollow Waveguide FT-IR Spectroscopy for Atmospheric Trace Gas Analysis: Determination of Atmospheric Ethene at the Lower ppb Level", Analytical Chemistry 76 (2), pp. 464-468, doi:10.1021/ac034396j, 2004.

[8] Werle, P., Slemr, F., Maurer, K., Kormann, R., Mücke, R. and Jänker, B.: "Near- and mid-infrared laser-optical sensors for gas analysis", Optics and Lasers in Engineering 37 (2), pp. 101-114, doi:10.1016/S0143-8166(01)00092-6, 2002.

[9] Esler, M.B., Griffith, D.W.T., Wilson, S.R. and Steele, L.P.: "Precision Trace Gas Analysis by FT-IR Spectroscopy. 1. Simultaneous Analysis of CO_2, CH_4, N_2O, and CO in Air", Analytical Chemistry 72 (1), pp. 206-215, doi:10.1021/ac9905625, 2000.

[10] Pereira, L., Pujol, M., Garcia-Mas, J. and Phillips, M.A.: "Non-invasive quantification of ethylene in attached fruit headspace at 1 p.p.b. by gas chromatography–mass spectrometry", Plant J 91, pp. 172–183. doi:10.1111/tpj.13545, 2017.

[11] Sinha, S.N., Bhatnagar, V.K., Doctor, P., Toteja, G.S., Agnihotri, N.P., Kalra, R.L.: "A novel method for pesticide analysis in refined sugar samples using a gas chromatography–mass spectrometer (GC–MS/MS) and simple solvent extraction method", Food Chemistry 126 (1), pp. 379-386, doi:10.1016/j.foodchem.2010.10.110, 2011.

[12] King, J., Mochalski, P., Kupferthaler, A., Unterkofler, K., Koc, H., Filipiak, W., Teschl, S., Hinterhuber, H. and Amann, A.: "Dynamic profiles of volatile organic compounds in exhaled breath as determined by a coupled PTR-MS/GC-MS study", Physiol. Meas. 31 (9), , pp. 1169-1184, doi:10.1088/0967-3334/31/9/008, 2010.

[13] Vesely, P., Lusk, L., Basarova, G., Seabrooks, J., and Ryder, D.: Analysis of Aldehydes in Beer Using Solid-Phase Microextraction with On-Fiber Derivatization and Gas Chromatography/Mass Spectrometry, J. Agric. Food Chem. 51 (24), pp. 6941–6944, doi:10.1021/jf034410t, 2003.

[14] Rahman, A., Kumar, P., Park, D.-S. and Shim Y.-B.: "Electrochemical Sensors Based on Organic Conjugated Polymers", Sensors 8 (1), pp. 118-141, doi:10.3390/s8010118, 2008.

[15] Wei, D. and Ivaska, A.: "Applications of ionic liquids in electrochemical sensors", Analytica Chimica Acta 607 (2), pp. 126-135, doi:10.1016/j.aca.2007.12.011, 2008.

[16] Riegel, J., Neumann, H., and Wiedenmann, H.-M.: "Exhaust gas sensors for automotive emission control", Solid State Ionics 152, pp. 783-800, doi:10.1016/S0167-2738(02)00329-6, 2002.

[17] Ivers-Tiffée, E., Härdtl, K.H., Menesklou, W. and Riegel, J.: "Principles of solid state oxygen sensors for lean combustion gas control", Electrochimica Acta 47 (5), pp. 807-814, doi:10.1016/S0013-4686(01)00761-7, 2002.

[18] Mikołajczyk, J., Bielecki, Z., Stacewicz, T., Smulko, J., Wojtas, J., Szabra, D., Lentka, Ł., Prokopiuk, A. and Magryta, P.: "Detection of Gaseous Compounds with Different Techniques", Metrology and Measurement Systems 23 (2), pp. 205-224, doi:10.1515/mms-2016-0026, 2016.

[19] Kumar, A., Kingson, T.M.G., Verma, R.P., Kumar, A., Mandal, R., Dutta, S., Chaulya, S.K. and Prasad, G.M.: "Application of Gas Monitoring Sensors in Underground Coal Mines and Hazardous Areas", International Journal of Computer Technology and Electronics Engineering 3 (3), pp. 9-23, ISSN 2249-6343, 2013.

[20] Barritault, P., Brun, M., Lartigue, O., Willemin, J., Ouvrier-Buffet, J.-L., Pocas, S. and Nicoletti, S.: "Low power CO_2 NDIR sensing using a micro-bolometer detector and a micro-hotplate IR-source", Sensors and Actuators B: Chemical 182, pp. 565-570, doi:10.1016/j.snb.2013.03.048, 2013.

[21] Schmitt, K., Müller, A., Huber, J., Busch, S. and Wöllenstein, J.: "Compact photoacoustic gas sensor based on broadband IR source", Procedia Engineering 25, pp. 1081-1084, doi:10.1016/j.proeng.2011.12.266, 2011.

[22] Wetchakun, K., Samerjai, T., Tamaekong, N., Liewhiran, C., Siriwong, C., Kruefu, V., Wisitsoraat, A., Tuantranont, A. and Phanichphant, S.: "Semiconducting metal oxides as sensors for environmentally hazardous gases", Sensors and Actuators B: Chemical 160 (1), pp. 580-591, doi:10.1016/j.snb.2011.08.032, 2011.

[23] Fine, G.F., Cavanagh, L.M., Afonja A. and Binions, R.: "Metal Oxide Semi-Conductor Gas Sensors in Environmental Monitoring", Sensors 10 (6), pp. 5469-5502, doi:10.3390/s100605469, 2010.

[24] Bastuck, M., Bur, C., Lloyd Spetz, A., Andersson, M. and Schütze, A.: "Gas identification based on bias induced hysteresis of a gas-sensitive SiC field effect transistor", Journal of Sensors and Sensor Systems 3, pp. 9-19, doi:10.5194/jsss-3-9-2014, 2014.

[25] Tsukada, K., Kariya, M., Yamaguchi, T., Kiwa, T., Yamada, H., Maehara, T., Yamamoto, T. and Kunitsugu S.: "Dual-gate field-effect transistor hydrogen gas sensor with thermal compensation", Japanese Journal of Applied Physics 49, doi:10.1143/JJAP.49.024206, 2010.

[26] Koistinen, K., Kotzias, D., Kephalopoulos, S., Schlitt, C., Carrer, P., Jantunen, M., Kirchner, S., McLaughlin, J., Mølhave, L., Fernandes, E.O. and Seifert, B.: "The INDEX project: executive summary of a European Union project on indoor air pollutants", Allergy 63, pp. 810–819, doi: 10.1111/j.1398-9995.2008.01740.x, 2008.

[27] Geiss, O., Giannopoulos, G., Tirendi, S., Barrero-Moreno, J., Larsen, B.R. and Kotzias, D.: "The AIRMEX study - VOC measurements in public buildings and schools/kindergartens in eleven European cities: Statistical analysis of the data", Atmospheric Environment 45 (22), pp. 3676-3684, doi:10.1016/j.atmosenv.2011.04.037, 2011.

[28] Daisey, J.M., Angell, W.J. and Apte, M.G.: "Indoor air quality, ventilation and health symptoms in schools: an analysis of existing information", Indoor Air 13, pp. 53–64. doi:10.1034/j.1600-0668.2003.00153.x, 2003.

[29] Sundell, J.: "On the history of indoor air quality and health", Indoor Air 14, pp. 51–58. doi:10.1111/j.1600-0668.2004.00273.x, 2004.

[30] Penza, M. and EuNetAir Consortium: "COST action TD1105: Overview of sensor-systems for air-quality monitoring", Proc. Eng. 87, pp. 1370-1377, doi:10.1016/j.proeng.2014.11.698, 2014.

[31] Jones, A.P.: "Indoor air quality and health", Atmospheric Environment 33 (28), pp. 4535-4564, 1999.

[32] Bernstein, J.A., Alexis, N., Bacchus, H., Leonard Bernstein., I, Fritz, P., Horner, E., Li, N., Mason, S., Nel, A., Oullette, J., Reijula, K., Reponen, T.,

Seltzer, J., Smith, A. and Tarlo, S.M.: “The health effects of nonindustrial indoor air pollution”, Journal of Allergy and Clinical Immunology 121 (3), pp. 585-591, 2008.

[33] Guo, H., Lee, S.C., Chan, L.Y. and Li, W.M.: “Risk assessment of exposure to volatile organic compounds in different indoor environments”, Environmental Research 94, pp. 57-66, doi:10.1016/S0013-9351(03)00035-5, 2004.

[34] Yin, S.-N., Hayes, R.B., Linet, M.S., Li, G.-L., Dosemeci, M., Travis, L.B., Li, C.-Y., Zhang, Z.-N., Li, D.-G., Chow, W.-H., Wacholder, S., Wang, Y.-Z., Jiang, Z.-L., Dai, T.-R., Zhang, W.-Y., Chao, X.-J., Ye, P.-Z., Kou, Q.-R., Zhang, X.-C., Lin, X.-F., Meng, J.-F., Ding, C.-Y., Zho, J.-S. and Blot, W.J.: “A cohort study of cancer among benzene-exposed workers in China: Overall results”, Am. J. Ind. Med. 29, pp. 227–235, doi:10.1002/(SICI)1097-0274(199603)29:3<227::AID-AJIM2>3.0.CO;2-N, 1996.

[35] Klepeis, N.E., Nelson, W.C., Ott, W.R., Robinson, J., Tsang, A.M., Switzer, P., Behar, J.V., Hern, S. and Engelmann, W.: “The National Human Activity Pattern Survey (NHAPS): A Resource for Assessing Exposure to Environmental Pollutants”, J. Expos. Analysis and Environ. Epidem. 11 (3), pp. 231–252, doi:10.1038/sj.jea.7500165, 2001.

[36] Brinke, J.T., Selvin, S., Hodgson, A.T., Fisk, W.J., Mendell, M.J., Koshland, C.P. and Daisey, J.M.: “Development of New Volatile Organic Compound (VOC) Exposure Metrics and their Relationship to ‘Sick Building Syndrome’ Symptoms”, Indoor Air 8, pp. 140–152. doi:10.1111/j.1600-0668.1998.t01-1-00002.x, 1998.

[37] Burge, P.S.: “Sick building syndrome”, Occup Environ Med 61 (2), pp. 185-190. doi:10.1136/oem.2003.008813, 2004.

[38] World Health Organization (WHO): “WHO guidelines for indoor air quality: selected pollutants”, The Regional Office for Europe of the World Health Organization, Ed. Copenhagen, Denmark, 2010.

[39] Bur, C., Andersson, M., Lloyd Spetz, A. and Schütze, A.: “Detecting Volatile Organic Compounds in the ppb Range with Gas Sensitive Platinum gate SiC-Field Effect Transistors”, IEEE Sensors Journal 14 (9), pp. 3221-3228, doi:10.1109/JSEN.2014.2326693, 2014.

[40] La ministre de l'écologie, du développement durable, des transports et du logement (France). Legifrance: “Décret n° 2011-1727 du 2 décembre 2011 relatif aux valeurs-guides pour l'air intérieur pour le formaldéhyde et le benzène,” Journal Officiel De La République Francaise, no. 2011-1727, p. 20529, 2011. available online: https://www.legifrance.gouv.fr/affichTexte.do?cidTexte=JORFTEXT000024909119&categorieLien=id, accessed: 06 Jan 2018.

[41] German Environmental Agency, Committee on Indoor Guide Values: „Richtwert für Formaldehyd in der Innenraumluft“, Bundesgesundheitsblatt 59, p. 1040-1044, doi:10.1007/s00103-016-2389-5, 2016. available online:

https://www.umweltbundesamt.de/sites/default/files/medien/360/dokumente/fa_rw.pdf, accessed 06 Jan 2018.

[42] World Health Organization (WHO): "WHO Air quality guidelines for particulate matter, ozone, nitrogen dioxide, and sulfur dioxide", Geneva, Switzerland, WHO/SDE/PHE/OEH/06.02., 2006.

[43] World Health Organization (WHO): "WHO handbook on indoor radon", Geneva, Switzerland, 2009.

[44] World Health Organization (WHO): "Air quality guidelines for Europe", 2nd ed., WHO Regional Publications, European Series, No. 91, 2000.

[45] German Environmental Agency, Committee on Indoor Guide Values: „Richtwerte für Toluol und gesundheitliche Bewertung von C7-C8-Alkylbenzolen in der Innenraumluft", Bundesgesundheitsblatt 59, p. 1522-1539, doi: 10.1007/s00103-016-2444-2, 2016. available online: https://www.umweltbundesamt.de/sites/default/files/medien/355/dokumente/toluol_2016.pdf, accessed 06 Jan 2018.

[46] Pilidis, G.A., Karakitsios, S.P., Kassomenos, P.A., Kazos, E.A. and Stalikas, C.D.: „Measurements of benzene and formaldehyde in a medium sized urban environment. Indoor/outdoor health risk implications on special population groups", Environ Monit Assess. 150 (1-4), pp. 285-94, doi:10.1007/s10661-008-0230-9, 2009.

[47] Hagen, J.A., Nafstad, P., Skrondal, A., Bjørkly, S. and Magnus, P.: „Associations between outdoor air pollutants and hospitalization for respiratory diseases", Epidemiology 11 (2), pp. 136-140, 2000.

[48] Yorifuji, T., Kashima, S., Tsuda, T., Ishikawa-Takata, K., Ohta, T., Tsuruta, K. and Doi, H.: "Long-term exposure to traffic-related air pollution and the risk of death from hemorrhagic stroke and lung cancer in Shizuoka, Japan", Science of The Total Environment 443, pp. 397-402, doi:10.1016/j.scitotenv.2012.10.088, 2013.

[49] Andersen, Z.J., Kristiansen, L.C., Andersen, K.K., Olsen, T.S., Hvidberg, M., Jensen, S.S., Ketzel, M., Loft, S., Sørensen, M., Tjønneland, A., Overvad, K. and Raaschou-Nielsen, O.: "Stroke and long-term exposure to outdoor air pollution from nitrogen dioxide: a cohort study", Stroke 43 (2), pp. 320–325., doi: 10.1161/STROKEAHA.111.629246, 2012.

[50] Shima, M. and Adachi, M.: "Effect of outdoor and indoor nitrogen dioxide on respiratory symptoms in schoolchildren", Int J Epidemiol 29 (5), pp. 862-870, doi:10.1093/ije/29.5.862, 2000.

[51] Lelieveld, J., Evans, J.S., Fnais, M., Giannadaki, D. and Pozzer, A.: "The contribution of outdoor air pollution sources to premature mortality on a global scale", Nature 525, pp. 367-371, doi: 10.1038/nature15371, 2015.

[52] Neidell, M.J.: “Air pollution, health, and socio-economic status: the effect of outdoor air quality on childhood asthma”, Journal of Health Economics 23 (6), pp. 1209-1236, doi:10.1016/j.jhealeco.2004.05.002, 2004.

[53] Pope, C.A. III, Burnett, R.T., Thun, M.J., Calle, E.E., Krewski, D., Ito, K. and Thurston, G.D.: “Lung cancer, cardiopulmonary mortality, and long-term exposure to fine particulate air pollution”, JAMA.287 (9), pp.1132-1141, doi:10.1001/jama.287.9.1132, 2002.

[54] D’Amato, G., Liccandi, G., D’Amato, M. and Cazzola, M.: “Outdoor air pollution, climatic changes and allergic bronchial asthma”, European Respiratory Journal 20, pp. 763-776, doi:10.1183/09031936.02.00401402, 2002.

[55] Spinelle, L., Gerboles, M., Villani, M.G., Aleixandre, M. and Bonavitacola, F.: “Field calibration of a cluster of low-cost available sensors for air quality monitoring. Part A: Ozone and nitrogen dioxide”, Sensors Actuators B: Chem. 215, doi:10.1016/j.snb.2015.03.031, 2015.

[56] Spinelle, L., Gerboles, M., Villani, M.G., Aleixandre, M. and Bonavitacola, F.: “Field calibration of a cluster of low-cost commercially available sensors for air quality monitoring. Part B: NO, CO and CO_2”, Sensors Actuators B Chem. 238, doi:10.1016/j.snb.2016.07.036, 2017.

[57] Heimann, I., Bright, V.B., McLeod, M.W., Mead, M.I., Popoola, O.A.M., Stewart, G.B. and Jones, R.L.: “Source attribution of air pollution by spatial scale separation using high spatial density networks of low cost air quality sensors”, Atmospheric Environment 113, pp. 10-19, doi:10.1016/j.atmosenv.2015.04.057, 2015.

[58] Lo Re, G., Peri, D. and Vassallo, S.D.: “Urban Air Quality Monitoring Using Vehicular Sensor Networks”, Advances onto the Internet of Things, Advances in Intelligent Systems and Computing 260, Springer International Publishing, doi:10.1007/978-3-319-03992-3_22, 2014.

[59] Hasenfratz, D., Saukh, O., Walser, C., Hueglin, C., Fierz, M., Arn, T., Beutel, J. and Thiele, L.: “Deriving high-resolution urban air pollution maps using mobile sensor nodes”, Pervasive and Mobile Computing 16, pp. 268-285, doi:10.1016/j.pmcj.2014.11.008, 2015.

[60] Westerdahl, D., Fruin, S., Sax, T., Fine, P.M. and Sioutas, C.: “Mobile platform measurements of ultrafine particles and associated pollutant concentrations on freeways and residential streets in Los Angeles”, Atmospheric Environment 39 (20), pp. 3597-3610, doi:10.1016/j.atmosenv.2005.02.034, 2005.

[61] Elen, B., Peters J., Van Poppel, M., Nico Bleux, N., Theunis, J., Reggente, M., and Standaert, A.: “The Aeroflex: A Bicycle for Mobile Air Quality Measurements”, Sensors 13 (1), pp. 221-240, doi:10.3390/s130100221, 2013.

[62] Nikzad, N., Verma, N., Ziftci, C., Bales, E., Quick, N., Zappi, P., K., Patrick, Dasgupta, S., Krueger, I., Šimunić Rosing, T. and Griswold, W.G.: "CitiSense: improving geospatial environmental assessment of air quality using a wireless personal exposure monitoring system", Proceedings of the conference on Wireless Health 2012, pp.1-8, Oct 23-25 2012, San Diego, California, doi:10.1145/2448096.2448107, 2012.

[63] Pereira, J., Porto-Figueira, P., Cavaco, C., Taunk, K., Rapole, S., Dhakne, R., Nagarajaram, H. and Câmara, J.S.: "Breath Analysis as a Potential and Non-Invasive Frontier in Disease Diagnosis: An Overview", Metabolites 5 (1), pp. 3-55. doi:10.3390/metabo5010003, 2015.

[64] Cao, W. and Duan, Y.: "Breath Analysis: Potential for Clinical Diagnosis and Exposure Assessment", Clinical Chemistry 52 (5), pp. 800-811, doi:10.1373/clinchem.2005.063545, 2006.

[65] Di Francesco, F., Fuoco, R., Trivella, M.G. and Ceccarini, A.: "Breath analysis: trends in techniques and clinical applications", Microchemical Journal 79 (1), pp. 405-410, doi:10.1016/j.microc.2004.10.008, 2005.

[66] Guo, D., Zhang, D., Zhang, L. and Lu, G.: "Non-invasive blood glucose monitoring for diabetics by means of breath signal analysis", Sensors and Actuators B: Chemical 173, pp. 106-113, doi:10.1016/j.snb.2012.06.025, 2012.

[67] Kharitonov, S.A., Yates, D., Robbins, R.A., Barnes, P.J., Logan-Sinclair, R. and Shinebourne, E.A.: "Increased nitric oxide in exhaled air of asthmatic patients", The Lancet 343 (8890), 133-135, doi:10.1016/S0140-6736(94)90931-8, 1994.

[68] Kolk, A.H.J., van Berkel, J.J.B.N., Claassens, M.M., Walters, E., Kuijper, S., Dallinga, J.W. and van Schooten, F.J.: "Breath analysis as a potential diagnostic tool for tuberculosis", The International Journal of Tuberculosis and Lung Disease 16 (6), pp. 777-782, doi:10.5588/ijtld.11.0576, 2012.

[69] Fuchs, P., Loeseken, C., Schubert, J.K. and Miekisch, W.: "Breath gas aldehydes as biomarkers of lung cancer", Int. J. Cancer 126, pp. 2663–2670. doi:10.1002/ijc.24970, 2010

[70] Kumar, S., Huang, J., Abbassi-Ghadi, N., Španěl, P., Smith, D. and Hanna, G.B.: "Selected Ion Flow Tube Mass Spectrometry Analysis of Exhaled Breath for Volatile Organic Compound Profiling of Esophago-Gastric Cancer", Anal. Chem. 85 (12), pp. 6121–6128, doi:10.1021/ac4010309, 2013.

[71] Phillips, M., Cataneo, R.N., Saunders, C., Hope, P., Schmitt P. and Wai, J.: "Volatile biomarkers in the breath of women with breast cancer", J. Breath Res. 4 026003, doi:10.1088/1752-7155/4/2/026003, 2010.

[72] Amal, H., Leja, M., Funka, K., Skapars, R., Sivins, A., Ancans, G., Liepniece-Karele, I., Kikuste, I., Lasina, I. and Haick, H.: "Detection of precancerous

gastric lesions and gastric cancer through exhaled breath", Gut 65, pp. 400-407, doi:10.1136/gutjnl-2014-308536, 2016.

[73] Schwoebel, H., Schubert, R., Sklorz, M., Kiskchel, S., Zimmermann, R., Schubert, J.K. and Miekisch, W.: „Phase-resolved real-time breath analysis during exercise by means of smart processing of PTR-MS data", Anal Bioanal Chem 401, pp. 2079-2091, doi:10.1007/s00216-011-5173-2, 2011

[74] Španěl, P. and Smith, D.: "Progress in SIFT-MS: Breath analysis and other applications", Mass Spectrom. Rev. 30, pp. 236–267, doi:10.1002/mas.20303, 2010.

[75] Gouma, P.-I., Wang, L., Simon, S.R. and Stanacevic, M.: "Novel Isoprene Sensor for a Flu Virus Breath Monitor", Sensors 17 (1) 199, doi:10.3390/s17010199, 2017.

[76] Righettoni, M., Tricoli, A., Gass, S., Schmid, A., Amann, A. and Pratsinis, S.E.: "Breath acetone monitoring by portable Si:WO gas sensors", Analytica Chimica Acta 738, pp. 69-75, doi:10.1016/j.aca.2012.06.002, 2012.

[77] Choi, S.-J., Lee, I., Jang, B.-H., Youn, D.-Y., Ryu, W.-H., Park, C.O. and Kim, I.-D.: "Selective Diagnosis of Diabetes Using Pt-Functionalized WO_3 Hemitube Networks As a Sensing Layer of Acetone in Exhaled Breath", Anal. Chem. 85 (3), pp 1792–1796, doi:10.1021/ac303148a, 2013.

[78] Vincent, T.A.,Wilson, A., Hattersley, J.G., Chappell, M.J. and Gardner, J.W.: "Development of a Handheld Side-Stream Breath Analyser for Point of Care Metabolic Rate Measurement", Bioinformatics and Biomedical Engineering, IWBBIO 2016, Lecture Notes in Computer Science 9656, pp. 13-21, doi:10.1007/978-3-319-31744-1_2, 2016.

[79] Mazzone, P.J., Wang, X.-F., Xu, Y., Mekhail, T., Beukemann, M.C., Na, J., Kemling, J.W., Suslick, K.S. and Sasidhar, M.: "Exhaled Breath Analysis with a Colorimetric Sensor Array for the Identification and Characterization of Lung Cancer", Journal of Thoracic Oncology 7 (1), pp. 137-142, doi:10.1097/JTO.0b013e318233d80f, 2012.

[80] Mondal, S.P., Dutta, P.K., Hunter, G.W., Ward, B.J., Laskowski, D. and Dweik, R.A.: "Development of high sensitivity potentiometric NO_x sensor and its application to breath analysis", Sensors and Actuators B: Chemical 158 (1), pp. 292-298, doi:10.1016/j.snb.2011.05.063, 2011.

[81] Brattoli, M., de Gennaro, G., de Pinto, V., Demarinis Loiotile, A., Lovascio S. and Penza, M.: "Odour Detection Methods: Olfactometry and Chemical Sensors", Sensors 11, pp. 5290-5322, doi:10.3390/s110505290, 2011.

[82] Yuwono, A.S. and Schulze Lammers, P.: "Odor Pollution in the Environment and the Detection Instrumentation", Agricultural Engineering International: the CIGR Journal of Scientific Research and Development 6, ISSN:1682-1130, 2004.

[83] Shusterman, D.: “Critical review: the health significance of environmental odor pollution”, Arch Environ Health 47 (1), pp. 76-87, doi:10.1080/00039896.1992.9935948, 1992.

[84] Reimringer, W., Conrad, T. and Schütze, A.: „Erfassung und Quantifizierung von Geruchsimmissionen durch Kombination hochempfindlicher Sensorsysteme mit einem Geruchsnetzwerk“, Proceedings 18. GMA/ITG-Fachtagung Sensoren und Messsysteme 2016, pp. 357-362, doi:10.5162/sensoren2016/5.2.4, 2016.

[85] Chen, L.-Y., Jeng, F.-T., Chang, M.-W. and Yen S.-H.: “Rationalization of an Odor Monitoring System: A Case Study of Lin-Yuan Petrochemical Park”, Environ. Sci. Technol. 34 (7), pp. 1166–1173, doi:10.1021/es990180g, 2000.

[86] Capelli, L., Sironi, S., Del Rosso, R., Céntola, P. and Il Grande, M.: “A comparative and critical evaluation of odour assessment methods on a landfill site”, Atmospheric Environment 42 (30), pp. 7050-7058, doi:10.1016/j.atmosenv.2008.06.009, 2008.

[87] Bruno, P., Caselli, M., de Gennaro, G., Solito, M. and Tutino, M.: “Monitoring of odor compounds produced by solid waste treatment plants with diffusive samplers”, Waste Management 27 (4), pp. 539-544, doi:10.1016/j.wasman.2006.03.006, 2007.

[88] Pan, L., Yang, S.X. and DeBruyn, J.: “Factor Analysis of Downwind Odours from Livestock Farms”, Biosystems Engineering 96 (3), pp. 387-397, doi:10.1016/j.biosystemseng.2006.10.017, 2007.

[89] Guo, H., Dehod, W., Feddes, J., Laguë C. and Edeogu, I.: “Monitoring odour occurrence in the vicinity of swine farms by resident observers - Part I: odour occurrence profiles”, Canadian Biosystems Engineering 47, pp. 6.57-6.65, 2005.

[90] Dincer, F., Odabasi, M. and Muezzinoglu, A.: “Chemical characterization of odorous gases at a landfill site by gas chromatography-mass spectrometry”, J. Chromatogr. A 1122, pp. 222-229, doi:10.1016/j.chroma.2006.04.075, 2006.

[91] Pacquit, A., Frisby, J., Diamond, D., Lau, K.T., Farrell, A., Quilty, B. and Diamond, D.: “Development of a smart packaging for the monitoring of fish spoilage”, Food Chemistry 102 (2), pp. 466-470, doi:10.1016/j.foodchem.2006.05.052, 2007.

[92] Chan, S.T., Yao, M.W.Y., Wong, Y.C., Wong, T., Mok, C.S and Sin, D.W.M.: “Evaluation of chemical indicators for monitoring freshness of food and determination of volatile amines in fish by headspace solid-phase microextraction and gas chromatography-mass spectrometry”, Eur Food Res Technol 224, pp. 67-74, doi:10.1007/s00217-006-0290-4, 2006.

[93] Keupp, C., Höll, L., Beauchamp, J. and Langowski, H.-C.: “Online monitoring of volatile freshness indicators from modified atmosphere packaged chicken

meat using PTR-MS", Proceedings of 27th IAPRI Symposium on Packaging 2015, pp. 267-272, 2015.

[94] Mayr, D., Margesin, R., Klingsbichel, E., Hartungen, E., Jenewein, D., Schinner F. and Märk, T.D.: "Rapid Detection of Meat Spoilage by Measuring Volatile Organic Compounds by Using Proton Transfer Reaction Mass Spectrometry", Appl. Environ. Microbiol. 69 (8), pp. 4697-4705, doi:10.1128/AEM.69.8.4697-4705.2003, 2003.

[95] Soukoulis, C., Cappellin, L., Aprea, E., Costa, F., Viola, R., Märk, T.D., Gasperi, F. and Biasioli, F.: "PTR-ToF-MS, A Novel, Rapid, High Sensitivity and Non-Invasive Tool to Monitor Volatile Compound Release During Fruit Post-Harvest Storage: The Case Study of Apple Ripening", Food Bioprocess Technol 6 (10), pp. 2831–2843, doi:10.1007/s11947-012-0930-6, 2013.

[96] Pesis, E.: "The role of the anaerobic metabolites, acetaldehyde and ethanol, in fruit ripening, enhancement of fruit quality and fruit deterioration", Postharvest Biology and Technology 37 (1), pp. 1-19, doi:10.1016/j.postharvbio.2005.03.001, 2005.

[97] Son, M., Cho, D., Lim, J.H., Park, J., Hong, S., Ko, H.J. and Park, T.H.: "Real-time monitoring of geosmin and 2-methylisoborneol, representative odor compounds in water pollution using bioelectronic nose with human-like performance", Biosensors and Bioelectronics 74, pp. 199-206, doi:10.1016/j.bios.2015.06.053, 2015.

[98] Muñoz, R., Sivret, E.C., Parcsi, G., Lebrero, R., Wang, X., Suffet, I.H. and Stuetz, R.M.: "Monitoring techniques for odour abatement assessment", Water Research 44 (18), pp. 5129-5149, doi:10.1016/j.watres.2010.06.013, 2010.

[99] Matatagui, D., Martí, J., Fernández, M.J., Fontecha, J.L., Gutiérrez, J., Gràcia, I., Cané, C., and Horrillo, M.C.: "Chemical warfare agents simulants detection with an optimized SAW sensor array", Sensors and Actuators B: Chemical 154 (2), pp. 199-205, doi:10.1016/j.snb.2010.01.057, 2011.

[100] Choi, N.-J., Kwak, J.-H., Lim, Y.-T., Bahn, T.-H., Yun, K.-Y., Kim, J.C., Huh, J.-S. and Lee, D.-D.: "Classification of chemical warfare agents using thick film gas sensor array", Sensors and Actuators B: Chemical 108 (1–2), pp. 298-304, doi:10.1016/j.snb.2004.11.022, 2005.

[101] Caygill, J.S., Davis, F. and Higson, S.P.J.: "Current trends in explosive detection techniques", Talanta 88, pp. 14-29, doi:10.1016/j.talanta.2011.11.043, 2012.

[102] Yinon, J.: "Field detection and monitoring of explosives", TrAC Trends in Analytical Chemistry 21 (4), pp. 292-301, doi:10.1016/S0165-9936(02)00408-9, 2002.

[103] Agarwal, B., Petersson, F., Jürschik, S., Sulzer, P., Jordan, A., Märk, T.D., Watts P. and Mayhew, C.A.: "Use of proton transfer reaction time-of-flight mass spectrometry for the analytical detection of illicit and controlled

prescription drugs at room temperature via direct headspace sampling", Anal Bioanal Chem 400, pp. 2631–2639, doi:10.1007/s00216-011-4892-8, 2011.

[104] Gentili, S., Cornetta, M. and Macchia, T.: "Rapid screening procedure based on headspace solid-phase microextraction and gas chromatography–mass spectrometry for the detection of many recreational drugs in hair", Journal of Chromatography B 801 (2), pp. 289-296, doi:10.1016/j.jchromb.2003.11.034, 2004.

[105] Harper, R.J., Almirall, J.R. and Furton, K.G.: "Identification of dominant odor chemicals emanating from explosives for use in developing optimal training aid combinations and mimics for canine detection", Talanta 67 (2), pp. 313-327, doi:10.1016/j.talanta.2005.05.019, 2005.

[106] Chiu S.-W. and Tang, K.-T.: "Towards a Chemiresistive Sensor-Integrated Electronic Nose: A Review", Sensors 13 (10), pp. 14214-14247, doi:10.3390/s131014214, 2013.

[107] Wilson, A.D. and Baietto, M.: "Applications and Advances in Electronic-Nose Technologies", Sensors 9 (7), pp. 5099-5148, doi:10.3390/s90705099, 2009.

[108] Röck, F., Barsan, N. and Weimar, U.: "Electronic Nose: Current Status and Future Trends", Chem. Rev. 108 (2), pp. 705–725, doi:10.1021/cr068121q, 2008

[109] Sironi, S., Eusebio, L., Capelli, L., Remondini, M. and Del Rosso, R.: "Use of an Electronic Nose for Indoor Air Quality Monitoring", Chemical Engineering Transactions 40, pp. 73-78, doi:0.3303/CET1440013, 2014.

[110] Zhang, L., Tian, F., Nie, H., Dang, L., Li, G., Ye, Q. and Kadri, C.: "Classification of multiple indoor air contaminants by an electronic nose and a hybrid support vector machine", Sensors and Actuators B: Chemical 174, pp. 114-125, doi:10.1016/j.snb.2012.07.021., 2012.

[111] De Vito, S., Piga, M., Martinotto, L. and Di Francia, G.: "CO, NO and NO urban pollution monitoring with on-field calibrated electronic nose by automatic bayesian regularization", Sensors and Actuators B: Chemical 143 (1), pp. 182-191, doi:10.1016/j.snb.2009.08.041, 2009.

[112] Martinelli, E., Zampetti, E., Pantalei, S., Lo Castro, F., Santonico, M., Pennazza, G., Paolesse, R., Di Natale, C., D'Amico, A., Giannini, F., Mascetti, G. and Cotronei, V.: "Design and test of an electronic nose for monitoring the air quality in the international space station", Microgravity Science and Technology 5-6, pp. 60-64, doi:10.1007/BF02919454, 2007.

[113] Wilson, A.D.: "Advances in Electronic-Nose Technologies for the Detection of Volatile Biomarker Metabolites in the Human Breath", Metabolites 5 (1), pp. 140-163, doi:10.3390/metabo5010140, 2015.

[114] Fens, N., Roldaan, A.C., van der Schee, M.P., Boksem, R.J., Zwinderman, A.H., Bel, E.H. and Sterk, P.J.: "External validation of exhaled breath profiling using an electronic nose in the discrimination of asthma with fixed

airways obstruction and chronic obstructive pulmonary disease", Clinical & Experimental Allergy 41 pp. 1371–1378, doi:10.1111/j.1365-2222.2011.03800.x, 2011.

[115] D'Amico, A., Pennazza, G., Santonico, M., Martinelli, E., Roscioni, C., Galluccio, G., Paolesse, R. and Di Natale, C.: "An investigation on electronic nose diagnosis of lung cancer", Lung Cancer 68 (2), pp. 170-176, doi:10.1016/j.lungcan.2009.11.003, 2010.

[116] Dragonieri, S., Annema, J.T., Schot, R., van der Schee, M.P.C., Spanevello, A., Carratú, P., Resta, O., Rabe, K.F. and Sterk, P.J.: "An electronic nose in the discrimination of patients with non-small cell lung cancer and COPD", Lung Cancer 64 (2), pp. 166-170, doi:10.1016/j.lungcan.2008.08.008, 2009.

[117] Eusebio, L., Capelli, L. and Sironi, S.: "Electronic Nose Testing Procedure for the Definition of Minimum Performance Requirements for Environmental Odor Monitoring", Sensors 16 (9), 1548, doi:10.3390/s16091548, 2016.

[118] Wilson, A.D.: "Review of Electronic-nose Technologies and Algorithms to Detect Hazardous Chemicals in the Environment", Procedia Technology 1, pp. 453-463, doi:10.1016/j.protcy.2012.02.101, 2012.

[119] Sohn, J.H., Hudson, N., Gallagher, E., Dunlop, M., Zeller, L. and Atzeni, M.: "Implementation of an electronic nose for continuous odour monitoring in a poultry shed", Sensors and Actuators B: Chemical 133 (1), pp. 60-69, doi:10.1016/j.snb.2008.01.053, 2008.

[120] Fuchs, S., Strobel, P., Siadat, M. and Lumbreras, M.: "Evaluation of unpleasant odor with a portable electronic nose", Materials Science and Engineering: C 28 (5), pp. 949-953, doi:10.1016/j.msec.2007.10.066, 2008.

[121] Loutfi, A., Coradeschi, S., Mani, G.K., Shankar, P. and Rayappan, J.B.B.: "Electronic noses for food quality: A review", Journal of Food Engineering 144, pp. 103-111, doi:10.1016/j.jfoodeng.2014.07.019, 2015.

[122] Cevoli, C., Cerretani, L., Gori, A., Caboni, M.F., Gallina Toschi, T. and Fabbri, A.: "Classification of Pecorino cheeses using electronic nose combined with artificial neural network and comparison with GC–MS analysis of volatile compounds", Food Chemistry 129 (3), pp. 1315-1319, doi:10.1016/j.foodchem.2011.05.126, 2011.

[123] Torri, L., Sinelli, N. and Limbo, S.: "Shelf life evaluation of fresh-cut pineapple by using an electronic nose", Postharvest Biology and Technology 56 (3), pp. 239-245, doi:10.1016/j.postharvbio.2010.01.012, 2010.

[124] Wongchoosuk, C., Wisitsoraat, A., Tuantranont, A. and Kerdcharoen, T.: "Portable electronic nose based on carbon nanotube-SnO gas sensors and its application for detection of methanol contamination in whiskeys", Sensors and Actuators B: Chemical 147 (2), pp. 392-399, doi:10.1016/j.snb.2010.03.072, 2010.

[125] Voss, A., Witt, K., Kaschowitz, T., Poitz, W., Ebert, A., Roser P. and Bär, K.-J.: "Detecting Cannabis Use on the Human Skin Surface via an Electronic Nose System", Sensors 14 (7), pp. 13256-13272, doi:10.3390/s140713256, 2014.

[126] Brudzewski, K., Osowski, S. and Pawlowski, W.: "Metal oxide sensor arrays for detection of explosives at sub-parts-per million concentration levels by the differential electronic nose", Sensors and Actuators B: Chemical 161 (1), pp. 528-533, doi:10.1016/j.snb.2011.10.071, 2012.

[127] Haddi, Z., Amari, A., Alami, H., El Bari, N., Llobet, E. and Bouchikhi, B.: "A portable electronic nose system for the identification of cannabis-based drugs", Sensors and Actuators B: Chemical 155 (2), pp. 456-463, doi:10.1016/j.snb.2010.12.047, 2011.

[128] Senesac, L. and Thundat, T.G.: "Nanosensors for trace explosive detection", Materials Today 11 (3), pp. 28-36, doi:10.1016/S1369-7021(08)70017-8, 2008.

[129] Helwig, N., Schüler, M., Bur, C., Schütze, A. and Sauerwald, T: "Gas mixing apparatus for automated gas sensor characterization", Meas. Sci. Technol. 25, doi:10.1088/0957-0233/25/5/055903, 2014.

[130] Li, Y., Täffner, T., Bischoff, M.,and Niemeyer, B.: "Test Gas Generation from Pure Liquids: An Application-Oriented Overview of Methods in a Nutshell", International Journal of Chemical Engineering 2012, 417029, doi:10.1155/2012/417029, 2012.

[131] Pogány, A., Balslev-Harder, D., Braban, C.F., Cassidy, N., Ebert, V., Ferracci, V., Hieta, T., Leuenberger, T., Martin, N.A. and Pascale, C.: "A metrological approach to improve accuracy and reliability of ammonia measurements in ambient air", Meas. Sci. Technol. 27, 115012, 10.1088/0957-0233/27/11/115012, 2016.

[132] Haerri, H.-P., Macé, T., Waldén, J., Pascale, C., Niederhauser, B., Wirtz, K., Stovcik, V., Sutour, C., Couette, J. and Waldén, T.: "Dilution and permeation standards for the generation of NO, NO_2 and SO_2 calibration gas mixtures", Meas. Sci. Technol. 28, 035801, doi:10.1088/1361-6501/aa543d, 2017.

[133] Spinelle, L., Aleixandre, M. and Gerboles, M.: "Protocol of evaluation and calibration of low-cost gas sensors for the monitoring of air pollution", Publications Office of the European Union, EUR 26112, doi:10.2788/9916, 2013.

[134] Kanazawa, E., Sakai, G., Shimanoe, K., Kanmura, Y., Teraoka, Y., Miura, N. and Yamazoe, N.: "Metal oxide semiconductor NO sensor for medical use", Sensors and Actuators B: Chemical 77 (1), pp. 72-77, doi:10.1016/S0925-4005(01)00675-X, 2001.

[135] Korotcenkov, G.: “Metal oxides for solid-state gas sensors: What determines our choice?”, Materials Science and Engineering: B 139 (1), 2007, pp. 1-23, doi:0.1016/j.mseb.2007.01.044, 2007.

[136] Barsan, N. and Weimar, U.: “Conduction Model of Metal Oxide Gas Sensors”, Journal of Electroceramics 7, pp. 143-167, doi:10.1023/A:1014405811371, 2001.

[137] Baur, T.: „Entwicklung eines Halbleitergasdetektors für gaschromatische Anwendungen“, Master Thesis, Saarland University, Lab for Measurement Technology, 2016.

[138] Madou, M.J. and Morrison, S.R.: “Chemical Sensing with Solid State Devices”, Academic Press, Boston, ISBN: 0-12-464965-3, 1989.

[139] Wang, C., Yin, L., Zhang, L., Xiang, D. and Gao, R.: “Metal oxide gas sensors: sensitivity and influencing factors”, Sensors 10 (3), pp. 2088-2106, doi:10.3390/s100302088, 2010.

[140] Yamazoe, N., Sakai, G. and Shimanoe, K.: “Oxide semiconductor gas sensors”, Catalysis Surveys from Asia 7, pp. 63-75, doi:10.1023/A:1023436725457, 2003.

[141] Rothschild, A. and Komem, Y.: “The effect of grain size on the sensitivity of nanocrystalline metal-oxide gas sensors”, Journal of Applied Physics 95, pp. 6374-6380, doi:10.1063/1.1728314, 2004.

[142] Kohl, D.: “Surface processes in the detection of reducing gases with SnO_2-based devices”, Sensors and Actuators 18 (1), pp. 71-113, doi:10.1016/0250-6874(89)87026-X, 1989.

[143] Simon, I., Bârsan, N., Bauer, M. and Weimar, U.: “Micromachined metal oxide gas sensors: opportunities to improve sensor performance”, Sensors and Actuators B: Chemical 73 (1), pp. 1-26, 10.1016/S0925-4005(00)00639-0, 2001.

[144] Udrea, F., Gardner, J.W., Setiadi, D., Covington, J.A., Dogaru, T., Lu, C.C. and Milne, W.I.: “Design and simulations of SOI CMOS micro-hotplate gas sensors”, Sensors and Actuators B: Chemical 78 (1), pp. 180-190, doi:10.1016/S0925-4005(01)00810-3, 2001.

[145] Semancik, S., Cavicchi, R.E., Wheeler, M.C., Tiffany, J.E., Poirier, G.E., Walton, R.M., Suehle, J.S., Panchapakesan, B. and DeVoe, D.L.: “Microhotplate platforms for chemical sensor research”, Sensors and Actuators B: Chemical 77 (1), pp. 579-591, doi:10.1016/S0925-4005(01)00695-5, 2001.

[146] Wang, J., Liu, L., Cong, S.-Y., Qi, J.-Q. and Xu, B.-K.: “An enrichment method to detect low concentration formaldehyde”, Sensors and Actuators B: Chemical 134 (2), pp. 1010-1015, doi:10.1016/j.snb.2008.07.010, 2008.

[147] Sun, Y.-F., Liu, S.-B., Meng, F.-L., Liu, J.-Y., Jin, Z., Kong, L.-T. and Liu, J.-H.: “Metal Oxide Nanostructures and Their Gas Sensing Properties: A

Review", Sensors 12 (3), pp. 2610-2631, doi:10.3390/s120302610, 2012. Figure licensed under CC BY-NC-SA 3.0.

[148] Lee, C.-Y., Chiang, C.-M., Wang, Y.-H. and Ma, R.-H.: "A self-heating gas sensor with integrated NiO thin-film for formaldehyde detection", Sensors and Actuators B: Chemical 122 (2), pp. 503-510, doi:10.1016/j.snb.2006.06.018, 2007.

[149] Elmi, I., Zampolli, S., Cozzani, E., Mancarella, F., and Cardinali, G.C.: "Development of ultra-low-power consumption MOX sensors with ppb-level VOC detection capabilities for emerging applications", Sensors and Actuators B: Chemical 135 (1), pp. 342-351, doi:10.1016/j.snb.2008.09.002, 2008.

[150] Baur, T., Schütze, A. and Sauerwald, T: „Optimierung des temperaturzyklischen Betriebs von Halbleitergassensoren", tm - Technisches Messen 82 (4), pp. 187–195, doi:10.1515/teme-2014-0007, 2015.

[151] Baur, T., Schütze, A. and Sauerwald, T: "Detection of short trace gas pulses", Proc. SENSOR 2017, Nuremberg, Germany, May 30 - June 01, doi:10.5162/sensor2017/A4.2, 2017.

[152] Gosangi, R. and Gutierrez-Osuna, R.: "Active temperature modulation of metal-oxide sensors for quantitative analysis of gas mixtures", Sensors and Actuators B: Chemical 185, pp. 201-210, doi:10.1016/j.snb.2013.04.056, 2013.

[153] Huang, X., Meng, F., Pi, Z., Xu, W. and Liu, J.: "Gas sensing behavior of a single tin dioxide sensor under dynamic temperature modulation", Sensors and Actuators B: Chemical 99 (2), pp. 444-450, doi:10.1016/j.snb.2003.12.013, 2004.

[154] Gramm, A. and Schütze, A.: "High performance solvent vapor identification with a two sensor array using temperature cycling and pattern classification", Sensors and Actuators B: Chemical 95 (1), pp. 58-65, doi:10.1016/S0925-4005(03)00404-0, 2003.

[155] Lee, A.P. and Reedy, B.J.: "Temperature modulation in semiconductor gas sensing", Sensors and Actuators B: Chemical 60 (1), pp. 35-42, doi:10.1016/S0925-4005(99)00241-5, 1999.

[156] Heilig, A., Bârsan, N., Weimar, U., Schweizer-Berberich, M., Gardner, J.W. and Göpel, W.: "Gas identification by modulating temperatures of SnO_2-based thick film sensors", Sensors and Actuators B: Chemical 43 (1), pp. 45-51, doi:10.1016/S0925-4005(97)00096-8, 1997.

[157] Baur, T: „Modell eines Halbleitergassensors im temperaturzyklischen Betrieb", Bachelor Thesis, Saarland University, Lab for Measurement Technology, 2014.

[158] Jung, R: „System für die hochpräzise Messungen von Halbleitergassensoren", Bachelor Thesis, Saarland University, Lab for Measurement Technology, 2016.

[159] Balandeh, M., Mezzetti, A., Tacca, A., Leonardi, S., Marra, G., Divitini, G., Ducati, C., Meda L. and Di Fonzo, F.: "Quasi-1D hyperbranched WO_3 nanostructures for low-voltage photoelectrochemical water splitting", J. Mater. Chem. A 3, pp. 6110-6117, doi:10.1039/C4TA06786J, 2015.

[160] Pervolaraki, M., Mihailescu, C.N., Luculescu, C.R., Ionescu, P., Dracea, M.D., Pantelica, D. and Giapintzakis, J.: "Picosecond ultrafast pulsed laser deposition of $SrTiO_3$", Applied Surface Science 336, pp. 278-282, doi:10.1016/j.apsusc.2014.12.026, 2015.

[161] Craciun, D., Socol, G., Stefan, N., Mihailescu, I.N., Bourne, G. and Craciun, V.: "High-repetition rate pulsed laser deposition of ZrC thin films", Surface and Coatings Technology 203 (8), pp. 1055-1058, doi:10.1016/j.surfcoat.2008.09.039, 2009.

[162] Preiß, E.M., Rogge, T., Krauß, A. and Seidel, H.: "Tin oxide-based thin films prepared by pulsed laser deposition for gas sensing", Sensors and Actuators B: Chemical 236, pp. 865-873, doi:10.1016/j.snb.2016.02.105, 2016.

[163] Huotari, J., Kekkonen, V., Haapalainen, T., Leidinger, M., Sauerwald, T., Puustinen, J., Liimatainen, J. and Lappalainen, J.: "Pulsed laser deposition of metal oxide nanostructures for highly sensitive gas sensor applications", Sensors and Actuators B: Chemical 236, pp. 978-987, doi:10.1016/j.snb.2016.04.060, 2016.

[164] Caricato, A.P., Luches, A. and Rella, R.: "Nanoparticle Thin Films for Gas Sensors Prepared by Matrix Assisted Pulsed Laser Evaporation", Sensors 9 (4), pp. 2682-2696, doi:10.3390/s90402682, 2009.

[165] Nam, H.-J., Sasaki, T. and Koshizaki, N.: "Optical CO Gas Sensor Using a Cobalt Oxide Thin Film Prepared by Pulsed Laser Deposition under Various Argon Pressures", J. Phys. Chem. B 110 (46), pp. 23081–23084, doi:10.1021/jp063484f, 2006.

[166] Zhao, Y., Feng, Z. and Liang, L.: "SnO_2 gas sensor films deposited by pulsed laser ablation", Sensors and Actuators B: Chemical 56 (3), pp. 224-227, doi:10.1016/S0925-4005(99)00067-2, 1999.

[167] de Koning, S., Janssen, H.-G. and Brinkman, U.A.T.: "Modern Methods of Sample Preparation for GC Analysis", Chroma 69 (Suppl 1), pp. 33-78, doi:10.1365/s10337-008-0937-3, 2009.

[168] Woolfenden, E.: "Sorbent-based sampling methods for volatile and semi-volatile organic compounds in air, Part 1: Sorbent-based air monitoring options", Journal of Chromatography A 1217 (16), pp. 2674-2684, doi:10.1016/j.chroma.2009.12.042, 2010.

[169] Zhang, S., Cai, L., Koziel, J.A., Hoff, S.J., Schmidt, D.R., Clanton, C.J., Jacobson, L.D., Parker, D.B. and Heber, A.J.: "Field air sampling and simultaneous chemical and sensory analysis of livestock odorants with sorbent

tubes and GC–MS/olfactometry", Sensors and Actuators B: Chemical 146 (2), pp. 427-432, doi:10.1016/j.snb.2009.11.028, 2010.

[170] Bart, J.C.J.: "Direct solid sampling methods for gas chromatographic analysis of polymer/additive formulations", Polymer Testing 20 (7), pp. 729-740, doi:10.1016/S0142-9418(01)00027-7, 2001.

[171] Curran, C., Underhill, M., Gibson, L.T. and Strlic, M.: "The development of a SPME-GC/MS method for the analysis of VOC emissions from historic plastic and rubber materials", Microchemical Journal 124, pp. 909-918, doi:10.1016/j.microc.2015.08.027, 2016.

[172] Tassi, F., Capecchiacci, F., Buccianti, A. and Vaselli, O.: "Sampling and analytical procedures for the determination of VOCs released into air from natural and anthropogenic sources: A comparison between SPME (Solid Phase Micro Extraction) and ST (Solid Trap) methods", Applied Geochemistry 27 (1), pp. 115-123, doi:10.1016/j.apgeochem.2011.09.023, 2012.

[173] Kusano, M., Mendez, E. and Furton, K.G.: "Development of headspace SPME method for analysis of volatile organic compounds present in human biological specimens", Anal Bioanal Chem 400, pp. 1817-1826, doi:10.1007/s00216-011-4950-2, 2011.

[174] Camara, M., Breuil, P., Briand, D., Viricelle, J.-P., Pijolat, C. and de Rooij, N.F.: "Preconcentration Modeling for the Optimization of a Micro Gas Preconcentrator Applied to Environmental Monitoring", Anal. Chem. 87 (8), pp 4455–4463, doi:10.1021/acs.analchem.5b00400, 2015.

[175] Brieger, O.: „Modellbasierte Optimierung eines Sensor-Präkonzentrator-Systems", Bachelor Thesis, Saarland University, Lab for Measurement Technology, 2017.

[176] Thommes, M., Kaneko, K., Neimark, A.V., Olivier, J.P., Rodriguez-Reinoso, F., Rouquerol, J. and Sing, K.S.W.: "Physisorption of gases, with special reference to the evaluation of surface area and pore size distribution (IUPAC Technical Report)", Pure Appl. Chem. 87(9-10), pp. 1051–1069, doi:10.1515/pac-2014-1117, 2015.

[177] Bolis, V.: "Fundamentals in Adsorption at the Solid-Gas Interface. Concepts and Thermodynamics", in: Auroux, A. (eds): "Calorimetry and Thermal Methods in Catalysis", Springer Series in Materials Science 154, Springer, Berlin, Heidelberg, doi:10.1007/978-3-642-11954-5_1, 2013.

[178] Ruthven, D.M.: "Fundamentals of Adsorption Equilibrium and Kinetics in Microporous Solids", in: Karge, H.G., Weitkamp, J. (eds): "Adsorption and Diffusion", Molecular Sieves 7. Springer, Berlin, Heidelberg, doi:10.1007/3829_007, 2006.

[179] Czaja, A.U., Trukhan N. and Müller, U.: "Industrial applications of metal–organic frameworks", Chem. Soc. Rev. 38, pp. 1284-1293, doi:10.1039/B804680H, 2009.

[180] Czeslik, K., Seemann, H and Winter, R.: „Basiswissen physikalische Chemie“, 4. Auflage, Vieweg+Teubner Verlag, doi:10.1007/978-3-8348-9359-8, 2010.

[181] Henry, W.: “Experiments on the Quantity of Gases Absorbed by Water, at Different Temperatures, and under Different Pressures”, Philosophical Transactions of the Royal Society of London 93, pp. 29–43, doi: 10.1098/rstl.1803.0004, 1803.

[182] Luebbers, M.T., Wu, T., Shen, L. and Masel, R.I.: “Trends in the Adsorption of Volatile Organic Compounds in a Large-Pore Metal−Organic Framework, IRMOF-1”, Langmuir 26 (13), pp. 11319–11329, doi10.1021/la100635r, 2010.

[183] Langmuir, I.: “The Constitution and Fundamental Properties of Solids and Liquids. Part I. Solids”, J. Am. Chem. Soc. 38 (11), pp. 2221–2295, doi:10.1021/ja02268a002, 1916.

[184] Brunauer, S., Emmett, P.H. and Teller, E.: “Adsorption of Gases in Multimolecular Layers”, J. Am. Chem. Soc. 60 (2), pp 309–319, doi:10.1021/ja01269a023, 1938.

[185] Sanchez, J.-B., Lahlou, H., Mohsen, Y., Gaddari, A. and Berger, F.: “Sub-ppm Detection of Ammonia Using a Microfabricated Gas Preconcentrator and a Room Temperature Gas Sensor”, Sensor Letters 13 (11), pp. 913-916, doi:10.1166/sl.2015.3529, 2015.

[186] Cho, S.M., Kim, Y.J., Heo, G.S. and Shin, S.-M.: “Two-step preconcentration for analysis of exhaled gas of human breath with electronic nose”, Sensors and Actuators B: Chemical 117 (1), pp. 50-57, doi:10.1016/j.snb.2005.10.050, 2006.

[187] McCartney, M.M., Zrodnikov, Y., Fung, A.G., LeVasseur, M.K. ,Pedersen, J.M., Zamuruyev, K.O., Aksenov, A.A., Kenyon, N.J. and Davis, C.E.: “An Easy to Manufacture Micro Gas Preconcentrator for Chemical Sensing Applications”, ACS Sensors 2 (8), pp. 1167-1174, doi:10.1021/acssensors.7b00289, 2017.

[188] Alfeeli, B., Cho, D., Ashraf-Khorassani, M., Taylor, L.T. and Agah, M.: “MEMS-based multi-inlet/outlet preconcentrator coated by inkjet printing of polymer adsorbents”, Sensors and Actuators B: Chemical 133 (1), pp. 24-32, doi:10.1016/j.snb.2008.01.063, 2008.

[189] Gràcia, I., Ivanov, P., Blanco, F., Sabaté, N., Vilanova, X., Correig, X., Fonseca, L., Figueras, E., Santander, J. and Cané, C.: “Sub-ppm gas sensor detection via spiral μ-preconcentrator”, Sensors and Actuators B: Chemical 132 (1), pp. 149-154, doi:10.1016/j.snb.2008.01.019, 2008.

[190] Lu, C.J. and Zellers, E.T.: “Multi-adsorbent preconcentration/focusing module for portable-GC/microsensor-array analysis of complex vapor mixtures”, Analyst 127, pp. 1061–1068, doi:10.1039/b111689d, 2002.

[191] Parkes, A.M., Lindley, R.E. and Orr-Ewing, A.J.: "Combining Preconcentration of Air Samples with Cavity Ring-Down Spectroscopy for Detection of Trace Volatile Organic Compounds in the Atmosphere", Anal. Chem. 76 (24), pp. 7329–7335, doi:10.1021/ac048727j, 2004.

[192] Sanderson, K.: "Materials chemistry: Space invaders", Nature 448, pp. 746-748, doi:10.1038/448746a, 2007.

[193] Rowsell, J.L.C. and Yaghi, O.M.: "Metal–organic frameworks: a new class of porous materials", Microporous Mesoporous Mater. 73 (1-2), pp. 3–14, doi:10.1016/j.micromeso.2004.03.034, 2004.

[194] Alhamami, M., Doan H. and Cheng, C.-H.: "A Review on Breathing Behaviors of Metal-Organic-Frameworks (MOFs) for Gas Adsorption", Materials 7, pp. 3198-3250, doi:10.3390/ma7043198, 2014.

[195] Férey, G., Mellot-Draznieks, C., Serre, C., Millange, F., Dutour, J., Surblé, S. and Margiolaki, I: "A Chromium Terephthalate-Based Solid with Unusually Large Pore Volumes and Surface Area", Science 309 (5743), pp. 2040-2042, doi:10.1126/science.1116275, 2005.

[196] Chui, S.S.Y., Lo, S.M.F., Charmant, J.P.H., Orpen, A.G. and Williams, I.D.: "A chemically functionalizable nanoporous material $[Cu_3(TMA)_2(H_2O)_3]n$", Science 283, pp. 1148–1150, doi:10.1126/science.283.5405.1148, 1999.

[197] Loiseau, T., Serre, C., Huguenard, C., Fink, G., Taulelle, F., Henry, M., Bataille, T., and Férey, G.: "A rationale for the large breathing of the porous aluminumterephthalate (MIL-53) upon hydration", Chemistry 10, pp. 1373–1382, doi:10.1002/chem.200305413, 2004.

[198] Rieger, M., personal communication, email, 25.09.2017.

[199] Bender, F., Barié, N., Romoudis, G., Voigt, A. and Rapp, M.: "Development of a preconcentration unit for a SAW sensor micro array and its use for indoor air quality monitoring", Sensors and Actuators B: Chemical 93 (1–3), pp. 135-141, doi:10.1016/S0925-4005(03)00239-9, 2003.

[200] Whalley, J., Sallis, P. and Bassey, E.: "Approaches to Cleaning Gas Response Signals from Metal Oxide Sensors: Optimisation and Generalizabilty", International Journal on Advances in Systems and Measurements 9 (1-2), pp. 12-23, 2016.

[201] Goschnick, J., Magapu, V., Kiselev, I. and Koronczi, I.: "New normalization procedure to improve signal pattern discrimination power in case of different concentration dependencies of the gas sensors in an array", Sensors and Actuators B: Chemical 116 (1–2), pp. 85-89, doi:10.1016/j.snb.2005.12.067, 2006.

[202] Proaki, J.G., and Manolakis, D.G.: "Digital Signal Processing: Principles, Algorithms, and Applications", 3rd ed., Prentice-Hall, Inc. Upper Saddle River, NJ, USA, 1996.

[203] Savitzky, A. and Golay, M.J.E.: “Smoothing and Differentiation of Data by Simplified Least Squares Procedures”, Anal. Chem. 36 (8), pp. 1627–1639, doi:10.1021/ac60214a047, 1964.

[204] Reimann, P. and Schütze, A.: “Sensor Arrays, Virtual Multisensors, Data Fusion, and Gas Sensor Data Evaluation”, in “Gas Sensing Fundamentals”, D. Kohl and T. Wagner, Eds., Springer, pp. 67-107, doi:10.1007/978-3-642-54519-1, 2014.

[205] Cizek, K., Prior, C., Thammakhet, C., Galik, M., Linker, K., Tsui, R., Cagan, A., Wake, J., La Belle, J. and Wang, J.: “Integrated explosive preconcentrator and electrochemical detection system for 2,4,6-trinitrotoluene (TNT) vapor”, Analytica Chimica Acta 661 (1), pp. 117-121, doi:10.1016/j.aca.2009.12.008, 2010.

[206] Leidinger, M., Huotari, J., Sauerwald, T., Lappalainen, J. and Schütze, A.: “Nanostructured WO_3 semiconductor gas sensor for selective detection of naphthalene”, Proc. SENSOR 2015 - 17th International Conference on Sensors and Measurement Technology, Nuremberg, Germany, May 19-21, pp. 723-728, doi:10.5162/sensor2015/E8.2, 2015.

[207] Bur, C.: “Selectivity Enhancement of Gas Sensitive Field Effect Transistors by Dynamic Operation”, Dissertation, Saarland University, Naturwissenschaftlich-Technischen Fakultät II - Physik und Mechatronik; also published in “Aktuelle Berichte aus der Mikrosystemtechnik – Recent Developments in MEMS”, Schutze., A and Seidel, H. (Eds), 27, ISBN:978-3-8440-3758-6, 2015.

[208] Reimann, P.: „Gasmesssysteme basierend auf Halbleitergassensoren für sicherheitskritische Anwendungen mit dem Ansatz der Sensorselbstüberwachung“, Dissertation, Saarland University, Naturwissenschaftlich-Technischen Fakultät II - Physik und Mechatronik; also published in “Aktuelle Berichte aus der Mikrosystemtechnik – Recent Developments in MEMS“, Schutze., A and Seidel, H. (Eds), 19, ISBN:978-3-8440-0232-4, 2011.

[209] Schneider, T.: „Methoden der automatisierten Merkmalsextraktion und –selektion von Sensorsignalen“, Master Thesis, Saarland University, Lab for Measurement Technology, 2015.

[210] Bastuck, M.: „Quantification of Volatile Organic Compounds“, Master Thesis, Saarland University, Lab for Measurement Technology, 2014.

[211] Bastuck, M., Puglisi, D., Huotari, J., Sauerwald, T., Lappalainen, J., Lloyd Spetz, A., Andersson, M. and Schütze, A: “Exploring the selectivity of WO_3 with iridium catalyst in an ethanol/naphthalene mixture using multivariate statistics”, Thin Solid Films 618, pp. 263-270, doi:10.1016/j.tsf.2016.08.002, 2016.

[212] Bur, C., Bastuck, M., Puglisi, D., Schütze, A., Lloyd Spetz, A. and Andersson, M.: “Discrimination and quantification of volatile organic compounds in the

ppb-range with gas sensitive SiC-FETs using multivariate statistics", Sensors and Actuators B: Chemical 214, pp. 225-233, doi:10.1016/j.snb.2015.03.016, 2015.

[213] Yan, J., Guo, X., Duan, S., Jia, P., Wang, L., Peng, C. and Zhang, S.: "Electronic Nose Feature Extraction Methods: A Review", Sensors 15 (11), pp. 27804–27831, doi:10.3390/s151127804, 2015.

[214] Vergara, A., Martinelli, E., Llobet, E., D'Amico, A. and Di Natale, C.: "Optimized Feature Extraction for Temperature-Modulated Gas Sensors", Journal of Sensors 2009, Article ID 716316, doi:10.1155/2009/716316, 2009.

[215] Backhaus, K.,Erichson, B, Plinke, P. and Weiber, R.: "Multivariate Analysemethoden", 14th ed., Springer Verlag Berlin Heidelberg, doi:10.1007/978-3-662-46076-4, 2016.

[216] Fisher, R.A.: "The use of multiple measurements in taxonomic problems", Annals of Eugenics 7 (2), pp. 179–188, doi:10.1111/j.1469-1809.1936.tb02137.x, 1936.

[217] Klecka, W.R.: "Discriminant Analysis", Beverly Hills, USA: Sage University Paper series on quantitative applications in the social sciences 19, doi:10.4135/9781412983938, 1980.

[218] Zhang, X. and Jia, Y.: "A linear discriminant analysis framework based on random subspace for face recognition", Pattern Recognition 40 (9), pp. 2585-2591, doi:10.1016/j.patcog.2006.12.002, 2007.

[219] Lu, J., Plataniotis, K.N. and Venetsanopoulos, A.N.; "Regularization studies of linear discriminant analysis in small sample size scenarios with application to face recognition", Pattern Recognition Letters 26 (2), pp. 181-191, doi:10.1016/j.patrec.2004.09.014, 2005.

[220] Etemad K. and Chellappa, R.: "Discriminant analysis for recognition of human face images", J. Opt. Soc. Am. A 14 (8), pp. 1724-1733, doi:10.1364/JOSAA.14.001724,1997.

[221] Leidinger, M., Sauerwald, T., Conrad, T., Reimringer, W., Ventura, G., and Schütze, A.: "Selective Detection of Hazardous Indoor VOCs Using Metal Oxide Gas Sensors", Procedia Engineering 87, pp. 1449-1452, doi:10.1016/j.proeng.2014.11.722, 2014.

[222] Wold, S., Sjöström, M. and Eriksson, L.: "PLS-regression: a basic tool of chemometrics", Chemometrics and Intelligent Laboratory Systems 58 (2), pp. 109-130, doi:10.1016/S0169-7439(01)00155-1, 2001.

[223] Geladi, P. and Kowalski, B.R.: "Partial least-squares regression: a tutorial", Analytica Chimica Acta 185, pp. 1-17, doi:10.1016/0003-2670(86)80028-9, 1986.

[224] Leidinger, M., Baur, T., Sauerwald, T., Reimringer, W., Spinelle, L., Gerboles, M. and Schütze, A.: "Highly sensitive benzene detection with MOS

gas sensors", Proc. SENSOR 2017, Nuremberg, Germany, May 30 - June 01, pp. 92-97, doi:10.5162/sensor2017/A4.3, 2017.

[225] Gutierrez-Osuna, R.: "Pattern analysis for machine olfaction: a review", IEEE Sensors Journal 2 (3), pp. 189-202, doi:10.1109/JSEN.2002.800688, 2002.

[226] MKS Instruments Inc.: „MF1 General Purpose Mass Flow Controller", data sheet, 2016

[227] Buttner, W.J., Burgess, R., Rivkin, C., Post, M.B., Boon-Brett, L., Black, G., Harskamp, F. and Moretto, P.: "Inter-laboratory assessment of hydrogen safety sensors performance under anaerobic conditions", International Journal of Hydrogen Energy 37 (22), pp. 17540-17548, doi:10.1016/j.ijhydene.2012.03.165, 2012.

[228] Gensterblum, Y., van Hemert, P., Billemont, P., Busch, A., Charriére, D., Li, D., Krooss, B.M., de Weireld, G., Prinz, D. and Wolf, K.-H.A.A.: "European inter-laboratory comparison of high pressure CO_2 sorption isotherms. I: Activated carbon", Carbon 47 (13), pp. 2958-2969, doi:10.1016/j.carbon.2009.06.046, 2009.

[229] Pein, M., Gondongwe, X.D., Habara, M. and Winzenburg, G.: "Interlaboratory testing of Insent e-tongues", International Journal of Pharmaceutics 469 (2), pp. 228-237, doi:10.1016/j.ijpharm.2014.02.036, 2014.

[230] Gonçalves, M.A., Gonzaga, F.B., Fraga, I.C.S., de Matos Ribeiro, C., Sobral, S.P., Borges, P.P. and de Carvalho Rocha, W.F.: "Evaluation study of different glass electrodes by an interlaboratory comparison for determining the pH of fuel ethanol", Sensors and Actuators B: Chemical 158 (1), pp. 327-332, doi:10.1016/j.snb.2011.06.029, 2011.

[231] Bockmon, E.E. and Dickson, A.G.: "An inter-laboratory comparison assessing the quality of seawater carbon dioxide measurements", Marine Chemistry 171, pp. 36-43, doi:10.1016/j.marchem.2015.02.002, 2015.

[232] Leidinger, M., Reimringer, W., Alépée, C., Rieger, M., Sauerwald, T., Conrad, T. and Schütze, A.: "Gas measurement system for indoor air quality monitoring using an integrated pre-concentrator gas sensor system", Proceedings Mikro-Nano-Integration - 6. GMM-Workshop, Oct. 05/06 2016, Duisburg, Germany, VDE Verlag, 2016.

List of Publications

Peer-reviewed publications

- Sauerwald, T., Baur, T., Leidinger, M., Reimringer, W., Spinelle, L.,Gerboles, M., Kok, G. and Schütze, A.: "Highly sensitive benzene detection with metal oxide semiconductor gas sensors - an inter-laboratory comparison", J. Sens. Sens. Syst. 7, pp. 235-243, doi: 10.5194/jsss-7-235-2018, 2018.
- Leidinger, M., Schultealbert, C., Neu, J., Schütze, A. and Sauerwald, T.: "Characterization and calibration of gas sensor systems at ppb level – a versatile test gas generation system", Meas. Sci. Technol. 29 (1), 015901, doi: 10.1088/1361-6501/aa91da, 2018.
- Schütze, A., Baur, T., Leidinger, M., Reimringer, W., Jung, R., Conrad, T. and Sauerwald, T.: "Highly Sensitive and Selective VOC Sensor Systems Based on Semiconductor Gas Sensors: How to?", Environments 4 (1), 20, doi:10.3390/environments4010020, 2017.
- Leidinger, M., Rieger, M., Sauerwald, T., Alépée C. and Schütze, A.: "Integrated pre-concentrator gas sensor microsystem for ppb level benzene detection", Sensors and Actuators B: Chemical 236, pp. 988-996, doi:10.1016/j.snb.2016.04.064, 2016.
- Leidinger, M., Huotari, J., Sauerwald, T., Lappalainen J. and Schütze, A.: "Selective detection of naphthalene with nanostructured WO_3 gas sensors prepared by pulsed laser deposition", J. Sens. Sens. Syst. 5, pp. 157-156, doi:10.5194/jsss-5-147-2016, 2016.
- Huotari, J., Kekkonen, V., Haapalainen, T., Leidinger, M., Sauerwald, T., Puustinen, J., Liimatainen, J. and Lappalainen, J.: "Pulsed laser deposition of metal oxide nanostructures for highly sensitive gas sensor applications", Sensors and Actuators B: Chemical 236, pp. 978-987, doi:10.1016/j.snb.2016.04.060, 2016.
- Leidinger, M., Sauerwald, T., Reimringer, W., Ventura, G., and Schütze, A.: "Selective detection of hazardous VOCs for indoor air quality applications using a virtual gas sensor array", J. Sens. Sens. Syst., 3, 253-263, doi:10.5194/jsss-3-253-2014, 2014.

Conference contributions

- Sauerwald, T., Baur, T., Leidinger, M., Spinelle, L., Gerboles, M. and Schütze, A.: „Laborübertragbare Kalibrierung von Sensoren für die Messung von Benzol", Tagungsband 13. Dresdner Sensor-Symposium, Dresden, 04.12.-06.12., pp. 105-110, doi: 10.5162/13dss2017/3.4, 2017.

- Leidinger, M., Baur, T., Sauerwald, T., Spinelle, L., Gerboles, M., Reimringer, W. and Schütze, A.: Highly sensitive benzene detection with MOS gas sensors, Proc. SENSOR 2017, Nuremberg, Germany, 30.05.-01.06., pp. 92-97, doi:10.5162/sensor2017/A4.3, 2017.
- Leidinger, M., Sauerwald, T., Alépée, C., Rieger, M. and Schütze, A.: „Integrated pre-concentrator gas sensor system for improved trace gas sensing performance“, IEEE Sensors 2016, Orlando, FL, USA, 30.10.-02.09., doi:10.1109/ICSENS.2016.7808668, 2016.
- Leidinger, M., Reimringer, W., Alépée, C., Rieger, M., Sauerwald, T., Conrad, T. and Schütze, A.: “Gas measurement system for indoor air quality monitoring using an integrated pre-concentrator gas sensor system”, Proceedings Mikro-Nano-Integration - 6. GMM-Workshop, 05.10.-06.10., Duisburg, Germany, VDE Verlag, 2016.
- Leidinger, M., Sauerwald, T., Alépée, C. and Schütze, A.: “Miniaturized Integrated Gas Sensor Systems Combining Metal Oxide Gas Sensors and Pre-concentrators”, Procedia Engineering 168, pp. 293-296, doi:10.1016/j.proeng.2016.11.199, 2016.
- Wilhelm, I., Rieger, M., Hürttlen, J., Wittek, M., Alépée, C., Leidinger, M. and Sauerwald, T.: “Novel Low-Cost Selective Pre-Concentrators Based on Metal Organic Frameworks”, Procedia Engineering 168, pp. 151-154, doi:10.1016/j.proeng.2016.11.186, 2016.
- Leidinger, M., Sauerwald, T., Rieger, M. and Schütze, A.: “Optimized Operation of an Integrated Pre-Concentrator Gas Sensor System, poster presentation”, IMCS2016, The 16th International Meeting on Chemical Sensors, Jeju Island, Korea, 10.07.-13.07., 2016.
- Stahl-Offergeld, M., Hohe, H.-P., Jung, R., Leidinger, M., Schütze, A. and Sauerwald, T.: “Highly Integrated Sensor System for the Detection of Trace Gases”, oral presentation, IMCS2016, The 16th International Meeting on Chemical Sensors, Jeju Island, Korea, 10.07.-13.07., 2016.
- Sauerwald, T., Leidinger, M., Schütze, A., Huotari, J. and Lappalainen, J.: “Nanostructured Semiconductor Gas Sensors for Detection of sub-ppm Concentration”, oral presentation, CIMTEC 2016, 5th International Conference "Smart and Multifunctional Materials, Structures and Systems", Perugia, Italy, 05.06.-09.06., 2016.
- Leidinger, M., Rieger, M., Sauerwald, T., Alépée, C. and Schütze, A.: „Integriertes Präkonzentrator-Gassensor-Mikrosystem zur Detektion von Spurengasen in Innenraumluft“, 18. GMA/ITG-Fachtagung Sensoren und Messsysteme, 10.05.-11.05., pp. 274-280, doi:10.5162/sensoren2016/4.2.4, 2016
- Leidinger, M., Schmitt, B., Sauerwald, T., Rieger, M., Alèpèe, C. and Schütze, A.: “Novel Integrated Gas Sensor Microsystem with Pre-Concentrator for Extremely High Sensitivity and Selectivity”, keynote presentation, COST Action TD1105 European Network on New Sensing Technologies for Air-Pollution Control and

Environmental Sustainability - EuNetAir, 5th Scientific Meeting, Sofia, Bulgaria, 16.12.-18.12., 2015.

- Bastuck, M., Leidinger, M., Sauerwald, T. and Schütze, A.: "Quantification of ppb-level volatile organic compounds", oral presentation, SGS 2015, IX International Workshop on Semiconductor Gas Sensors, Zakopane, Poland, 13.12.-16.12., 2015.
- Lappalainen, J., Huotari, J., Leidinger, M., Baur, T., Alépée, C., Komulainen, S., Puustinen, J. and Schütze A.: "Tailored Metal Oxide Nanoparticles, Agglomerates, and Nanotrees for Gas Sensor Applications", invited talk, SGS 2015, IX International Workshop on Semiconductor Gas Sensors, Zakopane, Poland, 13.12.-16.12., 2015.
- Leidinger, M., Sauerwald, T., Rieger, M., Alépée, C. and Schütze A.: „Integriertes Präkonzentrator-Gassensor-Mikrosystem zur Detektion von Spurengasen", Tagungsband Dresdner Sensor-Symposium, Dresden, 07.12.-09.12., pp. 72-77, doi: 10.5162/12dss2015/5.4, 2015.
- Schütze, A., Leidinger, M., Schmitt, B., Sauerwald, T., Rieger, M. and Alépée, C.: "A novel low-cost pre-concentrator concept to boost sensitivity and selectivity of gas sensor systems", Proceedings IEEE Sensors 2015, Busan, South Korea, 01.11.-04.11., pp. 735-738, doi:10.1109/ICSENS.2015.7370361, 2015.
- Schütze, A., Sauerwald, T., Leidinger, M., Huotari, J., Lappalainen, J., Rieger, M., Hürttlen, J., Alépée, C., Liimatainen, J. and Kekkonen, V.: "Increasing Sensitivity and Selectivity of Gas Sensor-Systems by PLD-deposited Sensitive Layers and Micromachined Pre-Concentrators with MOF Layers", Proceedings Fourth Scientific Meeting EuNetAir, Linköping, Sweden, 03.06.-05.06., doi:10.5162/4EuNetAir2015/04, 2015.
- Leidinger, M., Rieger, M., Weishaupt, D., Sauerwald, T., Nägele, M., Hürttlen, J. and Schütze, A.: "Trace gas VOC Detection Using Metal-organic Frameworks as Pre-concentrators and Semiconductor Gas Sensors", Procedia Engineering 120, pp. 1042-1045, doi:10.1016/j.proeng.2015.08.719, 2015.
- Kekkonen, V., Alépée, C., Liimatainen, J., Leidinger, M. and Schütze, A.: "Gas sensing characteristics of nanostructured metal oxide coatings produced by ultrashort pulsed laser deposition", EUROSENSORS 2015, XXIX edition of the conference series, poster presentation, Freiburg, Germany, 06.09.-09.09., 2015.
- Bastuck, B., Leidinger, M., Sauerwald, T. and Schütze, A.: "Improved Quantification of Naphthalene using non-linear Partial Least Squares Regression", ISOEN 2015, 16th International Symposium on Olfaction and Electronic Noses, poster presentation, Dijon, France, 28.06.-01.07., 2015.
- Leidinger, M., Huotari, J., Sauerwald, T., Lappalainen, J. and Schütze, A.: "Nanostructured WO_3 semiconductor gas sensor for selective detection of naphthalene", Proc. SENSOR 2015 - 17th International Conference on Sensors and Measurement Technology, Nuremberg, Germany, May 19-21, pp. 723-728, doi:10.5162/sensor2015/E8.2, 2015.

- Leidinger, M., Helwig, N., Sauerwald, T. and Schütze, A.: „Gasmischanlage zur automatischen Generierung von VOC-Spurengasen über einen weiten Konzentrationsbereich“, XXVIII. Messtechnisches Symposium des Arbeitskreises der Hochschullehrer für Messtechnik, Tagungsband, Shaker Verlag, Aachen, pp. 167-176, doi:10.5162/AHMT2014/P6, 2014.
- Leidinger, M., Sauerwald, T., Conrad, T., Reimringer, W., Ventura, G. and Schütze, A.: “Selective Detection of Hazardous Indoor VOCs Using Metal Oxide Gas Sensors”, Procedia Engineering 87, pp. 1449-1452, doi:10.1016/j.proeng.2014.11.722, 2014.
- Leidinger, M., Sauerwald, T. and Schütze, A.: „Optimierter dynamischer Betrieb und multivariate Signalauswertung zum selektiven Nachweis von VOC im ppb-Bereich“, 17. ITG / GMA Fachtagung Sensoren und Messsysteme, Nürnberg, 03.06.-04.06., ITG Fachbericht 250, VDE Verlag, 2014.
- Sauerwald, T., Leidinger, M. and Schütze, A.: “Selective Detection of VOC using a virtual gas sensor array”, E-MRS Spring Symposium, talk B.XII 5, Lille, France, 25.05.-29.05., 2014.
- Leidinger, M., Sauerwald, T., Pignanelli, E. and Schütze, A.: “Detection of CO_2 and Volatile Organic Compounds using a Combination of Semiconductor Gas Sensor and IR Spectroscopy”, poster presentation at the COST Action TD 1105 "EuNetAir" 2nd scientific meeting, Queens´ College, University of Cambridge, Cambridge, 18.12.-20.12., 2013.
- Leidinger, M., Sauerwald, T., Pignanelli, E. and Schütze, A.: „Detektion von CO_2 und flüchtigen organischen Komponenten mittels Kombination von Halbleiter-Gassensorik und Infrarotspektroskopie“, 11. Dresdner Sensor Symposium, Dresden, 09.12.-11.12., pp. 229-233, doi: 10.5162/11dss2013/B6, 2013.
- Leidinger, M., Pignanelli, E., Kühn, K., Sauerwald, T. and Schütze, A.: “High performance infrared gas measurement system based on a semiconductor gas sensor IR source with tunable Fabry-Pérot filter”, IRS² 2013 - 13th International Conference on Infrared Sensors & Systems, Nuremberg, Germany, 14.05.-16.05., doi: 10.5162/irs2013/i3.2, 2013.
- Kühn, K., Leidinger, M., Pignanelli, E. and Schütze, A.: “Investigations on a MOX Gas Sensor as an Infrared Source for an IR-based Gas Sensing System”, Proc. IMCS 2012: The 14th International Meeting on Chemical Sensors, 20.05.-23.05., Nuremberg, Germany, 2012.

Acknowledgment / Danksagung

Mein Dank gilt an erster Stelle Herrn Prof. Dr. Andreas Schütze, der mir die Möglichkeit der Bearbeitung einer interessanten Fragestellung im Bereich der Gassensorik gab. Seine Anregungen, Diskussionsbeiträge und Hinweise trugen wesentlich zum Gelingen dieser Arbeit bei.

Außerdem bedanke ich mich bei Herrn Prof. Dr. Helmut Seidel, der sich freundlicherweise bereiterklärt hat, das Zweitgutachten dieser Arbeit zu übernehmen.

Besonderer Dank gilt meinen ehemaligen Kollegen sowie den Abschlussarbeitern und Studenten des Lehrstuhls für Messtechnik, die alle gemeinsam zu einer sehr angenehme Arbeitsatmosphäre während meiner Zeit dort beigetragen haben. Die fachlichen und nicht-fachlichen Diskussionen, gemeinsamen Aktivitäten und sonstige Unterstützungen haben direkt und indirekt wertvolle Beiträge zum Gelingen dieser Arbeit geliefert.

Weiterhin möchte ich den Kollegen des SENSIndoor-Projekts danken für den guten wissenschaftlichen Austausch während der Projektlaufzeit, während der große Teile dieser Arbeit entstanden sind.

Nicht zuletzt möchte ich herzlich meiner Familie, meiner Freundin und meinen Freunden danken für die stetige Unterstützung während der Promotionszeit und insbesondere die Geduld während der Fertigstellung der Arbeit.

Affidavit / Eidesstattliche Versicherung

Hiermit versichere ich an Eides statt, dass ich die vorliegende Arbeit selbstständig und ohne Benutzung anderer als der angegebenen Hilfsmittel angefertigt habe. Die aus anderen Quellen oder indirekt übernommenen Daten und Konzepte sind unter Angabe der Quelle gekennzeichnet. Die Arbeit wurde bisher weder im In- noch im Ausland in gleicher oder ähnlicher Form in einem Verfahren zur Erlangung eines akademischen Grades vorgelegt.

Ort, Datum

_____

Unterschrift

_____

Martin Leidinger